Identification and characterisation of an overlapping open reading frame (ORF4) within the murine norovirus genome

by

Nora Ann McFadden

Thesis submitted for the degree of

Doctor of Philosophy

Imperial College London

2010

Department of Virology, Imperial College London, Faculty of Medicine,

St. Mary's Campus, Norfolk Place

London

Abstract

Caliciviruses are single-stranded positive-sense RNA viruses, most commonly associated with outbreaks of gastroenteritis in humans. In addition to the three open reading frames (ORFs) typical of caliciviruses a highly conserved fourth overlapping ORF within the murine norovirus (MNV) genome was identified and characterised during this project. ORF4 overlaps and is contained within the capsid encoding ORF2 in a +1 frame. Once a suitable antibody had been generated, immunoblotting was used to show that the ORF4 protein is produced during MNV infection. Although ORF4 mutant viruses were viable and replicated to wild-type MNV levels in tissue culture, pressure to restore ORF4 expression upon serial passage under specific conditions was demonstrated. Importantly, the ORF4 knockout virus was significantly attenuated in $STAT1^{-/-}$ mice. Proteomic analysis and a commercial yeast two-hybrid screen were used to identify host cell factors which interact with the ORF4 protein and confocal imaging was employed to examine cellular localisation. These approaches indicated that the ORF4 protein localises to the mitochondria and *in vitro* assays were subsequently used to demonstrate an involvement of the ORF4 protein in MNV induced apoptosis. As cells infected with the knockout virus showed an earlier and higher degree of apoptosis induction compared to wild-type infected cells, it is possible that the ORF4 protein may function to delay the onset of apoptosis during MNV infection. Whether or not the ORF4 protein has antiapoptotic activity or whether the difference in apoptotic phenotype is an indirect consequence of ORF4 protein function remains to be investigated. These data indicate that the ORF4 protein represents a novel, previously uncharacterised virulence determinant in MNV.

Table of contents

Abstract 2

Table of contents 3

List of figures 4

List of tables 4

List of appendices 4

Abbreviations 4

Acknowledgments 4

Declaration 4

1. Introduction 4

1.1 Caliciviruses 4

1.1.1 Disease and epidemiology 4

1.1.2 Morphology 4

1.1.3 Taxonomy 4

1.1.4 The study of Caliciviruses 4

1.1.5 MNV 4

1.1.6 Calicivirus life cycle and proteins 4

1.1.6.1 Attachment and entry 4

1.1.6.2 Translation of viral proteins 4

1.1.6.3 Genome replication and translation of the structural proteins 4

1.2 Overlapping reading frames 4

1.2.1 Positive-strand RNA viruses 4

1.2.1.1 Hepatitis E virus (HEV) 4

1.2.1.2 Hepatitis C virus (HCV) 4

1.2.1.3 Theiler's murine encephalitis virus (TMEV) 4

1.2.2 Negative-strand RNA viruses 4
1.2.2.1 Influenza A virus 4
1.2.2.2 Borna disease virus (BDV) 4
1.2.3 Further examples of overlapping reading frames 4
1.3 Project aims 4
2. Materials and Methods 4
2.1 Bioinformatics tools 4
2.2 Plasmid construction 4
2.3 Bacterial stocks, transformations and medium scale plasmid preparations 4
2.4 Polymerase chain reaction (PCR) and primers 4
2.4.1 PCR mutagenesis and cloning 4
2.4.2 PCR to determine the sequences of plasmid constructs and recombinant viruses 4
2.5 Agarose gel electrophoresis 4
2.6 T7 transcription and *in vitro* translation 4
2.7 Immunoprecipitation from *in vitro* transcription and translation (TNT) reactions 4
2.8 Recombinant protein production and purification 4
2.8.1 ORF4-his 4
2.8.2 Cherry ORF4 expression 4
2.9 Antisera 4
2.10 Western blot 4
2.11 Cell lines 4
2.12 DNA transfections 4
2.13 MNV reverse genetics 4

2.14 Reverse transcription-PCR (RT-PCR) and sequence verification of mutant viruses....4
2.15 Growth kinetic analysis....4
2.16 Determination of viral titre ($TCID_{50}$/ ml)....4
2.17 Analysis of ORF4 mutant virus stability....4
2.18 Analysis of virulent clones....4
2.19 *In vivo* virulence analysis....4
2.20 Quantification of viral load....4
2.21 Analysis of restoration of ORF4 expression....4
2.22 Statistical analysis....4
2.23 Tandem affinity purification....4
2.23.1 NTAP-ORF4 in the $CdCl_2$ inducible system....4
2.23.2 ORF4 in the tetracycline inducible system....4
2.24 Yeast-two hybrid screen....4
2.25 Confocal microscopy....4
2.25.1 Green fluorescent protein (GFP) transfections and slide preparation....4
2.25.2 Antibody-specific staining....4
2.26 Biochemical localisation....4
2.27 Apoptosis assays....4
3. Confirmation of ORF4 expression and *in vitro* characterisation of the ORF4 protein....4
3.1 Introduction....4
3.2 Results and discussion....4
3.2.1 Bioinformatic analysis....4
3.2.1.1 Location and Kozak context....4

3.2.1.2 Conservation of the ORF4 protein amino acid sequence 4
3.2.2 Detection of MNV ORF4 expression 4
3.2.2.1 *In vitro* transcription and translation reactions 4
3.2.2.2 Generation of an ORF4 protein reactive antibody 4
3.2.2.3 Western blot analysis 4
3.2.3 Generation and characterisation of ORF4 mutants 4
3.2.3.1 ORF4 mutants: Design, generation and recovery by reverse genetics 4
3.2.3.2 Initial characterisation of mutants 4
3.2.3.3 Loss of ORF4 results in a fitness cost 4
3.3. Conclusion 4
4. Characterisation of the role of ORF4 in MNV virulence 4
4.1 Introduction 4
4.2 Results and discussion 4
4.2.1 Generation and rescue of virulent MNV-1 ORF4 mutants 4
4.2.2 Characterisation of the role of ORF4 in MNV induced virulence 4
4.2.2.1 Experimental design 4
4.2.2.2 Analysis of bodyweight 4
4.2.2.3 Symptoms and pathology 4
4.2.2.4 Viral loads 4
4.2.2.4 Restoration of ORF4 expression not observed in M1-v 4
4.3 Conclusion 4
5. Identification of proteins which interact with the ORF4 protein 4
5.1 Introduction 4
5.2 Results and Discussion 4
5.2.1 Tandem affinity purification 4
5.2.1.1 Generation of stable cell lines 4

5.2.1.2 Identification of ORF4 protein interacting host cell proteins..... 4

5.2.1.2.2 Nuclear and nuclear associated proteins..... 4

5.2.1.2.3 Golgi and endoplasmic reticulum (ER) transport proteins..... 4

5.2.1.2.4 Binding partners associated with proteosomal degradation 4

5.2.1.2.5 Other identified NTAP-ORF4 binding partners..... 4

5.2.2 Yeast two-hybrid screen..... 4

5.3 Conclusions and future directions 4

6. Localisation studies 4

6.1 Introduction 4

6.2. Results and Discussion 4

6.2.1 Confocal microscopy demonstrating mitochondrial localisation 4

6.2.2 Biochemical localisation of the MNV ORF4 protein 4

6.3 Presentation and discussion of further work performed by Guia Carrara 4

6.3.1. Further characterisation of MNV ORF4 protein localisation..... 4

6.3.2 Analysis of the ORF4 protein equivalent of Sapovirus 4

6.4 Final conclusion..... 4

7. Investigation into the role of ORF4 in apoptosis 4

7.1 Introduction 4

7.1.1 The extrinsic and intrinsic pathways of apoptosis..... 4

7.1.2 The nuclear transport system in apoptosis 4

7.1.3 Viruses and apoptosis 4

7.2 Results and Discussion 4

7.2.1 Investigation of the role of ORF4 in viral induced apoptosis 4

7.3 Conclusion 4

8. Conclusion and future work..... 4

8.1 Overall conclusions 4

8.2 Hypothetical model of function.....4

8.3 Final summary.....4

Bibliography 4

List of figures

Figure 1.1. Calicivirus Electron microscopic images …….. 22
Figure 1.2. Phylogenetic relationship between caliciviruses…… ……... 23
Figure 1.3. Genome organisation of four genera within the *Caliciviridae* …….. 25
Figure 1.4. Diagrammatic representations of the MNV and FCV genomes ……... 30
Figure 1.5. Proposed models for the synthesis of MNV subgenomic RNAs …….. 35
Figure 1.6. Bioinformatic analysis of ORF4 ……... 37
Figure 1.7. HEV genome organisation …… 41
Figure 1.8. Organisation of the HCV genome ……. 43
Figure 1.9. Genome organisation of TMEV …… 45
Figure 1.10. Layout of an mRNA transcript of the influenza virus PB1 segment …….. 47
Figure 1.11. BDV genome organisation and transcriptional cleavage map …..……. 49
Figure 3.1. The location, size and reading frame of MNV ORF4 ……... 79
Figure 3.2. Bioinformatic analysis of ORF4 protein amino acid sequences ..….. 82, 83
Figure 3.3. *In vitro* translations and immunoprecipitations ……. 84
Figure 3.4. Generation of an ORF4 protein reactive antibody……. 86
Figure 3.5. Position of the ORF4 peptides and production of CH-P3-his …….... 87
Figure 3.6. Differences in the specific cross-reactivity of antibodies ……. 88
Figure 3.7. Detection of the ORF4 protein during virus infection …….……. 89
Figure 3.8. Generation of ORF4 mutants ……92
Figure 3.9. ORF4 expression is not required for virus replication in tissue culture … 93
Figure 3.10. Serial passage of ORF4 mutant viruses revealed phenotypic reversion 94
Figure 3.11. Virus yield experiment and effects of seeding density of protein production …… 96
Figure 4.1. Sequencing chromatograms of M1-v viral stock at genome positions 2151, 5118 and 5941 .....…… 100
Figure 4.2. Analysis of growth kinetics of M1-v and WT-v in RAW26.7 cells and BMMΦs …….. 101
Figure 4.3. Experimental design for *in vivo* virulence analysis ……. 103
Figure 4.4. ORF4 contributes to MNV virulence *in vivo* …….. 105
Figure 4.5. Viral RNA loads in the tissues of M1-v and WT-v infected mice …….. 109

Figure 4.6. Viral RNA loads in the faeces of M1-v and WT-v infected mice …….. 110
Figure 4.7. Sequencing chromatograms of all tissues and the faeces sample of an M1-v infected animal ……..... 112
Figure 5.1. Overview of the tandem affinity purification procedure ……. 117
Figure 5.2. NTAP-ORF4 in the $CdCl_2$ inducible system ……... 119
Figure 5.3. ORF4-CTAP in the tetracycline inducible system …….…. 120
Figure 5.4. Silver stained SDS-PAGE gel of the final eluate of the TAP purification ..……. …….. 122
Figure 5.5. Diagram of mitochondria and brief overview of mitochondrial import .. 124
Figure 5.6. Brief overview of the nuclear transport pathway ……..... 130
Figure 6.1. Confocal microscopy analysis of ORF4 protein localisation in infected cells...……... 146
Figure 6.2. Confocal microscopy analysis of ORF4 protein localisation using GFP fusion proteins ……..……... 147
Figure 6.3. Confocal microscopy analysis of ORF4 GFP fusions in BHK cells…… 148
Figure 6.4. Biochemical characterisation of ORF4 protein localisation…… 151
Figure 6.5. Confocal microscopy analysis of ORF4 GFP fusions in COS-7 cells … 152
Figure 6.6. Partial nuclear localisation of ORF4 GFP fusions …….. 153
Figure 6.7. Confocal microscopy images underlining mitochondrial localisation of GFP-ORF4…….. 154
Figure 6.8. Co-localisation of GFP-ORF4 with AIF, particularly at the nuclear membrane …….. 155
Figure 6.9. Design of N-terminal truncations of the ORF4 protein in ORF4-GFP ... 156
Figure 6.10 Confocal microscopy images demonstrating mitochondrial localisation of all three N-terminal truncations of ORF4-GFP ……. 157
Figure 6.11. The SV ORF4E protein does not localise to mitochondria ……... 159
Figure 6.12. ER localisation of the SV ORF4E protein …… 160
Figure 7.1. The different pathways of apoptosis ……... 165
Figure 7.2. *In vitro* measurement of caspase 3 activity and caspase levels in M1 vs. WT infected cells ……..... 171
Figure 7.3. Timecourse of apoptosis …….. 173
Figure 8.1. Proposals of ORF4 protein function …… 182

List of tables

Table 2.1 Genbank accession numbers of sequenced full-length MNV cDNA …….. 54

Table 2.2 Lists of various primers used during the course of this work ……57, 58

Table 5.1 Proteins identified by ORF4 TetR and LexA yeast two-hybrid screens …140

List of appendices

Appendix 1. Maps of plasmids used during the course of this work ……. 186-192

Appendix 2. Proteins identified in the NTAP-ORF4 purification which were not identified in the purification of other NTAP-MNV proteins …… 193, 194

Appendix 3. Proteins identified in the NTAP-ORF4 purification which were also identified in the purification of other NTAP-MNV proteins ……. 195, 196

Appendix 4. Proteins which interacted with the ORF4 protein by TetR yeast two hybrid screen …… 197

Appendix 5. Proteins which interacted with the ORF4 protein by LexA yeast two hybrid screen …… 198

Abbreviations

AIF	apoptosis inducing factor
ADP	adenosine diphosphate
Apaf-1	apoptotic protease activating factor 1
ARF	ADP ribosylation factor
ARL	ADP-ribosylation factor-like
ATP	adenosine triphosphate
BHK-21	baby-hamster kidney cells
BIG	Brefeldin A inhibited guanine nucleotide exchange factor
BMMΦ	primary bone-derived macrophages
BSA	bovine serum albumin
BSRT7	BHK-derived cell line expressing T7 polymerase
CAD	caspase-activated DNase
cDNA	copy DNA
CMV	cytomegalovirus
COP	coatomer proteins
COS7	cell line derived from adult African green monkey
Cre	cis-acting replication element
DAPI	4',6-diamidino-2-phenylindole
ddH_2O	double distilled H2O
DISC	death induced signalling complex
DMEM	Dulbecco's MEM
DMSO	dimethyl sulphoxide
DNA	deoxyribonucleic acid
dsRNA	double-stranded RNA
DTT	dithiothreitol
ECM	extracellular matrix
EDTA	ethylenediaminetetraacetic acid
eIF	eukaryotic initiation factor
EXP	exportin
FANC	Fanconi anemia group protein
FAZF	Fanconi anemia zinc finger
FCS	foetal calf serum
FCV	feline calicivirus
FMDV	foot and mouth disease virus
GAPDH	glyceraldehyde-3-phosphate dehydrogenase
GCN1	general control of amino-acid synthesis 1-like protein
GE	gastroenteritis

GEF	guanine nucleotide exchange factor
GFP	green fluorescence protein
gRNA	genomic RNA
GST	glutathione-S-transferase
h	hours
HAV	hepatitis A virus
HAX-1	HCLS1 associated protein X-1
HCV	hepatitis C virus
HEK	human embryonic kidney
HEPES	4-(2-hydroxyethyl)-1piperazineethane sulfonic acid
HRP	horseradish peroxidase
Hsp	heat shock protein
ICAD	inhibitor of caspase activated DNase
IFN	interferon
IP	immunoprecipitation
IRES	internal ribosomal entry site
IRS	insulin receptor substrate
kb	kilobases
kDa	kilo Dalton
LB	Luria Bertani media
LC	leader capsid
LFE	Lipofectamine 2000
LPS	lippopolysaccharide
m.o.i.	multiplicity of infection
min	minutes
MNV	murine norovirus
mRNA	messenger RNA
MTS	mitochondrial targeting sequence
NE	nuclear envelope
NMR	nuclear magnetic resonance
NPC	nuclear pore complex
NS	non-structural
nt(s)	nucleotide(s)
NTPs	nucleotide (A,U,G,C) triphosphates
NUP	nucleoporin
NV	Norwalk virus
OMM	outer mitochondrial membrane
ORF	open reading frame
ORF4	open reading frame 4 found in MNV

ORF4E	(sapovirus) open reading frame 4 equivalent
p.i.	post-infection
p.o.	per oral
PABP	polyA-binding protein
PAGE	poly acrylamide gel electrophoresis
PAR	poly ADP ribose
PARP	poly (ADP-ribose) polymerase 1
PBS	phosphate buffered saline
PBST	PBS-tween 20
PBX1	pre-B-cell leukaemia transcription factor interacting protein 1
PCBPs	polyC-binding proteins
PCR	polymerase chain reaction
Peci	peroxisomal delta3, delta2-enoyl-coenzyme A isomerase
PI	isolelectric point
PP	polyproline
PRP8	pre-mRNA processing factor 8
PTB	polypyrimidine tract-binding protein
PV	poliovirus
PVDF	polyvinylidene fluoride
qPCR	quantitative real time PCR
RAG1	recombination-activating gene 1
RAG2	recombination-activating gene 2
RAW264.7	mouse leukaemia monocyte macrophage cell line
Rbmx	RNA binding motif protein, X-linked
RdRp	RNA-dependent RNA polymerase
RHDV	rabbit hemorrhagic disease virus
RIPA	radioimmunoprecipitation
RNase	ribonuclease
ROS	reactive oxygen species
RRL	rabbit reticulocyte lysate
rRNA	ribosomal RNA
RT	room temperature
RT	reverse transcription
RT-PCR	reverse transcription PCR
Rz	ribozyme
SBP	streptavidin binding peptide
SDS	sodium dodecyl sulphate
SDS-PAGE	sodium dodecyl sulphate polyacrylamide gel electrophoresis
sgRNA	subgenomic RNA

siRNAs	small interfering RNAs
SMSV	San Miguel sea lion virus
SOC	super optimal broth with catabolite repression
ssRNA	single-stranded RNA
SSSV	suppression of synonymous site variability
STAT-1	signal transducer activator of transcription 1
SV	Sapovirus
TAP	tandem affinity purification
TBE	TRIS/borate/EDTA
$TCID_{50}$/ml	50% tissue culture infective dose
THSD1	thrombospondin, type I, domain 1
Tim	transport of inner mitochondrial membrane protein
TIM	transport of inner mitochondrial membrane complex
TMEV	Theiler's murine encephalitis virus
TNF	tumour necrosis factor
TNT	in vitro transcription and translation reaction
Tom	transport of outer mitochondrial membrane protein
TOM	transport of outer mitochondrial membrane complex
T-REX	tetracycline-regulated expression
tRNA	transfer RNA
UTR	untranslated region
VP1	virus capsid protein 1
VP2	virus capsid protein 2
VPg	virus protein linked to genome
vRNA	viral RNA
WRNIP1	Werner helicase interacting protein 1
XIAP	X-linked inhibitor of apoptosis
ZBTB32	zinc finger and BTB domain containing 32
ZNF294	zinc finger protein 294

Acknowledgments

First and foremost I would like to thank my supervisor Dr Ian Goodfellow for his endless help, fantastic support and lots of encouragement during my time in his laboratory. I'd also like to thank all remaining members of the Calicivirus lab past and present for some great times. Particularly Dalan Bailey for his input into the project and lots of great advice, as well as Guia Carrara, who was also involved in the ORF4 work. Yannis, Yaz, Akos, Surender, Lil, Amir, Luis, Lucy and Chloi thanks for lots of laughs alongside all the hard work.

I've also made some great friends during my stay in London, particularly Carol, Trevor, Goran, Valentina, Christin, Rohan, Rachel, Philip, Dalan, Laila, Goeff, Kev, Matt, Walter, Gareth and Claudio for lots fun. Who could forget the Christmas roast, Croatia day and barbeques at Goran's to Birthday picnics in Regents Park, the German pub in Fulham, dog racing, karaoke, dim sum, indoor camping, riding in Hyde Park and of course those Fridays in the Fountain. Those non-science friends (German and English) have also been fantastic, Konni, Julie, Julie, Basti, Mehwish, Jon and Ann for always being there to have a laugh with or lend an ear.

Linda and Dan you have been more than true friends. Thank you for all you help, generosity, sharing so many giggles and never doubting me. Grandpap, I hope you are now in a better place along with the grandparents I sadly never knew as well as those many other friends and acquaintances, many of whom died far too young. And of course my family: Grandma, Bev, Aaron, David and most of all Mum and Dad for always being there and without whom this would not be possible. Thank you.

Declaration

All the work presented in this thesis is the result of my own work (except where indicated) and in no way forms part of any other thesis. The work was performed at the Department of Virology, Faculty of Medicine, Imperial College London. Part of the work presented in chapter 4 was carried out at the University of Texas Southwestern Medical Center, USA during two visits in July and October 2008. All work was performed under the supervision of Dr Ian Goodfellow.

Taipan
Forever young

1. Introduction

1.1 Caliciviruses

1.1.1 Disease and epidemiology

Although caliciviruses are responsible for many important diseases in animals and humans, there remains a lot to be learned about the molecular mechanisms of pathogenesis, protein synthesis and replication. Human caliciviruses from the *Norovirus* and *Sapovirus* genera are frequently associated with outbreaks of gastroenteritis or "projectile vomiting" on cruise ships, in hospitals, schools, nursing homes and military camps. Approximately 90% of all non-bacterial gastroenteritis can be attributed to human caliciviruses (Fankhauser et al., 1998). Gastroenteritis caused by Norwalk virus was first described after an outbreak in a school in Norwalk Ohio in 1968 and since then the number of reported outbreaks has increased to such an extent that noroviruses were responsible for over 85% of non-bacterial gastroenteritis cases in Europe between 1995 and 2000 (Estes et al., 2006, Lopman et al., 2003). In the US there is estimated to be more than 23 million norovirus infections annually (Estes et al., 2006). In the UK outbreaks of norovirus infections in healthcare settings were estimated to cost $184 million between 2002 and 2003 and in other areas these viruses are also a considerable economic burden (Estes et al., 2006, Lopman et al., 2004).

Comparable to other gastrointestinal pathogens human caliciviruses are transmitted via the faecal – oral route, through contaminated food or water as well as via contaminated surfaces (Gallimore et al., 2006, Patel et al., 2009). Airborne transmission has also been demonstrated (Marks et al., 2000) and the infectious dose is extremely low, with less than 10 virus particles being required to establish an infection (Donaldson et al., 2008, Teunis et al., 2008).

Although human caliciviruses are most commonly associated with acute, rapidly resolving outbreaks of gastroenteritis, it is often extremely difficult to control outbreaks and very often highly susceptible individuals such as hospital patients, children and the elderly are subjected to continuous cycles of infection and re-infection. This is partly explained by the fact that immunity to these viruses is short-lived (6-14 weeks) and caliciviruses undergo antigenic drift which contributes to the large genetic diversify seen between strains (Johnson et al., 1990, Parrino et al., 1977).

In nursing homes and hospitals, noroviruses are the most common cause of gastroenteritis and often exacerbate pre-existing conditions and lead to a patient's

deterioration (Estes et al., 2006). Humans with impaired immunity have been shown to suffer from persistent norovirus infections where virus shedding can continue for weeks or even months (Estes et al., 2006, Gallimore et al., 2004, Gallimore et al., 2006, Murata et al., 2007). Recently, a link between norovirus infections and serious conditions such as necrotizing enterocolitis in neonates (Turcios-Ruiz et al., 2008) as well as convulsions in infants (Chen et al., 2009) have been reported. Globally, it is difficult to estimate the impact of human caliciviruses on the 3.5 – 5 million annual deaths from non-bacterial gastroenteritis, as the majority of these deaths occur in the developing world, which lacks adequate healthcare, diagnostics and surveillance (Bailey & Goodfellow, 2009). Currently there is no licensed vaccine or antiviral agents against human noroviruses.

Similar to human caliciviruses, animal caliciviruses are also extremely common and widespread. Murine norovirus (MNV) is an extremely common enteric pathogen of laboratory mice and studies have revealed that up to 64.3% of mice can test seropositive to MNV infection (Muller et al., 2007). In farming, porcine noroviruses (Farkas et al., 2005) and bovine noroviruses (Scipioni et al., 2008) are extremely common enteric pathogens. Feline caliciviruses (FCV) on the other hand are not associated with gastrointestinal disease, but are responsible for frequently persistent upper respiratory tract disease, with high infection rates associated with cats housed in shelters or colonies (Radford et al., 2007).

1.1.2 Morphology

Caliciviruses are non-segmented single-stranded positive-sense RNA viruses, with the name "calici" derived from the Latin word *calyx* (meaning cup or goblet), which was used to describe the cup like depressions found on the virion surface. Calicivirus particles (figure 1.1) were first visualised by immunoelectronmicroscopy in 1972. Virus particles are icosahedral in shape with a diameter of 28-35 nm and are of similar buoyant density (1.36 ± 0.04 g/cm^3) (Duizer et al., 2004, Estes et al., 2006, Kapikian, 2000, Karst et al., 2003, Wobus et al., 2006). One of the problems in terms of controlling outbreaks of gastroenteritis

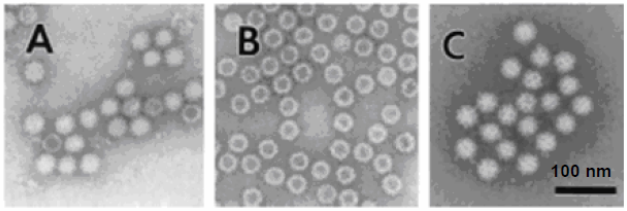


Figure 1.1. Calicivirus Electron microscopic images (Atmar and Estes, 2001). A) Norwalk virus, **B)** Baculovirus expressed Norwalk-virus particles **C)** Sapovirus.

caused by caliciviruses is the fact that caliciviruses are heat stable up to 60°C and are very resistant to many commonly used disinfectants, including high chlorine concentrations, acidity, ethanol and quaternary ammoniums (Baert et al., 2008, Dolin, 2007, Estes et al., 2006).

1.1.3 Taxonomy

In terms of taxonomy, the *Caliciviridae* consist of 4 recognised genera although there are two additional proposed genera (Farkas et al., 2008, Oliver et al., 2006). Phylogenetic analysis has revealed that there is a close genetic relationship between human caliciviruses and animal caliciviruses, and novel caliciviruses are continually being identified (Bergin et al., 2009, Vashist et al., 2009) (figure 1.2).

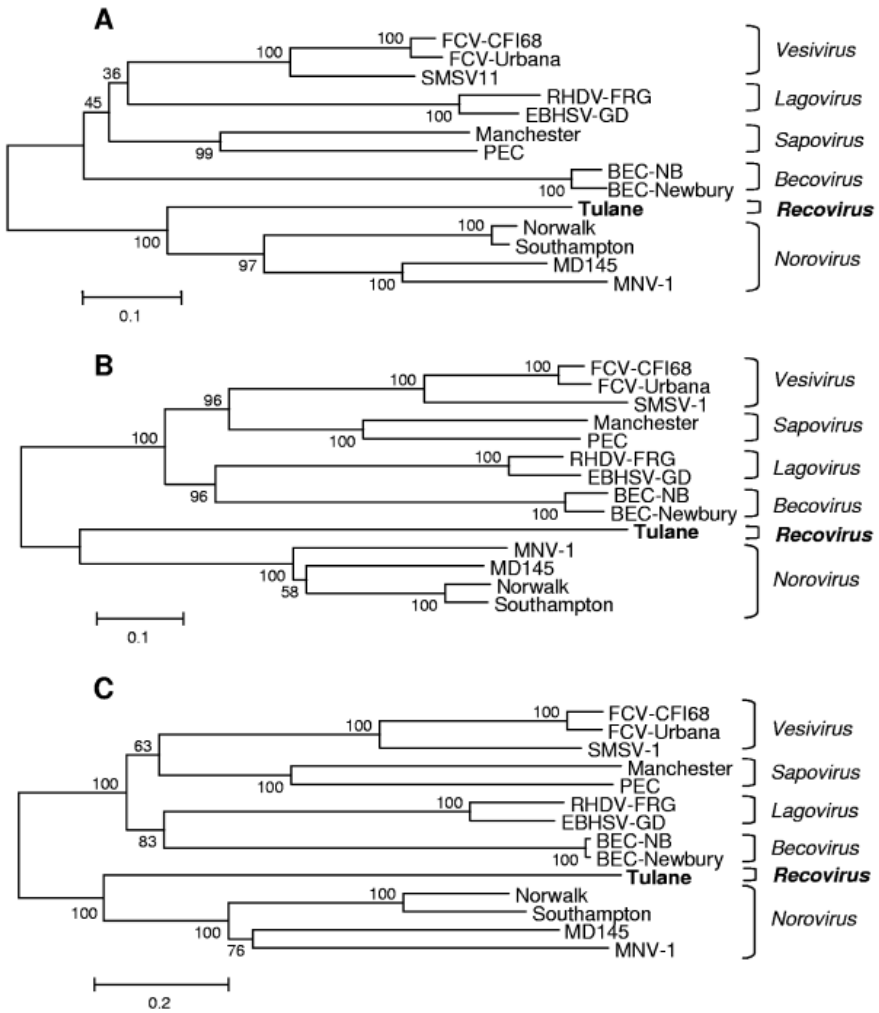


Figure 1.2. Phylogenetic relationship between caliciviruses. Unrooted tree phylogram as shown by Farkas et al., 2008. Phylogram is based on amino acid sequence alignments of the calicivirus NTPase (A), polymerase (B) and VP1 (C). The degree of divergence is reflected as units of amino acid substitutions per site which are represented by the scale bars.

Of the recognised genera, the *Sapovirus* genus includes human sapoviruses such as Manchester virus as well as porcine enteric caliciviruses (PECs). The *Lagovirus* genus includes rabbit hemorrhagic disease virus (RHDV) and European brown hare syndrome virus, both of which are associated with significant problems in the rabbit industries (Green et al., 2000, McIntosh et al., 2007). The *Vesivirus* genus includes feline calicivirus (FCV), swine vesicular exanthema virus (SVEV) and San Miguel Sea lion virus (SMSV) (Pringle, 1998). The *Norovirus* genus is comprised of several genogroups (reviewed by Bailey et al., 2009). Human noroviruses are contained within genogroups I, II and IV. Genogroup II also contains porcine strains, whereas genogroup III comprises bovine and ovine noroviruses. Canine and lion noroviruses are classified within genogroups IV (Martella et al., 2007, Martella et al., 2008) and MNV is a member of genogroup V noroviruses (Bailey & Goodfellow, 2009).

Whereas the *Norovirus* and *Vesivirus* genera contain three distinct open reading frames (ORFs) which show a small degree of overlap at the 5' and 3' junctions, there is no overlap at the ORF1/ORF2 junction in sapoviruses or lagoviruses (figure 1.3) (Clarke & Lambden, 2000). In addition, MNV contains a fourth overlapping open reading frame (ORF4) which overlaps ORF2 in a +1 frame, the characterisation of which was performed during the course of this work. Importantly, MNV is the only norovirus predicted to contain an overlapping reading frame in this position. However, a comparably located ORF4 equivalent (ORF4E) overlapping reading frame has been predicted in some members of the *Sapovirus* genus, including Manchester virus, Sapporovirus and Parkeville virus (Clarke & Lambden, 2000).

The proposed genera within the *Caliciviridae* include the *Recovirus* genus, of which Tulane virus, a virus found in rhesus macaques is a representative (Farkas et al., 2008). In addition, the *Beco/Nabovirus* genus which includes the bovine calicivirus Newbury-1 has also been proposed (Oliver et al., 2006). Although the beco/nabovirus genome organisation is typical to that seen of lago- and sapoviruses, several differences led to the proposal of a new genus. These include differences in the length of the 5' untranslated region (UTR), the fact that no overlap between ORF1 and ORF2 was observed and the higher resemblance of the minor capsid protein to that of noroviruses. The genome organisation of Tulane virus on the other hand is comparable to that seen for noro- and vesiviruses, as three ORFs are present, although ORF1 is considerably shorter (Farkas et al., 2008).

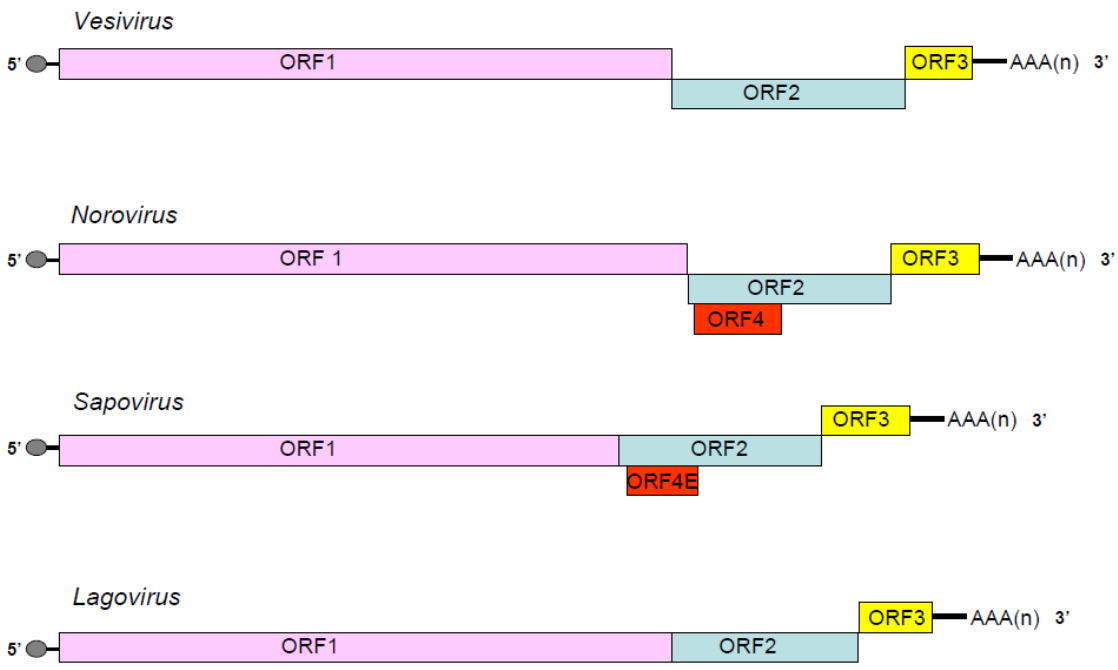


Figure 1.3. Genome organisation of four genera within the *Caliciviridae* (adapted from Atmar & Estes 2001). Whereas the first (ORF1) and second (ORF2) open reading frames show a small degree of overlap in the *Noro-* and *Vesivirus* genera, no overlap is seen in the *Sapo-* and *Lagovirus* genera. A fourth overlapping ORF (ORF4) is only thought to exist in MNV and not in other noroviruses, and only some sapovirus members possess an overlapping open reading frame at the equivalent position (ORF4E). Minor size differences between the reading frames are represented in the diagrams.

1.1.4 The study of Caliciviruses

In comparison to what is known about other positive-strand RNA viruses such as picornaviruses, relatively little is known about the molecular biology of caliciviruses. One of the reasons behind this is the fact that despite numerous efforts (Duizer et al., 2004), there is no effective tissue culture system enabling *in vitro* cultivation of human caliciviruses to date. However, a number of advances have been made in recent years. For example, Norwalk virus RNA was infectious in mammalian cells, although replication only proceeded for a single cycle (Guix et al., 2007). These findings support the long-held belief that *in vitro* calicivirus cultivation is restricted at the level of viral entry into the cells, either through receptor specificity or restrictions in viral particle uncoating (Guix et al., 2007). Evidence that polarisation of cells is required for *in vitro* calicivirus propagation is supported by findings that human noroviruses can be passaged and replicated to low titres in 3-D differentiated cells in tissue culture (Straub et al., 2007). However as this system is extremely costly, labour intensive, and difficult to establish, these findings remain to be confirmed by other independent research

groups. Consequently, the widespread use of this system in order to study human caliciviruses is extremely unlikely. Although a study with gnotobiotic pigs has demonstrated that it is possible to successfully passage a genogroup II human norovirus, the use of pigs is also extremely costly and labour intensive (Cheetham et al., 2006). Passage was also only possible in a proportion of gnotobiotic pigs in which the development of mild diarrhoea with virus shedding and seroconversion was reported (Cheetham et al., 2006). With the lack of an *in vitro* propagation system for human caliciviruses, alternative approaches to studying caliciviruses include the generation of stable cell lines expressing replicating Norwalk virus RNA (Chang et al., 2006) as well as the use of recombinant virus-like particles (Huang et al., 2005, Taube et al., 2005).

In addition, animal caliciviruses which grow in tissue culture are often used as model systems for studying human calicivirus biology. For a considerable time, FCV was the most common model system for studying caliciviruses, as FCV was the first calicivirus to grow efficiently in cell culture and have a reverse genetics system (Sosnovtsev & Green, 1995). However, a major difference between human caliciviruses and FCV is the fact that FCV is associated with frequently persistent upper respiratory tract and not gastrointestinal disease. Consequently, other caliciviruses such as PECs and particularly MNV have become the systems of choice as these viruses spread via the faecal-oral and possibly respiratory route. Recent advances have also ensured that reverse genetics systems for studying PEC or MNV mutants are now also available (Chang et al., 2005, Chaudhry et al., 2007, Ward et al., 2007). A preference for MNV has resulted due to the close genetic relatedness between MNV and human noroviruses and the fact that studying the virus in the natural host is extremely cost-effective in comparison to other caliciviruses.

1.1.5 MNV

In 2003, the first MNV strain (MNV-1) was identified in mice lacking recombination-activation gene 2 (RAG2) and signal transducer and activation of transcription 1 (STAT1) (Karst et al., 2003, Wobus et al., 2006). $STAT1^{-/-}$ mice or those lacking both type I and II IFN receptors rapidly succumb to a fatal systemic disease when inoculated with MNV-1 (Karst et al., 2003, Mumphrey et al., 2007, Wobus et al., 2006). Symptoms of this lethal infection include meningitis, encephalitis, pneumonia,

hepatitis and vasculitis of the cerebral vessels (Karst et al., 2003). In $RAG^{-/-}$ mice MNV-1 infection is not lethal but causes a persistent infection with continuous virus shedding (Karst et al., 2003, Wobus et al., 2006). These observations led to the conclusion that whilst the innate immune system is required for infection control, the adaptive immune system is needed for viral clearance (Wobus et al., 2006). Interestingly, mice lacking either type I or type II interferon receptors, protein kinase RNA activated (PKR) or inducible nitric oxide synthase were no more susceptible to systemic disease than wild-type 129 mice (Karst et al., 2003). The fact that mice lacking either type I or type II interferon receptors did not succumb to fatal disease whereas those lacking both did, demonstrates the importance of IFN in clearing MNV-1 infection and is an example of how type I and type II interferon receptors can substitute each other if necessary (Karst et al., 2003). In inbred mice MNV-1 causes a subclinical infection and disease is perturbed by a functioning STAT-1 pathway, which is critical for the interferon (IFN) response (Mumphrey et al., 2007). Although the infection is subclinical, the virus replicates in the intestine and spleen and is associated with histopathological changes (Mumphrey et al., 2007).

Later it was discovered that similar to human noroviruses, MNV is a widespread pathogen and there are a number of other murine norovirus strains (Hsu et al., 2007, Wobus et al., 2006). Surprisingly, studies in a research facility have shown that up to 67.5% of research mouse colonies contain MNV reactive antibodies, which could potentially have an impact on research experiments (Muller et al., 2007). Recent studies using a number of viruses including influenza-, vaccinia-, cytomegalo- as well as retroviruses have shown that MNV infection does not significantly affect the immune response or the viral titres of these secondary agents (Ammann et al., 2009, Doom et al., 2009, Hensley et al., 2009). However, an alternative study has demonstrated that disease progression in the mouse model of inflammatory bowel disease is affected by MNV infection (Lencioni et al., 2008), which suggests that the study of intestinal pathogens could be affected in research facilities in which MNV is inherent. Although very similar at the genomic level, the phenotype seen upon infection with MNV strains other than MNV-1 differs significantly to MNV-1 (Hsu et al., 2007). Rather than establishing a subclinical infection similar to that caused by MNV-1, all other murine norovirus strains are associated with persistent infections and prolonged faecal shedding in inbred mice (Hsu et al., 2007).

In vitro, MNV replicates well in haematopoietic cells, particularly in macrophages and dendritic cells (Wobus et al., 2004, Wobus et al., 2006). MNV is commonly propagated in RAW264.7 cells, an immortalised mouse macrophage cell line which was established from a lymphocytic lymphoma induced by Abelson murine leukaemia virus (Raschke et al., 1978). The first isolated strain of MNV-1 (CW1) (Karst et al., 2003, Wobus et al., 2004) was used to establish two reverse genetics systems. The system presented by Ward *et al* is based on a polymerase II driven system to recover MNV and a number of variations of this approach have been described (Ward et al., 2007). An alternative system described by Chaudhry *et al*, employs Fowlpox virus (FPV) expressing T7 RNA polymerase in order to drive the expression of MNV cDNA clones under the control of a T7 promoter (Chaudhry et al., 2007). As this latter system is associated with higher virus yields, it is currently the preferential approach to studying MNV.

As with all model systems however, some aspects of the study of MNV may not apply to human noroviruses, and it is important to remember that differences do exist. For one, mice can not vomit due to the lack of an emetic reflex, and they also do not routinely develop diarrhoea after MNV infection. Secondly, prolonged faecal shedding and viral persistence is commonly associated with MNV infection, even in immunocompetent mice. In humans however, persistent norovirus infections are usually associated with an immunocompromised status (Estes et al., 2006, Gallimore et al., 2004, Gallimore et al., 2006, Murata et al., 2007). However, in spite of these differences, on a molecular biology basis MNV has and can continue to contribute to knowledge of the calicivirus life cycle and the functions of proteins produced during infection.

1.1.6 Calicivirus life cycle and proteins

1.1.6.1 Attachment and entry

In humans, susceptibility to norovirus infections is determined by a person's histo-blood group antigens (HBGA) and secretor status, thus explaining why people with an O blood group phenotype are more susceptible to infection and suffer frequent bouts of disease in comparison to others (Dolin, 2007, Estes et al., 2006). HBGA are carbohydrates present on gut epithelial cells and are the most probable norovirus receptors, although co-receptors may also be involved (Dolin, 2007, Estes et al., 2006,

Hutson et al., 2002). *In vitro*, noroviruses have indeed been shown to bind to a number of histo-blood group antigens (Nilsson et al., 2009, Rydell et al., 2009) as well as heparin sulphate (Tamura et al., 2004). For FCV, the transmembrane, immunoglobulin-like superfamily member junctional adhesion molecule 1 (JAM-1) and α-2,6-sialic acid can act as functional receptors (Makino et al., 2006, Stuart & Brown, 2007). Using murine macrophages it has recently been demonstrated that terminal sialic acid moieties present on gangliosides can also act as receptors for MNV (Taube et al., 2009). Following JAM-1 binding of FCV, conformational changes in the capsid structure take place (Bhella et al., 2008) and similar to many other non-enveloped viruses such as picornaviruses, adenoviruses, and coxsackievirus B3, FCV enters cells by clathrin-mediated endocytosis (Stuart & Brown, 2006). Whereas acidification of the endosome enables FCV uncoating which allows the viral genome to enter the cytoplasm (Stuart & Brown, 2006), recent studies using MNV have shown that viral entry into permissive cells is pH independent (Perry et al., 2009).

1.1.6.2 Translation of viral proteins

Upon entering the cell, the 7-8 kb positive-sense polyadenylated viral genome can immediately act as mRNA for protein synthesis (Carter et al., 1992, Sosnovtsev et al., 2006). However, unlike the host mRNAs, the genome does not possess the classic 5' cap structure which is essential for translation (figure 1.4). Instead, caliciviruses employ a unique mechanism of translation in order to ensure the preferential translation of the viral RNA over that of the host. Caliciviruses possess a 13-15 kDa VPg protein (viral protein genome linked) which acts as a cap substitute and recruits translation initiation factors (Chaudhry et al., 2006, Daughenbaugh et al., 2003, Goodfellow et al., 2005).

The involvement of host cell proteins such as polypyrimidine tract binding protein (PTB), La and poly-C binding protein (PCBP) in FCV translation has also been demonstrated (Karakasiliotis et al., 2006) (and unpublished observations from my colleagues). Although the closely related picornaviruses also have a VPg protein covalently linked to the 5' end, there is no sequence homology and the calicivirus VPg is approximately 10 kDa larger. Instead of VPg-dependent translation, picornaviruses utilise the 650-1300 nucleotides located in the 5' UTR which forms an internal ribosomal entry site (IRES). With the extremely short 5' UTR found in caliciviruses (5 nucleotides in MNV, 19 nucleotides in FCV), it is clear that IRES-dependent

translation does not occur, and in contrast to picornaviruses, the larger VPg is required for translation (Sosnovtsev et al., 2006).

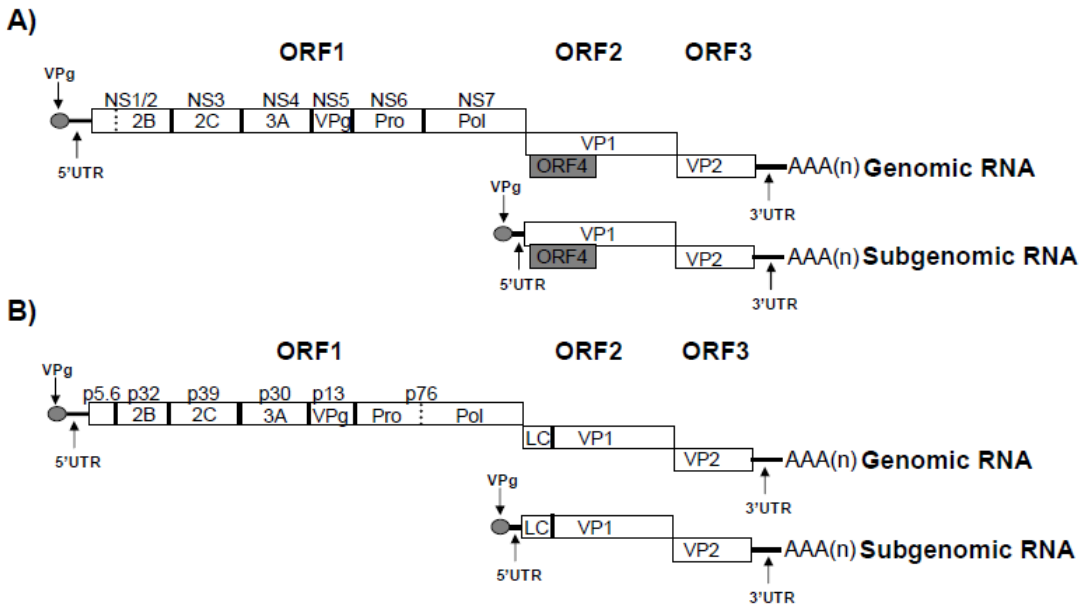


Figure 1.4. Diagrammatic representations of the MNV (A) and FCV (B) genomes. The calicivirus genomic and subgenomic RNAs have a protein (VPg) covalently linked to the 5' end and have a 3' poly adenylated tail. A short 5' and 3' untranslated region (UTR) is also found on either end of the protein-coding sequence. Caliciviruses encode three characterised ORFs with ORF1 being proteolytically processed into 6 non-structural proteins, whereas ORF2 encodes the major capsid protein VP1 and ORF3 the minor capsid protein VP2. In MNV, a fourth open reading frame (ORF4) has been identified. Differences exist in the nomenclature between MNV **(A)** and FCV **(B)** proteins, although the relative genome positions are equivalent. In MNV non-structural (NS) proteins are labelled NS1-7, with NS1/2 not being proteolytically cleaved despite the presence of a protease cleavage site (dashed line) (Sosnovtsev et al., 2006). In FCV, non-structural proteins are labelled according to size, with the largest protein (p76) being the protease polymerase fusion (Sosnovtsev et al., 2002). Some proteins are also named after picornavirus homologues (2B, 2C, 3A), pro = protease, pol = polymerase, LC = leader capsid.

The precise role of the polyA tail in the calicivirus life cycle remains to be elucidated, as *in vitro* studies with RHDV have shown that the 3' poly-A tail can in fact be deleted without having much impact on virus replication (Liu et al., 2008b). However, studies using MNV have shown that the correct nucleotide sequence immediately upstream of the 3' poly-A tail is essential for virus recovery *in vitro* (Chaudhry et al., 2007) and that conserved RNA secondary structures present in the 3' end of the viral genome play a role in viral virulence (Bailey et al., 2010b).

Until recently, with the exception of Manchester virus, the calicivirus genome was thought to encode three ORFs (Carter et al., 1992, Karst et al., 2003, Liu et al., 1995, Sosnovtsev et al., 2006). Translation of the first open reading frame yields a large polyprotein containing the non-structural proteins (figure 1.4). *In vitro* as well as in

infected cells, this product is cleaved by the virus encoded 3C-like protease (Pro) to release the six mature non-structural proteins (Sosnovtsev et al., 2006, Wobus et al., 2006). Comparable to picornaviruses, uncleaved precursor proteins such as that of the protease and polymerase and the first and second non-structural proteins can also be detected (Sosnovtsev et al., 2006, Wobus et al., 2004). Although the polyprotein layout is comparable for both FCV and MNV, differences do exist. In FCV infected cells, the viral capsid is produced as an immature protein which requires proteolytic removal of the leader capsid sequence (LC). For FCV, the viral protease and polymerase are merged (p76), whereas in MNV infected cells these proteins must be separated into the protease (NS6) and polymerase (NS7) in order to be functional (Sosnovtsev et al., 2006, Sosnovtsev et al., 2002, Ward et al., 2007). In MNV infected cells the first two non-structural proteins (NS1/2) are found as a fusion, unlike the FCV equivalent proteins p32 and p39 (Sosnovtsev et al., 2006, Sosnovtsev et al., 2002). Additional to the protease cleavage sites, the MNV polyprotein also contains three caspase 3 cleavage sequences in NS1/2 (Sosnovtsev et al., 2006, Thackray et al., 2007). Caspases (cysteine aspartic acid proteases) are cellular proteases which are activated following stimulation of apoptosis (Chowdhury et al., 2008). Although MNV infection of RAW264.7 cells is associated with apoptosis induction and subsequent caspase 3 activation (Bok et al., 2009, Furman et al., 2009), two of the known cleavage sites are not conserved among MNV stains, whilst a highly conserved predicted third cleavage site was not experimentally cleaved (Sosnovtsev et al., 2006, Thackray et al., 2007).

The first non-structural protein in MNV is NS1/2, which is predicted to have a similar function to the picornavirus 2B protein. In picornaviruses, 2B is thought to insert into the membrane via hydrophobic membrane spanning domains where it is involved in membrane rearrangements, including vesicle formation and alteration of membrane permeability (Agirre et al., 2002, Madan et al., 2007). In FCV infected cells, p32 associates with membranous replication complexes (Green et al., 2002), and like all MNV non-structural proteins NS1/2 has also been associated with replication complexes (Hyde et al., 2009). However, cytoplasmic labelling of MNV infected cells with NS1/2 also suggest a role outside the replication complex (Hyde et al., 2009). Evidence from the Norwalk virus analogue p48 suggest that the protein localises to the Golgi apparatus and disrupts vesicle transport (Ettayebi & Hardy, 2003). Consistent

with these data, p48 was shown to interact with the vesicle-associated membrane protein-associated protein A (VAP-A) (Ettayebi & Hardy, 2003).

Because of a predicted nucleotide triphosphate (NTP) binding domain, MNV NS3 and related calicivirus equivalents are thought to be similar to the 2C NTPase of picornaviruses. NTPase activity has been demonstrated *in vitro* for RHDV and the norovirus Southampton virus (Marin et al., 2000, Pfister & Wimmer, 2001). Although the protein shares sequence motifs similar to superfamily 3 helicases, *in vitro* assays have not been able to show helicase activity, which stands in contrast to what has been demonstrated for the HCV NS3 protein (Pfister & Wimmer, 2001). An association with the viral replication complex has been shown for FCV (Sosnovtsev et al., 2002) as well as MNV (Hyde et al., 2009). MNV NS3 also demonstrated distinct foci of cytoplasmic localisation, indicating that the protein may not just be involved in viral replication. Little is known about the fourth non-structural protein of the calicivirus ORF1 (NS4 in MNV and p30 in FCV). However, mutations in MNV NS4 are thought to play a role in tissue culture adaptation of MNV (Bailey et al., 2008). The predicted amphipathic helix is thought to have membrane association properties and like the picornavirus 3A protein, NS4 is thought to recruit VPg to membrane vesicles in the replication complex (Green et al., 2002, Hyde et al., 2009, Sosnovtsev et al., 2002).

MNV NS5 (and related calicivirus equivalents) is more commonly known as VPg, which is covalently linked to the viral genomic and subgenomic RNA (Herbert et al., 1997). VPg is essential for virus infectivity, as treatment with proteinase K results in the viral RNA being non-infectious (Burroughs & Brown, 1978, Schaffer et al., 1980). Similarly, *in vitro* translation of FCV RNA was inhibited following removal of VPg (Herbert et al., 1997), whereas *in vitro* transcribed capped FCV RNAs derived from cDNA clones were infectious when transfected into cells (Sosnovtsev & Green, 1995). In MNV, VPg removal also renders the virus non-infections and *in vitro* translation does not occur (Chaudhry et al., 2006). *In vitro*, MNV, FCV and Lordsdale virus have all been shown to bind the cap-binding eIF4F component eIF4E, and GST- pulldowns using Norwalk virus VPg have demonstrated other eIF4F components such as the eIF4A helicase and the scaffold protein eIF4G also associate with the translation complex (Chaudhry et al., 2006, Daughenbaugh et al., 2006, Goodfellow et al., 2005). However, differences exist between FCV and MNV in the requirement for eIF4E, with *in vitro* depletion of eIF4E severely affecting VPg-dependent FCV, but not MNV translation (Chaudhry et al., 2006). Differences were also observed in the requirement

for eIF4A *in vitro* as well as in tissue culture, with an increased requirement of MNV for eIF4A (Chaudhry et al., 2006). As eIF4A has RNA helicase activity, the increased requirement seen for MNV may well be due to the higher levels of RNA secondary structure present in the genome of MNV (Simmonds et al., 2008). Other studies have demonstrated a direct interaction between recombinant Norwalk virus VPg and the eIF3d component of the eIF3 translation initiation complex, and the whole eIF3 complex could be isolated from cells expressing Norwalk virus GST-tagged VPg (Daughenbaugh et al., 2003). Calicivirus VPg has also been shown to interact with the viral polymerase and capsid protein (Kaiser et al., 2006), demonstrating that VPg is likely to play many roles in the virus life cycle.

The viral 3C-like protease (NS6 in MNV) is released from the polyprotein through autocatalytic cleavage and subsequently cleaves the ORF1 polyprotein with high specificity (Sosnovtsev et al., 2002). In FCV, the protease is fused to the polymerase as a single functional entity (p76), which is the only form found during infection (Wei et al., 2001a). All calicivirus proteases belong to the chymotrypsin-like serine protease superfamily and cleave the non-structural polyprotein precursor molecule (Sosnovtsev et al., 2006). It has been demonstrated that the calicivirus protease cleaves host cell poly(A) binding protein (PABP) (Kuyumcu-Martinez et al., 2004) as well as the eukaryotic initiation factor eIF4G (Willcocks et al., 2004), both essential components of host cell mRNA translation. The purpose of this cleavage is thought to be the shutoff of host translation, and it is likely that the viral protease also cleaves other host factors.

1.1.6.3 Genome replication and translation of the structural proteins

The C-terminal non-structural protein encodes the viral RNA-dependent RNA polymerase (NS7 in MNV), which comparable to other RNA dependent RNA polymerases lacks proofreading activity, therefore supporting the ability of caliciviruses to undergo antigenic drift (Estes et al., 2006, Sosnovtsev et al., 2006, Wobus et al., 2006). The viral polymerase replicates the viral genome via a negative-sense intermediate, and northern blot analysis has revealed that negative-sense genomic as well as subgenomic RNA can be detected during infection (Green et al., 2002). The RHDV polymerase has been shown to transfer nucleotides to VPg (Machin et al., 2001), thus explaining the covalent linkage between the VPg protein and viral RNA.

In MNV, cleavage of the protease-polymerase precursor molecule into separate subunits is essential for virus replication (Ward et al., 2007). The preservation of conserved RNA secondary structures within the MNV genome is also required for viral replication (Simmonds et al., 2008). During replication, intracellular membrane rearrangement as well as the loss of an intact Golgi apparatus can be observed (Hyde et al., 2009, Wobus et al., 2006).

Both norovirus and sapovirus RNA-dependent RNA polymerases can act in a primer independent manner and can initiate *de novo* RNA synthesis (Fukushi et al., 2004, Fullerton et al., 2007). Currently, there are two proposed mechanisms (figure 1.5) for the production of an approximately 2.4 kb VPg-linked polyadenylated subgenomic RNA which is expressed during calicivirus replication (Herbert et al., 1997, Meyers et al., 1991, Neill, 2002). The first is that during negative-sense RNA synthesis, premature termination of the polymerase activity produces a negative-sense subgenomic RNA, which then acts as a template for positive-sense subgenomic RNA synthesis. A second and more widely held belief is that synthesis of the subgenomic RNA is primed from a subgenomic promoter present upstream of ORF2 on the full-length negative-strand. In support of the latter theory are the requirement for conserved RNA secondary structures upstream of ORF2 for efficient replication, as well as the fact that some RNA secondary structures were predicted to be more stable in the negative-sense template than the positive (Simmonds et al., 2008).

As the vast proportion of produced capsid proteins are translated from the subgenomic RNA, the production of a subgenomic message may act to delay the production of structural proteins until viral replication has taken place (Wobus et al., 2006). On the subgenomic RNA, ORF2 encodes the 58.9 kDa major capsid protein (VP1) and ORF3 encodes the 22.1 kDa minor capsid protein (VP2) (Clarke & Lambden, 1997, Clarke & Lambden, 2000, Wobus et al., 2006). Studies with RHDV have shown that VP2 is not essential for virus infectivity (Liu et al., 2008a). Interestingly, for FCV, RHDV and MNV it has been shown that translation of the minor capsid protein VP2 occurs though a novel translation mechanism, dependent on a motif termed TURBs (termination upstream ribosome binding site motif), which is located immediately upstream of the VP1 stop codon (Meyers, 2003). The TURBs actually contains two important sequences, with the 5' sequence though to be important in binding the ribosome (it contains 18S rRNA complementary sequence), whilst the other sequence is though to be important in positioning the ribosome to enable translation of VP2 at the correct site

(Meyers, 2003, Meyers, 2007, Napthine et al., 2009). Another proposed model is that eIF3 binds to the TURBs motif preventing disassembly of the ribosome following VP1 termination, which is supported by the fact that purified eIF3 stimulates translational re-initiation (Poyry et al., 2007).

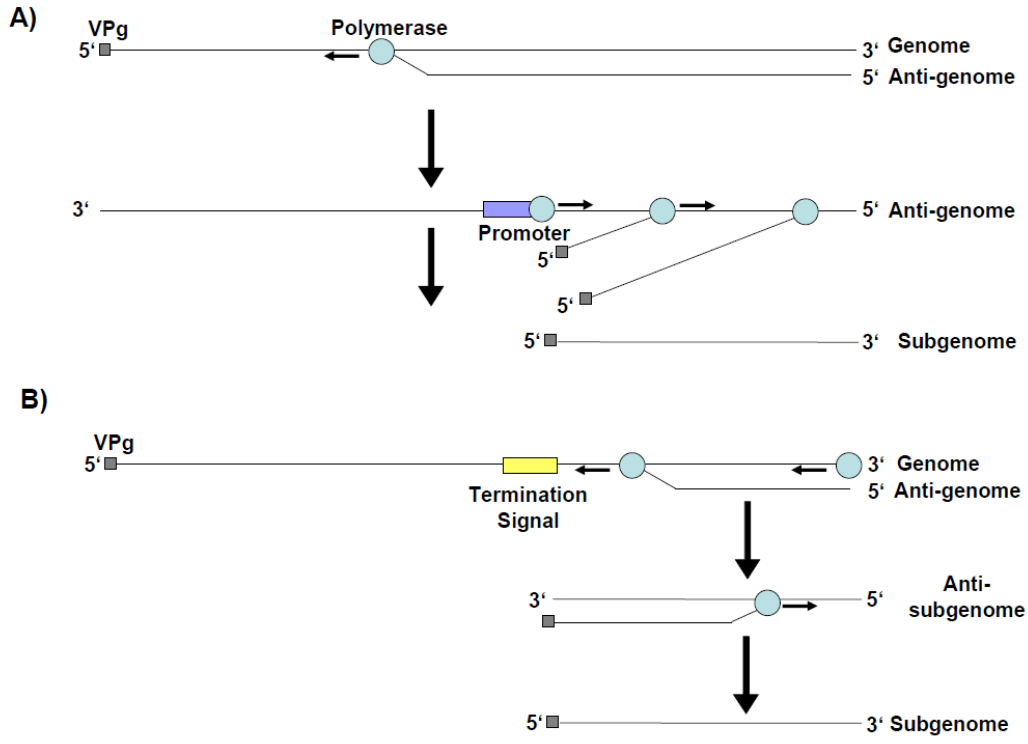


Figure 1.5. Proposed models for the synthesis of MNV subgenomic RNAs. Either the viral polymerase binds to a promoter present in the full-length negative-sense anti-genome strand of MNV, thus resulting in the MNV subgenomic RNA (A), or premature termination of anti-genome synthesis results in a negative-sense subgenomic RNA which is then copied into the positive-sense subgenomic RNA (B). Adapted from a review (Putics et al., in press).

VP1 contains two domains with P1 and P2 forming the protruding domain and the S domain forming the capsid icosahedron (Muller et al., 2007). The P2 domain has been implicated in the virus-cell interaction and probably represents the main immune recognition domain as it exhibits a high degree of genetic sequence diversity (Muller et al., 2007). VP2 is predicted to stabilise VP1 in the capsid structure (Muller et al., 2007). Expression of VP1, with or without the co-expression of VP2 leads to self-assembled virus-like particles (VLPs) (Green et al., 1997, Jiang et al., 1992, Taube et al., 2005). VLPs have been used to study a variety of virus-host interactions as they are morphologically and antigenically indistinguishable from real virus particles (Estes et al., 2006). Recent cryo-electon microscopic images of MNV have shown that MNV differs to previously characterised caliciviruses as the protruding domain is lifted off

the shell domain and is rotated such that new interactions are formed at the P1 base to generate a cage-like structure which engulfs the shell domains (Katpally et al., 2008). This structure has been suggested to be a form of capsid maturation which may occur in some caliciviruses (Katpally et al., 2008).

Once protein synthesis and genome replication has occurred, the viral RNA is packaged into viral particles. Evidence suggests that the subgenomic RNA is encapsidated in RHDV as well as in FCV (Meyers et al., 1991, Neill, 2002). Unfortunately, little is known about the mechanisms of viral release, but as many calicivirus infections induce apoptosis, it can be speculated that apoptosis-induced membrane collapse serves the release of virus particles (Al-Molawi et al., 2003, Alonso et al., 1998, Bok et al., 2009, Furman et al., 2009, Sosnovtsev et al., 2003).

The aim of this project was to characterise a previously unidentified fourth open reading frame (ORF4) in the MNV genome. Bioinformatic evidence strongly suggests the existence of this fourth ORF in the MNV genome, which overlaps with the capsid encoding region at the start of the subgenomic RNA in a +1 frame (figure 1.4). Analysis of the degree of suppression of synonymous site variability (SSSV) within the MNV genome was examined and published in 2008 by Simmonds et al. Using the programme Sequence Scan in the Simmonic sequence editor (Simmonds et al., 2008), the codon variability was examined for all the available MNV genomes. This approach analyses the frequency with which each codon for a particular amino acid is used at a particular position in the genome and compares it to how often that codon could be employed due to the degeneracy of the genetic code. As can be seen (figure 1.6a), a high degree of SSSV exists within the first 650 nucleotides of the MNV subgenomic RNA. For example, within ORF4 leucine is encoded by the triplet UUG at a far higher frequency (15 out of 33 codons = 45%) than leucine is encoded for in ORF1 (17 of 128 = 13%) or indeed any of the other single coding ORFs, which encode leucine at a comparable rate to ORF1 (data not shown). Even though SSSV can be indicative of evolutionarily conserved RNA secondary structure(s) within coding sequences, such as in the *cis*-replicating element in the 2C coding region of human enteroviruses (Goodfellow et al., 2000), in this case the area of SSSV in MNV overlaps precisely with the region predicted to encode ORF4 (figure 1.6a). As the ORF4 coding region represents the start to the subgenomic RNA, RNA secondary structures important for virus translation and/or replication are likely to be present in this region. However, SSSV over such a significant stretch of the genome is not seen in the related norovirus

GII family (figure 1.6a), or in fact any of the other related caliciviruses (vesiviruses, lagoviruses or sapoviruses) (Simmonds et al., 2008). These findings correlate with previous observations (Muller et al., 2007, Thackray et al., 2007), where low genetic diversity beginning at the ORF1-ORF2 junction but extending well into the ORF4 region was observed for a number of different MNV strains.

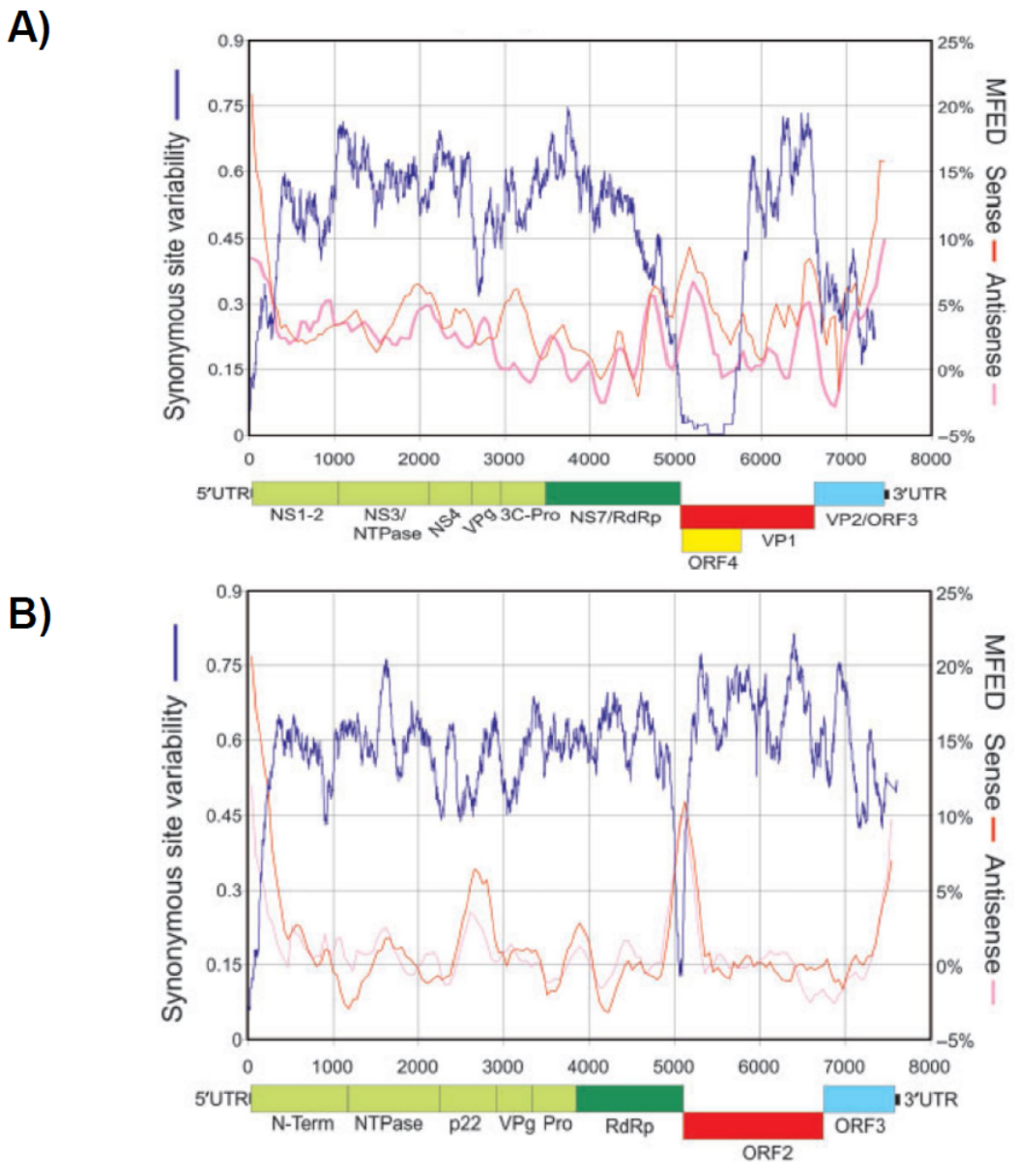


Figure 1.6. Bioinformatic analysis of ORF4. A) Suppression of synonymous site variation (SSSV) within all the currently sequenced MNV strains reveals a high SSSV within the ORF4 region which cannot be seen in the related sequenced Norovirus GII strains **(B).** Similarly, higher MFED values are also seen in the ORF4 region for MNV. Diagram as depicted by Simmonds et al., 2008.

Similarly, higher mean fold energy difference (MFED) values are required for maintaining conserved RNA secondary structures (Simmonds et al., 2008). MFED

values are essentially comparative thermodynamic values between the free energies generated when folding sequence specific RNA fragments to the free energies generated when the sequence of those fragments is randomised. Importantly, within these randomised sequences, the amino acid sequence order of the protein is maintained. For caliciviruses higher MFED values are also seen upstream of the ORF1/2 junction and this region potentially contains a small RNA structure involved in subgenomic RNA synthesis. For MNV, the higher MFED values at the beginning of the subgenomic RNA extend further into ORF2 (and therefore into ORF4) than for the other related viruses, although the extension does not cover the entire ORF4 coding region (figure 1.6a).

Interestingly, although the related human SV are also predicted to encode an overlapping open reading frame within the VP1 coding region (Liu et al., 1995), the analysis by Simmonds et al., did not reveal a high degree of SSSV for sapoviruses as seen for MNV (Simmonds et al., 2008). One reason for this could be that unlike MNV, the SV ORF4E is not present in all SV strains. Furthermore, the lack of available genome sequences for SV also restricted this analysis because all individual genogroups were pooled, thus providing difficulties in identifying and demonstrating the position of an overlapping reading frame using this approach. Closer bioinformatic analysis of the lagovirus RDHV during the course of this work also revealed a potential 120 amino acid overlapping reading frame initiated from a GTG with a G being present in positions +4. Similarly, ATG initiation could give rise to an 82 amino acid protein for SMSV, although this ATG is not surrounded by an optimal Kozak context. However, further approaches would be required to characterise the true nature of these potential reading frames which are significantly shorter than the 214 amino acid protein encoded by MNV. The lack of available sequences for SMSV virus make such a bioinformatic approach difficult, and the lack of significant SSSV within lagoviruses (Simmonds et al., 2008), suggest that comparable to sapoviruses, differences in the presence of this uncharacterised reading frame may be strain specific.

After this project had commenced a number of publications have referred to the existence of ORF4 (Chachu et al., 2008a, Hyde et al., 2009, McCartney et al., 2008, Thackray et al., 2007), although in all cases the ORF4 is referred to as uncharacterised and the question as to whether a functional protein product is actually encoded is frequently posed (Chachu et al., 2008a, Hyde et al., 2009, McCartney et al., 2008).

The MNV ORF4 protein shares no homology with any previously characterised proteins, yet it is highly conserved between MNV isolates. During the course of this project evidence has been generated to suggest that MNV ORF4 encodes an accessory virulence factor which is involved in the process of programmed cell death (apoptosis). Although there is no homology between the MNV ORF4 protein and other characterised viral overlapping ORF proteins, many of these overlapping ORF proteins also act as accessory virulence factors. The following sections will therefore describe some examples of overlapping ORFs in both positive- as well as negative-strand RNA viruses.

1.2 Overlapping reading frames

Overlapping ORFs exist in many viral genomes regardless of the nucleic acid type or genome polarity. Optimal usage of limited genome capacity which must be restricted due to the nature of the error prone polymerase is certainly an advantage of overlapping reading frames. The requirement for conservation of two reading frames can also constrain genetic diversity resulting from the high error prone polymerase activity of RNA viruses (Belshaw et al., 2007). The use of overlapping frames can also be seen as a means to regulate the production of protein as ribosomes effectively compete for reading frames. Although often not essential for survival in tissue culture, the products of these overlapping frames are frequently virulence factors and as will be shown, this is also thought to be the case for the MNV ORF4 protein. As MNV is a positive-sense RNA virus, the first three examples of characterised overlapping reading frames will be from positive-stranded RNA viruses, after which there will also be two examples from negative-strand RNA viruses, where the similarities between the overlapping reading frame proteins and MNV ORF4 protein will later become apparent. However, it is important to remember that although these examples were chosen, there are many other examples of overlapping reading frames in RNA viruses, DNA viruses and even in pro- and eukaryotes, with further examples being named at the end of this section.

1.2.1 Positive-strand RNA viruses

1.2.1.1 Hepatitis E virus (HEV)

Hepatitis E virus (HEV) is a positive-sense single-stranded RNA virus, which is currently classified in the sole genus of *Hepevirus* (Huang et al., 2007, Panda et al., 2007). HEV is responsible for acute viral hepatitis and endemic HEV is particularly a problem in developing countries as HEV is an enteric zoonotic pathogen, which can spread via contact with infected animals or the consumption of contaminated meat (Panda et al., 2007). Amongst others, animals shown to faecally excrete HEV or show HEV specific antibodies include pigs, deer, cattle, donkeys, mules, rodents and mongoose (Panda et al., 2007).

The 7.2 kb HEV genome is polyadenylated and contains a 5' cap structure (Panda et al., 2007, Zhang et al., 2001). Due to similarities in genome organisation and the fact that HEV is an enteric pathogen, HEV was originally classified as a member of the *Caliciviridae*, with the non-structural genes encoded in the first ORF at the 5' end of the genome and the structural genes encoded in the second ORF at the 3' end (figure 1.7) (Tam et al., 1991). However, HEV also contains an overlapping reading frame (ORF3) beginning in the ORF1- ORF2 junction, which is expressed from a bicistronic subgenomic RNA (Graff et al., 2006). Until recently it was thought that HEV ORF3 overlaps with ORF1 at the 5' end by one nucleotide and then significantly overlaps with ORF2 (figure 1.7) (Huang et al., 2007, Surjit et al., 2004). However, current evidence suggests that instead of initiating at this predicted position and encoding a 123 amino acid protein, ORF3 initiates at a downstream AUG to produce a 114 amino acid protein (Huang et al., 2007).

The ORF3 protein, which is essential for viral infectivity *in vivo* (Huang et al., 2007) but not *in vitro* (Emerson et al., 2006), has structural as well as non-structural functions. In terms of acting as a structural protein, the ORF3 protein forms homodimers (Tyagi et al., 2001) and associates with viral particles (Tyagi et al., 2002). Sequence alignments between the HEV ORF3 protein and the MNV minor capsid protein VP2 which is produced from MNV ORF3 have shown a significant degree of sequence homology between the two proteins (Bailey, unpublished observations). ORF3 is phosphorylated at a single serine residue via the mitogen-activated protein kinase signalling pathway and associates with the cytoskeleton (Zafrullah et al., 1997). By associating with the cytoskeletal network (in particular microtubules), the ORF3

protein has been proposed to act as a cytoskeletal anchor which recruits ORF2 for particle assembly (Kannan et al., 2009, Panda et al., 2007).

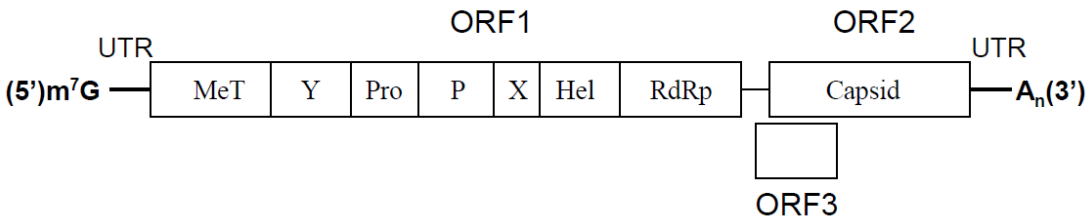


Figure 1.7. HEV genome organisation. The viral genome is flanked at both the 5' and 3' ends by a short untranslated region (UTR). Genomes are capped and possess a polyA tail. Translation occurs from 3 ORFs. ORF1 encodes the non-structural proteins which include the methyltransferase (MeT), the uncharacterised Y domain (Y), protease (Pro), proline-hinge region (P), protease associated X domain (X), helicase (Hel) and RNA-dependent RNA polymerase (RdRp) (Panda et al., 2007). The capsid protein is encoded by ORF2 and structural as well as non-structural properties have been attributed to the ORF3 overlapping reading frame protein.

In addition to having structural functions, the ORF3 protein has been shown to interact with src-homology 3 (SH3) domain containing proteins via carboxy located conserved polyproline motifs (sequence PxxP) (Korkaya et al., 2001, Panda et al., 2007). SH3 domains are common to numerous proteins and are involved in intracellular signalling and cytoskeletal organisation (Korkaya et al., 2001, Lee et al., 1995, Macdonald et al., 2005). Dimerised phosphorylated ORF3 binds to numerous SH3 domain containing proteins including the signal transduction pathway proteins Src, Hck, Fyn, the p58α regulatory subunit of phosphatidylinositol 3-kinase, phospholipase Cγ and the adaptor protein Grb2 (Korkaya et al., 2001, Surjit et al., 2004). It is thought that interaction with these SH3 domain containing proteins serves to perturb host antiviral signalling cascades as has been demonstrated for a number of viral proteins including NS5A of HCV (Macdonald et al., 2005) and the Nef protein of human immunodeficiency virus (HIV) (Macdonald et al., 2005, Saksela et al., 1995). The ORF3 protein also localises to early and recycling endosome where the protein interferes with epidermal growth factor (EGFR) signalling (Chandra et al., 2008). As EGFR endocytosis is required for the nuclear translocation of signal transducer and activator of transcription (STAT3) in response to cellular stress, interference from the ORF3 protein is thought to promote cell survival and down-regulate the inflammatory response (Chandra et al., 2008).

1.2.1.2 Hepatitis C virus (HCV)

Hepatitis C virus (HCV), a member of the *Hepacivirus* genus within the *Flaviviridae* family also contains a conserved overlapping reading frame in a 9.5 kb positive-sense RNA genome (Vassilaki & Mavromara, 2003, Walewski et al., 2001). Although asymptomatic infection with HCV is frequent, once HCV infection is established it causes liver hepatitis, with persistent infections leading to liver cirrhosis and hepatocellular carcinoma. HCV infection is currently a major global health problem in developed as well as developing countries and extensive treatment consisting of pegylated interferon alpha and ribavirin is often not successful.

Until 2001 reviews were reporting that HCV contains a single ORF (Moradpour et al., 2001). The translation of this ORF is IRES mediated and yields a large polyprotein which is processed into structural and non-structural proteins by viral and cellular proteases (figure 1.8) (Dubuisson, 2007, Qureshi, 2007, Suzuki et al., 2007a, Suzuki et al., 2007b). However, early bioinformatic evidence suggested that in addition to the core protein, the N-terminus of HCV also encodes another protein in a +1 ORF relative to the core-encoding region (figure 1.8) (Ina et al., 1994, Smith & Simmonds, 1997).

The protein encoded by this overlapping reading frame is known as the frameshift (F) protein, alternative reading frame protein (ARFP) or core+1 protein (Vassilaki & Mavromara, 2009). A number of *in vitro* studies such as the rabbit reticulocyte lysate system and tissue culture expression have demonstrated that the F protein is expressed from this ORF (Baril & Brakier-Gingras, 2005, Varaklioti et al., 2002, Vassilaki & Mavromara, 2003, Xu et al., 2001). Although to date the F protein has not been detected during *in vivo* infection, a T-cell specific immune response (Bain et al., 2004) and antibodies to the F protein have been detected in the sera of HCV infected patients (Cohen et al., 2007, Komurian-Pradel et al., 2004, Varaklioti et al., 2002, Walewski et al., 2001).

Studies have demonstrated that the F protein is not essential for HCV replication in tissue culture or *in vivo* and that the region encoding the F protein contains functional RNA secondary structures (McMullan et al., 2007, Vassilaki et al., 2008b). The requirement of these RNA secondary structures rather than F protein expression for optimal virus replication has therefore raised the question whether the overlapping reading frame is in fact authentic. Disputes also exist over the actual translational start site of the F protein and until recently, it was widely believed that F protein expression was the result of ribosomal frameshift between codons 8 and 11 of the core-encoding

region (Basu et al., 2004). However, it has now been demonstrated that internal AUG-mediated initiation of translation at codons 85 and 87 of the core+1 encoding region yields a smaller F protein known as core+1/S (Vassilaki et al., 2008a, Vassilaki et al., 2008c, Wolf et al., 2008). To date it has not been excluded that multiple versions of the F protein generated by differing cellular translation events exist during infection.

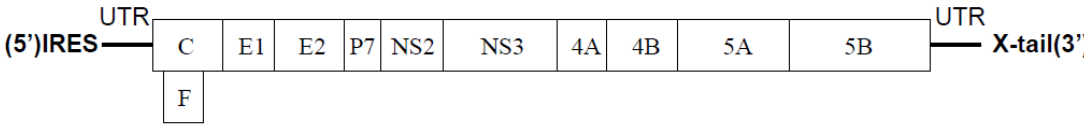


Figure 1.8. Organisation of the HCV genome. Translation is mediated by an internal ribosomal entry site (IRES) and yields the polyprotein from ORF1, as well as the F protein which is produced from an overlapping, core-encoding overlapping reading frame. HCV does not possess a polyA tail, but a stretch of 98 nucleotides known as the X tail, which comparable to the polyA tail also plays a role in viral translation (Ito et al., 1998). Structural ORF1 products include the core (C) and two envelope proteins (E1 and E2). Non-structural proteins include the P7 ion channel, NS2 is a component of the NS2/3 protease, NS3 has N-terminal protease and C-terminal helicase/NTPase activity, NS4A is a co-factor of NS3 protease, NS4B induces membrane alterations, NS5A is phosphoprotein and NS5B is RNA dependent RNA polymerase (Dubuisson, 2007).

Although the function of the F protein is currently unknown, it is likely that the F protein is an accessory virulence factor. Expression of the F protein *in vitro* has been shown to induce cytokines involved in hepatic injuries (Fiorucci et al., 2007). Both full-length and core+1/S versions of the F protein are cytoplasmic proteins which associate with the endoplasmic reticulum (ER) in resting cells (Vassilaki et al., 2007), but associate with the mitotic spindle and microtubules in dividing cells (Vassilaki et al., 2007). Both versions of the F protein are highly basic, are very unstable and are rapidly degraded by the proteasome (Roussel et al., 2003, Vassilaki et al., 2007, Xu et al., 2003). The F protein directly interacts with the proteasome subunit α3 and is rapidly degraded in a ubiquitin-independent manner, which has led to the suggestion that the F protein regulates protein degradation in infected cells (Yuksek et al., 2009). Regulation of F protein expression by the core protein has also been recorded and could prevent accumulation of the F protein (Vassilaki et al., 2007, Vassilaki & Mavromara, 2003). Consistent with these data is the observation that the F protein interacts with prefoldin 2, a member of a chaperone complex which plays a role in stabilising cytoskeletal proteins such as actin and tubulin prior to folding (Tsao et al., 2006). An interaction between the F protein and prefoldin 2 perturbs cytoskeletal organisation, even though an intact cytoskeleton is required for virus replication. Hence it has been proposed that by blocking intact microtubule and actin

polymerisation, the F protein limits virus replication, thus promoting a persistent infection, which indeed is common for HCV (Tsao et al., 2006). Other studies suggest a role of the F protein in the development of hepatocellular carcinoma, as F protein expression in cells is associated with up-regulation of the oncogene c-myc and down-regulation of antioncogenic p53 (Ma et al., 2008, Wu et al., 2007). Recently, antiapoptotic activity of the F protein has also been described with expression of the F protein leading to overexpression of nuclear factor kappa B (NF-kB) signalling pathway, thus preventing TNF mediated apoptosis (Shao et al., 2009). However, as the various HCV proteins have been attributed pro- as well as antiapoptotic functions (Kang et al., 2009, Lee et al., 2005, Lee et al., 2007), the consequence of any apoptotic activity of the F protein in the context of infection is unclear. In conclusion, despite numerous efforts relatively little is known about the HCV F protein(s), and it is hoped that future research may yield interesting results into the expression and function of this highly disputed reading frame.

1.2.1.3 Theiler's murine encephalitis virus (TMEV)

Theiler's murine encephalitis virus (TMEV) or Theiler's virus is a cardiovirus within the *Picornaviridae* (Kong & Roos, 1991, van Eyll & Michiels, 2002). Different strains of TMEV are associated with different pathologies in infected weanling mice. Whereas the GDVII subgroup family members are associated with an acute fatal neuronal infection, members of the TO subgroup are first associated with a subclinical infection which is then followed by persistent demyelinating disease (Ghadge et al., 1998). The DA strain has been shown to persist in glial cells and microglia for the lifespan of the mouse (Aubert et al., 1987, Cash et al., 1986). Due to similarities in CNS pathology seen between persistent TMEV strains and multiple sclerosis, TMEV acts as a model for immune mediated demyelinating disease (Drescher & Sosnowska, 2008, Stavrou et al., 2010).

The genome of TMEV is a positive-sense single-stranded RNA genome of approximately 7 kb. IRES dependent translation yields a polyprotein which is predominantly cleaved by the viral 3C-like protease (figure 1.9) (Kong & Roos, 1991, van Eyll & Michiels, 2002). The TO subgroup of TMEV which includes the DA strain contain a further overlapping ORF situated 13 nucleotides downstream of the polyprotein ORF and encoding the highly conserved 18 kDa L* protein (Kong &

Roos, 1991, Stavrou et al., 2010). Translation of L* is thought to occur through leaky scanning of the ribosome (van Eyll & Michiels, 2002).

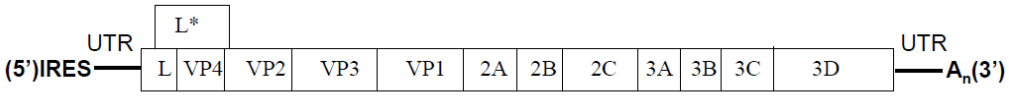


Figure 1.9. Genome organisation of TMEV. Translation of the TMEV genome is IRES-mediated. The first open reading frame encodes a polyprotein which contains the same protein layout and function as all members of the *Picornaviridae* (Whitton et al., 2005). Translation of the L* protein in an overlapping reading frame is thought to occur though leaky scanning and the protein is unique to TMEV. The leader (L) protein inhibits interferon production (van Pesch et al., 2001) and interferes with nucleocytoplasmic trafficking (Delhaye et al., 2004), whereas VP1-4 represent the viral structural proteins. Non-structural proteins include 2A, which plays a role in host cell protein shutoff; 2B inhibits cellular secretory pathways and induces increased membrane permeability, 2C acts as an NTPase and functions in vesicle formation. 3A inhibits intracellular transport (including MHC expression), 3B is viral protein genome linked (VPg), which in contrast to caliciviruses is only required for genome replication, 3C is the viral protease which also cleaves host factors and the C-terminal protein 3D is the viral RNA-dependent RNA polymerase (Whitton et al., 2005).

In vitro L* has been shown to prevent premature shutoff of host cell protein synthesis and has antiapoptotic activity (Ghadge et al., 1998, Himeda et al., 2005). In infected cells L* associates with microtubules (Obuchi et al., 2001). Overall, it is thought that the L* protein contributes to viral persistence and demyelination by delaying the onset of apoptosis caused by TMEV infection of certain cell types (Ghadge et al., 1998, Obuchi & Ohara, 1999). However, the precise molecular function of the L* protein remains to be investigated to date.

1.2.2 Negative-strand RNA viruses

Like positive-strand RNA viruses, there are many examples of negative-sense RNA viruses which encode proteins from overlapping open reading frames. In contrast to positive-strand RNA viruses however, theses viruses must utilise the activity of the viral polymerase protein contained within the viral particle in order to convert their genome into positive-sense RNA which can be translated.

1.2.2.1 Influenza A virus

Influenza A virus is an extremely common and antigenically versatile respiratory virus belonging to the *Orthomyxoviridae*, which has the ability to cause seasonal epidemics as well as pandemics (review by Coleman, 2007). Some of the reasons for influenza's success as a pathogen is the fact that the high error prone polymerase of this virus

ensures successful antigenic drift, which is responsible for seasonal epidemics (Coleman, 2007). Due to the segmented nature of the negative-strand viral genome and the variety of permissive species, influenza also undergoes antigenic shift, which results in pandemics. Pandemics arise because the entire global population is susceptible to infection due to the lack of any pre-existing protective immunity. In terms of human deaths, the most devastating pandemic occurred in 1918/19, when it is estimated that between 20 and 50 million people died globally as a consequence of infection (Lamb & Takeda, 2001). Recently, there are concerns that a novel influenza A virus (subtype H1N1) derived from pigs will be responsible for the next global pandemic (Chang et al., 2009). The primary cause of death from influenza A is in fact due to secondary bacterial infection, and recent evidence suggests that an overlapping reading frame protein called PB1-F2 which is encoded by some influenza virus strains may be involved in viral virulence. Evidence from avian influenza isolates suggests that in birds the PB1-F2 transcript is under extremely high selective pressure for nonsynonymous substitutions and PB1-F2 was highly conserved amongst the studied strains (Obenauer et al., 2006).

The PB1-F2 protein is 87 amino acids in size and is encoded on the polymerase gene PB1 in a +1 frame located 120 bases downstream of the PB1 initiation site (Chen et al., 2001). AUG-dependent translation of PB1-F2 is thought to occur through ribosomal scanning of the capped PB1 mRNA transcript (figure 1.10) (Chen et al., 2001), which like all influenza virus mRNAs is produced in the nucleus and enters the cytoplasm for translation. Very recent reports also suggest that an N-terminal truncated version of the PB1 gene (termed N40) is also produced through ribosomal scanning (figure 1.10) (Wise et al., 2009).

Although PB1-F2 is not required for replication in tissue culture, the protein is an accessory factor with is required for increased virulence and mortality in mice (Zamarin et al., 2006). The short-lived PB1-F2 protein has proapoptotic activity and targets the mitochondria via a C-terminal mitochondrial targeting sequence (MTS) (Chen et al., 2001, Gibbs et al., 2003, Yamada et al., 2004). Phosphorylation of PB1-F2 is required for apoptotic activity (Mitzner et al., 2009). Oligomerisation and membrane insertion properties are thought to be responsible for pore formation in the mitochondrial membrane, through which apoptotic signalling molecules such as cytochrome *c* are released (Bruns et al., 2007). PB1-F2 can also induce apoptosis in macrophages when expressed extracellularly, which is likely due to pore-forming

activity in the cellular membrane (Lamb & Takeda, 2001). Similarly, an interaction between PB1-F2 and the mitochondrial proteins VDAC1 (voltage-dependent anion channel 1) and ANT3 (adenine nucleotide translocator 3) has been demonstrated (Danishuddin et al., 2010, Zamarin et al., 2005). ANT3 is an inner mitochondrial membrane protein, whereas VDAC1 is an outer mitochondrial membrane protein. Both ANT3 and VDAC1 play a role in mitochondrial membrane permeabilisation during the process of apoptosis. The importance of apoptosis induction during the replication of influenza virus is demonstrated by reduced viral replication in cell lines expressing antiapoptotic Bcl-2 family proteins (Olsen et al., 1996).

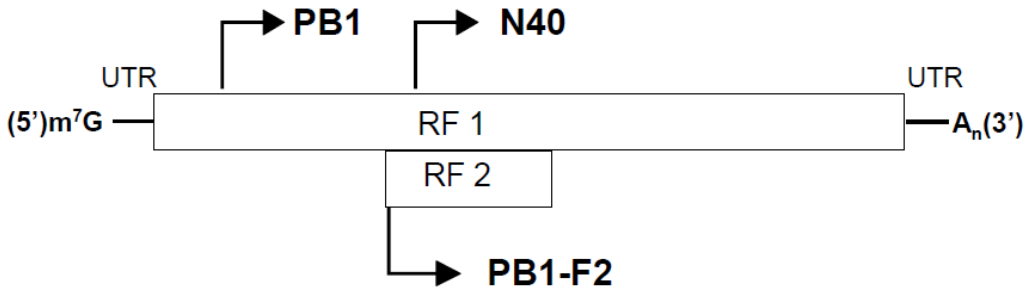


Figure 1.10. Layout of an mRNA transcript of the influenza virus PB1 segment. The polymerase PB1 and a newly identified truncated version (N40) are encoded by one reading frame (RF), whereas the accessory virulence factor PB1-F2 is encoded by an overlapping reading frame in a +1 frame. Translation of PB1-F2 and N40 is thought to occur through ribosomal scanning.

To date, the precise involvement of PB1-F2 in viral virulence remains unclear. On the one hand, knocking out PB1-F2 expression attenuated the virus's ability to induce apoptosis in immune cells (Chen et al., 2001). There is also evidence to suggest that PB1-F2 deliberately targets alveolar macrophages and CD8 T-cells for degradation, thus delaying the immune response to infection (Conenello & Palese, 2007, Zamarin et al., 2005). In epithelial cells on the other hand, PB1-F2 knockout viruses did not differ significantly in the ability of influenza to induce apoptosis (Chen et al., 2001). In infected mice, the knockout virus did not show reduced viral titres, but more rapid viral clearance was observed in comparison to wild-type virus, indicating that PB1-F2 is involved in a delayed immune response (Zamarin et al., 2006). Interestingly, PB1-F2 probably played a key role in the virulence of the pandemic 1918 virus and mice infected with a laboratory strain of influenza containing the 1918 PB1-F2 gene (with an unaltered PB1 sequence) exhibited severe lung pathology and an increase in

secondary bacterial pneumonia (McAuley et al., 2007). It is thought that increased secondary bacterial infection is caused by the ability of PB1-F2 to cause immune cell infiltration into the lungs, which could even be observed after intranasal inoculation of mice with the C-terminal fragment of PB1-F2 (McAuley et al., 2007). However, a direct link between apoptosis induction by PB1-F2 *in vitro* and viral virulence remains to be established.

Interestingly, recent evidence suggests that the novel H1N1 strain does not produce full-length PB1-F2, but an 11 amino acid truncated form of the protein which lacks the C-terminal domain required for mitochondrial targeting and apoptosis induction (Ramakrishnan et al., 2009, Trifonov & Rabadan, 2009). It is speculated that this truncation may be a reason for the reduced virulence of this virus in comparisons to other pandemic strains (Ramakrishnan et al., 2009, Trifonov & Rabadan, 2009). Consequently there is great emphasis on understanding the precise role of PB1-F2 in influenza virus virulence, especially as current concerns are that the novel H1N1 strain may gain a functional PB1-F2 gene by acquiring a PB1 segment from avian origin or from the seasonal H3N2 strains which also contain a functional PB1-F2 gene (Zell et al., 2007). The recent identification of the N40 truncated version of the PB1 gene produced through internal initiation also means that future investigations into PB1-F2 must take this newly identified gene into account. As yet, the function of N40 remains to be characterised, but preliminary evidence suggests that expression of all three genes encoded on the PB1 segment is affected by the expression levels of other proteins (Wise et al., 2009). Consequently, elucidating the precise function of PB1-F2 as an additional virulence factor may prove to be a difficult task.

1.2.2.2 Borna disease virus (BDV)

Borna disease virus (BDV) is an enveloped neurotropic virus belonging to the *Mononegavirales*, which posses an approximately 9.9 kb non-segmented negative-sense RNA genome. BDV most commonly affects horses and sheep although natural infection has been reported in a wide range of species (review by Jordan & Lipkin). BDV infection causes immune-mediated meningoencephalitis, and infection in humans may be linked to neuropsychiatric disorders (Jordan & Lipkin, 2001). In spite of continuous virus gene expression, BDV causes persistent infections in tissue culture as well as *in vivo*, and a number of species can be infected experimentally (Jordan & Lipkin, 2001).

Comparable to influenza virus and unique to non-segmented negative-strand RNA viruses, BDV replicates in the cell nucleus. Different capped and polyadenylated mRNAs are expressed from three different transcription units by alternative transcriptional termination and alternative splicing (Jordan & Lipkin, 2001). Six ORFs are expressed from 3 transcription units, with the second transcription unit encoding the phosphoprotein (P), as well as the X-protein from overlapping ORFs (figure 1.11). Recently an upstream ORF (uORF) has also been identified on this mRNA, and the stop codon overlaps the X-protein initiation site by 1 nucleotide (Watanabe et al., 2009). To date, the putative 8 amino acid peptide encoded by this ORF remains to be detected in infected cells, and it is possible that uORF plays a role in translational regulation from the mRNA (Watanabe et al., 2009). The X-protein is expressed upstream of the P protein in a +1 frame. Regulation of translation from this polycistronic mRNA is thought to occur though a unique, previously unknown mechanism, whereby the RNA helicase DDX21 which binds to the 5'UTR is regulated (potentially by phosphorylation) by the P protein (Watanabe et al., 2009). Phosphorylated DDX21 detaches from the 5' UTR, which results in an increase in termination-coupled re-initiation of translation from the uORF4 into the X ORF (Watanabe et al., 2009).

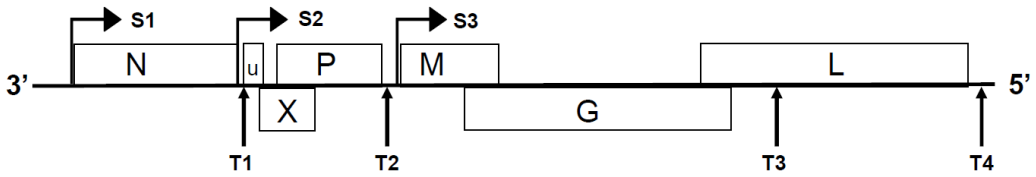


Figure 1.11. BDV genome organisation and transcriptional cleavage map showing transcriptional start (S) and termination sites (T). The nucleoprotein (N) is transcribed from the first mRNA, the X protein and phosphoprotein (P) are produced from the second mRNA in overlapping reading frames, whilst it is not known whether the small upstream uORF (u) actually expresses a peptide. The matrix protein (M), envelope glycoprotein (G) and polymerase protein (L) are produced from the third mRNA transcript. Alternative termination sites and alternative splicing produces variants of several gene products. Figure adapted from a review (Schneider, 2005).

Copious amounts of the non-structural X protein can be detected in infected cells and tissues, and although the protein does not associate with viral particles, the X protein is essential for virus viability and rescue from cDNA (Poenisch et al., 2007, Schwardt et al., 2005). The X protein plays a crucial role in regulating levels of the P protein which together with the nucleoprotein and polymerase form the polymerase complex

(Poenisch et al., 2008, Schwemmle et al., 1998). Protein X is predicted to act as a regulator of BDV gene expression by sequestering excessive amounts of P, as the P protein has a negative effect on polymerase activity (Poenisch et al., 2008, Schneider et al., 2003). The X protein directly interacts with P, a co-factor of the RNA-dependent RNA polymerase via the amino terminus, which also contains a potential nuclear export signal (Jordan & Lipkin, 2001). Because of this export signal it has been suggested that the X-protein is involved in nucleocytoplasmic shuttling during BDV replication. Indeed, the P protein efficiently localise to the cytoplasm of infected cells in the presence of the X protein (Kobayashi et al., 2003).

In terms of localisation, the X protein can be detected in both the cytoplasm and the nucleus. Interestingly, recent evidence suggests that the 87 amino acid X protein also localises to the mitochondria and has antiapoptotic activity (Poenisch et al., 2009a). This study showed that the X protein is required for viral persistence, as *in vivo* inoculation with BDV expressing a mutant form of the X protein lacking the mitochondrial localisation sequence caused acute but not persistent infections (Poenisch et al., 2009a). Examination of the brains of these acutely infected animals revealed a high number of apoptotic cells, suggesting antiapoptotic activity of the X-protein is directly linked to viral persistence (Poenisch et al., 2009a). Indeed, further studies to precisely identify the mode of action of the X protein are currently ongoing and this alternative function of the X protein is the first reported case of a mitochondrial localised protein of an RNA virus which has significant antiapoptotic activity (Poenisch et al., 2009a).

1.2.3 Further examples of overlapping reading frames

The list of presented overlapping reading frame proteins is not exhaustive and many other examples exist. In positive- strand RNA viruses, for example in toroviruses, which infect livestock and are members of the *Coronaviridea*, bioinformatic analysis has recently identified a highly conserved overlapping reading frame, although expression and function are currently unknown (Firth & Atkins, 2009). Members of the *Potyviridae* which contain more than 30% of known plant viruses also contain an overlapping reading frame in a +2 frame, the expression of which is essential for virus viability (Chung et al., 2008). Other plant viruses with an overlapping reading frame are waikaiviruses, which belong to the *Picornavirales* order (Firth & Atkins, 2008a).

In non-segmented negative-sense RNA viruses, many members of the *Paramyxovirinae* (for example measles virus, rinderpest virus and mumps virus), some vesiculoviruses (for example vesicular stomatitis virus) and some rhabdoviruses (for example Tupai virus, which infects tree shrews) posses an overlapping reading frame in the phosphoprotein gene (Liston & Briedis, 1995, Spiropoulou & Nichol, 1993, Springfeld et al., 2005). These accessory proteins are thought to interfere with interferon signalling (Gotoh et al., 2001).

Although examples from positive or negative-sense RNA viruses were chosen due to the relatedness to MNV or because the discussed proteins are relevant to findings related to the ORF4 protein, it is important to remember that overlapping reading frame products are not just encoded in positive or negative-sense RNA viruses. Members of the *Reoviridae*, which are segmented double-stranded RNA viruses also have examples of overlapping ORFs which are translated via leaky scanning (Firth & Atkins, 2008b). Examples include translation of genome segments of cypoviruses, which are insect viruses (Firth & Atkins, 2008b), phytoreoviruses, which are plant and insect replication competent viruses (Suzuki et al., 1996), as well as human reovirus (Ernst & Shatkin, 1985). In human reoviruses, the S1 gene segment encodes the large structural virion surface protein σ1, thought to play a role in viral attachment, whereas the overlapping reading frame protein σ1s is an accessory virulence factor (Hoyt et al., 2005). σ1s has been shown to be a proapoptotic protein which localises to the nucleus and plays a role in viral induced apoptosis (Hoyt et al., 2004, Hoyt et al., 2005). In tissue culture σ1s is a dispensable protein, with mutant viruses not affected in replication ability but in ability to induce apoptosis (Hoyt et al., 2005). Similarly, the related orbiviruses are also predicted to contain an overlapping overlapping reading within the helicase encoding region (Firth, 2008). Orbiviruses include a number of viruses which infect livestock, for example Bluetongue virus and African horse sickness virus. Retroviruses also contain a number of overlapping reading frames, products of which contribute to virulence and immunogenicity (Gaur & Green, 2005, Yewdell & Hickman, 2007).

Although less common, alternative translation has also been described for DNA viruses with examples ranging from papillomaviruses (Narechania et al., 2005) to bacteriophages (Rodriguez et al., 2005). In hepatitis B virus, a DNA virus which replicates via an RNA intermediate, mutations which favour the production of alternative reading frame products are thought to play a role in viral virulence,

especially in the advanced stages of disease (Faure, 2006). To date, extensive studies on the expression of these overlapping reading frame products remains to be investigated.

Importantly, translation of overlapping reading frames is not just limited to viruses and examples of alternative gene products have also been documented in bacteria (Higashi et al., 2006), as well as in eukaryotes (Manktelow et al., 2005, Matsufuji et al., 1995, Saulquin et al., 2002, Shigemoto et al., 2001). It is highly likely that with the increasing understanding and identification of viral overlapping reading frames, further examples of eukaryotic overlapping reading frame proteins will be identified in the future. Especially the increased use of bioinformatics should aid the identification of "hidden genes". Overall, it is thought that understanding the nature of these reading frames as well as methods of translation are likely to aid in understanding not just viral infections but also human diseases such as cancer and autoimmune diseases, conditions in which expression of overlapping reading frame proteins are suspected to play a role (Ho & Green, 2006).

1.3 Project aims

The objective of this project was to determine the role (if any) that ORF4 plays in the MNV life cycle. Individual project aims included to:

1) Determine if the ORF4 protein is expressed during virus infection
2) Examine if ORF4 expression is required for virus replication in tissue culture
3) Investigate the role of ORF4 in MNV virulence
4) Identify host cell factors which interact with the ORF4 protein
5) Examine cellular location of the ORF4 protein
6) Characterise the function of the ORF4 protein

2. Materials and Methods

2.1 Bioinformatics tools

Vector NTI from Invitrogen was used to generate vector maps (depicted in Appendix 1) of MNV cDNA clones and expression plasmids. These were then used in subsequent analysis, for example for identification of restriction sites, designing PCR primers and analysis of sequencing reactions submitted to the MRC sequencing Service at Imperial College London. Alignments of MNV sequences were performed with ClustalW online software (www.ebi.ac.uk/Tools/clustalw/index.ht ml) and Vector NTI using sequences found in GenBank (www.ncbi.nlm.nih.gov/Genbank/index.ht ml). A list of MNV sequences analysed can be seen in table 2.1. Analysis of SSSV and calculation of MFED values was carried out by Prof Peter Simmonds as described (Simmonds et al., 2008).

Genbank accession numbers				
AB435514	EU004655	EU004662	EU004671	EU004678
AB435515	EU004654	EU004664	EU004672	EU004679
AY228235	EU004657	EU004665	EU004673	EU004681
DQ911368	EU004658	EU004667	EU004674	EU004682
EF531290	EU004659	EU004668	EU004675	FJ446719
EF531291	EU004660	EU004669	EU004676	FJ446720
EU004656	EU004661	EU004670	EU004677	

Table 2.1 Genbank accession numbers of sequenced full-length MNV cDNA. Accession numbers used to generate an amino acid alignment of all putative ORF4 proteins using the bioinformatic programme vector new technology informax (VNTI) from Invitrogen.

For identifying the ORF4 polyproline motifs, the ORF4 sequence was analysed by SH3 Hunter (http://cbm.bio.uniroma2.it/SH3-Hunter), a web server designed to recognise polyproline motifs which are putative SH3 domain interaction sites of proteins. Predicted protein characteristics such as hydrophobicity, molecular weight and charge were analysed using the online software found at http://www.athina.biol.uoa.gr and http://www.scripps.edu, as well as using Vector NTI from Invitrogen. Secondary structure predictions were performed with PSIPRED (Bryson et al., 2005), which give graphical representations as well as confidence prediction scores of predicted helical, coil, and strand regions. Membrane topology prediction was analysed using MEMSAT3 (Jones et al., 1994). Predicted subcellular localisation was investigated using the prediction algorithm LOCtree (Nair & Rost,

2005) and mitochondrial localisation was analysed using MitoProt (Claros & Vincens, 1996), PSORT II (Nakai & Horton, 1999, Nakai & Kanehisa, 1992) and MuliLoc (Hoglund et al., 2006) and CELLOv2.5 (Yu et al., 2006). The biochemically determined RNA structure of the 5' end of the MNV subgenomic RNA was supplied by Dr Surender Vashist. Thermodynamic structure prediction of the ORF4 sequence was also carried out using mfold (frontend.bioinfo.rpi.edu/applications/mfold/cgi-bin/RNA-form1.cgi) (Zuker, 2003). Densitometry analysis to compare protein expression levels in western blots was performed using ImageJ software obtainable from http://rsbweb.nih.gov/ij/download.html.

2.2 Plasmid construction

A list of all primers containing the relevant restriction sites used for plasmid generation can be found in table 2.2. For overview purposes, maps of these plasmids can be found within Appendix 1. The ORF4 expression plasmid pcDNA-ORF4 was generated by cloning the PCR amplified ORF4 encoding sequence into the expression plasmid pcDNA3.1+ which contains a cytomegalovirus (CMV) and T7 polymerase promoter. For the production of full-length ORF4 protein, VPg and peptide 3 and 4 fragments of the ORF4 protein fused to the Cherry tag, these PCR amplified fragments were cloned into the Cherry- his encoding pSCherry 2 (Eurogentech). Green fluorescent protein (GFP) fusions of the ORF4 protein were generated by cloning PCR fragments of both MNV ORF4 and the SV ORF4E encoding sequence into the GFP plasmids pEGFP-N1 and pEGFP-C1 (Clontech). Both C-terminal (ORF4-GFP and ORF4E-GFP) and N-terminal (GFP-ORF4 and GFP-ORF4E) GFP fusion expression constructs were generated. Using PCR mutagenesis (primers listed in table 2.2), C-terminal-GFP plasmids expressing N-terminal truncations of the MNV ORF4 protein were generated. Truncations include Δ 1-19 ORF4-GFP, Δ 1-56 ORF4-GFP and Δ 1-123 ORF4-GFP.

Full-length infectious MNV-1 clones (pT7MNV3'Rz) encoding ORF4 mutations were generated by PCR mutagenesis (primers listed in table 2.2) which placed the stop codon TAG at previously identified positions within ORF4 without disrupting the amino acid coding sequence of the capsid. The ORF4 knockout virus M1 contains a stop codon through mutation of T to A at genome position 5118 and hence translation terminates after 17 amino acids. The ORF4 truncated virus M10 contains a T to A

mutation at genome position 5364 terminating translation after 99 amino acids, and the truncated M20 contains a G to A mutation at genome position 5655 terminating translation after 196 amino acids. Using pT7MNV3'Rz as a template, the first round of PCRs was used to generate two products for each mutant to be generated. One product was made by using the respective mutant forward primer in combination with the MNV reverse sequencing primer 6034R, whilst the other used the MNV sequencing forward primer 4450F in combination with the ORF4 mutant reverse primer. The products were gel purified to remove any template and equal amounts were combined in a second PCR reaction using the primers 4450F and 6034R. The resulting 1.6kb fragment was subsequently cloned into pT7MNV3'Rz using the naturally occurring restriction sites AfeI and SacII.

For proteomic identification of proteins which interact with the ORF4 protein, ORF4 was cloned into the $CdCl_2$ inducible N-terminal tandem affinity purification (TAP) Tag expression vector pMEP4 generated by Dr Dalan Bailey. MNV ORF4 was also cloned into the tetracycline inducible TAP expression plasmids pcDNA4/TO-NTAP and pcDNA4/TO-CTAP.

Expression primers			
Oligo name	Oligo sequence	Polarity	Description
Primers for cloning into the expression plasmid pcDNA3.1+			
IGIC38	CCCCAAGCTTGCCACCATGGCGCAGCGCCAAAAGCC	5'	MNV-1 ORF4 into pcDNA3.1+, HindIII site and Kozak
IGIC39	ATAAGAATGCGGCCGCTTAGGTAGACAAAATTGAAATCAGC	3'	MNV-1 ORF4 into pcDNA3.1+, NotI site
Primers for cloning into pSCherry2			
IGIC172	GGGAATTCCATATGGGAAAGAAGGGCAAGAAC	5'	MNV-1 VPg into pSCherry2, EcoRI site
IGIC173	ATAGTTTATGCGGCCGCCTCAAAGTTGATCTTCTCGCC	3'	MNV-1 VPg into pSCherry2, NotI site
IGIC174	GGGAATTCCATATGGCGCAGCGCCAAAAG	5'	full-length MNV-1 ORF4 into pSCherry2, EcoRI site
IGIC175	ATAGTTTATGCGGCCGCGGTAGACAAAATTGAAATCAG	3'	full-length MNV-1 ORF4 into pSCherry2, Not I site
IGIC176	GGGAATTCCATATGCCGGGCAAATTAACCAAATT	5'	MNV-1 ORF4 peptide 3 into pSCherry2 , EcoRI site
IGIC177	ATAGTTTATGCGGCCGCTGTTTCGAGGCGAGATGGAAAACTCAC	3'	MNV-1 ORF4 peptide 3 into pSCherry2, NotI site
IGIC178	GGGAATTCCATATGCTCGAAACACCCCAGGTGAAATACT	5'	MNV-1 ORF4 peptide 4 into pSCherry2 , EcoRI site
IGIC179	ATAGTTTATGCGGCCGCGGTGGGCAAGGTAGGGGTTAAGCC	3'	MNV-1 ORF4 peptide 4 into pSCherry2, NotI site
Primers for cloning MNV and SV ORF4E into GFP expression plasmids pEGFPN1 and pEGFPC1			
IGIC 214	GGGAATTCGTCGACATGGCGCAGCGCCAAAAG	5'	MNV-1 ORF4 into PEGFP-C1, SalI site
IGIC 215	GCATTCCCGGATCCTTAGGTAGACAAAATTGAAAT	3'	MNV-1 ORF4 into pEGFP-C1, BamHI site
IGIC 216	GGGAATTCGTCGACGCCACCATGGCGCAGCGCCAAAAG	5'	MNV-1 ORF4 into pEGFP-N1, SalI site and Kozak
IGIC 217	GCATTCCCGGATCCCGGCCGGTAGACAAAATTGAAAT	3'	MNV-1 ORF4 into pEGFP-N1, BamHI site and +2 frameshift
IGIC 443	GGGAATTCGTCGACATGGCTCCAACCCAGAGCC	5'	SV ORF4E into pEGFP-C1, SalI site
IGIC 444	GAATTCCCGGATCCTCATGAAAGAAACTGGCTCAG	3'	SV ORF4E into pEGFP-C1, BamHI site
IGIC 445	GGGAATTCGTCGACGCCACCATGGCTCCAACCCAGAGCC	5'	SV ORF4E into pEGFP-N1, SalI site and Kozak
IGIC 446	GAATTCCCGGATCCCGTGAAAGAAACTGGCTCAG	3'	SV ORF4E into pEGFP-N1, BamHI site and +2 frameshift
IGIC 476	GGGAAGTCGACGCCACCATGTACCACCCTATTTTCCCAAG	5'	MNV-1 ORF4 N-terminal Δ1-123 into pEGFP-N1, SalI site and Kozak
IGIC 475	GGGAAGTCGACGCCACCATGTCCAGTGCCCCCTTGGTG	5'	MNV-1 ORF4 N-terminal Δ1-56 into pEGFP-N1, SalI site and Kozak
IGIC 474	GGGAAGTCGACGCCACCATGCTGCCGCCGTTGAACAGG	5'	MNV-1 ORF4 N-terminal Δ1-19 into pEGFP-N1, SalI site and Kozak
Primers for cloning MNV ORF4 into TAP Tagging plasmids			
IGIC 125	TTTAAACGTACGGTGATGGCGCAGCGCCAAAAGCCAATGGCTCTG	5'	MNV-1 ORF4 into pMEP4 N-terminal TAP Tag, BsiWI site
IGIC 126	TTTAAAGCGATCGCTTATTAGGTAGACAAAATTGAAATCAGCCGCCGGC	3'	MNV-1 ORF4 into pMEP4 N-terminal TAP Tag, SgfI site
IGIC 385	AAAATCGATACCATGGTGATGGCGCAGCGCCAAA	5'	MNV-1 ORF4 into pcDNA4/TO C-Terminal TAP tag, Cla1 site
IGIC 394	TTTCGTACGGGTAGACAAAATTGAAATCAGC	3'	MNV-1 ORF4 into pcDNA4/TO C-Terminal TAP tag , BsiWI site
IGIC 432	GCGAGCCTATAGATGAAAATCTGTACTTCCAGGGGATAGATGAGAACCTG	5'	Primer to remove two ClaI sites in pcDNA4/TO-CTAP
IGIC 433	CAGGTTCTCATCTATCCCCTGGAAGTACAGATTTTCATCTATAGGCTCGC	3'	Primer to remove two ClaI sites in pcDNA4/TO-CTAP

Oligo name	Oligo sequence	Polarity	Description
	Mutagenic primers		
	Primers for generating MNV-1 ORF4 mutants		
IGIC61	CCAGCGGCCAGGATCTAGTTCCTGCCGCCGTTG	5'	MNV-1 ORF4 M1 CTT -> CTA (L) (TAG into ORF4) position 5118
IGIC62	CAACGGCGGCAGGAACTAGATCCTGGCCGCTGG	3'	MNV-1 ORF4 M1 CTT -> CTA (L) (TAG into ORF4) position 5118
IGIC63	CCATGTACACCGGCTGGGTAGGGAACATGGAGGTTC	5'	MNV-1 ORF4 M10 GTT -> GTA (V) (TAG into ORF4) position 5364
IGIC64	GAACCTCCATGTTCCCTACCCAGCCGGTGTACATGG	3'	MNV-1 ORF4 M10 GTT -> GTA (V) (TAG into ORF4) position 5364
IGIC65	GTGATGAGTCTTTTGTAGTCTCTGGCCGCCTTC	5'	MNV-1 ORF4 M20 GTG -> GTA (V) (TAG into ORF4) position 5655
IGIC66	GAAGGCGGCCAGAGACTACAAAAGACTCATCAC	3'	MNV-1 ORF4 M20 GTG -> GTA (V) (TAG into ORF4) position 5655
	qPCR primers		
Oligo name	Oligo sequence	Polarity	Description
IGIC 464	CAAACATCTTTCCCTTGTTC	5'	Forward qRT-PCR primer for MNV-1 genomic RNA
IGIC 465	TGGACAACGTGGTGAAGGAT	3'	Reverse qRT-PCR primer for MNV-1 genomic RNA
	Sequencing primers		
Oligo name	Oligo sequence	Polarity	Description
3734F	GCGAGATCAGCTTAAGCCCTATTCAGAACCACGCG	5'	MNV-1 sequencing primer
4450F	GCCCTTGCACCACACAGCTGAATAGTTTGG	5'	MNV-1 sequencing primer
5052F	GTGAATGAGGATGAGTGATGGCGCAGCGCCAAAAGCCAATGGC	5'	MNV-1 sequencing primer
4450R	CCAAACTATTCAGCTGTGTGGTGCAAGGGC	3'	MNV-1 sequencing primer
4839R	GCAGGGCCATTAGTTGGGAGGGTCTCTGAGCATGTCC	3'	MNV-1 sequencing primer
5332R	GTTCCCAACCCAGCCGGTGTACATGGCTGAGAGGTGGGC	3'	MNV-1 sequencing primer
5722R	CACGGGCAAGTCGACCATCCGGTAGATGGTTCTCTC	3'	MNV-1 sequencing primer
6034R	GGACCTCGATCTCCAGTTGCCCAGAGAAATCGGGGTAACC	3'	MNV-1 sequencing primer
IGIC463	CCCGATGGTCGTTGACCCGCCTGGCACAAC	5'	Internal SV ORF4E sequencing primer
IGIC462	GGAAGGAGCTGACTGGGTTG	5'	Internal N-terminal TAP tag sequencing primer

Table 2.2. Lists of various primers used during the course of this work. For MNV sequencing primers the number in the oligo name reflects the genome position in the full-length MNV-1 clone pT7MNV3'Rz' from which the oligo sequences, with F depicting a forward sequencing primer (5' to 3') and R depicting a reverse sequencing primer (3' to 5'). The sequences of all primers are depicted in 5' to 3' direction. Polarity indicates whether the primer was used as a forward (5') or reverse (3') primer.

2.3 Bacterial stocks, transformations and medium scale plasmid preparations

The bacterial strains used for transformation were *E. coli* DH5α and NEB Turbo (New England Biolabs). Transformations were carried out according to the manufacturer's instructions. Plasmid preparations were carried out using the Pureyield Plasmid Midiprep System (Promega) according to the manufacturer's protocol. The purity and concentration of the plasmid DNA was determined by spectrophotometry.

2.4 Polymerase chain reaction (PCR) and primers

For PCR amplifications an Eppendorf thermal cycler was used and Go Taq Flexi Polymerase (Promega) or KOD Hot Start Polymerase (Novagen) was used according to the manufacturer's protocol. KOD polymerase was preferentially used for PCR mutagenesis as the high fidelity polymerase is extremely accurate and (unlike most commercially available DNA polymerases) exhibits 3′→5′exonuclease-dependent proofreading activity, thus resulting in a low PCR mutation frequency. A list of primers used during the course of this work can be seen in table 2.2. All PCR products were purified with GFX PCR DNA and Gel Band Purification Kit (GE Healthcare).

2.4.1 PCR mutagenesis and cloning

Using KOD polymerase, 50 µl PCR reactions were prepared using 100 ng template DNA, 1 µl forward primer (10 pmol / µl stock), 1 µl reverse primer (10 pmol / µl stock), 1 µl KOD polymerase, 25 µl KOD Hot start Mastermix (provided by Novagen, consisting of dNTPs, buffer, $MgCl_2$) and ddH_20 to 50 µl. Reactions were placed on a PCR block and were incubated at 95^oC for 2 min in order to activate the hot start polymerase. PCR amplification was subsequently performed for 25 cycles which consisted of a denaturation step at 95^oC for 20 s, annealing step at 50^oC for 10 s and extension at 72^oC for 15 s/kb to be amplified. Reactions were subsequently placed at 4^oC followed by storage at -20^oC until further use. A list of the primers used for PCR mutagenesis can be seen in table 2.2.

2.4.2 PCR to determine the sequences of plasmid constructs and recombinant viruses

In order to determine and verify the sequences of plasmid constructs as well as the generated cDNA sequences of recombinant viruses, Go Taq Flexi Polymerase® (Promega) reactions were prepared according to the manufacturer's protocol. Briefly, reactions were prepared consisting of 100 ng input DNA, 5 µl GoTaq® Flexi buffer (5 x stock), 1 µl dNTPs (10 mM stock), 1 µl forward primer (10 pmol / µl stock), 1 µl reverse primer (10 pmol / µl stock), 2.5 µl $MgCl_2$ (25mM stock) and 0.1 µl GoTaq polymerase®. The volume was then made up to 25 µl using ddH_2O. The reactions were placed on a PCR block and the initial denaturation was performed at 95°C for 2 min. 30 cycles were subsequently performed consisting of denaturation at 95°C for 30 s, annealing at 60°C for 30 s and extension at 72°C for 90 s. A final extension step was performed at 72°C for 5 min which was followed by incubation at 4°C. All PCR products were stored at -20°C until further use.

2.5 Agarose gel electrophoresis

DNA was visualised and analysed by agarose gel electrophoresis. Agarose gels with percentages varying from 0.8-3% (w/v) were produced by dissolving agarose in 0.5 x TBE (TRIS/Borate/EDTA) buffer. After brief cooling, ethidium bromide (stock 5 mg/ ml) was added at 1:100,000 dilution and the gel was poured and left to set. Once set, gels were run in 0.5 x TBE with voltage depending on the size of the DNA fragment as well as the percentage of the gel.

2.6 T7 transcription and *in vitro* translation

In vitro transcription and translation (TNT) reactions from 1 µg of DNA were carried out using 20 µl TNT Quick (Promega) reaction with 1 µl (0.56 MBq) ^{35}S methionine (GE Healthcare). Reactions were incubated for 120 min before an equal volume of 2x reducing SDS-PAGE sample buffer was added.

For the immunoprecipitation of *in vitro* translated ORF4 protein, a large reaction was performed containing 31.25 µl rabbit reticulocyte lysates (RRLs) (Promega), 2.5 µl TNT buffer, 1.25 µl T7 polymerase, 1.25 µl amino acid mix minus methionine, 2.5

µl (1.4 MBq) ^{35}S methionine (GE Healthcare), 1.25 µl RNAsin and 5 µg of the template pcDNA-ORF4. Reactions were incubated at 30^{o}C on a PCR block. 10 µl of the total reaction (62.5 µl) was added to an equal volume of 2x reducing SDS-PAGE sample buffer and kept for analysis by SDS-PAGE. The remaining reaction was used for immunoprecipitation as detailed below.

The TNT products were analysed on a 15% (w/v) SDS-PAGE gel which was Coomassie blue stained (Coomassie blue in 10% (v/v) ethanol and 10% (v/v) glacial acetic acid in ddH_2O) to check equal loading. The gel was destained in a solution containing 10% (v/v) ethanol and 10% (v/v) glacial acetic acid in ddH_2O. After drying the radiolabelled proteins were visualised by autoradiography and phosphoimager.

2.7 Immunoprecipitation from *in vitro* transcription and translation (TNT) reactions

A 50% (v/v) protein A bead slurry was prepared in radioimmunoprecipitation (RIPA) buffer (50 mM Tris–HCl pH 8.0, 150 mM NaCl, 1 mM EDTA, 1% (v/v) Triton X-100 and 0.1% (v/v) SDS). 50 µl of the 50% slurry was aliquoted into pre-siliconised tubes containing either 50 µl of purified polyclonal ORF4 protein cross-reactive antibody, 20 µl of VP1 or VP2 cross-reactive antibody, or 5 µl of rabbit pre-immune sera. The antibody-protein A slurry was incubated at room temperature (RT) for 1 h with regular mixing. After 1 h the antibody-bead complexes were washed 3 times in RIPA buffer to remove excess antibody. Before incubation with the antbodies the product of the TNT reaction was pre-cleared by incubating for 20 min at 4^{o}C with the 50% slurry of protein A agarose beads and the total volume was topped up to 1 ml with RIPA buffer. The pre-clear acted to remove proteins from the reaction which non-specifically bound to the protein A agarose beads. The pre-cleared reaction was then centrifuged at 10,000 x g for 3 min and the supernatant was divided equally between the antibody-protein A-sepharose containing tubes. The volume was topped up to a total of 500 µl and the reactions were incubated overnight on a rotor at 4^{o}C. After incubation the reactions were washed 3 times in high-stringency RIPA buffer (500 mM NaCl) and twice in standard RIPA buffer. After these washes an equal volume of reducing SDS-PAGE sample buffer was added and the proteins were separated by SDS-PAGE, stained, fixed and visualised as described above.

2.8 Recombinant protein production and purification

2.8.1 ORF4-his

For protein induction, BL21 DE3* bacterial cells were transfected with the plasmid encoding the N-terminal ubiquitinated and C-terminal his-tagged ORF4 protein under the control of a T7 promoter (pET26UB MNV ORF4) generated previously by Dr Ian Goodfellow. Cells were also transfected with T7 polymerase and ubiquitin protease encoding pCG1 vector under the control of the inducible lacUV5 promoter as described previously (Gohara et al., 1999). Ubiquitin protease cleavage of the ORF4 fusion protein was used to ensure the expression of "authentic" ORF4 protein which possibly employs GTG initiation. Hence without this system bacterial expression would require an additional methionine encoding N-terminal ATG, which could affect protein properties.

Transfected cells were grown for 24 h in Overnight Express^{TM} instant TB medium at 37^{o}C. The next day cells were centrifuged at 1,500 x g for 30 min. Cell pellets were washed in phosphate buffered saline (PBS) and were centrifuged at 1,500 x g for 15 min. Cells were lysed in a buffer containing 10 mM immidazol, 500 mM NaCl, 8 M urea, 50 mM Tris pH 8.0. Lysis was aided by sonication (2 min total). The lysate was centrifuged at 10,000 x g for 15 min. 2 ml of a 50% (v/v) Ni-NTA resin slurry in lysis buffer was added to the supernatant and the reaction was incubated overnight on a rotor at room temperature. The next day the reaction was centrifuged at 200 x g for 5 min and the resin containing fraction was washed and resuspended in lysis buffer. The reaction was transferred to a polyprep column (Biorad) which was washed with lysis buffer containing 15 mM immidazol. An elution buffer containing 200 mM immidazol was added and the eluted protein was collected in 1 ml fractions. The fractions containing the ORF4-his protein were pooled and the protein concentration was quantified on a Coomassie stained SDS-PAGE gel using standard bovine serum albumin (BSA) concentrations.

2.8.2 Cherry ORF4 expression

Full-length ORF4 protein, ORF4 peptide 3 (amino acids 41-69, sequence PGKLTKLTPGSSKILSSAPLVSFPSRLETP) and peptide 4 (amino acids 67-90, sequence LETPQVKYCLIWPSGQGLTPTLPT) and MNV VPg were cloned into

pSCherry2, which encodes the haeme binding protein of cytochrome *c* (known as the Cherry tag) as well as a his tag. The proteins N-terminally fused to the Cherry tag and containing a C-terminal his-tag were expressed in T7 polymerase encoding SE1 bacteria (supplied by Eurogentech) by growing in overnight Express^{TM} instant TB medium at 37^{o}C. Cells containing the empty plasmid without the cherry tag (pSCodon1.2) acted as a negative control and the plasmid containing the cherry tag alone (pSCherry2) acted as a positive control. 5 ml of overnight culture was centrifuged and protein expression could be observed by the presence of a red pellet. Induction of expression was visualised on a gel by centrifuging the equivalent amount of bacteria to give and optical density (OD) of 0.8 at 600 nm. The bacterial pellets were resuspended in 100 µl 1x reducing SDS-PAGE sample buffer and 10 µl were run on an SDS-PAGE gel which was subsequently Coomassie stained and fixed as described above.

2.9 Antisera

All antibody dilutions given in this section refer to western blot analysis, for dilutions used for confocal microscopy please consult the confocal microscopy section in this chapter. Antisera to the RNA dependent RNA polymerase of MNV-1 was generated by immunisation of New Zealand white rabbits by Eurogentech after providing them with recombinant viral polymerase (NS7) previously purified in the lab. An anti-NS7 serum was used at a dilution of 1:1000.

The first antibody raised against the ORF protein was generated using the standard immunisation programme by Eurogentech. Briefly, New Zealand white rabbits were immunised with recombinant full-length his-tagged ORF4 protein provided in 8 M urea, and the rabbits received additional boosts of the protein on days 14 and 28. On day 36 sera were taken for a test ELISA performed by Eurogentech, which demonstrated that the sera were capable of cross reacting with his-tagged ORF4 protein *in vitro*. After an additional boost on day 56 rabbits were sacrificed on day 65 for the final bleed. When used in our laboratory for western blot and co-immunoprecipitation, the antibody demonstrated good cross-reactivity against ORF4-his and other his-tagged proteins but was unable to detect the ORF4 protein alone.

Using a 28-day immunisation programme, antibodies raised against 2 N-terminal peptide components of the ORF4 protein (peptide 1 from amino acids 41-55, which

represents the amino acid sequence PGKLTKLTPGSSKIL, and peptide 2 from amino acids 62-74, which represents the amino acid sequence SFPSRLETP QVKY) were generated by Eurogentech. The peptides used for immunisation were chosen and were produced and purified by Eurogentech. The peptides were coupled to keyhole limpet hemocyanin (KLH) as a carrier in order to enhance immunogenicity. Selection of these peptides was based on hydrophilicity, antigenic index, surface probability as well as alpha helix predictions. Briefly, the 28 day protocol performed by Eurogentech consisted of immunisation of New Zealand white rabbits with the two peptides and subsequent boosts were performed on days 7, 10 and 18. On day 21, sera generated from a test bleed were used by Eurogentech in an ELISA, which demonstrated good cross reactivity between the sera and the two peptides. After 28 days a terminal bleed was performed and the two anti-peptide antibodies were affinity purified on the above peptides by Eurogentech. For detection of the ORF4 protein by western blot analysis the antibody raised against peptide 1 was used at a dilution of 1:100, whereas that raised against peptide 2 was unsuccessful regardless of dilution.

Thirdly, a better ORF4 protein reactive antibody (used at a dilution of 1:250) was generated by Eurogentech by immunising New Zealand white rabbits with peptide 1, which was repeated on day 21. On day 49 a boost was performed with full-length ORF4-his. Preliminary enzyme-linked immunosorbent assays (ELISAs) performed by Eurogentech on test bleeds demonstrated little cross- reactivity of the sera with ORF4-his. Therefore, rabbits were further boosted with ORF4-his (day 77). On day 91, rabbits were immunised with ORF4 peptide 3 N-terminally fused to the Cherry tag and C-terminally fused to a his tag (CH-P3-his), generated as described above. On day 105 a further boost with peptide 1 was performed and a final boost with CH-P3-his was carried out on day 119, which was followed by a terminal bleed on day 143. This antibody was purified by Eurogentech by affinity purification against peptide 1.

A mouse monoclonal antibody to glyceraldehyde-3-phosphate dehydrogenase (GAPDH) (Cat # AM4300) was purchased from Ambion and was used at a dilution of 1:20,000. A goat polyclonal antibody raised against the C-terminus of AIF was purchased from Santa Cruz Biotechnology and was used at a dilution of 1:500 (Cat # AIF (D-20): sc-9416). Polyclonal rabbit antibodies against full-length caspase 3 (Cat # 9662), Asp175 cleaved caspase 3 (Cat # 9661), mouse specific full-length caspase 9 (Cat # 9504), mouse specific Asp353 cleaved caspase 9 (Cat # 9509) were purchased from Cell Signalling Technology and were used at the recommended dilution of

1:1000. A rabbit monoclonal antibody against survivin (Cat # 2808) was also purchased from Cell Signalling Technology and was used at the recommended dilution of 1:1000. A rabbit polyclonal antibody to calnexin used for confocal microscopy analysis was purchased from Santa Cruz Biotechnology (Cat # Calnexin (H-70): sc-11397).

Anti-mouse secondary antibody coupled with horseradish peroxidase (HRP) was used at 1:15,000, anti-rabbit antibody coupled with HRP was used at 1:10,000 and anti-goat antibody coupled with HRP (Santa Cruz Biotechnology) was used at 1:3000 dilution. Alexa Fluor® 546 goat anti-rabbit and Alexa Fluor® 546 donkey anti-goat IgG were purchased from Invitrogen.

2.10 Western blot

For western blot analysis, cells were lysed in RIPA buffer (50 mM Tris–HCl pH 8.0, 150 mM NaCl, 1 mM EDTA, 1% (v/v) Triton X-100 and 0.1% (v/v) SDS). The BCA protein assay (Pierce) was used to quantify the protein in the lysates. From each lysate an equal amount of protein was mixed with SDS sample buffer (reducing) and heated at 95^{o}C for 5 min after which proteins were separated by SDS-PAGE. Proteins were transferred to a polyvinylidene fluoride (PVDF) Immobilon-P transfer membrane (Millipore) by semi-dry blotting according to the manufacturer's instructions (Biorad). The transfer of the ORF4 protein was run slightly longer at 15 V for 60 min. Following transfer the membrane was blocked with PBST (0.1% (v/v) Tween 20 in PBS) containing 5% (w/v) milk powder. After blocking, the membrane was incubated with primary antibody diluted in PBST, 5% milk for a minimum of 2 h and was washed 3 times in PBST, 5% milk. The secondary, HRP conjugated antibody diluted in PBST, 5% milk was applied for 1 h and the membrane was washed twice in PBST and twice in PBS. For the final visualisation, enhanced chemiluminescent substrate (ECL) (GE Healthcare) was used according to manufacturer's instructions. Briefly, 3 ml of reagent 1 was added to 3 ml of reagent 2 and each membrane was incubated for 30 s in the mixture, prior to placing between two acetate sheets in a film cassette. Exposures to X-ray film were subsequently performed in a dark room.

2.11 Cell lines

MNV was propagated in the murine leukaemia macrophage cell line RAW 264.7 using Dulbecco's modified Eagle medium (DMEM) with 10% (v/v) foetal calf serum (FCS),

penicillin (100 U/ ml) and streptomycin (100 µg/ml) and 10 mM HEPES buffer. Bone derived macrophages (BMMΦ) from BALB/c mice were isolated from the thigh bone, differentiated and maintained as detailed (Munder, 1971). Baby-hamster kidney cells (BHK-21) expressing T7 RNA polymerase (BSRT7 cells) used during reverse genetics recovery of MNV from cDNA clones, were cultured in DMEM (+FCS and pen/strep as above) containing G418 at a concentration of 1 mg/ ml. COS-7 cells (CV-1 cell line derived from adult male African green monkey kidney) and 293T cells were grown in DMEM (+FCS and pen/strep as above).

Stable 293T cell lines expressing $CdCl_2$ inducible NTAP-ORF4 and NTAP were grown in DMEM containing 10% FCS, pen/strep, 50 µg/ml hygromycin and non-essential amino acids. Tetracycline-regulated expression (T-REX) 293T cells were cultured in DMEM containing 10% FCS, pen/strep and blasticidin at a concentration of 5 µg/ml. 293T TRex cell lines stably transfected with tetracycline inducible NTAP-ORF4, ORF4-CTAP, NTAP or CTAP were cultured as T-REX 293T cells but additionally contained zeocin at a concentration of 200 µg/ml. All cells were maintained at 37^{o}C with 10% CO_2.

2.12 DNA transfections

Cells were transfected with DNA diluted in Optimem (Gibco) using Lipofectamine 2000 (Invitrogen) according to the manufacturer's instructions. Transfections were always performed in antibiotic free media, as antibiotics entering the cells as a result of the transfection protocol results in toxicity to the cells.

2.13 MNV reverse genetics

ORF4 mutant viruses were recovered using the reverse genetics principle previously described by Chaudhry *et al* 2007. Briefly, BSRT7 were seeded at $7.5x10^5$ cells/well in $9cm^2$ in antibiotic free DMEM with 10% FCS and incubated overnight at 37^{o}C, 10% CO_2. Antibiotic free media was used in preparation for transfection. The next day cells were infected with Fowlpox virus (FPV) expressing T7 polymerase at a multiplicity of infection (m.o.i.) of 0.5 plaque forming units (p.f.u.) per cell, (titred in chick embryo fibroblasts). 700 µl of virus inoculum in antibiotic free DMEM with 10% FCS was left on the cells for 1 h after which a further 2 ml of antibiotic free DMEM with 10% FCS was added for 1 h. After incubation at room temperature, cells were washed in antibiotic free DMEM with 10% FCS and using Lipofectamine 2000 according to the

manufacturer's protocol, cells were subsequently transfected with 1 µg of the MNV infectious cDNA. 24 h post-transfection two freeze–thaw cycles were used to release cell-associated virus which was subsequently titred by $TCID_{50}$/ml in RAW 264.7 cells, using microscopic visualisation for the appearance of cytopathic effect. As cytopathic effect was easily visualised, no staining protocol was necessary to distinguish between infected and non-infected wells. Cytopathic effect was apparent by cell shrinkage, rounding, loss of contact inhibition and cell death. Protein expression was analysed by harvesting the cells into RIPA buffer and performing western blot analysis.

2.14 Reverse transcription-PCR (RT-PCR) and sequence verification of mutant viruses

Reverse transcription was carried out on RNA extracted from cells infected at high m.o.i. for 12 h, after which RNA extractions were performed using the mammalian total RNA extraction kit from Sigma. 5 µg of RNA and SuperScript II reverse transcriptase (Invitrogen) was used according to the manufacturer's instructions. In the first step a supermix consisting of 1 µl dNTPs (10mM stock), 1 µl primer (2 pmol / µl stock), 5 µg RNA and ddH_20 to 12 µl was prepared on ice in PCR tubes. Samples were incubated at 65°C for 5 min in a PCR block before placing back on ice. To each reaction were added 5 µl of 5 x SuperScript II buffer, 2 µl DTT, 1 µl RNAsin and 1 µl SuperScript II RT enzyme. Samples were then incubated at 42°C for an additional 50 min, followed by 70°C for 15 min to inactivate the enzyme before placing on ice and subsequently storing at -20^{o}C.

The MNV genome specific primer 6034R was used for the reverse transcription to determine the sequence of all ORF4 mutant viral stocks. ORF4 was subsequently amplified from the resulting cDNA using the MNV-1 sequencing primers 4450F and 6034R. The ORF4 region was then sequenced using the MNV-1 sequencing primers 5722R and 5054F.

2.15 Growth kinetic analysis

RAW264.7 cells seeded at $3.2x10^5$ cells per well of a 24-well plate were subsequently infected with the ORF4 mutant viruses M1, M10 or M20 at an m.o.i. of 0.01. The assay was performed in triplicate for each virus. At given time points (0, 6, 12, 24, 48,

72 h post-infection) the infections were frozen and upon thawing the viral titres were determined by $TCID_{50}$. Protein samples over the given timecourse were also taken, standardised and analysed by western blot.

2.16 Determination of viral titre ($TCID_{50}$/ ml)

The MNV titre was determined by serial dilutions of the virus in a 96 well plate using DMEM (10% FCS + pen/strep) as the diluent. Dilutions ranged from 10^{-1} to 10^{-8} in a total volume of 250 µl. From each dilution series four 50 µl aliquots were transferred to 96 well plates, to which $1x10^4$ RAW264.7 cells were added per well. After incubation for 5 days the percentage of infected wells in each repeat titration was scored by microscopic analysis for cytopathic effect of the virus on the cells. Viral titres were calculated using the standard formula based on the Reed-Muench method (Reed & Muench, 1938). The dilution at which 50 % of the wells were infected was then calculated using the following equation:

$$\frac{(\%\ \textit{positive above}\ 50\%) - 50\%}{(\%\ \textit{positive above}\ 50\%) - (\%\ \textit{positive below}\ 50\%)} = \textit{proportionate distance}$$

The result of the equation gave the proportionate distance between the two dilutions which gave a percentage infection either side of 50 %. The distance between the dilutions was calculated by using the following equation:

(log dilution above 50%) + (proportionate distance x log dilution factor) = log $TCID_{50}$

The reciprocal of the $TCID_{50}$ was then used to express the virus titre as $TCID_{50}$ / unit volume, i.e. $TCID_{50}$ / ml.

2.17 Analysis of ORF4 mutant virus stability

RAW264.7 cells were seeded at $3.75x10^6$ cells per well (9 cm^2) of a 6-well dish and were subsequently infected with the ORF4 mutant viruses M1, M10 or M20 at an m.o.i. of 0.01. After 48 h, passage 1 viruses were freeze-thawed and were used for the subsequent low m.o.i. round of infection. This style of passage was continued for 5 cycles after which cells were infected at high m.o.i. for 12 h and RNA was isolated for

subsequent RT-PCR and sequencing. RT reactions and PCR were performed as for viral stocks described above.

2.18 Analysis of virulent clones

An infectious clone harbouring the wild-type virulent MNV-1defining mutations at genome positions 2151 and 5941 was generated by Dr Dalan Dalan Bailey and the recovered recombinant virus is subsequently referred to as WT-v. The ORF4 knockout mutation was built into this infectious clone by Yasmin Chaudhry and the generated virulent recombinant viruses are referred to as M1-v. Following the generation of stocks the sequences of these viruses were verified by high m.o.i. infection of RAW 264.7 cells with passage 1 virus for 12 h and subsequent RNA extraction as described. RT-PCR reactions using the sequencing primer 2616R and 6034R were prepared. PCR reactions using 5 µl cDNA were subsequently set up. The primers 1954F and 2616R were used to amplify the region from the 2616R cDNA reaction and the primers 4450F and 6034R were used to amplify the ORF4 region from the 6034R reaction. For sequencing of the virulent stocks at genome position 2151, sequencing reactions were prepared using the primer 1954F. For sequencing of the virulent stocks at genome position 5941 sequencing reactions were prepared using the primer 6034R. For sequencing of the ORF4 mutation sequencing reactions were prepared using the primer 5332R.

2.19 *In vivo* virulence analysis

All work involving live animals was carried with the help of Dr Dalan Bailey and in collaboration with Dr Felix Yarovinsky at the University of Texas Southwestern Medical Center, USA. Mice were housed in a category 2 laboratory on the campus. In order to analyse virulence 16 male and female $STAT1^{-/-}$ mice (six to eight weeks in age, purchase from Taconic) were inoculated by oral gavage with either WT-v, or M1-v. 6 control mice were inoculated with lysates from uninfected cells using the same method. For this experiment mice were inoculated with 1000 $TCID_{50}$ units. A previous smaller scale trial experiment involving only male mice and using 10,000 $TCID_{50}$ units inoculum was used to analyse bodyweight only. Animals were weighed and checked daily post-infection for signs of clinical disease characteristic of MNV-1 infection. 8 mice in each virus infected group were left for the duration of the experiment with

blood and faeces samples being collected on days 0, 3 and 7 post-infection. Blood was collected by eye bleeding using heparinised blood collection tubes. Upon appearance of extremely severe symptoms such as ataxia, MNV specific symptoms on 3 consecutive days or more than 20% loss in bodyweight, mice were sacrificed by complete dislocation of the neck at the level of cervical vertebrae. The remaining 8 mice from each virus infected group were used to collect tissue samples. For this, two females and two males from each group were sacrificed on days 3 and 5 post-infection. Tissue samples collected for analysis include the mesenteric lymph node, spleen, liver, kidney, intestine, heart and lung. Lastly, faeces samples were also taken directly from the small intestine of these sacrificed mice. Upon harvesting, samples were immediately placed in Trizol® reagent (Invitrogen) and were frozen at -80^{o}C for subsequent RNA extraction.

2.20 Quantification of viral load

Viral loads in the harvested tissue samples were quantified by real time quantitative PCR (qPCR) of viral cDNA generated by performing RT-reactions using tissue sample extracted RNA as a template. Firstly, tissue samples stored in Trizol® reagent (Invitrogen) were thawed and homogenised. RNA extraction from the Trizol® reagent was performed through chloroform/isopropanol precipitation according to the manufacturer's instructions. Pelleted RNA was resuspended in 150 µl ddH_2O and RNA concentrations were quantified spectrophotometrically. 1µg of total RNA from each tissue sample was added to an RT reaction using recombinant Avian Myeloblastosis Virus (AMV) RT enzyme (Fermentas) according to the manufacturer's instructions.

A viral standard RNA corresponding to nucleotides 1085 – 1986 of the MNV genome (containing 10^{10} viral genome copies/ 2 µl) previously prepared by *in vitro* transcription reaction and quantified by Dr Surender Vashist was subsequently diluted by performing 10-fold serial dilutions in RNA dilution buffer (yeast RNA, Ambion Cat #AM7118 diluted 1:100 in nuclease free water) to give viral RNA standards ranging between 10^7 and 10^1genome copies per µg total RNA. For each sample, duplicate qPCR reactions were then prepared in 96-well qPCR plates (Thermo Scientific) using the MESA Blue qPCR MasterMix Plus for Syber Assay (Eurogentech). 10% of the total amount of RT-generated cDNA or viral RNA standard

was placed into 20 µl reactions containing the MNV genomic primers IGIC464 and IGIC465. The enzyme-containing buffer and ddH_2O were added according to the manufacturer's protocol. Reactions containing ddH_2O and RNA dilution buffer were used as a control. DNA was amplified in an ABI 7900 real time PCR machine using a 10 min heat denaturing step (95°C for 10 min) followed by 40 cycles of 94°C for 15 sec, 58°C for 30 sec and 72°C for 30 sec.

Viral genome copy number was calculated by interpolation from the standard curve. This was generated using serial dilutions of standard RNA. The detection limit was established by setting the threshold of detection to the values seen by qPCR reaction of a non-infected negative control mouse. To ensure that these negative control values were not due to contamination of the tissue samples with DNA from the laboratory, the melting curves of these qPCR reactions were analysed and compared to the viral standards. A melting curve measures the melting temperature of the product obtained by qPCR. If only one specifically primed product is produced, then a single curve corresponding to the melting temperature can be seen. If the products are multiple and non-specifically primed, then several curves are seen, which do not overlap with the curve of the desired product.

2.21 Analysis of restoration of ORF4 expression

In order to analyse the ORF4 sequences from viral RNA isolated from the tissues of $STAT1^{-/-}$ mice, cDNA was generated by performing RT-PCR reactions using 1 µg of tissue sample extracted RNA as a template. Reverse transcriptions were performed using the sequencing primer 6034R as described above. The cDNA products were subsequently PCR amplified by hemi-nested PCR. The first PCR reaction was carried out using 5 µl cDNA and the MNV sequencing primers 5052F and 5722R, whilst the second reactions contained 2 µl of the first PCR reaction and the primers 5052F and 5332R. The M1 defining mutation was subsequently sequenced using the MNV sequencing primer 5332R.

2.22 Statistical analysis

For comparing viral yields at high vs. low cell seeding density an unpaired T-test at 95% confidence level was performed. Statistical analysis of mouse bodyweight in the

days following infection was performed by Two-way ANOVA with Bonferroni post-tests. Viral loads in the faeces of infected mice were measured using an unpaired T-test at 95% confidence level. For the Glo3/7 assays, caspase activity at 16 h post-infection was statistically compared using an unpaired T-test at 95% confidence level. For the apoptosis timecourse, difference in luminescent signal over time was compared by two-way ANOVA with Bonferroni post-tests.

2.23 Tandem affinity purification

2.23.1 NTAP-ORF4 in the $CdCl_2$ inducible system

ORF4 was cloned into the TAP plasmid pMEP4:NTAP which contains a GS tag (protein G and streptavidin binding sequence). 293T cells expressing the NTAP-ORF4 (stably selected with 50 µg/ml hygromycin B from Roche) were induced by adding 10 µM $CdCl_2$ for 16 h. The cells from 10 x F175 flasks (approximately $2x10^8$ cells) were trypsinised, pooled and washed 3 times in ice-cold PBS. Cell pellets were lysed in an equal volume (approximately 2 ml) of lysis buffer (50 mM Tris-HCl (pH 7.5), 125 mM NaCl, 5% (v/v) glycerol, 0.2% (v/v) NP-40, 1.5 mM $MgCl_2$, 25 mM NaF, 1 mM Na_3VO_4 and protease inhibitors) for 10-15 min. Lysates were freeze thawed twice (liquid N_2 then 37°C water bath) and centrifuged in a 4°C centrifuge at 15,000 x g for 10 min. 30 µl sample (sample 1) was kept for analysis.

For the first immunoprecipitation the cleared lysates were added to 60 µl packed beads of rabbit IgG agarose (Sigma-Aldrich Cat# A2909) which had been washed in lysis buffer. Rabbit IgG agarose contained polyclonal rabbit sera, which bound to the TAP tagged proteins due to the ability of the protein G binding domain to bind IgG. The reactions were incubated at 4°C for 2-3 h and were subsequently centrifuged at 500 x g and the supernatant was removed and kept for analysis (sample 2). The pelleted beads were washed 3 times with 1 ml lysis buffer followed by three washes in TEV-protease cleavage buffer (10 mM Tris-HCl (pH 7.5), 100 mM NaCl, and 0.2% NP-40). Bound proteins were eluted by adding 20 units of TEV protease to the approximate 40 µl of packed beads together with 10 µl 20x TEV buffer (Invitrogen), 2 µl 0.1 M DTT and 125 µl ddH_20. Before the addition of the enzyme, 20 µl of sample (beads included) was kept for analysis and the reactions were incubated overnight at 4°C.

For the second immunoprecipitation, IgG beads were centrifuged at 500 x g. An aliquot of the supernatant (20 µl) containing the cleaved protein was kept for analysis and the rest was added to 250 µl lysis buffer containing the remaining beads. The reaction was resuspended and centrifuged. After three repeats the beads were retained as sample 5 and the supernatant containing the protease cleavage product was incubated with 40 µl of packed Ultralink Immobilized Streptavidin Plus (Pierce) beads prepared in lysis buffer at 4^{o}C for 2-3 h. After incubation the reactions were centrifuged at 500 x g, the supernatant was kept for analysis (sample 6) and the beads were washed four times in lysis buffer. The SBP-tagged proteins were eluted by adding 1 mM D-biotin in 100 µl PBS and shaking at 4^{o}C for 1-2 hrs. The reactions were centrifuged at 500 x g and the supernatant was retained as sample 7 (the final eluate) and the remaining streptavidin beads were resuspended in an equal volume of 2x reducing SDS sample buffer (sample 8) and retained for measuring the efficiency of the biotin elution.

15% of available purified protein (S7) in 5x SDS sample buffer was separated on NuPAGE Novex Bis-Tris Mini Gels (Invitrogen) and analysed with silver stain (Invitrogen) according to the NuPAGE basic staining protocol. The remaining 85% of sample 7 was also separated by SDS-PAGE and was analysed by Coomassie stain. Coomassie stained bands were excised and were sent for mass spec analysis.

2.23.2 ORF4 in the tetracycline inducible system

293T T-REX cells (expressing the tetracycline repressor, selected for with blasticidin at 5 µg /ml media) generated previously in the lab were transfected with pcDNA4/TO-NTAP-ORF4, pcDNA4/TO-ORF4-CTAP as well as pcDNA4/TO-CTAP. After 24 h, media was replaced with antibiotic (including blasticidin) containing media and after a further 24 h cells were harvested into filter sterilised conditioned selection media from 293T T-REX cells containing blasticidin (5 µg/ml). To this, zeocin was added at a concentration of 200 µg/ml. Serial dilutions were set up and selection media was regularly replaced until single distinct colonies were detected. Under sterile conditions, single colonies were isolated and grown up as clonal cell lines.

Once enough cells had grown, each clonal cell line was seeded into two wells of 6-well plates. Upon confluency, expression of the TAP tagged fusion protein was induced in one set of each cell line by adding 1 µg/ml doxycycline (Sigma) whilst the

other set was left non-induced. After incubation at 37°C overnight cells were harvested, washed in PBS, lysed into RIPA buffer, standardised, separated by SDS-PAGE and analysed by western blot as described previously. Best-inducible clones with least leaky expression were chosen for continual passage and TAP pulldown. In order to perform TAP purification, TAP expressing selected clones were grown in 10 T-175 flasks (approximately 2 x 10^8 cells), and were induced with 1 μg/ml doxycycline (Sigma) for 16 h after which cells were washed 3 times in ice-cold PBS and lysed in 5 ml TAP lysis buffer (as above) for 10-15 min. Subsequent TAP purification was performed as described above.

2.24 Yeast-two hybrid screen

For the ORF4 yeast-two hybrid screen the company Proteinlinks (San Diego, CA, USA) was employed. They carried out both LexA and the more specific TetR screen with subsequent identification of binding partners. Full-length ORF4 fused in-frame to the DNA binding domains encoded within the pCWX200 (TetR) and pEG202 (pLexA) yeast expression plasmids did not transform into yeast, predictably due to toxicity. A 176 amino acid truncation of the protein generated by Dr Ian Goodfellow and cloned into the expression plasmids transformed into yeast and did not self-activate transcription. Using this truncated version of the protein a library of 1.4 x 10^7 cDNA clones derived from mouse spleen was screened for the ability to interact with the ORF4 protein. After identification of positive interactors by growth on selective media (X-Gal/Gal and Leu2-/Gal), colonies were retransformed. Growth on selective media using the p53-PIAS1 interaction as a positive control indicated interaction, and positive clones were extracted and sequenced. Sequences of clones were used to identify the binding partners and the information was passed on to our laboratory. Using VNTI and the NCBI BlastX programme the authenticity of the sequences were confirmed and it was verified if multiple interactors were indeed identical clones.

2.25 Confocal microscopy

2.25.1 Green fluorescent protein (GFP) transfections and slide preparation

Cells were seeded at $1x10^5$ cells/ml in antibiotic-free media into 6-well (9 cm^2) dishes containing coverslips, and transfected with either C-terminal (ORF4-GFP) -and N-terminal (GFP-ORF4) GFP fusion constructs using the empty GFP expressing plasmids pEGFPC1 and pEGFPN1 as controls. Analysis of SV ORF4E C-terminal (ORF4E-GFP) and N-terminal (GFP-ORF4E) fusions was also carried out by this approach. On separate occasions the plasmids encoding MNV ORF4 C-terminal truncations Δ 1-19 ORF4-GFP, Δ 1-56 ORF4-GFP and Δ 1-123 ORF4-GFP were transfected into cells. After overnight incubation cells were stained for 30 min at 37°C with a 1:250 dilution of MitoTracker Red 580 (Invitrogen) in DMEM containing 10% FCS and pen/strep. After incubation cells were washed three times in ice cold PBS. Cells were fixed at RT with 4% (w/v) paraformaldehyde (PFA) in 250 mM HEPES for 15 min, after which they were washed 3 times in PBS and quenched using 50 mM ammonium chloride for 10 min followed by 3 PBS washes. Coverslips were subsequently mounted onto slides using moviol containing 4'-6-Diamidino-2-phenylindole (DAPI). Confocal microscopy was carried out using the Zeiss Meta 510 confocal microscope, and images were taken using the LSM 3.2 image software.

2.25.2 Antibody-specific staining

Cells fixed as above were permeabilised with PBS containing 0.2% (v/v) Triton X-100. Slides were washed in PBS, followed by blocking in PBS containing 0.2% (w/v) BSA. In the case of AIF staining of the mitochondria, cells were incubated with Goat anti-AIF D-20 (Santo Cruz Biotechnology). In the case of ER staining cells were incubated with rabbit anti-calnexin antibody (H70 Santa Cruz biotechnology). In the attempt to use the ORF4 protein cross-reactive antibody, cells were incubated with anti-ORF4 generated by the modified immunisation protocol described above. Primary antibodies were diluted in PBS containing 0.2% BSA at antibody dilutions of 1:50, 1:250 and 1:500. After incubation in a humidified chamber for 45 min at RT, slides were washed 3 times in PBS and were incubated for 45 min at RT in a humidified chamber with 1:300 Alexa Fluor® 546 conjugated anti-IgG secondary antibody. Alexa Fluor® 546 donkey anti-goat IgG was used in the case of AIF staining, whereas Alexa

Fluor® 546 goat anti-rabbit IgG was used in the case of calnexin and ORF4 staining. Following incubation and three PBS washes, coverslips were mounted onto slides using moviol containing DAPI and were analysed as above. In all cases, images of the slides incubated with a 1:250 antibody dilution were taken.

2.26 Biochemical localisation

2 x 10^7 RAW264.7 cells were infected with either WT or ORF4 M1 virus at an m.o.i. of 5. After 12 h at 37^{o}C, the control total cell lysates were prepared by washing in PBS and lysing directly into reducing SDS sample buffer. The mitochondria and cytosol of infected cells were separated using a mitochondria isolation kit for mammalian cells (Thermo scientific). The isolated mitochondria were directly suspended into reducing SDS sample buffer whilst due to the high volume the cytosolic fraction was concentrated using the UPPA-protein concentrate kit from G-Biosciences. Fractions were separated on a 15% SDS-PAGE gel and a western blot against the ORF4 protein was performed. In further western blots, a rabbit antibody against poly C-binding protein (PCBP-1) acted as a control for the cytosolic fraction and the AIF antibody acted as a control for the mitochondrial fraction.

2.27 Apoptosis assays

For apoptosis assays, RAW264.7 or BMMΦ cells were seeded at 5x10^5 cells per well of a 24-well plate. After settling in the wells for 24 h cells were infected with an m.o.i. of 5 or treated with 5 µM staurosporine (Sigma). For the RAW264.7 16 h post-infection analysis samples were taken in triplicate with three independent repeats, for the BMMΦ analysis timepoints were taken in duplicate. For the timecourse analysis each timepoint was set up in triplicate. At given timepoints (9, 12, 15, 18 and 21 h post-infection) cells were PBS washed and lysed in 1 ml of 1x cell culture lysis reagent (Promega). 100 µl of lysed cells were the incubated with 100 µl of Glo3/7 assay reagent (Promega) and after incubating at RT for 40 min, luminescence was read using a TD20/20 luminometer (Turner Designs). After separation of lysates by SDS-PAGE, levels of cleaved caspase 3, full-length caspase 3, cleaved caspase 9, full-length caspase 9 and survivin were determined by western blot analysis.

3. Confirmation of ORF4 expression and *in vitro* characterisation of the ORF4 protein

3.1 Introduction

Prior to this study, the potential ORF4 present in the MNV VP1 coding region had not been characterised. Indeed, the initial MNV publication in 2003 (Karst et al., 2003) did not identify this potential fourth open reading frame, but preliminary analysis by our laboratory identified that an ORF existed. On this basis bioinformatic analysis was performed in order to characterise the potential protein that ORF4 encoded. One of the first questions raised was of course whether or not this potential overlapping reading frame protein possessed any similarity to other previously characterised proteins. Additionally, an *in vitro* approach was taken in order to express and subsequently detect a protein from this open reading frame. By employing the MNV reverse genetics system established in our laboratory (Chaudhry et al., 2007) ORF4 mutant viruses were generated and were characterised in tissue culture. The overall aim of this chapter was therefore to preliminarily characterise the ORF4 protein using bioinformatics as well as a number of *in vitro* techniques.

3.2 Results and discussion

3.2.1 Bioinformatic analysis

3.2.1.1 Location and Kozak context

The 642 nucleotide ORF4 is located at the beginning of the MNV subgenomic RNA in a +1 frame relative to ORF2, which encodes the viral capsid protein VP1 (figure 3.1a). The potential ORF4 protein AUG initiating triplet is found at genome position 5069, and the flanking sequences contain a G both at positions -3 and +4, placing it in a strong Kozak context (Kozak, 1984). Interestingly, a GTG immediately before the AUG is highly conserved and could also act as a potential initiation codon, although there is currently no direct evidence to suggest that this is the case (figure 3.1b). However, translation initiation of several viral proteins from codons other than ATG has been documented for many viruses, especially in the context of overlapping open reading frames. Example include the HCV F protein, which uses a GUG or GCG initiation codon (Baril & Brakier-Gingras, 2005); the newly identified overlapping reading frame product of the coronavirus torovirus utilises a conserved CUG codon (Firth & Atkins, 2009); and human T-cell lymphotropic virus type 1 (HTLV-1) can use

GUG and CUG in-frame initiation codons which ensure enhanced translation of the Rex and Tax proteins encoded on a dicistronic mRNA (Corcelette et al., 2000). In recent years, the use of dicistronic mRNAs as a regulatory means of gene expression in eukaryotes has become ever more evident, and includes for example the expression of endogenous fibroblast growth factor-2 (FGF-2) (Blaustein et al., 2009). Hence, regulated expression of the ORF4 protein may also be the case due to the nature the overlapping reading frames.

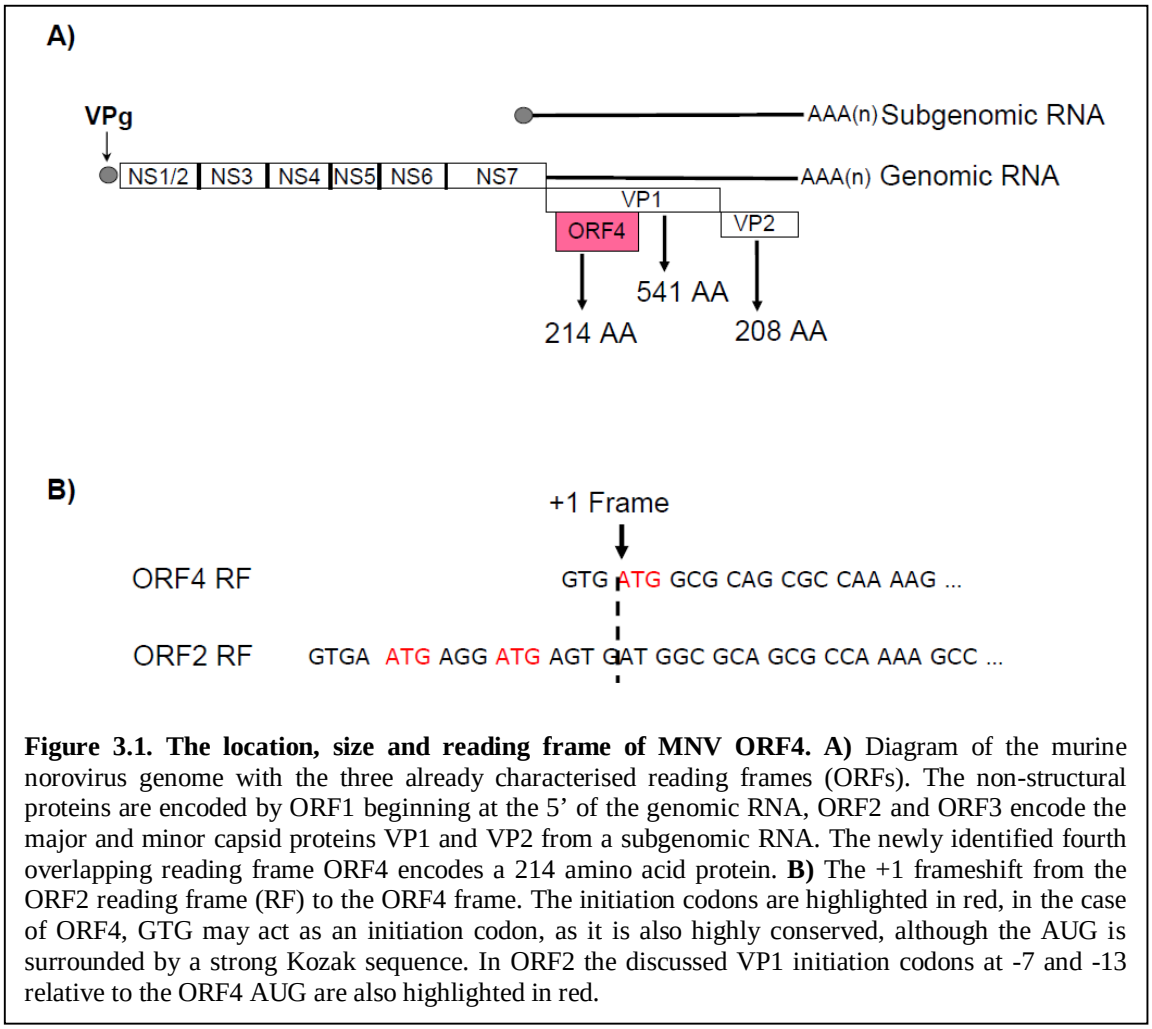


Figure 3.1. The location, size and reading frame of MNV ORF4. A) Diagram of the murine norovirus genome with the three already characterised reading frames (ORFs). The non-structural proteins are encoded by ORF1 beginning at the 5' of the genomic RNA, ORF2 and ORF3 encode the major and minor capsid proteins VP1 and VP2 from a subgenomic RNA. The newly identified fourth overlapping reading frame ORF4 encodes a 214 amino acid protein. **B)** The +1 frameshift from the ORF2 reading frame (RF) to the ORF4 frame. The initiation codons are highlighted in red, in the case of ORF4, GTG may act as an initiation codon, as it is also highly conserved, although the AUG is surrounded by a strong Kozak sequence. In ORF2 the discussed VP1 initiation codons at -7 and -13 relative to the ORF4 AUG are also highlighted in red.

The authentic MNV VP1 initiation codon has yet to be identified as the VP1 ORF contains two potential AUG codons. Whereas the first AUG initiation codon is in a weak Kozak context (U at -3 and A at +4), the initiation codon positioned at -7 is in a stronger, but still not presented in an optimal Kozak context (A at -3 and +4) (figure 3.1b). Indeed, dicistronic mRNAs sometimes contain strong Kozak context initiation codons surrounded by weaker ones (Matsuda & Dreher, 2006, Smith et al., 2005). Translation from different initiation codons in bicistronic RNAs is ensured by leaky

scanning of the ribosome, which involves forward or backward movement of the ribosome from the strong Kozak initiation site. A precedent for this has already been reported in turnip yellow mosaic virus, where the ORF encoding the p69 protein is in a weak Kozak context 7 bases upstream from the strong context ORF encoding the p206 protein (Matsuda & Dreher, 2006). However, it is unclear whether or not leaky scanning actually occurs in the VPg-dependent translation employed by MNV, or whether the ORF4 strong Kozak initiation codon plays a role in ribosome recruitment and leaky scanning assisting VP1 translation.

3.2.1.2 Conservation of the ORF4 protein amino acid sequence

Another interesting observation is that in addition to the genomic conservation (discussed in chapter 1), the primary amino acid sequence of the ORF4 protein is highly conserved and also contains several conserved polyproline motifs in the N-terminus (figure 3.2). Polyproline motifs (minimum sequence PxP) are frequently involved in SH3 binding and recent studies performed by Dr Andrew MacDonald, have demonstrated that the ORF4 protein has SH3 binding activity (data not shown).

Comparison of the MNV ORF4 protein with the SV ORF4E protein showed that there is relatively little homology between the smaller, 161 amino acid SV protein and the 214 amino acid protein encoded by MNV ORF4 (data not shown). Similarly, little homology was observed in comparisons between the RHDV and SMSV potential overlapping reading frame proteins and MNV ORF4 and SV ORF4E (data not shown). Between MNV ORF4 protein amino acids 84-124 and SV ORF4E protein amino acids 92-132, there is 39% amino acid identity of 41 amino acids [using LALIGN server, (Huang & Miller, 1991)]. Similarly, alignment of MNV ORF4 protein amino acids 10-155 and SV ORF4E protein amino acids 23-161 reveals 29.4% identity over this 138 amino acid region [using EMBOSS alignment programme, (Rice et al., 2000)]. Such a low percent identity does suggest there may be differences in function between the MNV ORF4 protein and the SV ORF4E protein, although SV also contains a number of proline motifs which align with the proline residues present in MNV (data not shown). Most interestingly, alignments of the MNV ORF4 protein with hypothetical proteins translated from the ORF2 coding region in a +1 frame relative to VP1 for a number of caliciviruses (Human norovirus GII, SV, PEC, FCV, SMSV, RHDV, Tulane, and Newbury-1) revealed that although stop codons are frequently encountered in this reading frame, putative amino acid stretches do align with the MNV ORF4

protein (data not shown). Like the SV ORF4E protein, this was the case for a number of proline residues. Hence even though many related caliciviruses may have lost the functionality of this ORF, the presence of putative amino acid sequences which align with ORF4 protein may suggest these sequences are in fact evolutionary remnants. In an experimental approach, comparative analysis between the MNV and SV overlapping reading frame proteins was examined and results can be seen in chapter 6. Noteworthy is that no significant homology can be seen between the MNV ORF4 protein and other overlapping reading frame proteins such as those of influenza, HCV, TMEV, HEV or indeed any previously described protein present in various databases.

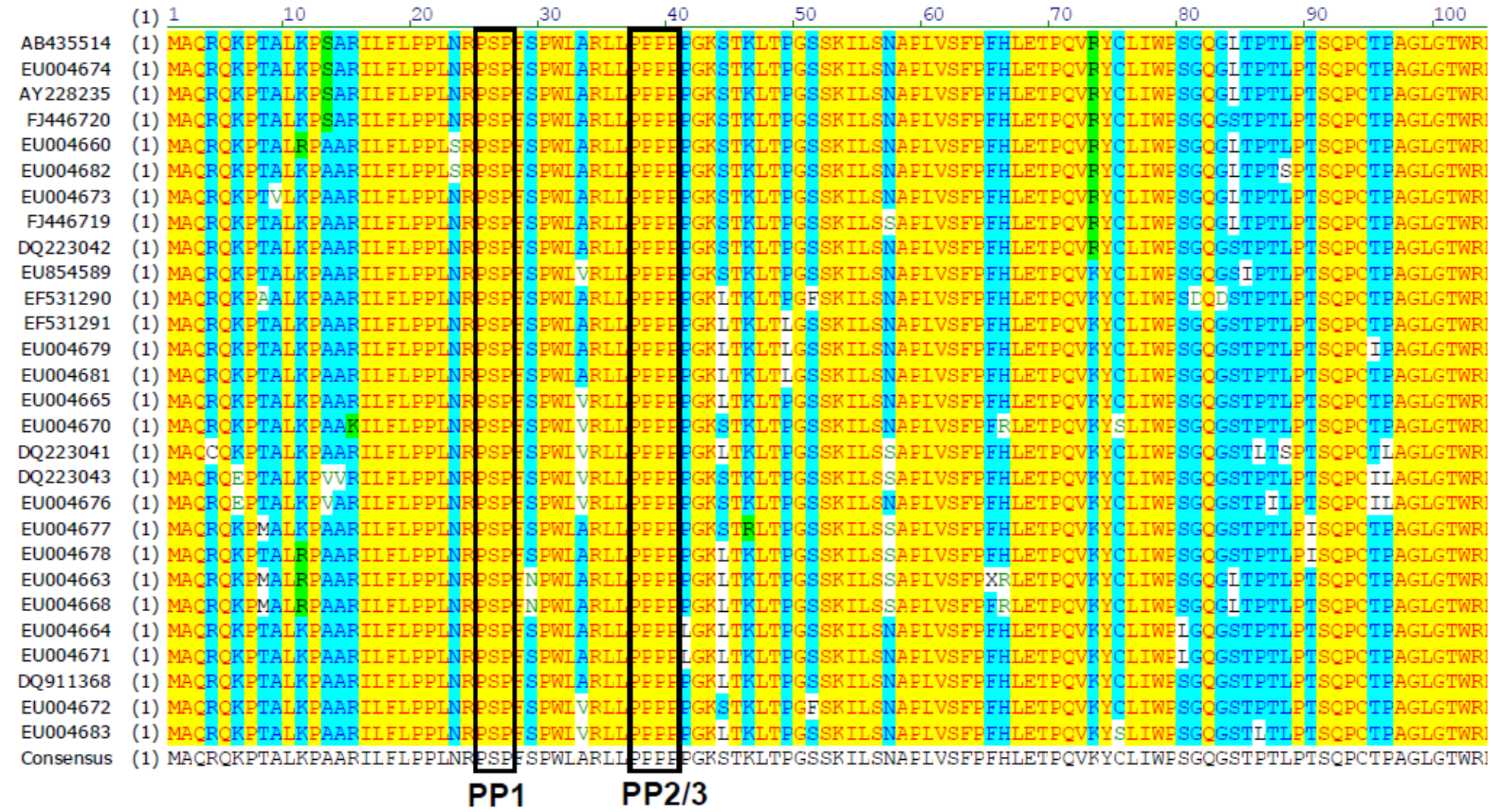


Figure 3.2. Bioinformatic analysis of ORF4 protein amino acid sequences (continued overleaf). Alignment of the amino acid sequence of all the currently published MNV strains (duplicates removed) also revealed a high degree of conservation of all the putative ORF4 proteins at the amino acid level. Between the highlighted lines are the positions of four highly conserved polyproline motifs.

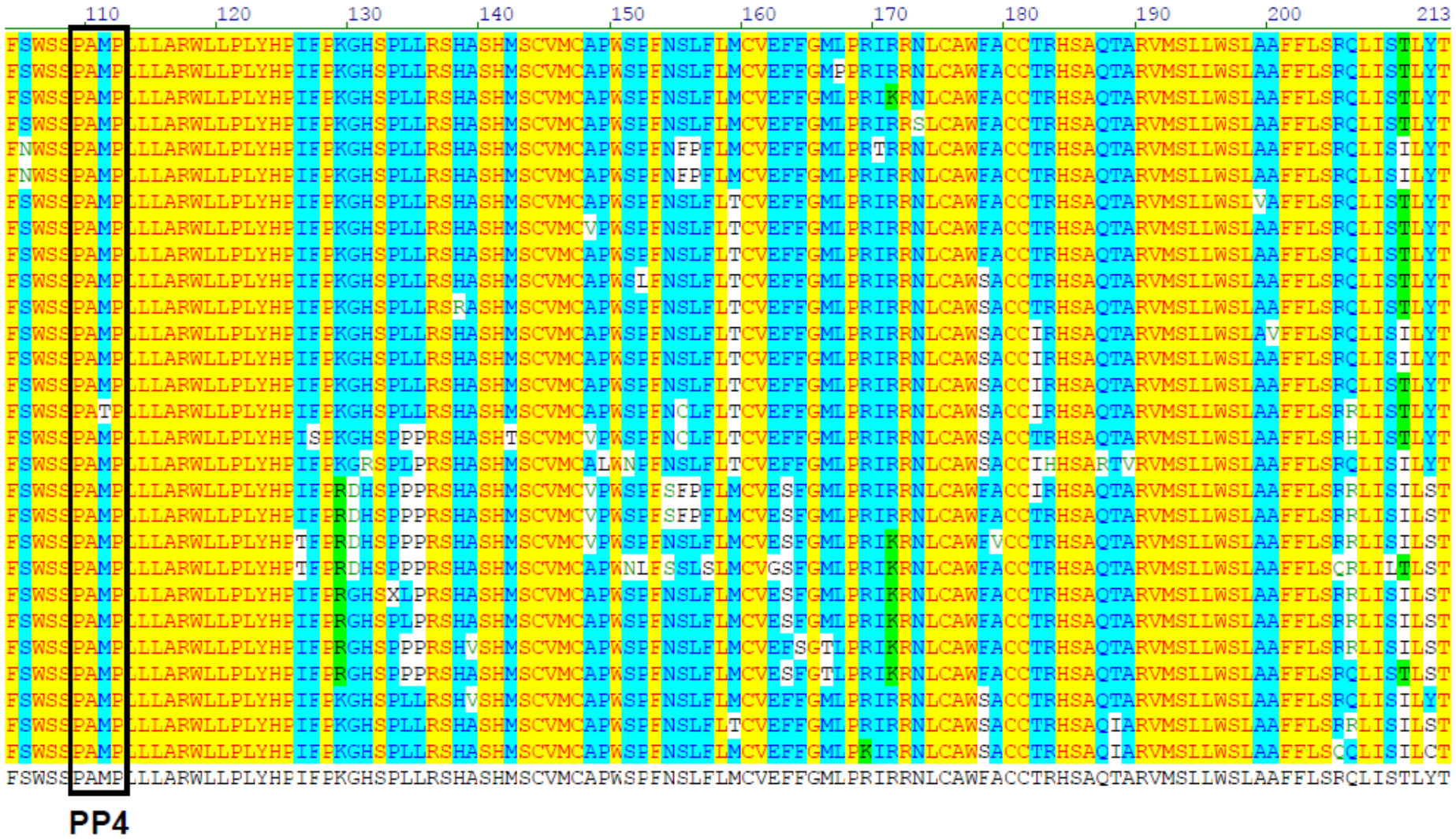


Figure 3.2 (continued)

3.2.2 Detection of MNV ORF4 expression

3.2.2.1 *In vitro* transcription and translation reactions

In order to determine if a protein could be produced from the MNV potential fourth open reading frame, ORF4 was cloned into an expression plasmid (pcDNA3.1+) which, in addition to a T7 polymerase promoter also contains a CMV promoter to allow expression once transfected into cells. S^{35} methionine radiolabelled TNTs were performed with the ORF4 expression plasmid (pcDNA3.1+ORF4) and a construct encoding the subgenomic RNA from a tissue-culture adapted MNV strain (pSportMNVSG4*). Results revealed that a protein of a similar size (approximately 23 kDa) was produced from both constructs (figure 3.3a). The identity of VP1 and VP2 was subsequently confirmed by immunoprecipitation (figure 3.3b). Once a successful ORF4 protein cross-reactive antibody was generated using a modified immunisation programme (detailed in section 3.2.2.2), the identity of the ORF4 protein was also confirmed by immunoprecipitation from these TNTs (figure 3.3b).

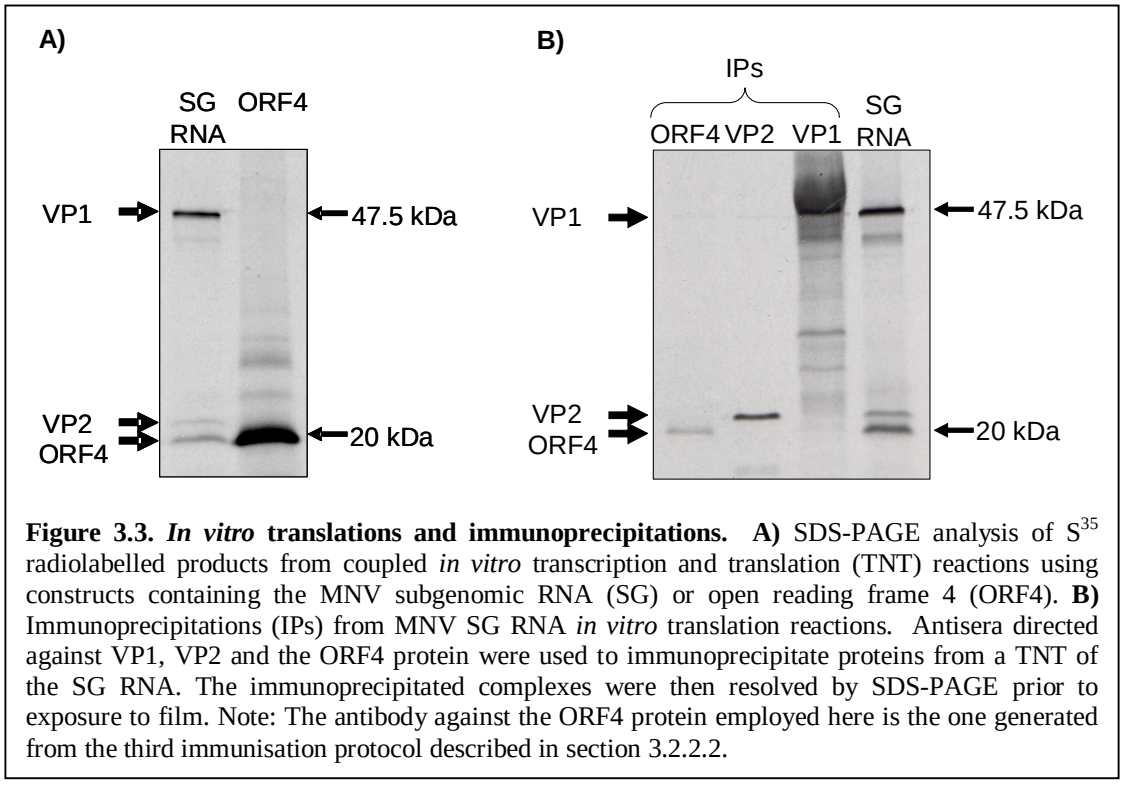


Figure 3.3. *In vitro* translations and immunoprecipitations. A) SDS-PAGE analysis of S^{35} radiolabelled products from coupled *in vitro* transcription and translation (TNT) reactions using constructs containing the MNV subgenomic RNA (SG) or open reading frame 4 (ORF4). **B)** Immunoprecipitations (IPs) from MNV SG RNA *in vitro* translation reactions. Antisera directed against VP1, VP2 and the ORF4 protein were used to immunoprecipitate proteins from a TNT of the SG RNA. The immunoprecipitated complexes were then resolved by SDS-PAGE prior to exposure to film. Note: The antibody against the ORF4 protein employed here is the one generated from the third immunisation protocol described in section 3.2.2.2.

Although the predicted product of ORF4 is slightly larger than that of ORF3, it appeared to run at a lower position on the SDS-PAGE gel, which may be because the protein is processed by cellular proteases or may simply be due the characteristics of the protein (charge, hydrophobicity, etc.). Bioinformatic analysis does predict that the

ORF4 protein possesses an extremely high isoelectric point (PI) of 11.8. The PI is the pH at which the protein carries no net electrical charge, and consequently the ORF4 protein is predicted to be highly basic. The detection of the ORF4 protein from an expression construct, as well as from the MNV subgenomic RNA was one of the first indications that this fourth reading frame is authentic, and so further experiments were performed to investigate the role of ORF4 in the virus life cycle.

3.2.2.2 Generation of an ORF4 protein reactive antibody

One of the most definitive approaches to confirm that an ORF is expressed is the ability to detect the protein it encodes using specific antisera. Therefore, the generation of an antibody capable of detecting the ORF4 protein was a main priority at the beginning of the project. Unfortunately, similarly to characterised MNV non-structural proteins, mouse MNV immune sera were not capable of detecting recombinant his-tagged ORF4 protein or a protein of the predicted size from infected cell lysates by western blot (data not shown). The production of an ORF4 protein reactive antibody was particularly difficult as recombinant C-terminal his-tagged ORF4 protein (ORF4-his) expressed and purified from *E. coli* was insoluble. Additionally, due to bioinformatically predicted transmembrane regions present in the C-terminus (data not shown), the ORF4 protein is believed to be very hydrophobic, properties which make production and purification to the quantities required for immunisation difficult. The first approach in generating an ORF4 protein cross-reactive polyclonal antibody was to produce recombinant full-length his-tagged ORF4 protein and immunise rabbits using a traditional approach as illustrated in figure 3.4a.

Unfortunately, the antibody generated by this method (protocol 1) was incapable of detecting virus expressed ORF4 protein by western blot. Although this could have simply indicated that the ORF4 protein is not expressed during infection, the antibody also failed to detect the protein expressed from cDNA transfected into cells. Similarly it was incapable of immunoprecipitating the ORF4 protein expressed *in vitro*. Even though the antibody detected full-length recombinant ORF4-his, this was due to specific cross reactivity with the his-tag (data not shown).

In an attempt to produce a second antibody, several GST-fused peptide fragments of the ORF4 protein were designed with the aim of expressing and purifying them for subsequent immunisation. This also proved to be difficult as various fragments of the protein failed to express in *E. coli* (data not shown). One successful approach (protocol

2) was finally achieved by immunising rabbits (figure 3.4b) with two distinct potentially immunogenic peptides (peptide 1 and 2) chosen by the immunisation company Eurogentech and present in the N-terminus of the ORF4 protein (figure 3.5a). Selection of these peptides was based on hydrophilicity, antigenic index, surface probability as well as alpha helix predictions. In order to enhance immunogenicity, peptide 1 (ORF4 protein amino acid sequence 41-55) and peptide 2 (ORF4 protein amino acids 62-74) were coupled to KLH as a carrier and immunisation was performed using a rapid 28 day immunisation programme, after which the two anti-peptide antibodies were affinity purified on the above peptides (figure 3.4b). Subsequent analysis revealed that only one of these anti-peptide antibodies (α-P1) was successful in detecting the ORF4 protein by western blot (figure 3.6a) and immunoprecipitation of *in vitro* translated ORF4 product (data not shown). Drawbacks of this antibody included a substantial amount of cross-reactive non-specific bands, and the fact that a high concentration of antibody (1:100 dilution for western blot) was required to detect the protein (figure 3.6a).

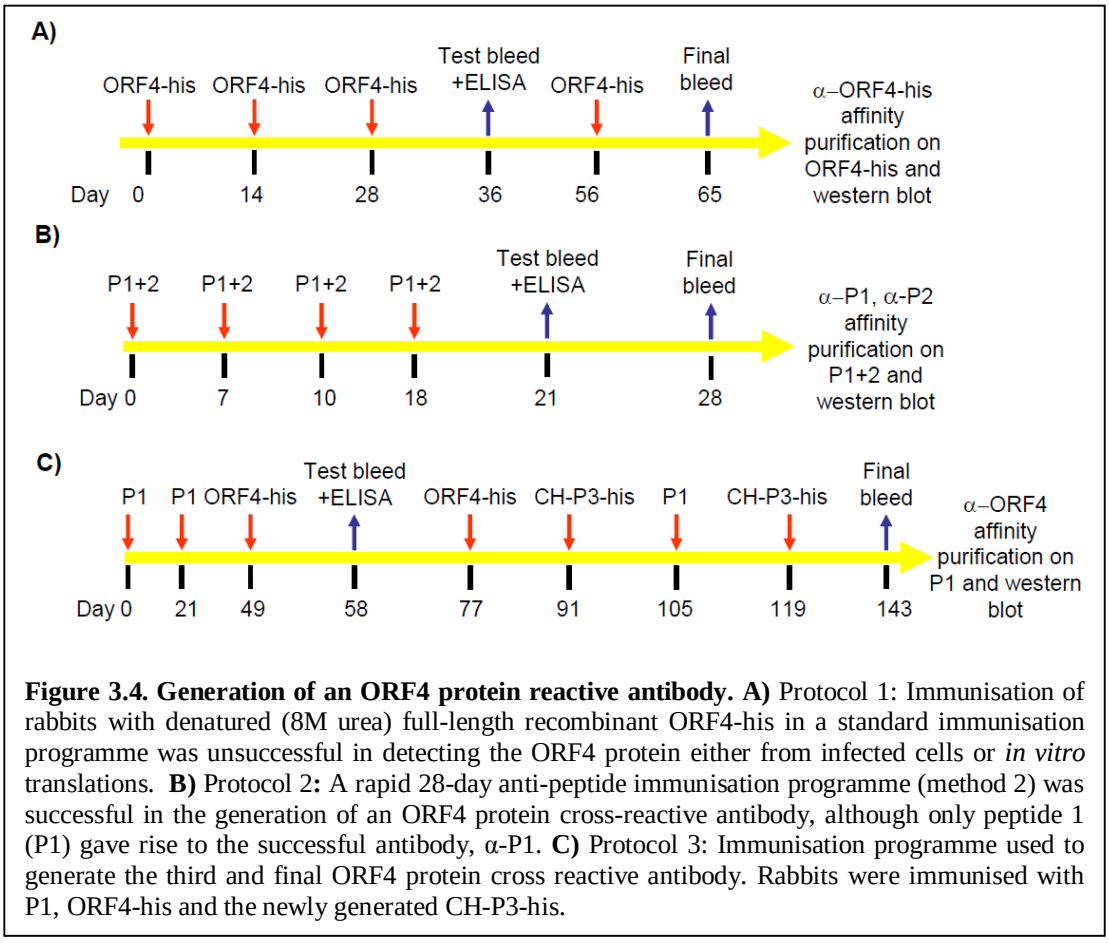


Figure 3.4. Generation of an ORF4 protein reactive antibody. A) Protocol 1: Immunisation of rabbits with denatured (8M urea) full-length recombinant ORF4-his in a standard immunisation programme was unsuccessful in detecting the ORF4 protein either from infected cells or *in vitro* translations. **B)** Protocol 2**:** A rapid 28-day anti-peptide immunisation programme (method 2) was successful in the generation of an ORF4 protein cross-reactive antibody, although only peptide 1 (P1) gave rise to the successful antibody, α-P1. **C)** Protocol 3: Immunisation programme used to generate the third and final ORF4 protein cross reactive antibody. Rabbits were immunised with P1, ORF4-his and the newly generated CH-P3-his.

Finally, a more specific ORF4 protein-reactive antibody was produced in rabbits using a modified prime boost strategy (protocol 3). Rabbits were first immunised with

peptide 1 (previously found to be immunogenic by protocol 2), and were then boosted with recombinant full-length ORF4-his (figure 3.4c). Although ELISAs on the peptide and ORF4-his performed by Eurogentech showed that ORF4 protein reactivity was good (data not shown), initial western blot analysis of infected cells revealed very little improvement over the previous antibody in terms of non-specific cross reactivity and quantity of the antibody required to detect the protein (data not shown). This may well be linked to the fact that ELISA assays recognise conformational epitopes in contrast to western blot analysis of lysates separated by SDS-PAGE where linear epitopes are presented.

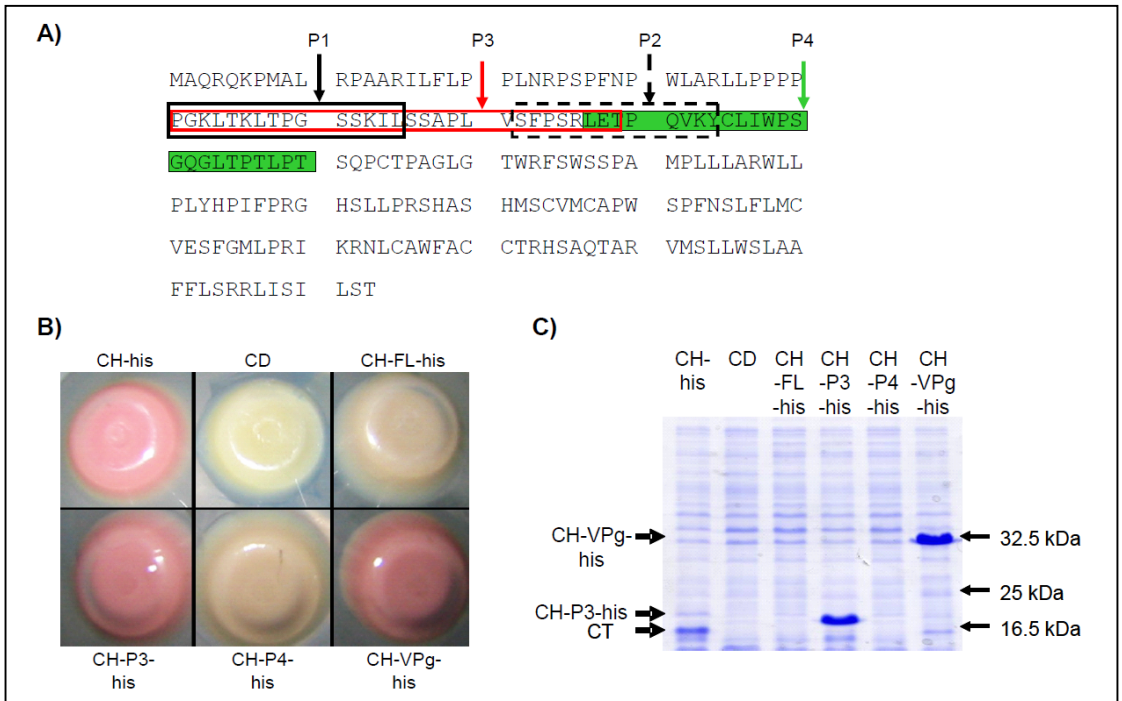


Figure 3.5. Position of the ORF4 peptides and production of CH-P3-his. A) To detect the ORF4 protein two N-terminal anti-peptide antibodies were generated against the highlighted peptide 1 (P1) and peptide 2 (P2). Expression of two longer fusion peptides (P3 and P4) was attempted in order to generate a more efficient ORF4 protein cross-reactive antibody. **B)** Characteristic red colour of bacterial pellets expressing either the cherry tag alone pSCherry2 (CH-his) or cherry tagged proteins (CH-VPg-his, CH-P3-his) over the yellow pellets of the negative control pSCodon1.2 (CD). Those proteins expressed in low levels (CH-P4-his, CH-FL-his) showed a slightly orange colour. **C)** Coomassie stained 15% SDS-PAGE gel containing lysates of *E.coli* expressing the various Cherry-fusion proteins: The gel indicates that CH-P3-his and CH-VPg-his were induced. As above, pSCherry2 (CH) acted as a positive control, whereas pSCodon1.2 (CD) was a negative control. Induction was not seen for the full-length cherry tagged ORF4 protein (CH-FL-his) or CH-P4-his.

It was anticipated that immunisation with a further antigenic peptide could generate a good ORF4 protein reactive antibody. Therefore, attempts were made to express the full-length ORF4 protein as well as two ORF4 encoded peptides (peptide 3 and 4) as soluble recombinant proteins fused to a red polypeptide (cherry tag), which is the 11

kDa haeme binding domain of cytochrome *c* (figure 3.5a). The colouration allows instant identification of expressed proteins and as the cherry tag is highly soluble this can increase the solubility of the target protein. The cherry expressing plasmid, pSCherry2 also expresses tRNAs for six rare codons, and so enables expression of proteins which contain rare codons. As immunisation with peptide 1 was known to give an ORF4 protein cross-reactive antibody, the sequence was incorporated into peptide 3, which contained amino acids 41-69 (figure 3.5a). Peptide 4 (which overlaps with peptide 3 at the N-terminus) contains the amino acid sequences 67-90 of the ORF4 protein. MNV VPg acted as a positive control as it is known to be soluble and expresses in bacterial cells. As expected, the bacteria (*E. coli*) produced a characteristic red colour upon protein expression (figure 3.5b). Upon induction, cherry fused full-length ORF4 protein (CH-FL-his) and peptide 4 (CH-P4-his) showed low levels of expression seen by the slight orange colour compared to the negative control pSCodon1.2 (CD). Cherry fused peptide 3 (CH-P3-his) on the other hand had the characteristic red colour seen for the positive control pSCherry2 (CH-his), which contains the cherry tag alone (figure 3.5b). SDS-PAGE confirmed the initial visual confirmation that CH-P3-his was expressed (figure 3.5c). This allowed large scale induction and purification for immunisation. Therefore, rabbits were subsequently boosted twice with CH-P3-his and once with peptide 1 (figure 3.4c). This approach gave a good reactive antibody against the ORF4 protein (figure 3.6b).

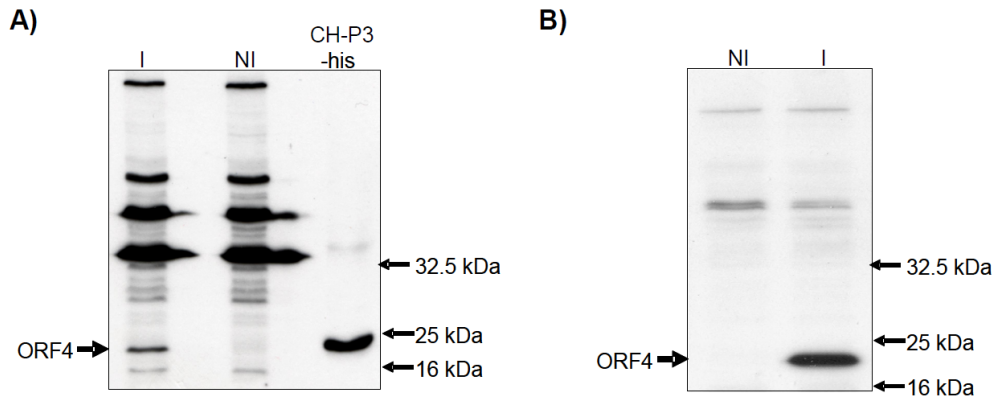


Figure 3.6. Differences in the specific cross-reactivity of antibodies generated by protocols 2 and 3 (as described in figure 3.5). Infected (I) and non-infected (NI) RAW264.7 mouse macrophage cells were lysed 12 hours post-infection and were separated by SDS-PAGE. Western blot analysis was performed using the anti-peptide antibody generated by protocol 2 **(A)** and the antibody generated by the more successful protocol 3 **(B).** In the case of (A), CH-P3-his acted as a positive control.

3.2.2.3 Western blot analysis

After generation of a suitable ORF4 protein reactive antibody, the ORF4 protein was detected in RAW264.7 mouse macrophage cells lysed 12 h after m.o.i. of approximately 4 (figure 3.7a).

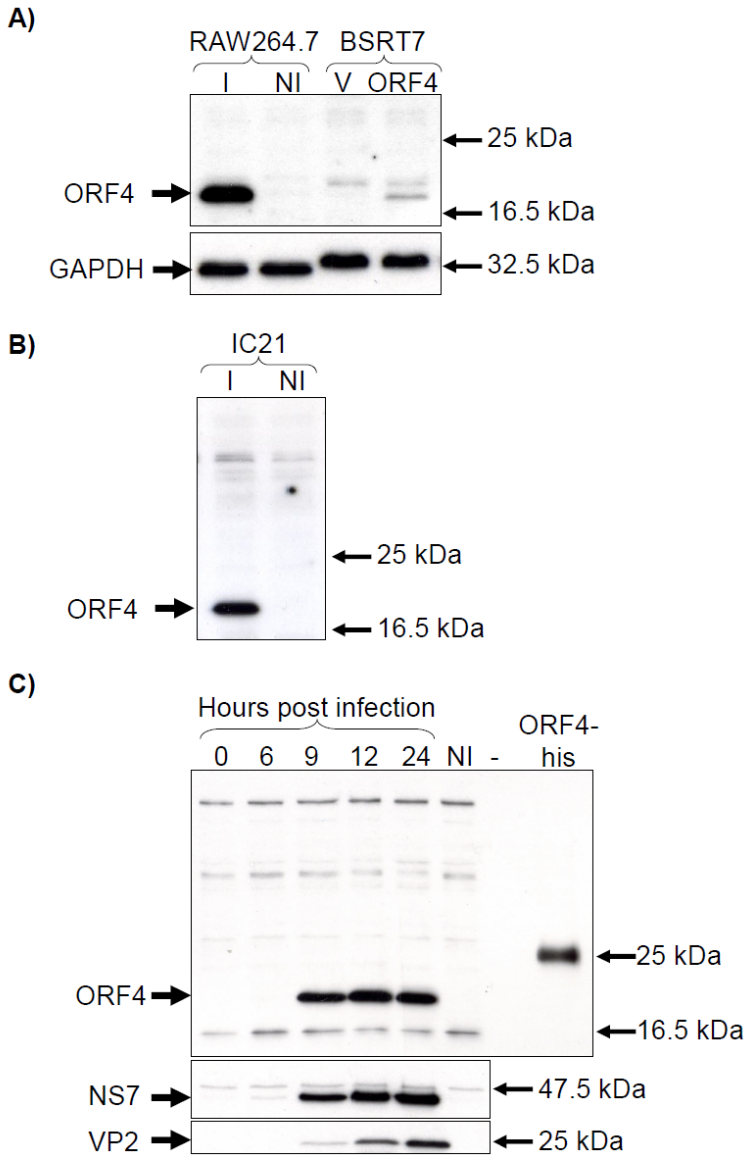


Figure 3.7. Detection of the ORF4 protein during virus infection. A) Western blot of infected (I) and non-infected (NI) RAW264.7 mouse macrophages lysed 12 hours post-infection and separated by SDS-PAGE, showing the ORF4 protein and the cellular GAPDH as a control. Adjacent are cell lysates from BSRT7 cells infected with FPV-T7 and subsequently transfected with the vector (V) pcDNA3.1+ or the ORF4 protein expression construct pcDNA3.1+ORF4. Cells were harvested 16 hours post transfection. **B)** Western blot of infected IC21 mouse macrophages treated as RAW264.7 cells described above. **C)** Western blot of SDS-PAGE separated lysates from infected RAW264.7 cells taken during a timecourse of infection demonstrating ORF4 protein expression, as well as other viral proteins such as the viral polymerase NS7 and the minor capsid protein VP2. Non-infected cells acted as a negative control and recombinant ORF4-his acted as a positive control.

Western blot analysis revealed that this protein is the same molecular weight as a protein present in BSRT7 cells (cell line derived from BHK cells) transfected with the ORF4 expression construct pcDNA3.1+ORF4 (figure 3.7a). However, the ORF4 protein was only detected if expression was boosted by infecting with FPV-T7 (Fowlpox virus expressing T7 polymerase) prior to transfection, which was possibly due to a fast turnover rate of the ORF4 protein in BSRT7 cells. This western blot provided the first evidence in infected cells that ORF4 is an authentic open reading frame and that the protein is expressed during infection of RAW264.7 cells. Furthermore, the ORF4 protein was also detected following infection of IC21 mouse macrophages (figure 3.7b), confirming that expression of the ORF4 protein during infection was not limited to the RAW264.7 macrophage cell line.

In order to examine the kinetics of ORF4 protein expression during infection, RAW264.7 cells were infected at high m.o.i. and protein samples were harvested at various times post-infection. The ORF4 protein was detected from 9 h post-infection, which is comparable to the appearance of the viral minor capsid protein VP2 (figure 3.7c). In contrast, detection of NS7 was observed as early as 6 h post-infection, although such differences are frequently influenced by the affinity of a particular antibody.

3.2.3 Generation and characterisation of ORF4 mutants

3.2.3.1 ORF4 mutants: Design, generation and recovery by reverse genetics

To examine the requirement for ORF4 in the MNV life cycle, three mutants, which introduced stop codons at different locations in ORF4 (figure 3.8a) were generated by overlap PCR mutagenesis initially using the full-length infectious MNV clone pT7MNV3'Rz as a template. The resulting 1.6 kb fragment was subsequently cloned into pT7MNV3'Rz using naturally occurring restriction sites. Due to the nature of the overlapping reading frames, the mutations were designed not to affect the amino acid sequence of the major capsid protein VP1. Three mutants (figure 3.8b) containing the stop codon TAG at different positions in ORF4 were generated through single point mutations of the leucine encoding TTG (M1 and M10), and the tryptophan encoding TGG (M20). The mutants M1, M10 and M20 contain stop codon insertions at codon positions 17, 99 and 196 of ORF4. These correspond to the following nucleotide substitutions M1 T5118A, M10 T5364A and M20 G5655A.

To ensure that the inserted stop codons (confirmed by sequencing) did indeed terminate ORF4 protein translation and did not disrupt the production of the capsid proteins, the subgenomic RNA of these mutants was *in vitro* translated. As anticipated, the production of VP1 and VP2 was not affected in any of the ORF4 mutants (figure 3.8c). For the mutants M1 and M10 no ORF4 protein was seen, and for M20, which is only a C-terminal ORF4 protein truncation, the translated protein was slightly smaller than WT ORF4 protein (figure 3.8c). A feature common to *in vitro* translation of the MNV subgenomic RNA is internal initiation of the capsid protein. Interestingly, internal initiation appeared to be significantly stronger from the subgenomic RNA of the M1 mutant (figure 3.8c). One explanation for this phenomenon could be that the ORF4 region is no longer occupied by translating ribosomes, thus there is a higher probability of VP1 internal initiation.

It was also confirmed that the knockout mutation M1 lay in a region of the 5' MNV subgenomic RNA previously shown to be single-stranded by biochemical structure probing of the 5' end of the subgenomic RNA (performed by Dr Surender Vashist) (data not shown). Unfortunately the positions of M10 and M20 extended beyond this mapped region, although predictions using the server m-fold also confirmed that the mutations were located in loop regions rather than stems. Consequently, it was concluded that RNA secondary structure was largely unaltered in all mutants.

Once the cDNA clones had been generated, ORF4 mutant viruses were recovered using the established MNV reverse genetics system (Chaudhry et al., 2007). Analysis by western blot revealed that there was no difference in expression levels of NS7 during the recovery of M1, M10 or M20 compared to wild-type (WT) virus (data not shown). Western blot of SDS-PAGE separated lysates of cells transfected with the clone of virus encoding a frameshift in the polymerase (FS) (thus showing a truncated band by western blot) as well as non-transfected cells acted as a negative control. Titrations of the recovered mutant viruses also showed them to have a similar titre to WT ranging between 10^3 and 10^4 virus particles per ml of lysate (data not shown).

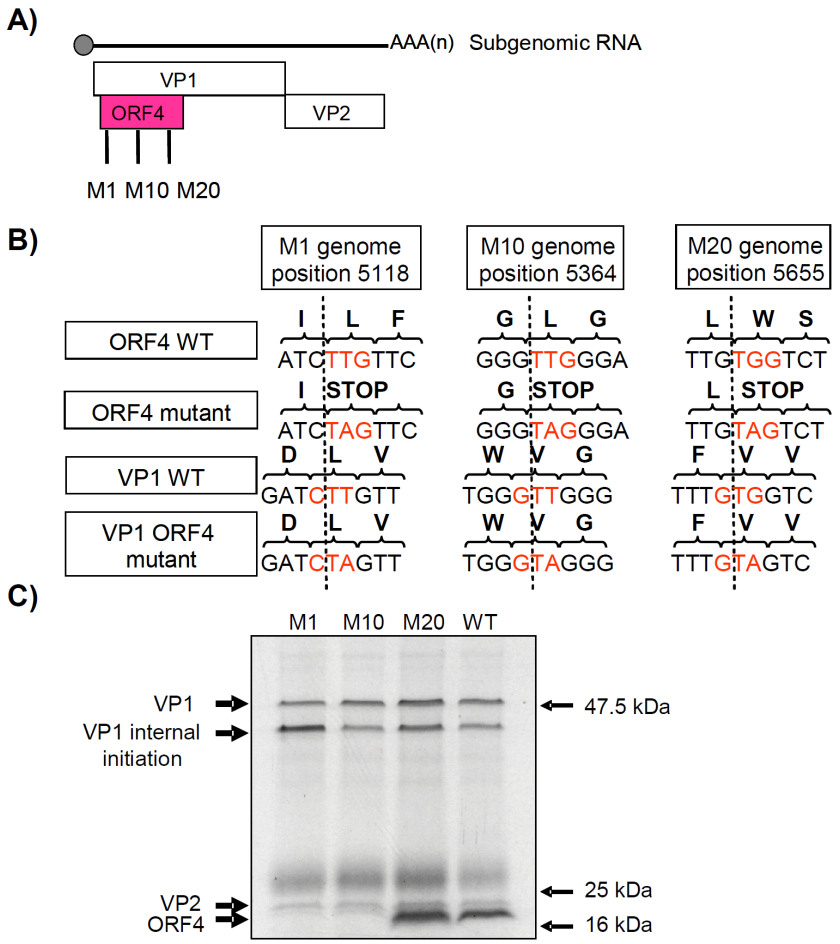


Figure 3.8. Generation of ORF4 mutants A) Schematic diagram showing the three positions into which stop codons were inserted into the ORF4 protein coding sequence in order to generate mutants. **B)** Genome position of the ORF4 mutants highlighting the changes in nucleotide sequence required to generate the mutants, although the amino acid sequence (highlighted above the codons) of VP1 remained unaffected due to the degeneracy of the genetic code. **C)** *In vitro* translation of ORF4 mutated MNV subgenomes. The subgenomic region of the wild-type full-length MNV clone (pT7MNV3'Rz) and the full-length clone containing the ORF4 mutations was amplified by PCR to incorporate a T7 promoter and products were used for *in vitro* transcription and translation assays prior to analysis by SDS-PAGE.

3.2.3.2 Initial characterisation of mutants

After recovery, the ORF4 mutant viruses were used to infect RAW264.7 cells in order to generate high titre stocks. RT-PCR and sequencing confirmed that after recovery and initial passage the viruses still contained the mutations in ORF4 (data incorporated as part of figure 3.10b - see next section). Thus, these results suggested that expression of the ORF4 protein is not essential for virus recovery or viability in tissue culture. To confirm the lack of ORF4 expression in the mutants, western blot analysis of lysates from RAW264.7 cells infected with the ORF4 mutants was performed. As expected,

no protein was detected in cells infected with either M1 or M10 (data incorporated as part of figure 3.10c - see next section).

In cells infected with virus encoding the C-terminally truncated M20, a slightly larger faint band could be seen (figure 3.10c). Such an observation for M20 was not surprising as like any truncated protein, the ORF4 product from M20 was likely to be misfolded and was probably ubiquitinated in preparation for subsequent degradation. Single (data not shown) and multi-step growth curve analysis indicated that there was no significant difference in the growth kinetics of wild-type and mutant viruses (figure 3.9), indicating that a lack of the ORF4 protein was not associated with reduced replication efficiency tissue culture.

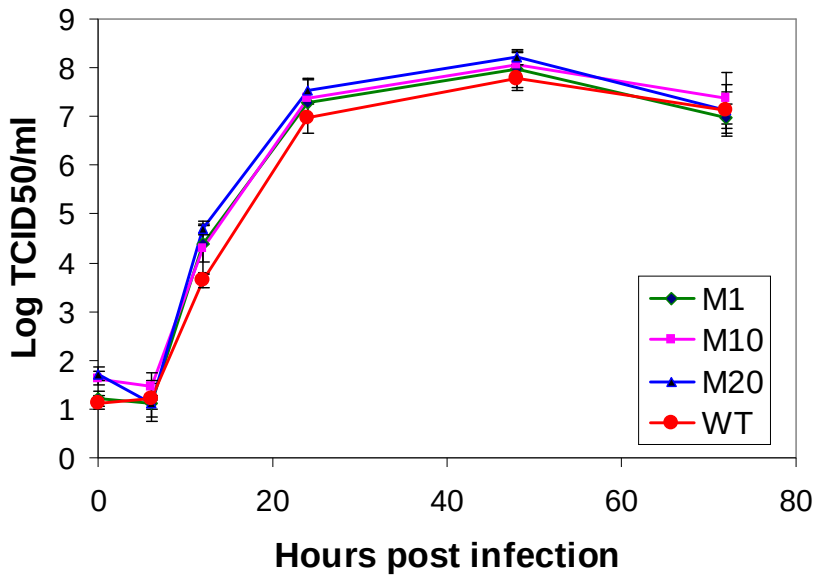


Figure 3.9. ORF4 expression is not required for virus replication in tissue culture. A) Multi-step growth curves (low m.o.i.) infection demonstrating no observable difference in viral titres between the ORF4 mutants and WT virus. RAW264.7 cells were infected at an m.o.i. of 0.01 and infections were frozen at given timepoints. Viral titres were subsequently determined by tissue culture infectious dose 50 assays (TCID50). Timepoints for individual viruses represent the means of three independent repeats; error bars represent the standard error between repeats.

3.2.3.3 Loss of ORF4 results in a fitness cost

Although no difference in growth kinetics of the ORF4 mutants was seen in tissue culture, the high degree of genetic conservation between isolates indicates that there is evolutionary pressure to conserve this reading frame. Mutant viruses can also be studied by other approaches in cell culture in order to detect any possible attenuation, for example by assaying viral fitness in direct comparison to the WT virus, or simply through serial passage. Therefore, the generated ORF4 mutants described above were

passaged five times by low m.o.i. infection of RAW264.7 mouse macrophages as depicted in figure 3.10a.

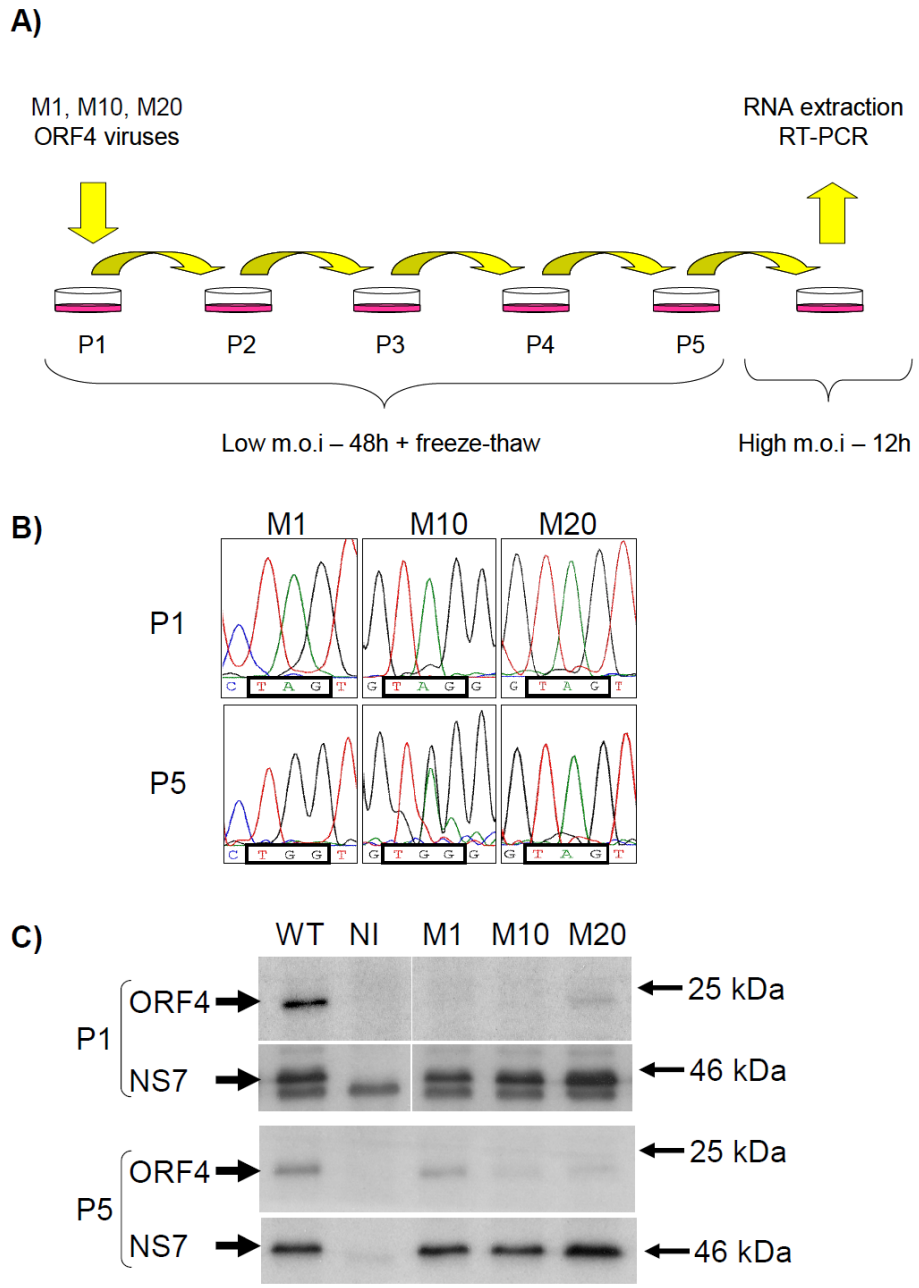


Figure 3.10. Serial passage of the ORF4 mutant viruses revealed phenotypic reversion. A) The ORF4 mutant viruses M1, M10 and M20 were used to infect RAW 264.7 cells at low m.o.i. for 5 passages. Passage 5 viruses were then used to infect RAW264.7 cells at the high m.o.i. required for viral RNA extraction and RT-PCR. Note: Passage 1 refers to this experiment, and the virus used to inoculate the cells was sequence verified high titre passage 2 virus following virus recovery as described previously. **B)** Chromatograms from sequencing reactions of passage 1 (P1) and passage 5 (P5) viruses. **C)** Lysates were generated by infecting RAW264.7 cells with passage 1 and 5 viruses of the ORF4 mutants M1, M10 and M20. Lysates were also prepared from non-infected cells (NI) and cells infected with WT MNV. Lysates were separated by SDS-PAGE prior to western blot analysis using antibodies against the ORF4 protein and viral polymerase (NS7).

After 5 passages in tissue culture, alterations of the TAG stop codon in M1 and M10 to TGG, restoring ORF4 expression were observed (figure 3.10b). Most importantly, the inserted TGG codon is not seen at either of these positions in any of the currently sequenced murine norovirus strains indicating that there was clear pressure on the virus to restore this reading frame. The reason as to why in both cases a G is preferentially inserted rather than the original wild-type base (T for both M1 and M10) is however unclear. The viral polymerase may preferentially insert a certain base when undergoing an error, which is estimated to occur at a frequency similar to related RNA viruses of approximately 10^{-3} to 10^{-4} (Castro et al., 2005). Noteworthy is that in all three cases, (i.e. wild-type, ORF4 mutant, and ORF4 expression restored virus), the amino acid sequence of the capsid remains unaltered due to the degeneracy of the genetic code. Western blot analysis from viruses infected cells after 5 passages in tissue culture confirmed the restoration of ORF4 expression in M1 and M10 (figure 3.10c). As previously mentioned, the slightly larger fainter band seen for M20 was most likely a ubiquitinated form of the truncated protein (figure 3.10c). The reason why no revertants were seen for M20 may lie in the fact that as the protein is only truncated by 19 amino acids, it still contains some, if not all of its function, hence there was less pressure to restore expression of the C-terminal 20 amino acids.

Interestingly, the restoration of ORF4 expression (repeated in two independent experiments for M1) could only be seen when cells were seeded at the high density of $1.2x10^6$/well in $9cm^2$. When viruses were passaged in cells seeded at low cell seeding density ($6x10^5$/well in $9cm^2$), no reversion was seen for any of the mutants by passage 5 or indeed passage 10 (data not shown). This raised concerns over whether or not growth curves, which were performed at low cell seeding density, gave an accurate representation of the effect of ORF4 mutations on virus growth kinetics. Consequently, a virus yield assay at 48 h post-infection, using the ORF4 knockout virus M1 was performed at low vs. high cell seeding density. There was no statistically significant difference between the yield of M1 vs. WT virus in cells seeded at high or low density (analysis performed using the unpaired T-test at 95% confidence) (figure 3.11a). However, a single-step growth curve performed at high seeding density revealed that from 15 h post-infection, the levels of viral VP1 were reduced for M1 in comparison to WT (figure 3.11b). Whilst densitometry analysis revealed that at 15 h VP1 levels were 22% higher in WT infected cells, the difference at 18 h (79%) and 21 h (60%) was significantly higher. This observation was also made when levels of the viral

polymerase (NS7) were compared (data not shown). In contrast, no significant difference between the viral protein levels could be seen at the two earlier timepoints (9 and 12 h), and the levels of the cellular control GAPDH was comparable in all samples (figure 3.11b). These findings contrast previous and frequently repeated data performed at low seeding density, where no difference was seen in viral protein levels in either multi- (data not shown) or single-step growth curves (3.11c).

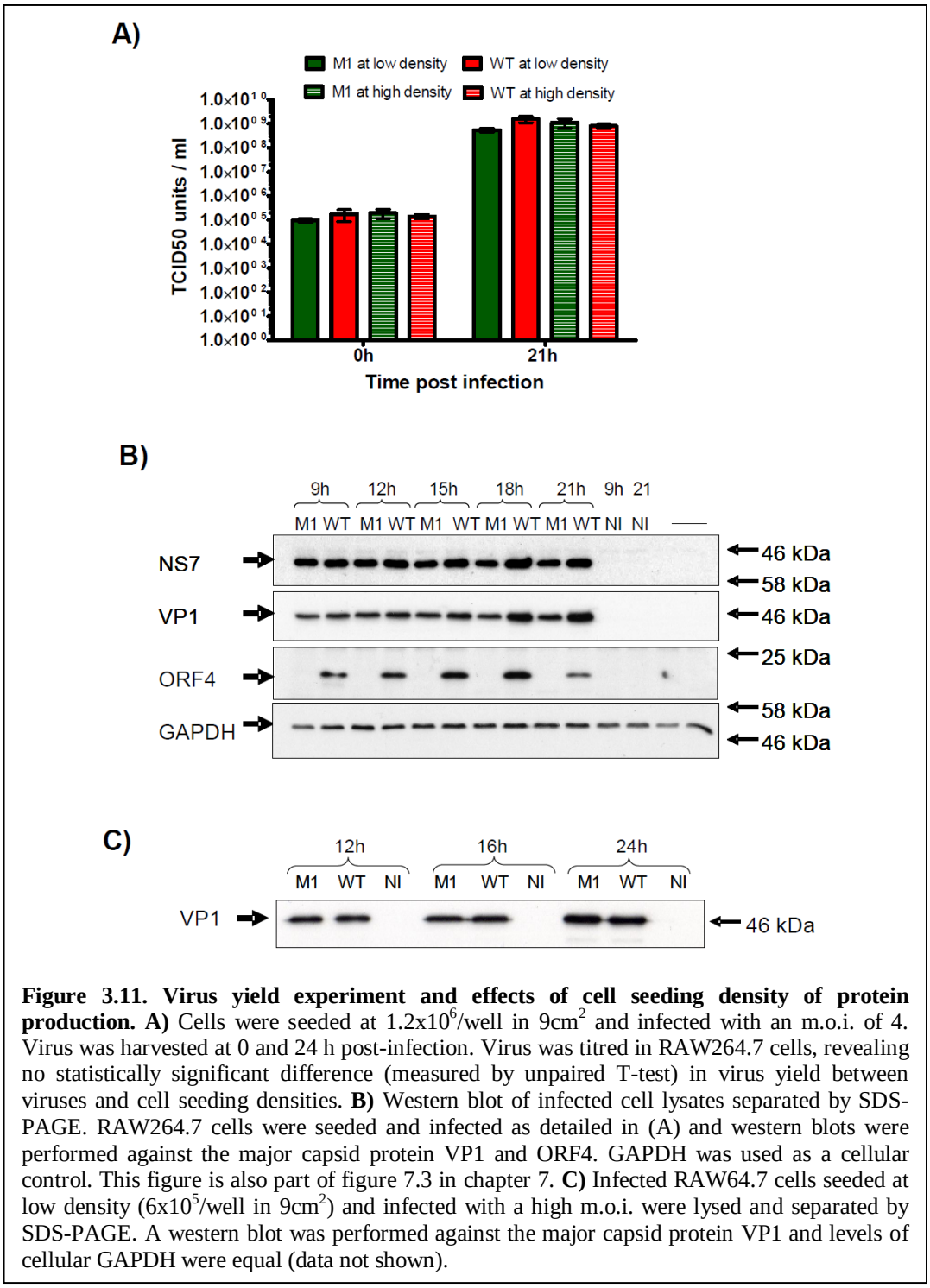


Figure 3.11. Virus yield experiment and effects of cell seeding density of protein production. A) Cells were seeded at $1.2x10^6$/well in $9cm^2$ and infected with an m.o.i. of 4. Virus was harvested at 0 and 24 h post-infection. Virus was titred in RAW264.7 cells, revealing no statistically significant difference (measured by unpaired T-test) in virus yield between viruses and cell seeding densities. **B)** Western blot of infected cell lysates separated by SDS-PAGE. RAW264.7 cells were seeded and infected as detailed in (A) and western blots were performed against the major capsid protein VP1 and ORF4. GAPDH was used as a cellular control. This figure is also part of figure 7.3 in chapter 7. **C)** Infected RAW64.7 cells seeded at low density ($6x10^5$/well in $9cm^2$) and infected with a high m.o.i. were lysed and separated by SDS-PAGE. A western blot was performed against the major capsid protein VP1 and levels of cellular GAPDH were equal (data not shown).

.

3.3. Conclusion

Both bioinformatic as well as *in vitro* evidence were used to successfully demonstrate that MNV ORF4 is an authentic overlapping reading frame which encodes a protein expressed during infection in tissue culture. Interestingly, the ORF4 protein displayed no homology to any currently identified proteins. Unfortunately, the lack of sequence homology between the MNV ORF4 protein and the related SV ORF4E suggests separate functions and would require a more in-depth *in vitro* comparative analysis, which is partly addressed in chapter 6. However, the current lack of a cell culture system for human sapoviruses would severely limit an approach similar to the one taken for MNV in this chapter. Additionally, large scale bioinformatic analysis using available RHDV and SMSV sequences needs to be performed in order to investigate the possible existence of an MNV ORF4 equivalent reading frame. However, the potential 82 - 120 amino acid products would be significantly smaller than the 214 amino acid MNV ORF4 protein.

Although *in vitro* analysis revealed that the ORF4 mutant viruses did not show a replicative defect in comparison to WT viruses, this may not be the case during *in vivo* infections. Therefore, as will be described in chapter 4, investigations examining the phenotype of ORF4 mutants in $STAT1^{-/-}$ mice were performed. Interestingly, more extensive *in vitro* analysis did show that restoration of protein expression occurred in two ORF4 mutants serially passaged under conditions of high cell seeding density, providing evidence that even in tissue culture viruses containing an intact ORF4 had a fitness advantage. In conclusion, the data presented in this chapter was used as a basis for investigating the role of ORF4 *in vivo* as well as subsequent *in vitro* experiments to identify ORF4 protein interacting proteins, identify cellular localisation and involvement in apoptosis, all of which will be described in subsequent chapters.

4. Characterisation of the role of ORF4 in MNV virulence

4.1 Introduction

Although not essential for MNV viability in cell culture, it is possible that similar to other viral overlapping reading frame proteins, such as the PB1-F2 protein of influenza A (McAuley et al., 2007), the ORF4 protein functions as an accessory protein which enhances virulence. Consequently, to determine if ORF4 was involved in MNV virulence the virulence of the ORF4 knockout virus M1 was examined in the STAT $1^{-/-}$ mouse model. As described previously, MNV-1 causes a lethal systemic infection in $STAT1^{-/-}$ mice or mice lacking both type I and type II IFN receptors (Karst et al., 2003, Mumphrey et al., 2007). STAT1 is critical for IFN signalling and controls MNV-1 replication and dissemination (Karst et al., 2003). Mice lacking only type I or type II interferon do not suffer from fatal MNV-1 infection as the presence of one can at least partially compensate for the lack of the other (Karst et al., 2003). Infection of wild-type 129 mice with MNV-1 results in a subclinical infection, although histopathological changes and viral RNA can be detected within 24 h post-infection in the proximal intestine, spleen and liver (Karst et al., 2003, Mumphrey et al., 2007, Wobus et al., 2006). After peroral inoculation of immunocompetent adult 129 mice, MNV-1 is rapidly disseminated from the small intestine to the spleen, liver and occasionally lungs, but in contrast to immunocompromised mice where viral RNA loads continually increase, viral RNA in adult 129 mice is cleared by day 3 post-infection (Karst et al., 2003, Wobus et al., 2006). The steady increase in viral RNA in the intestines of $STAT1^{-/-}$ mice and subsequent viral dissemination, has been attributed to the inability of these mice to control viral replication and dissemination through IFN signalling (Karst et al., 2003). Although MNV-1 was initially identified in $RAG/STAT1^{-/-}$ mice it was shown that only $STAT1^{-/-}$ was required for lethality and that RAG was required for viral clearance by the adaptive immune system (Karst et al., 2003). To date, the precise cause of death from MNV-1 infection remains unknown.

4.2 Results and discussion

4.2.1 Generation and rescue of virulent MNV-1 ORF4 mutants

The repeated passage of MNV in tissue culture has been demonstrated to result in attenuation (Bailey et al., 2008, Mumphrey et al., 2007). Therefore, all previous ORF4 studies were performed using the MNV-1 tissue culture adapted strains, also the basis

for the MNV reverse genetics system generated and employed in our laboratory (Chaudhry et al., 2007). Studies in our laboratory demonstrated that the attenuation occurring after tissue culture passage was the result of a single amino acid change in the capsid protein, although another mutation in NS4 may also contribute to tissue culture adaptation (Bailey et al., 2008). Therefore, an infectious virulent MNV-1 cDNA clone encoding the virulence determining amino acid in VP1 as well as the original amino acid in NS4 was constructed and rescued by Dr Dalan Bailey (Bailey et al., 2008). In collaboration with Yasmin Chaudhry, the ORF4 knockout mutation M1 was introduced into the infectious clone encoding the virulent cDNA and mutant virus (termed M1-v) was recovered alongside wild-type virulent MNV-1 (termed M1-v). In both cases (M1-v and WT-v), the recovered virus was only passaged once in tissue culture in order to prevent tissue culture adaptation. The presence of the virulence defining codons at positions 2151 and 5941 as well as the ORF4 stop codon (position 5118) were confirmed in M1-v by sequencing (figure 4.1). Sequencing at positions 2151 and 5941 was also performed for WT-v (data not shown).

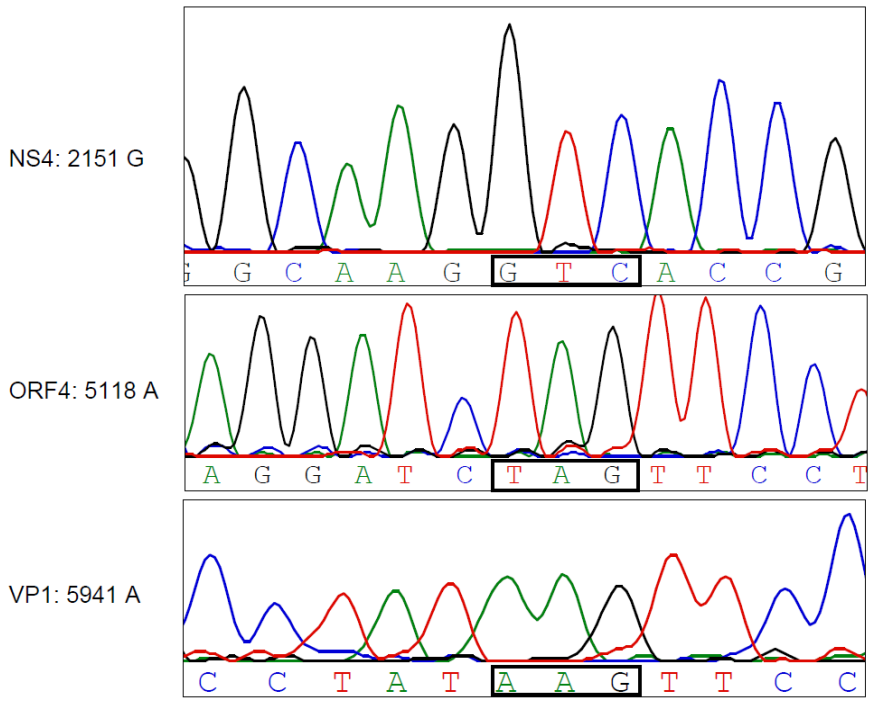


Figure 4.1 Sequencing chromatograms of M1-v viral stock at genome positions 2151, 5118 and 5941. The codons containing the desired base are boxed. The virulent clones are defined by a G at genome position 2151 in the NS4 encoding region, and an A at position 5941 in the VP1 encoding region. In contrast, in tissue culture adapted MNV the GTC encoding valine in NS4 mutates to ATC encoding isoleucine and the AAG encoding lysine in VP1 mutates to glutamate encoded by GAG (Bailey et al., 2008). In addition M1-v encodes an A at genome position 5118, inserting the stop codon TAG into the ORF4 reading frame.

To ensure that ORF4 expression was not essential for viral replication in the virulent MNV infectious clone, Dr Bailey performed multistep growth curves (m.o.i. of 0.01) using M1-v and WT-v in both immortalised (RAW264.7) as well as primary bone derived mouse macrophage cells (BMMΦ) isolated from the thigh bone of BALB/c mice. As expected, viral titres of both M1-v and WT-v were reduced in infected bone derived macrophages in comparison to RAW264.7 cells (figure 4.2). The lower virus yields from BMMΦ were most likely linked to primary cells being less permissive to viral replication than the tissue culture adapted macrophages. As these macrophages were derived from WT mice, they most likely mounted an effective anti-viral response as a result of MNV infection. It is therefore likely that the antiviral function of interferon reduced viral yield due to regulation of viral infection.

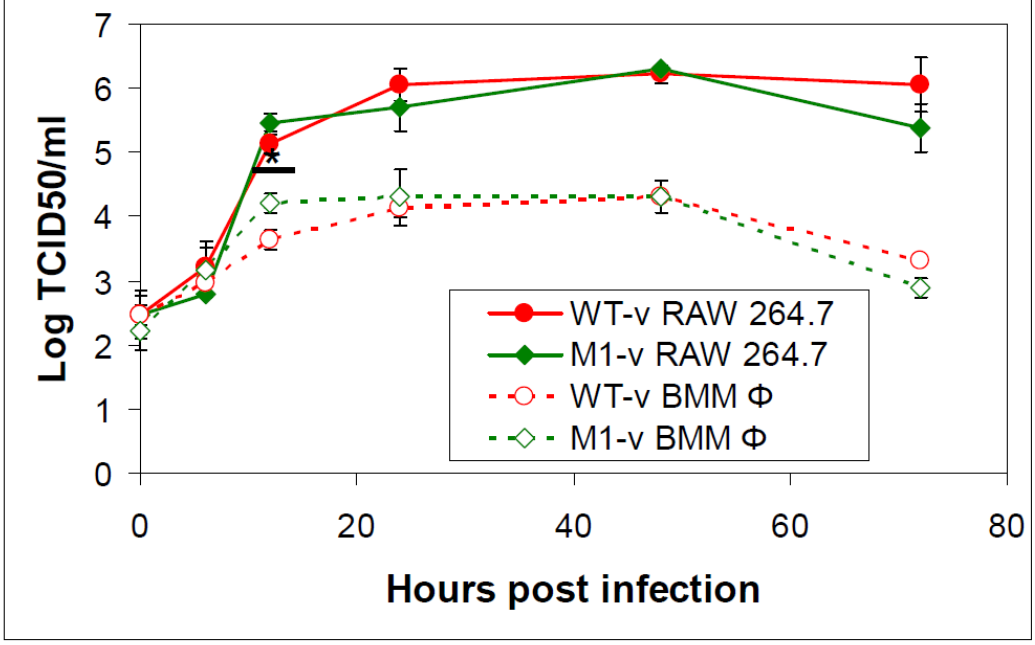


Figure 4.2. Analysis of growth kinetics of M1-v and WT-v in RAW26.7 cells and BMMΦs. Growth curve analysis was performed by Dr Dalan Bailey. Cells were infected at an m.o.i. of 0.01 in triplicate and were frozen at given timepoints before subsequent titration by TCID50 in RAW264.7 cells in triplicate. Error bars reflect the standard deviation seen between the replicate titrations, ***** depicts the statistically significant difference ($P<0.05$) between WT-v and M1-v at 12 h post-infection in BMMΦ.

The unpaired T-test was used to statistically compare the means of the two groups (i.e. M1-v infected cells against WT-v infected cells). The results are reflected in the P-value which displays the chance that random sampling would result in means differing to the extent as observed in the experiment. If overall the P value is large ($P>0.05$), the difference is not significant, whereas the reverse is the case for small P-values, with $P<0.01$ being of moderate and $P<0.001$ being of major significance. Interestingly, the

viral titres in BMMΦs at 12 h post-infection revealed a significant difference (P=0.0149) between M1-v and WT- v, with WT-v displaying an almost 10-fold higher average titre. As the assays were performed in triplicate and only small deviations were observed, it is possible that this difference between M1-v and WT-v is authentic and that M1-v can grow to slightly higher titres in the first 12 h post-infection. In order to be confident of these observations however, this assay would need to be repeated. However, despite the differences seen at 12 h post-infection in BMMΦs the final viral titres did not show statistical significant differences between M1-v and WT-v.

4.2.2 Characterisation of the role of ORF4 in MNV induced virulence

4.2.2.1 Experimental design

Together with Dr Dalan Bailey and working in collaboration with Dr Felix Yarovinsky at the University of Texas Southwestern Medical Center 6-8 week old $STAT1^{-/-}$ mice were challenged with either M1-v or WT-v. For this experiment two cohorts were established (figure 4.3) and groups of 8 mice (4 females and 4 males) were inoculated with 1000 $TCID_{50}$ units of either M1-v or WT-v. In a previously performed smaller-scale trial experiment, groups of 6 male mice had been inoculated with 10,000 TCID0 units and weight loss was monitored post-infection. The results of this trial were encouraging but led us to decrease the infectious dose for reasons detailed below. To exclude the possibility of cross-contamination or contamination through external sources (MNV is after all a prevalent pathogen of laboratory mice), 6 mice were inoculated with mock lysate from non-infected cells as a negative control.

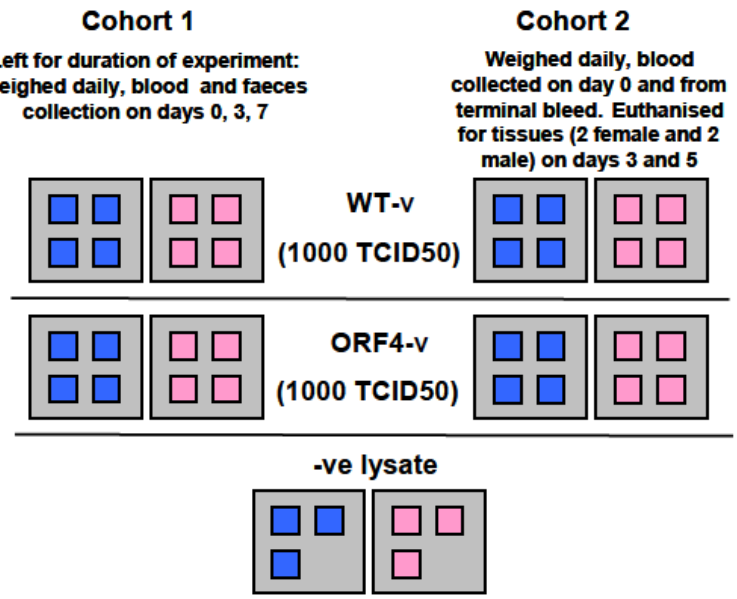


Figure 4.3 Experimental design for *in vivo* virulence analysis. 2 cohorts of male (represented in blue) and female (represented in pink) mice infected with either WT-v or M1-v at 1000 TCID50 units, whereas 6 control mice were treated with non-infected virus negative (-ve) lysate. Control mice were left for the duration of the experiment (as cohort 1) and were sacrificed for tissues and blood samples on day 14 post-infection.

Mice in cohort 1 were weighed daily, and blood and faeces were taken on days 0, 3 and 7 post-infection, which is comparable to what had taken place during the 10,000 $TCID_{50}$ infectious dose trial. Cohort 2 was also weighed daily and blood samples were taken on day 0. However, on days 3 and 5 post-infection, 2 males and 2 females from each of the infected groups were sacrificed for terminal blood and tissue samples, which included the mesenteric lymph node, spleen, liver, kidney, heart, lung and small intestine. Faeces samples were also directly harvested from the small intestine during the post mortems. Animals were arbitrarily selected for tissue sampling via ear-tag identification irrespective of symptoms. All tissue samples were used for the isolation of viral RNA. As this work was performed overseas and samples were shipped to the UK for subsequent processing all virus was inactivated in compliance with custom regulations for the import of biological material. Local rules at Southwestern Medical Center also required all viruses contained in tissue samples to be inactivated. Therefore, the isolation of live virus particles from harvested tissue samples was unfortunately not possible. Control mice were sacrificed for tissues on day 14 (on day 7 for the 10,000 $TCID_{50}$ infectious dose experiment), due to restrictions placed by the animal facility. For humane purposes, a 20% loss of bodyweight, the development of

severe symptoms or the presence of MNV-1 specific symptoms for 3 consecutive days was set in order to prevent undue suffering to the animal.

4.2.2.2 Analysis of bodyweight

One of the first indications that M1-v was attenuated in STAT1$^{-/-}$ mice came from analysis of the bodyweights of the infected animals. Whilst the weights of mice inoculated with the mock lysate control gradually increased following inoculation (figure 4.4a), weights of mice infected with WT-v dropped significantly in the first few days post-infection, consistent with previous findings (Mumphrey et al., 2007). Although some of the mice inoculated with M1-v demonstrated weight loss at the same time as those inoculated with WT-v, overall the bodyweights of mice inoculated with M1-v increased or remained constant in the first 5 days post-infection, although drops in bodyweight comparable to WT-v infected mice were seen in individual cases (figure 4.4a).

Weight loss was accompanied by the onset of symptoms typical of MNV-1 infection, to be described later. Animals removed from the study include those sacrificed on days 3 and 5 post-infection, as well as those exhibiting severe symptoms, showing more than 20% loss of bodyweight or exhibiting MNV-1 specific symptoms on 3 consecutive days. In order to determine whether or not differences seen in bodyweight were not due to chance, statistical analysis was performed by two-way ANOVA. This analysis determines how a response (in this case weight loss) is determined by two factors (in this case time and type of inoculum) and compares the likelihood that differences amongst the means in bodyweight could have been caused by chance alone. As for the T-test, the results are reflected in the P-value and the use of post-tests. If overall the P value is large ($P>0.05$), the difference is not considered significant, whereas the reverse is the case for small P-values. A statistical significant difference in the weights of mice infected with WT-v compared to the mock lysate was not seen for the first 3 days post-infection ($P>0.05$) (figure 4.4a). From day 4 onwards however, there was a major significant difference between WT-v and mock lysate treated mice ($P<0.001$). Interestingly, and most importantly, for the first 5 days post-infection, the weights of mice infected with M1-v showed no statistical significant difference ($P>0.05$) to the weights of mice inoculated with the control lysate. By day 6, the difference between mock and M1-v was of minor significance ($P<0.05$) although there was still a major significant difference between M1-v and WT-v ($P<0.001$).

Statistical analysis by two-way ANOVA past day 6 was not possible due to the removal of the WT infected mice from the study. Corresponding to visual predictions, an unpaired T-test in order to analyse statistically significant differences between the weights of the control mice and the remaining M1-v infected mice between days 7 and 10 post-infection demonstrated that there was a significant statistical difference ($P<0.05$) in all cases (data not shown).

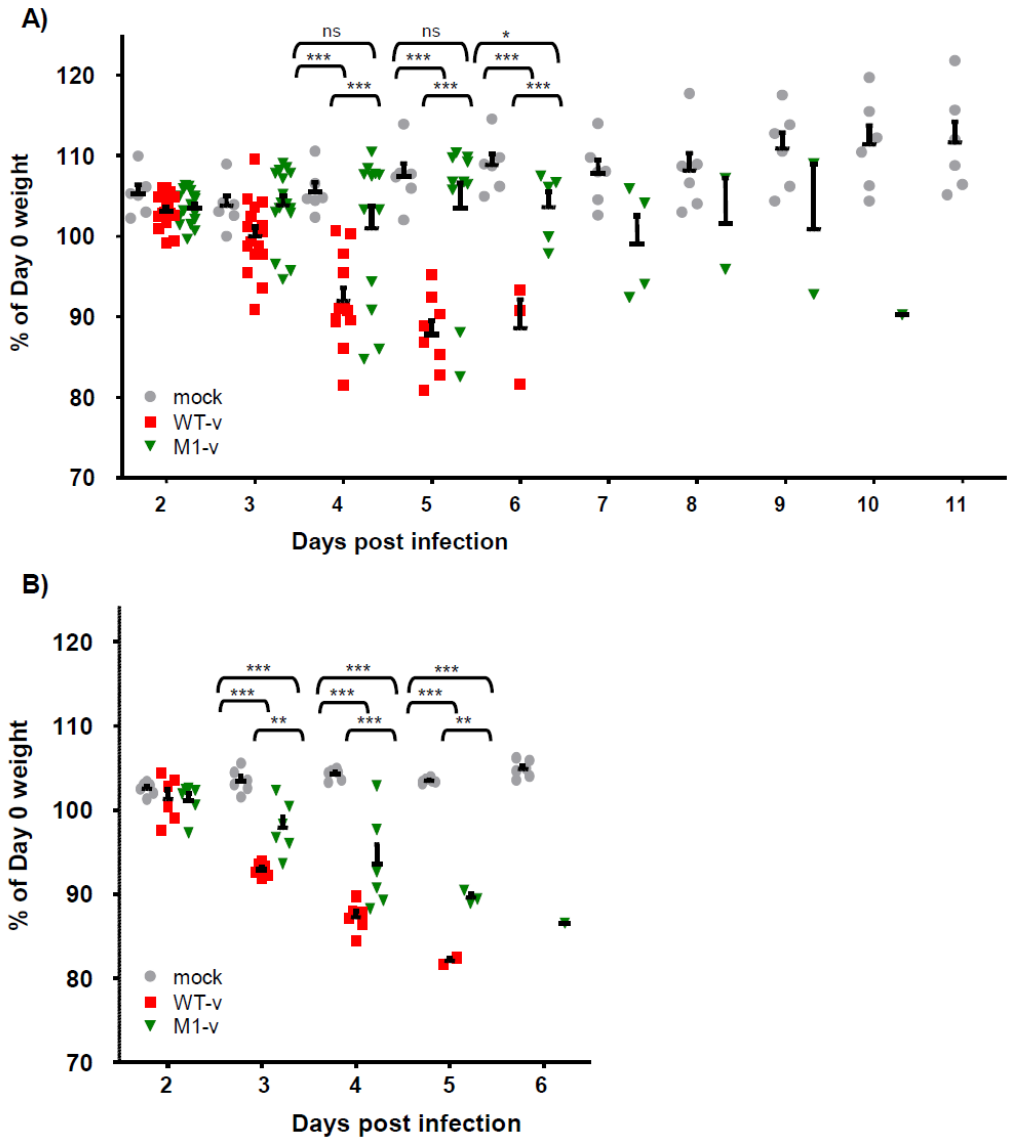


Figure 4.4. ORF4 contributes to MNV virulence *in vivo*. A) Daily bodyweights of mice inoculated with either negative lysate or virus (M1-v or WT-v) at 1000 TCID50 units. Statistical differences (calculated by two-way ANOVA with Bonferroni post-tests) are represented by the P-values. P values of $P<0.001$, $P<0.01$ and $P<0.05$ are represented as ***, ** and *. Non-significant differences ($P>0.5$) are represented as ns. Statistical significances between M1-v and WT-v are depicted in the lower brackets, differences between WT-v and mock are represented in the middle brackets and differences between mock and M1-v in the top brackets. Error bars represent the standard error and lines represent the means of the weights of mice treated with a specific inoculum on each day. **B)** Daily bodyweights and statistical differences between mice infected with 10,000 TCID50 units of M1-v or WT-v.

This data represented the first real evidence that ORF4 is involved in MNV-1 virulence. However, although the means showed no statistical difference between the weight-gaining control mice and M1-v infected mice, cases of dramatic weight loss corresponding to onset of disease was observed in a number of M1-v infected mice from days 3 post-infection. In fact, between days 6 and 10 post-infection all remaining M1-v infected animals showed signs of weight loss and all animals eventually succumbed to the disease. Weight loss in M1-v infected mice correlated with the same clinical manifestation of disease as were seen in mice infected with WT-v.

Noteworthy is that the observed statistical differences in weight loss between mice inoculated with WT-v and M1-v was not as prominent in a previous experiment performed with the higher infectious dose of 10,000 $TCID_{50}$ units. Although statistical analysis (also by two-way ANOVA with Bonferroni post-tests) revealed a significant difference ($P<0.001$) in bodyweight by day 3 post-infection between control mice and mice infected with either M1-1 or WT-v, there were statistically significant differences in bodyweight between M1-v and WT-v on days 3, 4 and 5 post-infection ($P<0.01$ on days 3 and 5, $P<0.001$ on day 4) (figure 4.4b). Consequently, attenuation of M1-v appeared more significant when the lower infectious dose was used.

4.2.2.3 Symptoms and pathology

In all cases, weight loss for both M1-v and WT-v was accompanied by symptoms typical of MNV infection (Karst et al., 2003, Mumphrey et al., 2007, Ward et al., 2006). Early symptoms (seen by day 3 for WT-v) included matted and dull fur, along with a related decrease in grooming activity. Apparently healthy animals also physically disassociated themselves from those clearly displaying symptoms. These first symptoms were rapidly followed by hunched appearance, disorientation and reduced mobility leading to ataxia. At the later stages of infection all M1-v and WT-v infected mice exhibited ocular and mucosal discharge. Infected mice showed significantly reduced defecation and faeces were generally smaller, lighter and more fibrous than for the control mice. Excessive urination seen in infected mice also indicated potential kidney problems and the skin of these mice was noticeably dehydrated. Hair loss was also seen in a number of WT-v and M1-v infected mice.

Once the post mortems of cohort 2 animals was performed, it became clear that reduced defecation was most likely due to gastrointestinal bloating and blockage, where the stomachs and intestines contained a large amount of undigested food.

Indeed, previous experiments measuring gastric emptying of MNV-1 infected STAT1$^{-/-}$ mice demonstrated a striking increase in stomach contents of infected STAT1$^{-/-}$ but not WT mice (Mumphrey et al., 2007). Severe gastrointestinal blockage and yellow coloured intestinal infiltrate and fluid accumulation was only seen during the later stages of infection in day 5 sacrificed animals (all WT-v and two M1-v infected animals). Gastrointestinal blockage could thus explain the observed decrease in defecation, and a decrease in intestinal stool content following MNV-1 infection of STAT1$^{-/-}$ mice has also previously been reported (Mumphrey et al., 2007). Interestingly, gastric bloating could potentially be caused by decreased gastric motor function, which could also be the case for human noroviruses. Because mice can not vomit due to the lack of an emetic reflex, gastric blockage occurs, whereas in humans vomiting ensues (Meeroff et al., 1980, Mumphrey et al., 2007).

On day 3, many of the spleens of WT-v infected animals had a dark red discoloration, indicative of an intense immune response. This discolouration was also seen for a number of M1-v infected animals. By day 5, the spleens of a number of mice (both WT-v and M1-v infected) were darker, indicating necrosis. Similarly, the livers of infected animals were paler than for the control mice, indicating hepatitis, either through infiltrate of immune or bacterial cells which had infiltrated the peritoneum from the gut. Importantly, these symptoms were both the same for M1-v and WT-v infected animals, although the pathology seen by post mortem was generally not as severe and apparent for M1-v infected as for WT-v infected mice. At the time of writing histopathology slides of tissues taken from M1-v and WT-v infected animals were not available as they were prepared by a company at the University of Texas Southwestern Medical Center in collaboration with Dr Yarovinsky. Following communication with the lab it has since been established that the randomly selected M1-v tissue samples left for histopathology analysis closer resembled the tissues of the control mice rather than the WT-v infected mice.

4.2.2.4 Viral loads

Although analysis of symptoms and bodyweight can be used to compare the phenotype of two viruses, a more accurate approach is quantitative analysis of viral load. For viruses which cause systemic disease, such as MNV-1 in STAT1$^{-/-}$ mice, analysis of viral load in various tissues can strongly reflect on a virus's ability to spread from the initial site of infection and cause systemic disease. In order to investigate viral load,

RNA in the tissues (mesenteric lymph node (MLN), spleen, liver, kidney, heart, lung, intestine) of animals sacrificed on days 3 and 5 post-infection was reverse transcribed to generate cDNA, and quantitative real-time PCR (qPCR) analysis was performed. Unfortunately, the limit of virus detection (10^3 viral genome copies per µg of total RNA) in complex RNA samples derived from animal tissues, was higher than the limit for RNA samples derived from tissue culture infected cells (10^2 viral genome copies per µg of RNA). Viral genome copy number was determined by comparison to a known amount of standard viral RNA. The viral detection limit was determined by melting curve as specified in the materials and methods (chapter 2). On day 3, viral genome copy numbers in the tissues of M1-v infected animals was either below or very close to the detection limit by this analysis and not exceeding the copy number of 10^4 (figure 4.5a).

By day 5, viral genome copy number for WT-v infected tissues ranged from 10^7-10^{10} viral genomes per µg of total RNA (figure 4.5b). In contrast, only one of the four M1-v sacrificed mice showed levels of viral RNA in all tissues which were several logs above the detection limit. The viral genome levels in the tissues of this infected mouse ranged from 10^5 to 10^7 per µg of RNA, depending on the tissue. These values were still significantly lower than for WT-v infected mice. In contrast, the viral genome levels of the remaining mice were either below or marginally above the detection threshold, ranging between 10^3 and 10^4 genome copies per µg of RNA. Even though the genome copy number was low, for the two animals above the detection threshold, the viral RNAs were verified as viral genomes as the melting curves were comparable to those of the viral RNA standard and the WT-v infected tissues (data not shown). On day 5, viral titres generally appeared higher in the MLN and spleen, consistent with previous findings and the hypothesis that MNV spreads from the initial site of infection (i.e. intestine) and disseminates via the lymphatic system to cause a systemic infection (Karst et al., 2003, Mumphrey et al., 2007).

Unfortunately, qPCR analysis of the blood of infected animals did not give rise to detectable levels of viral RNA, which was more likely due to technical difficulties such as having sufficient quantities of extracted RNA, rather than the virus not being present. Previous observations have indeed reported high levels of viral RNA in the blood of MNV-1 infected $STAT1^{-/-}$ mice (Karst et al., 2003, Wobus et al., 2006). Terminal bleeds were taken by eye bleeding, but in hindsight cardiac puncture to bleed out the animals would have been a preferable method of blood collection. This

technique would have ensured sufficient quantities of extractable RNA were obtained to enable the isolation of viral RNA.

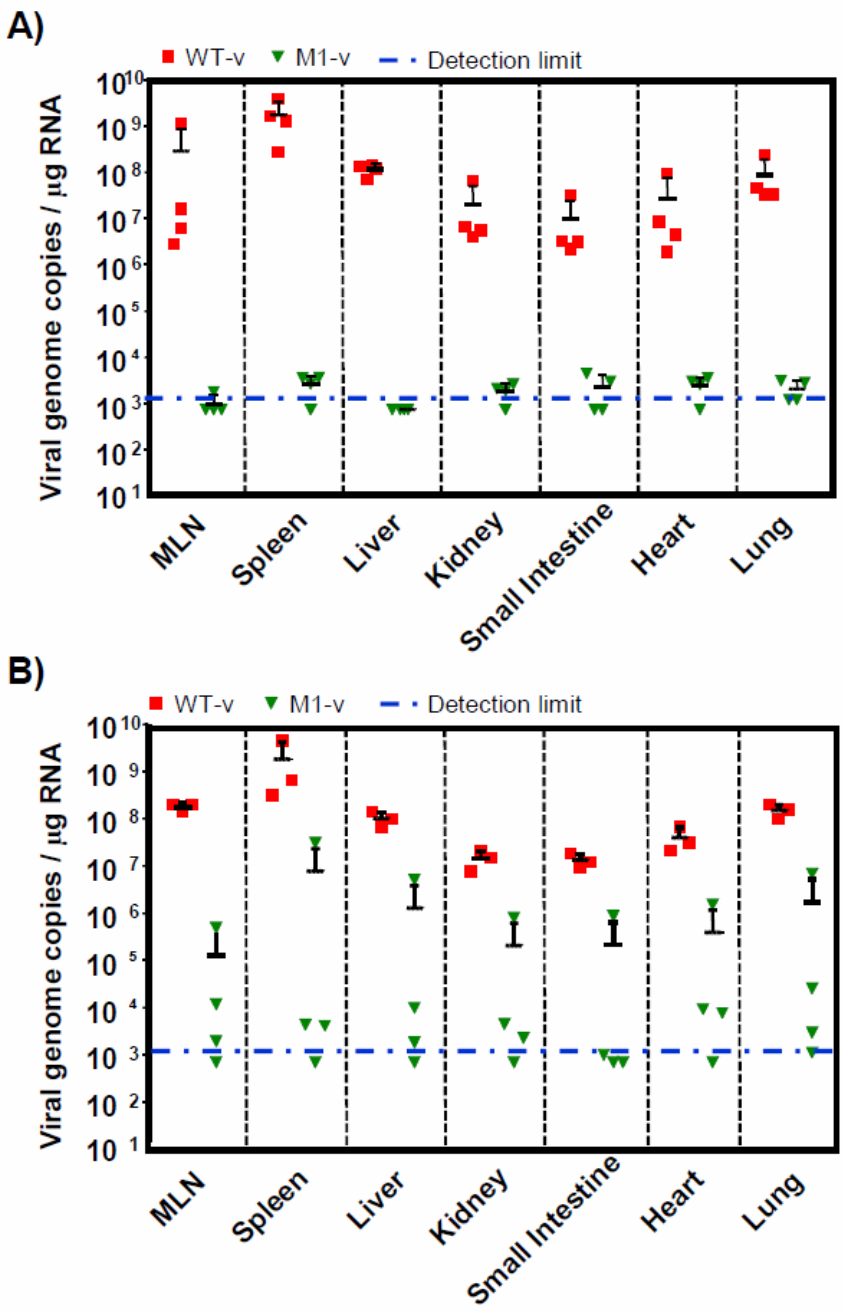


Figure 4.5. Viral RNA loads in the tissues of M1-v and WT-v infected mice sacrificed on days 3 (A) and days 5 (B) post-infection. Viral loads were determined by qPCR analysis of viral cDNA generated by MNV genomic primer specific reverse transcription of viral RNA harvested from infected tissues. Viral loads are depicted as genome copy number per µg of total RNA. The viral detection limit is highlighted by the blue lines. Error bars represent the standard error and lines represent the means between viral genome copy numbers determined in individual mice treated with the same inoculum.

Viral RNA was also detected in the faeces of all (days 3 and 5) sacrificed WT-v animals, with genome copy numbers per µg input RNA ranging between 10^6-10^7 on

day 3 and between 10^7-10^8 on day 5 (figure 4.6). The faeces of these animals were collected by harvesting directly from the intestine during the post mortems. This ensured that the faeces samples were fresh as the reduced defection caused by gastrointestinal blockage no longer enabled faeces sample collection when mice were weighed during their daily examination. On day 3, two M1-v infected animals had viral genome copy numbers slightly above the detection limit of 10^3 genome copies per µg of RNA (figure 4.6).

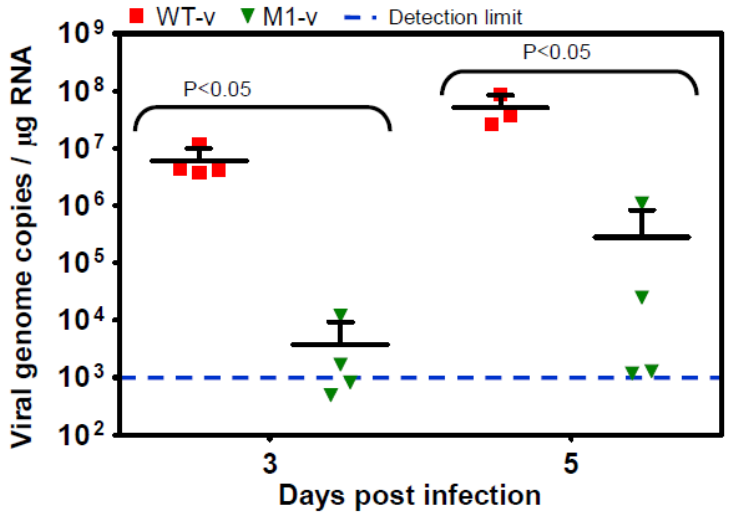


Figure 4.6. Viral RNA loads in the faeces of M1-v and WT-v infected mice sacrificed on days 3 and 5 post infection. Viral loads were determined by qPCR analysis of viral cDNA generated by MNV genomic primer specific reverse transcription of viral RNA harvested from intestinally extracted faeces. Viral loads are depicted as genome copy number per µg of total RNA. The viral detection limit is highlighted by the blue line. Error bars represent the standard error and lines represent the means between viral genome copy numbers determined in individual mice treated with the same inoculum. Statistical differences between the viral loads of WT-v and M1-v at both timepoints (P<0.05) were calculated using the standard unpaired T-test.

For one of these M1-v infected animals the viral genome number per µg of RNA was 10^4. On day 5, two M1-v infected mice had viral genome copy numbers around the detection limit, whilst the genome copy numbers were several logs higher for the two other M1-v sacrificed mice. For one M1-v animal viral genome copy number per µg of RNA was 10^6, whilst the other animal contained values above 10^4. The mouse with the highest levels of viral RNA was the same M1-v infected animal which had high viral RNA loads in all tissue samples (figure 4.5). However, on both days, M1-v viral genome copy numbers in the faeces of infected animals were significantly lower (determined using an unpaired T-test) than those of WT-v infected animals, with P<0.05 in both cases. Consequently, the viral genome copy number in the faeces

corresponded with the results obtained from the infected tissue samples, and indicated that M1-v was attenuated in STAT1$^{-/-}$ mice.

4.2.2.4 Restoration of ORF4 expression not observed in M1-v

The observed bodyweight and viral load differences between WT-v and M1-v infected animals, as well as differences in disease onset between individual M1-v infected animals led to the examination whether ORF4 expression was restored during the course of the infection. As described in chapter 2, mutations restoring ORF4 expression were observed in the ORF4 knockout virus upon serial passage in tissue culture. However, RT-PCR and sequencing analysis of RNA from tissue samples of a day 5 and day 7 sacrificed mouse (cohort 1 animal, sacrificed due to severe symptoms) revealed that the M1-v defining TAG stop codon was still present (figure 4.7). Consequently, the differences in disease onset between individual M1-v infected animals was not associated with restoration of ORF4 expression. However, it must be noted that although restoration was not observable from the sequencing chromatogram, where no significant mixture of bases higher than background level can be observed at the TAG site in question (figure 4.7), the sequencing analysis may not have been sensitive enough to detect a small quasispecies population of revertants. Therefore, sequencing of individual viral clones may have been a more appropriate approach to detect restoration of ORF4 expression. Additionally, if mouse to mouse transmission was allowed to continue, restoration of ORF4 may well have been observed. Unfortunately, the costs of these experiments, and the containment facilities required prevented such an analysis.

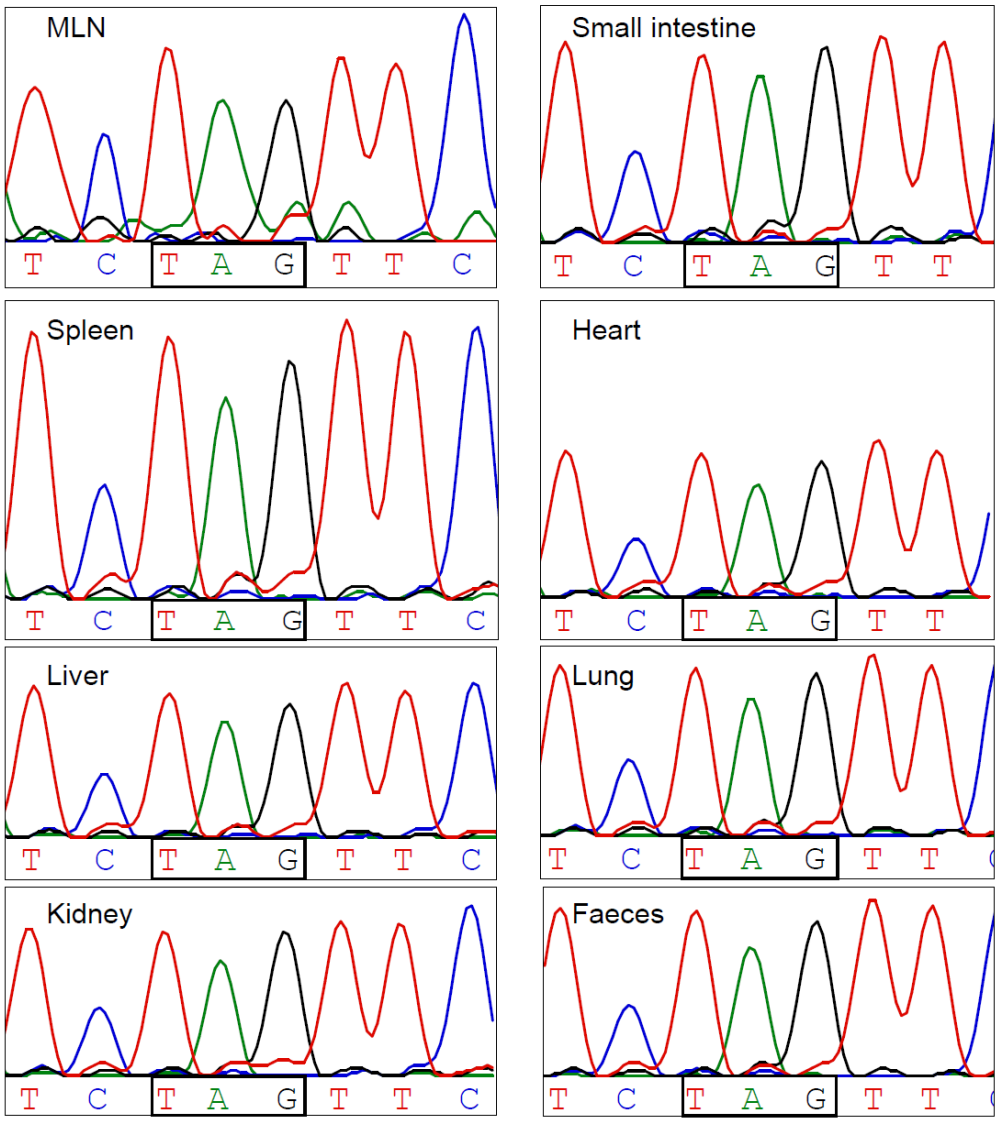


Figure 4.7. Sequencing chromatograms of all tissues and the faeces sample of an M1-v infected animal. The viral RNA isolated from the infected animal sacrificed on day 7 was subjected to RT-PCR followed by PCR amplification and subsequent sequencing, which demonstrated the presence of the TAG stop codon in all harvested tissues as well as the faeces sample.

4.3 Conclusion

In order to investigate the role of the ORF4 protein in MNV-1 induced virulence, genetically engineered viruses harbouring the ORF4 knockout mutation were used to infect STAT1$^{-/-}$ mice. Because MNV-1 is associated with a lethal infection in STAT1$^{-/-}$ mice, the virulence of mutant viruses can be analysed. The aim of this experiment was to compare the virulence of M1-v to WT-v by analysing lethality, bodyweight and viral load at given time points post-infection. Although the lack of ORF4 expression did not alter the final outcome of MNV-1 infection in STAT1$^{-/-}$ mice, study of bodyweight and qPCR analysis of viral load demonstrated that M1-v was attenuated *in*

vivo in comparison to WT-v. As the ORF4 knockout mutation M1 only contained a single base change in comparison to WT, it was plausible to suggest that M1-v was in fact restoring ORF4 expression, similar to what was observed upon serial passage in tissue culture (chapter 3). However, sequencing analysis performed on the tissues and faeces of two M1-v infected mice revealed that this was not the case.

Analysis by qPCR demonstrated a reduced viral load in M1-v infected tissues on days 3 and 5 post-infection in comparison to WT-v. In combination with weight analysis data, this suggests that M1-v was attenuated and had thus not replicated as efficiently as WT-v in the same timeframe (i.e. from infection until tissue harvest). The reason why such large differences in viral RNA load were seen between infected M1-v infected mice on day 5 could be that whilst infection was well established in the mouse with high viral RNA levels, productive viral replication in the remaining three mice was only beginning to be established. Even if attenuated, it is difficult to explain why such large differences existed in the onset of disease between individual M1-v infected mice. Although restoration of ORF4 expression was excluded, one other possible explanation is that in some animals initial M1-v infection was in fact abortive. However, once successfully infected mice had developed severe disease and were excreting large quantities of virus, these sentinel mice then became infected by their cage companions. To date, no studies have been performed on the transmissibility of MNV, although the resilience of viral particles to environmental assault and the high transmission rates of human noroviruses suggest that MNV is also highly transmissible and could easily be spread between mice from contaminated water, food and fomites. In future, in order to limit the possibility of interspecies transmission occurring mice could be housed in the smallest possible group of 2 animals per cage rather than 4.

As MNV-1 infection in $STAT1^{-/-}$ mice is associated with apoptotic cells in the liver and intestine (Mumphrey et al., 2007) and as data presented in chapter 7 indicates a role of the ORF4 protein in the process of apoptosis, it would be important to compare the tissues of M1-v to WT-v infected $STAT1^{-/-}$ mice. Although histopathology data from tissue samples taken from the liver, spleen and small intestine of arbitrarily selected M1-v and WT-v infected mice was not available at the time of writing, it has since been established that no difference could be observed between the tissue samples of M1-v infected and control mice in comparison to WT-v infected mice.

Although studies using this highly virulent MNV strain in $STAT1^{-/-}$mice gave vital insights into the attenuated phenotype of M1-v, it must be remembered that MNV-1 is

unique in the ability to cause lethal infection in severely immunocompromised mice. As previously described, MNV-1 infection of immunocompetent mice is subclinical and all other MNV strains are involved in persistent infections of immunocompetent as well as immunocompromised mice. Consequently, the use of persistent MNV stains would probably be more representative in elucidating the role of ORF4 during MNV infection. Indeed, the high genetic conservation of ORF4 between all currently sequenced MNV stains (as shown in chapter 3), supports the idea that ORF4 also plays a role in persistent strains and not just in MNV-1. Because of the lack of widespread systemic disease caused by non-MNV-1 strains, studies would be limited to analysis of bodyweight, quantification of viral load in liver, spleen and intestine shortly after infection, as well as analysis of faecal shedding. Cytokine production in response to infection could also be analysed. In contrast to the MNV-1 studies in $STAT1^{-/-}$ mice, seroconversion to MNV could also be monitored, an aspect which could not be examined in the STAT1 system as mice die before a protective immune response can be mounted. Indeed, antibody production is critical for the clearance of MNV (Chachu et al., 2008b), and a comparative analysis between WT and ORF4 knockout viruses could yield some interesting results. Therefore, in order to investigate the role of ORF4 in a persistent MNV strain, the ORF4 knockout mutation M1 was built into an MNV-3 infectious clone which was generated in our laboratory. The rescued virus was viable in tissue culture and did not restore ORF4 expression after passage in tissue culture at low cell seeding density (data not shown). Although the aim was to investigate the phenotype of M1-MNV-3 in comparison to WT-MNV-3 in immunocompetent mice, unfortunately time constraints prevented any further analysis of this mutant virus.

In conclusion, it is clear that loss of ORF4 expression results in a significant fitness cost to MNV-1 in $STAT1^{-/-}$ mice. Consequently, the ORF4 protein is strongly implicated in MNV-1 virulence in immunocompromised $STAT1^{-/-}$ mice. Although not required for virus viability in tissue culture or *in vivo*, the ORF4 protein appears to act as an accessory virulence factor in $STAT1^{-/-}$ mice. This phenotype is reminiscent of the non-essential but enhanced virulent phenotype in infections caused by influenza A virus harbouring the overlapping reading frame protein PB1-F2 (McAuley et al., 2007). Lastly, although the use of $STAT1^{-/-}$ mice gave vital insights into the role of the ORF4 protein in MNV-1 virulence, future work will focus on understanding the role of ORF4 in MNV strains which cause persistent infections such as MNV-3.

5. Identification of proteins which interact with the ORF4 protein

5.1 Introduction

In order to begin to determine the function of the ORF4 protein, host cell proteins which interact with the ORF4 protein were identified. There are several methods to identify host cell interacting proteins to a protein of interest, one of which is tandem affinity purification. Tandem affinity purification is a protocol which allows the purification of a tagged protein and associated binding partners from cells under mild conditions, whilst maintaining protein-protein interactions (Janin & Seraphin, 2003). This approach has been used to identify and elucidate a number of protein-protein interactions, from those associated with ribosomal networks (Fleischer et al., 2006, Jao & Chen, 2006) to proteins required for nuclear pre-mRNA retention and splicing (Dziembowski & Seraphin, 2004, Dziembowski et al., 2004). The protocol employed here was developed based on a modified TAP tag designed by Burckstummer et al in 2006, in which the tag consists of two streptococcal immunoglobulin G (IgG)-binding units of protein G and streptavidin binding peptide (SBP). Like the conventional TAP tag (consisting of two IgG-binding units of protein A from *Staphylococcus aureus* and a calmodulin binding peptide), the protein G and SBP domains are separated by a tobacco etch virus (TEV) protease cleavage site (Burckstummer et al., 2006). The protein of interest and binding partners are purified during a series of immunoprecipitations as illustrated in figure 5.1. Because the purification is performed under mild conditions, in many cases direct binding partners are isolated with associated proteins in a large complex. Purified final samples are then analysed by mass spectrometry and software such as Mascot can interpret a mass spectrum. Obtained peptide molecular masses are combined with sequence data, composition and fragment ion data (Mann & Wilm, 1994). By scanning databases, the peptide mass sequences are then used to identify the peptides, which if unique, can subsequently be categorised to belonging to a particular protein.

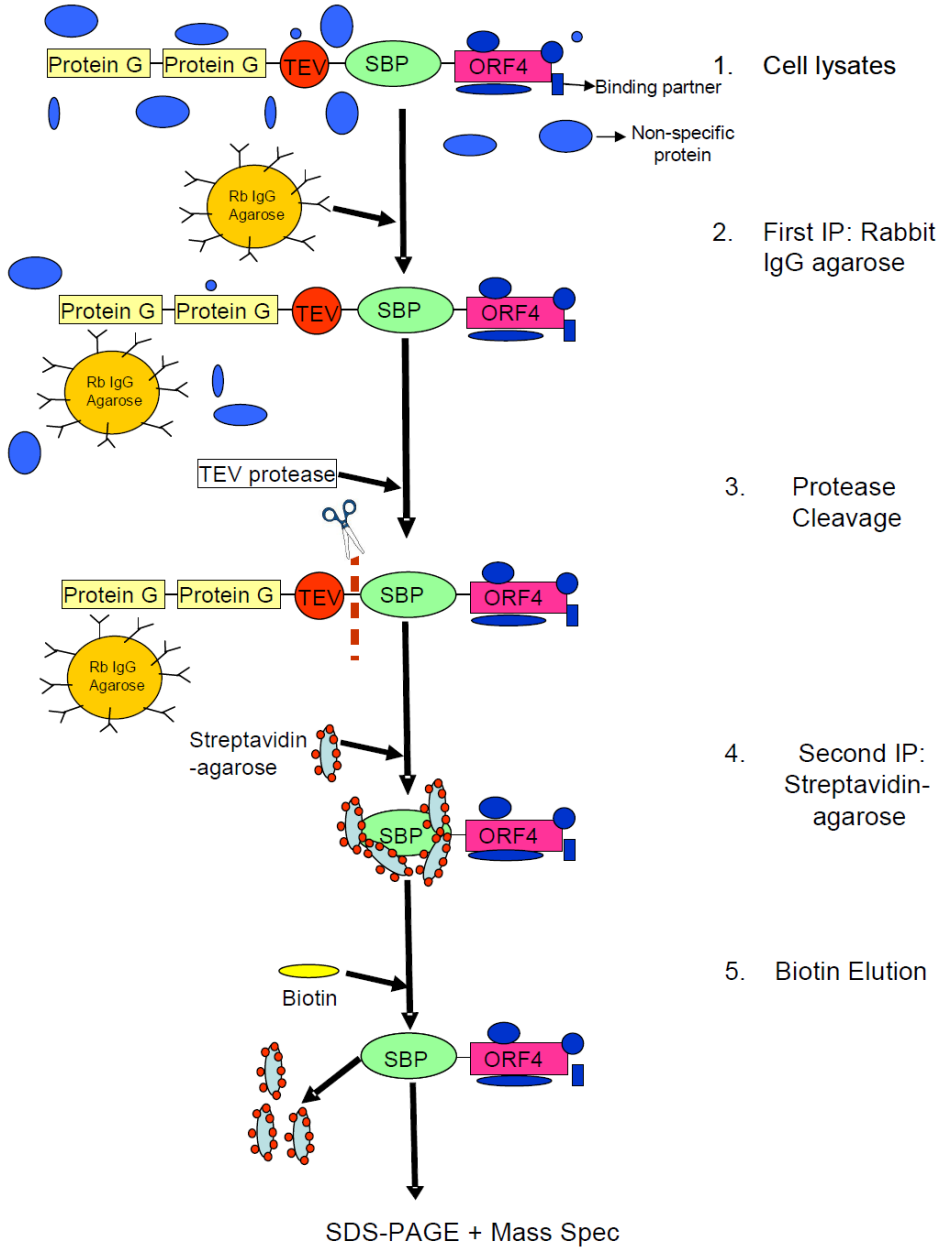


Figure 5.1. Overview of the tandem affinity purification procedure. For a detailed account of the procedure please refer to the materials and methods section (chapter 2). An abridged version is described in the text (section 5.1). IP = immunoprecipitation, SBP = streptavidin binding peptide, TEV = tobacco etch virus cleavage site, Rb = rabbit, IgG = immunoglobulin G.

Another approach to identifying proteins which interact with a protein of interest is yeast two-hybrid screen. The technique of a yeast two-hybrid screen was originally described in 1991 (Chien et al., 1991) and employs transcriptional activation of a reporter gene such as LacZ as a method of screening protein-protein interactions within the nucleus of yeast cells. Since the first description of this method, many variations and modifications of the screen have been developed. In the commonly used LexA screen the DNA binding and transcription activation domains are both derived

from yeast. Although this screen has the disadvantage that interactions from closely related yeast proteins may cause interference from yeast proteins binding to the DNA binding and activation domains, the screen has successfully identified a number of protein-protein interactions (Gorska et al., 2006, Stanasila et al., 2006). In an alternative screen the DNA binding domain of the bait fusions is derived from the bacterial tetracycline repressor (TetR), whereas the reporter genes URA3 and LacZ are under the control of the tetracycline operator, to which TetR binds (Xu et al., 1997). As for the LexA screen, transcription can only occur when DNA binding domains of the bait and transcription activation domains of the prey interact. However, because the TetR DNA binding domain is not derived from yeast, this system reduces endogenous interference from yeast proteins binding to the DNA binding and activation domains preventing an interaction between bait and prey.

5.2 Results and Discussion

5.2.1 Tandem affinity purification

5.2.1.1 Generation of stable cell lines

In an attempt to identify host cell factors which interact with the ORF4 protein, a tandem affinity purification protocol developed by Dr Dalan Bailey for MNV proteins in 293T cells was employed. 293T cells were used because attempts to generate stable RAW264.7 cell lines expressing MNV ORF4 TAP fusion proteins were unsuccessful. These problems were most likely the consequence of the low transfection efficiency of the permissive RAW264.7 cells, and the possibility that overexpression of the ORF4 protein is potentially toxic to mouse macrophage cells.

An N-terminal TAP tagged MNV ORF4 expression construct (pMEP4 NTAP-ORF4) was generated and used to produce stable 293T cells. Expression of the fusion protein was regulated by a $CdCl_2$ inducible promoter, whereas an Epstein Barr virus (EBV) origin of replication ensured episomal maintenance by EBNA-1, also encoded by the plasmid (figure 5.2a). A hygromycin resistance gene ensured the continued selection of cells expressing the plasmid. Expression of the constructs was detected by western blot analysis of lysates separated by SDS-PAGE due to the ability of the protein G contained in the TAP tag to bind IgG. Overnight induction with $CdCl_2$ demonstrated the inducibility of the system for cells expressing the NTAP tag vector alone (figure

5.2b). Unfortunately, the NTAP-ORF4 protein was also produced from cells in the absence of induction, and hence induction had only a small stimulatory effect on the expression levels (figure 5.2b).

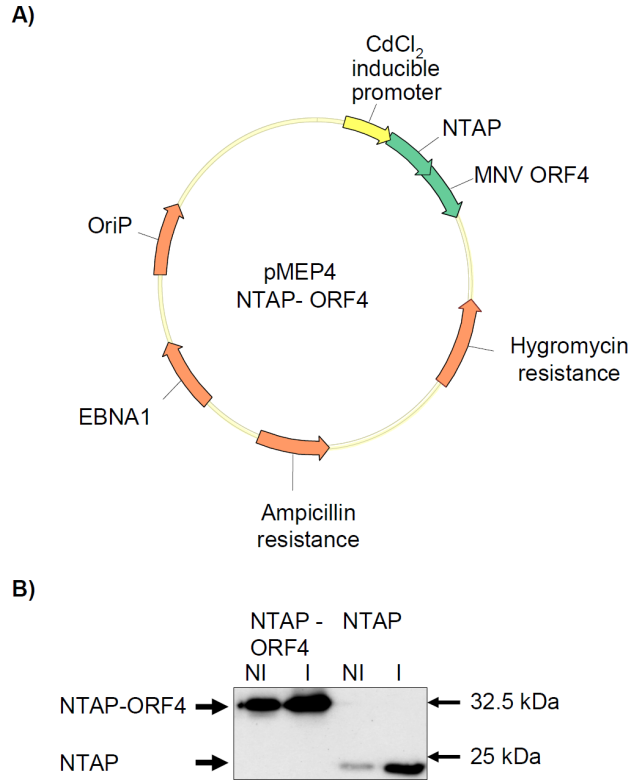


Figure 5.2. NTAP-ORF4 in the $CdCl_2$ inducible system. A) Diagram of the plasmid pMEP4 NTAP-ORF4 used to generate stable 293T cell lines expressing NTAP-ORF4 under a $CdCl_2$ inducible promoter. Stable clones of 293T cells harbouring the plasmid were selected using hygromycin, whereas an EBV origin of replication and the encoded EBNA1 ensured episomal maintenance. **B)** Inductions of stably transfected 293T cells expressing NTAP-ORF4 or NTAP. Cells were induced by the addition of $CdCl_2$ for 16 h and lysates from non-induced (NI) and induced (I) cells were separated by SDS-PAGE and analysed by western blot using antisera against MNV which reacted with the protein G domains present in TAP tag.

Although tandem affinity purification was carried out with this $CdCl_2$ inducible system (see below), concerns arose as to the toxicity of $CdCl_2$ on the cells following induction, as even low concentrations of $CdCl_2$ can alter gene expression (Cannino et al., 2008). Consequently, a change in protein expression may have altered the profile of proteins in the NTAP-ORF4 complex. For these reasons, both C- and N-terminal TAP tag ORF4 fusion constructs were generated in the tetracycline inducible plasmid pcDNA4/TO (figure 5.3a).

293T cells stably expressing the tetracycline repressor (TRex) were transfected with the tetracycline inducible TAP or TAP ORF4 expression constructs (both C an N-terminal) and stable, expressing clones were selected (figure 5.3b). In this example

(figure 5.3b), the ORF4-CTAP clone 2 was chosen, as in the absence of the inducer (doxycycline) ORF4-CTAP was not detectable, but high levels were observed following induction. Identification of clones stably expressing C- or NTAP alone or NTAP-ORF4 was performed in the same manner (data not shown).

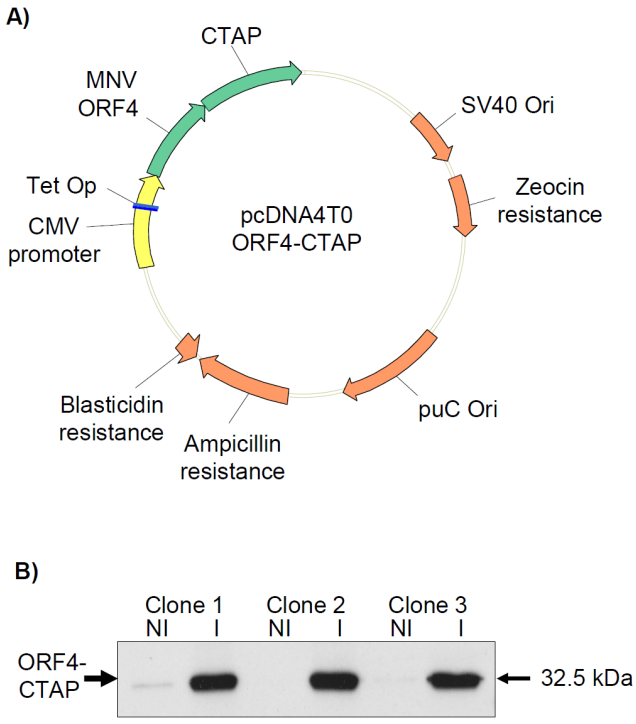


Figure 5.3. ORF4-CTAP in the tetracycline inducible system. **A)** Diagram of the plasmid pcDNA4T0-ORF4-CTAP used to generate ORF4-CTAP stable 293T TRex cells expressing the tetracycline repressor. Expression of ORF4-CTAP was under the control of a tetracycline inducible CMV promoter. Stable cell lines expressing the plasmid were selected for with zeocin and blasticidin **B)** Western blot analysis demonstrating ORF4-CTAP inductions. Cells were induced by adding doxycycline for 16 h and lysates of non-induced (NI) and induced (I) cells were separated by SDS-PAGE and analysed by western blot.

5.2.1.2 Identification of ORF4 protein interacting host cell proteins

After stable cell lines had been generated, the TAP protocol (figure 5.1) was employed in order to identify ORF4 protein binding partners. After the purification procedure (please refer to chapter 2 for details), 15% of the final eluate was separated by SDS-PAGE and silver stained, whilst the remaining 85% was separated by SDS-PAGE and Coomassie stained. After staining, Coomassie stained bands were excised and were sent for mass spec to enable subsequent identification by Mascot peptide sequence query. The identification of peptides within individual Coomassie stained excised

bands was used to identify bands on silver stained gels which had been run side by side.

A silver stained SDS-PAGE gel of the final eluate of the TAP purification of NTAP-ORF4 and NTAP alone in the $CdCl_2$ inducible system can be seen in figure 5.4. This purification was performed in conjunction with Dr Dalan Bailey and other lab members, as the procedure was performed on almost all MNV proteins simultaneously. Comparative SDS-PAGE analysis (figure 5.4) between the final eluates for NTAP-ORF4 and NTAP revealed a number of proteins specific for NTAP-ORF4. Due to the high number of proteins identified in the ORF4 complex, only a subset is highlighted in figure 5.4. The proteins in this subset are mainly proteins with high Mascot score, which were identified in the NTAP-ORF4 purification but not in the purification of other MNV proteins, although exceptions are the case, especially in examples where a number of related proteins were identified as unique NTAP-ORF4 interacting proteins. The remainder of the identified proteins not highlighted are contained within appendix 2 and 3, which lists the identified proteins based on scoring of the peptide sequences by Mascot sequence query. Appendix 2 contains proteins only identified by NTAP-ORF4, whilst appendix 3 lists NTAP-ORF4 binding proteins which were also identified in the TAP purification of other MNV proteins. It is important to remember that the proteins were identified in a large scale screen, and a direct interaction between NTAP-ORF4 and all the identified proteins is likely not to be the case. Therefore, this analysis not only identified proteins likely to interact with the ORF4 protein directly, but also those which bind indirectly via the direct binding partners. For all of the MNV proteins, Mascot sequence query identified keratin as a contaminant in many samples. Several proteins, particularly tubulin and heat shock proteins were present in virtually all MNV and NTAP final eluates. Consequently, these proteins were not incorporated into the final list of proteins identified in the NTAP-ORF4 screen. However, an exception to this is tubulin, as a much more substantial quantity of tubulin was observed in the case of NTAP-ORF4 than seen for any of the other MNV proteins. Therefore, tubulin was incorporated into the list of proteins isolated in the NTAP-ORF4 complex, as tubulin is also potentially involved in the function of the ORF4 protein (discussed in section 5.2.1.2). Based on peptide sequencing, 49 unique and 47 other proteins were identified in the NTAP-ORF4 purification, extensive lists of which are contained within appendix 2 and 3.

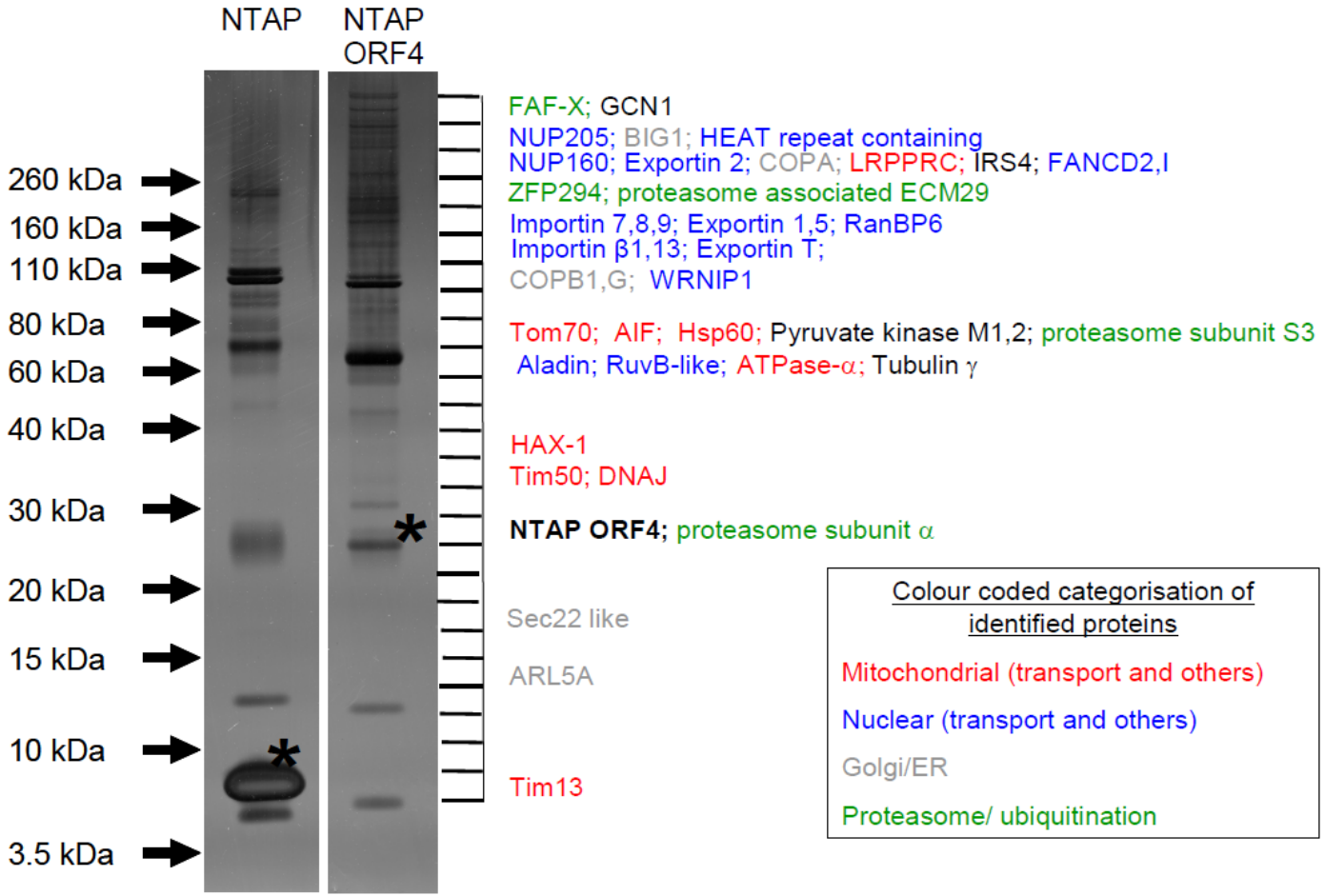


Figure 5.4. Silver stained SDS-PAGE gel of the final eluate of the TAP purification of NTAP-ORF4 and NTAP alone. TAP purification procedure, SDS-PAGE and Coomassie / silver stain were performed in collaboration with Dr Dalan Bailey for NTAP-ORF4 and other MNV proteins. By carrying out the SDS-PAGE at the same voltage for an equal duration, a direct comparison between identified proteins in the excised bands and their relative location on the silverstained gel could be drawn. Asteriks indicate the locations of NTAP or NTAP-ORF4. The location of the gel segments excised and sent for mass spec are depicted by the boxes to the left of the protein listings. Note: Although this list covers a great majority of identified proteins, a complete list of NTAP-ORF4 interacting proteins can be found in appendix 1 and 2.

When analysing the number of identified proteins, the vast majority could be divided into four categories based on cellular location and function as highlighted in figures 5.4. These included mitochondrial, nuclear, Golgi/ER as well as proteosomal proteins and their various functions and possible role of the MNV life cycle are discussed below. Importantly however it must be remembered that only a very small number of these proteins are likely to represent authentic binding partners and very few interactions would likely be maintained under high stringency binding conditions.Therefore, the discussed consequences of many interactions are highly speculative and require further investigation. Currently there is no direct evidence for an involvement of any of the discussed proteins in ORF4 protein function, and it is hoped that interactions for a number of proteins will be confirmed in the future.

5.2.1.2.1 Mitochondrial proteins

Of the mitochondrial proteins identified, several are involved in mitochondrial import, whereas others can be linked to apoptosis via the mitochondrial pathway. In order to aid the understanding of the locations of the identified proteins an overview of mitochondrial import can be seen in figure 5.5.

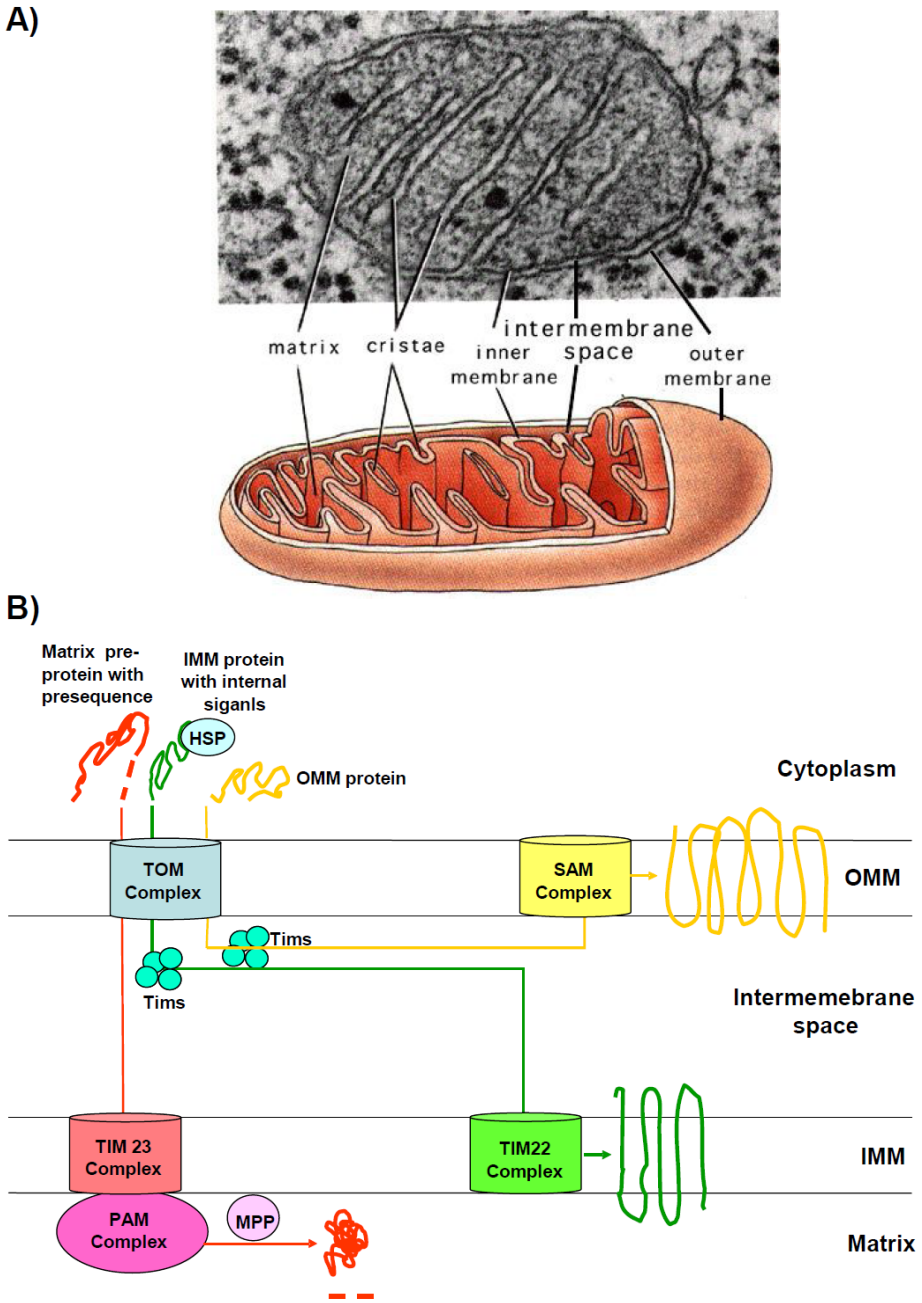


Figure 5.5. Diagram of mitochondria and brief overview of the mitochondrial import pathways. A) Mitochondria contain both an outer and an inner membrane. The space between the two membranes is referred to as the intermembrane space, whilst the matrix is surrounded by the inner membrane, which forms protrusions into the matrix also known as cristae. Various transport pathways are required to import mitochondrial proteins to their target destination. Diagram downloaded from http://cosmology.com/images. **B)** Matrix, inner mitochondrial membrane (IMM) and outer mitochondrial membrane (OMM) proteins all employ distinct transport pathways. In all cases, the first stage of import is mediated by the transport of outer mitochondrial membrane (TOM) complex, which transports proteins across the OMM. Matrix proteins which contain an N-terminal presequence are directly passed on to the transport of inner mitochondrial membrane 23 (TIM23) complex, which is associated with the presequence translocase associated import motor (PAM) complex. Presequences are removed by the mitochondrial processing peptidase (MPP). Presequence containing IMM proteins also pass through the TIM23 complex, whereas those with internal localisation signals bind to small Tims (9-10 and 8-13) upon passing though the OMM. The small Tim chaperones deliver IMM proteins to the TIM22 complex responsible for IMM insertion. Upon traversing the TOM complex, OMM targeted proteins also bind small Tims and OMM proteins are inserted to the OMM via the sorting and assembly machinery (SAM) complex. HSP = heat shock protein

A number of mitochondrial import proteins were identified in the NTAP-ORF4 complex, including the transport of outer mitochondrial membrane protein Tom70, as well as the transport of inner mitochondrial membrane proteins Tim5, Tim13 and DnaJ, which associates with the import machinery. Tom70 functions as a receptor for proteins destined for mitochondrial import and is N-terminally anchored to the outer mitochondrial membrane (OMM) (Mokranjac & Neupert, 2009). Tom70 is mainly responsible for binding precursors of inner mitochondrial membrane proteins which contain internal localisation signals rather than a pre-sequence (Mokranjac & Neupert, 2009, Rehling et al., 2004, Yamamoto et al., 2009). Whilst the N-terminus of Tom70 interacts with cytosolic chaperones such as Hsp70 and Hsp90 (also identified in the NTAP-ORF4 complex), the C-terminus interacts with the chaperone-bound proteins targeted for mitochondrial import (Mills et al., 2009, Mokranjac & Neupert, 2009). Following binding, proteins are passed on to the multimeric TOM complex, also known as the general insertion pore (GIP), which consists of a number of Tom proteins as well as chaperones (Mokranjac & Neupert, 2009). Whilst still in the TOM complex, those proteins targeted for insertion into the OMM and IMM bind to small Tims in the intermembrane space (Tims9-10 and Tims8-13) (Mokranjac & Neupert, 2009, Rehling et al., 2004). These Tims (of which Tim13 was identified as a component of the NTAP-ORF4 complex) act as chaperones which deliver the proteins destined for OMM or IMM insertion to the relevant insertion complex (Mokranjac & Neupert, 2009).

Another identified protein, Tim50 is an integral membrane protein preset on the intermembrane side of the inner mitochondrial membrane (IMM). Tim50 forms part of the transport of inner mitochondrial membrane complex by binding to the multimeric TIM23 complex (Rehling et al., 2004). Tim50 is believed to bind proteins with presequences coming from the TOM complex and direct them to the pore-forming TIM23 complex in the IMM (Rehling et al., 2004). The energy demand for this active transport process is met by the presequence translocase associated import motor (PAM) complex, responsible for ATP hydrolysis (Rehling et al., 2004). By binding to the PAM complex, DnaJ-like proteins (also identified as a component of the ORF4-containing complex) stimulate ATP hydrolysis (Rehling et al., 2004).

The identification of such a vast number of mitochondrial import proteins associated with OMM transport as well as IMM transport strongly suggests that the ORF4 protein is targeted to the IMM. However, a bioinformatic approach could not identify a

mitochondrial targeting sequence (MTS) within the ORF4 protein, although a non-canonical MTS may be present (discussed in detail in chapter 6). Alternatively, the ORF4 protein may associate with the mitochondrial proteins discussed below, and hence the import proteins may not directly bind to NTAP-ORF4 but rather bind as a consequence of being in a complex with NTAP-ORF4 associated proteins.

Interestingly, many of the identified mitochondrial proteins which are not directly involved in the mitochondrial import pathways could be associated with the process of programmed cell death (apoptosis). Given the fact that MNV infection has been associated with the induction of apoptosis via the mitochondrial pathway in RAW264.7 cells (Bok et al., 2009, Furman et al., 2009), these findings were of considerable interest. Of the identified proteins, mitochondrial heat shock protein 60 (Hsp60) was originally described as a mitochondrial chaperone which interacts with Hsp10 and Hsp70, aiding protein folding after mitochondrial import through both the OMM and IMM (Cappello et al., 2008, Ostermann et al., 1989). Although Hsp60 is not exclusive to the mitochondria, mitochondrial release of Hsp60 upon stimulation of apoptosis has been demonstrated (Chandra et al., 2007). Hsp60 has been implicated in pro-survival (Chandra et al., 2007, Ghosh et al., 2008, Gupta & Knowlton, 2002, Kirchhoff et al., 2002) as well as pro-death functions (Chandra et al., 2007, Xanthoudakis et al., 1999), which may vary between tissues, cell types as well as apoptotic stimuli. Because of these differences, it is difficult to speculate on the consequences of an interaction between the ORF4 protein and Hsp60, and further investigations would be required.

Another identified apoptosis-associated protein was AIF. AIF has been associated with both the intrinsic and extrinsic pathways of apoptosis induction and was the first protein shown to induce apoptosis via the mitochondrial pathway in the absence of caspases (Joza et al., 2001, Modjtahedi et al., 2006, Yu et al., 2009). Mitochondrial-mediated caspase-independent apoptosis has recently been termed parthanatos (Yu et al., 2009). Under normal cellular conditions, AIF is a mitochondrial protein with FAD associated oxioreductase activity (Modjtahedi et al., 2006). Upon apoptotic stimuli, AIF exits the mitochondria and translocates to the nucleus, where the protein plays a role in chromatin condensation and high molecular weight DNA fragmentation (Andrabi et al., 2006, Modjtahedi et al., 2006, Susin SA, 1999). During the process of apoptosis, mature AIF binds to the translation initiation factor 3 subunit eIF3g (Kim et al., 2006). eIF3g plays a key role in the large eIF complex in recruiting the initiator

methionyl-tRNA and mRNA to the 40S ribosomal subunit. The interaction between eIF3g and AIF inhibits translational initiation, and thus AIF plays a role in shutting off host cell protein synthesis during apoptosis (Kim et al., 2006). Similar to many mitochondrial proteins, AIF is translated as a 67 kDa precursor protein with an N-terminal MTS (Modjtahedi et al., 2006, Susin SA, 1999). Upon mitochondrial import, the MTS is cleaved off, and until very recently it was believed that mature AIF localised exclusively to the IMM as the 62 kDa form lacking the MTS. Upon apoptotic stimuli AIF is released from the IMM by cleavage to produce a 57 kDa soluble version (Yu et al., 2009). However, it has recently been demonstrated that approximately 30% of AIF localises to the OMM and that around 20% of this uncleaved AIF also translocates to the nucleus (Yu et al., 2009). The mechanism by which AIF locates to the OMM is unknown, but may involve retrograde movement of partially processed AIF through the OMM, as is seen for yeast fumarase (Knox et al., 1998, Yu et al., 2009).

An interaction between AIF and the ORF4 protein could be interesting from two aspects. Firstly, the ORF4 protein may directly interfere with the involvement of AIF in the processes of apoptosis during MNV infection. Supporting this hypothesis are results from co-localisation studies between the ORF4 protein and AIF (chapter 6), as well as the demonstration that the ORF4 protein is involved in the process of apoptosis during infection (chapter 7). Secondly, as eIF3 is required not only for host but also for viral translation (Daughenbaugh et al., 2003), it is possible that competitive binding of AIF to the ORF4 protein prevents the interaction between AIF and eIF3, thus translation is maintained for as long as possible during the course of viral induced apoptosis. This would most certainly explain why viral translation was reduced from 15 h post-infection in cells infected with the ORF4 knockout virus (chapter 3). As will be shown in detail in chapter 7, these differences in protein expression also coincide with apoptosis induction during MNV infection.

The isolated mitochondrial ATPase subunit alpha forms part of the electron transport complex which employs the mitochondrial membrane potential to generate ATP. Interestingly, studies have shown that expression of mitochondrial ATPase subunit alpha was enhanced upon stimulation of apoptosis and is probably related to an increased requirement for ATP in order to undergo apoptosis (Singh & Khar, 2005). Consequently, binding or sequestering of the subunit by the ORF4 protein may impair ATPase activity. This could result in the cells not containing sufficient ATP to execute

apoptosis as swiftly as possible during the course of infection, supporting evidence of which can be found in chapter 7.

Interestingly, although tubulin was present in virtually all samples, an extremely high score for various peptide components of tubulin were seen for one of the NTAP-ORF4 samples. The corresponding section on the silver stained gel also showed intense staining in comparison to NTAP alone for which tubulin was also identified at this position (figure 5.4). Hence, in this case tubulin may in fact authentically bind either directly or indirectly to NTAP-ORF4. Although highly ubiquitous, tubulin also localises to the mitochondrial membrane and has been shown to associate with the VDAC (Carre et al., 2002). VDAC is one of the many components of the permeability transition pore (PTP), which spans from the OMM to the IMM. Upon stimulation of apoptosis, the PTP is essential for mitochondrial membrane permeabilisation, which releases proapoptotic molecules such as cytochrome *c*, AIF, or Smac/Diabolo from the mitochondria (Carre et al., 2002). Therefore, a potential interaction between NTAP-ORF4 and the VDAC-associated tubulin could possibly serve to interfere with or even block the VDAC. This block would in turn delay the process of apoptosis, as many executioners of apoptosis would be unable to exit the mitochondria. Once again, evidence presented in chapter 7 could lend support to this theory.

The antiapoptotic HCLS1 associated protein X-1 (HAX-1) was also identified in the NTAP-ORF4 purification. HAX-1 associates with Omi/HtrA2, the proapoptotic serine protease which upon stimulation of apoptosis cleaves HAX-1, exits the mitochondria and induces apoptosis by caspase dependent as well as independent mechanisms (Cilenti et al., 2004). Antiapoptotic HAX-1 also acts as an effective inhibitor of caspase 9, one of the key components of apoptosis induction, also reported to be activated upon MNV-1 infection of RAW264.7 cells (Bok et al., 2009, Furman et al., 2009, Han et al., 2006). Interestingly, HAX-1 is the target for a number of viral proteins, and the potential interaction between the ORF4 protein and HAX-1 may share functional similarities. Kaposi's sarcoma-associated herpesvirus (KSHV) ORF K15 protein co-localises with HAX-1 in the mitochondria and ER and has been shown to interact with HAX-1 (Sharp et al., 2002). However, a positive or negative effect on the ability of K15 to interfere with HAX-1 inhibited apoptosis remains to be demonstrated (Sharp et al., 2002). Furthermore, the proapoptotic Vpr protein of HIV also interacts with HAX-1, and over-expression of Vpr leads to the depletion of HAX-

1 from the mitochondria, which possibly contributes to the ability of Vpr to disrupt mitochondrial membrane potential and induce apoptosis (Yedavalli et al., 2005).

5.2.1.2.2 Nuclear and nuclear associated proteins

In addition to the mitochondrial proteins discussed above, several nuclear proteins were also isolated using NTAP-ORF4. These include components and associated proteins of the nuclear pore complex such as nucleoporins (NUPs), as well as nuclear importins and exportins (figure 5.4). Transport of proteins greater than 40 kDa into the nucleus is achieved by active transport across the nuclear pore, a large nuclear membrane spanning multimeric complex (Stewart et al., 2001). Nuclear import requires binding of the target protein to import proteins (known as importins) via a nuclear localisation signal (NLS). Once in the nucleus, importins need to be recycled, which frequently requires export molecules (exportins). Exportins also function to export proteins targeted into the cytoplasm from the nucleus. In order to understand the relevancy of the proteins identified by TAP, a brief overview of the processes of nuclear transport and associated components can be seen in figure 5.6 (adapted from Stewart et al., 2001).

Disruption of nuclear transport is used by many viruses to perturb the host antiviral response, including poliovirus (Belov et al., 2003, Tolskaya et al., 1995), vesicular stomatitis virus (VSV) (Fontoura et al., 2005) and HCV (Chung et al., 2000). One of the identified proteins, NUP160 is a central core component of the NPC (Glavy et al., 2007, Vasu et al., 2001) and aladin was also recently identified as a constituent of the NPC (Kind et al., 2009). Interestingly, NUP160 associates with NUP107, which was identified in an ORF4 protein yeast two-hybrid screen (described later in this chapter). The isolated NUP205 is a member of the NUP93 subcomplex which is thought to regulate and stabilise NPC assembly (Krull et al., 2004).

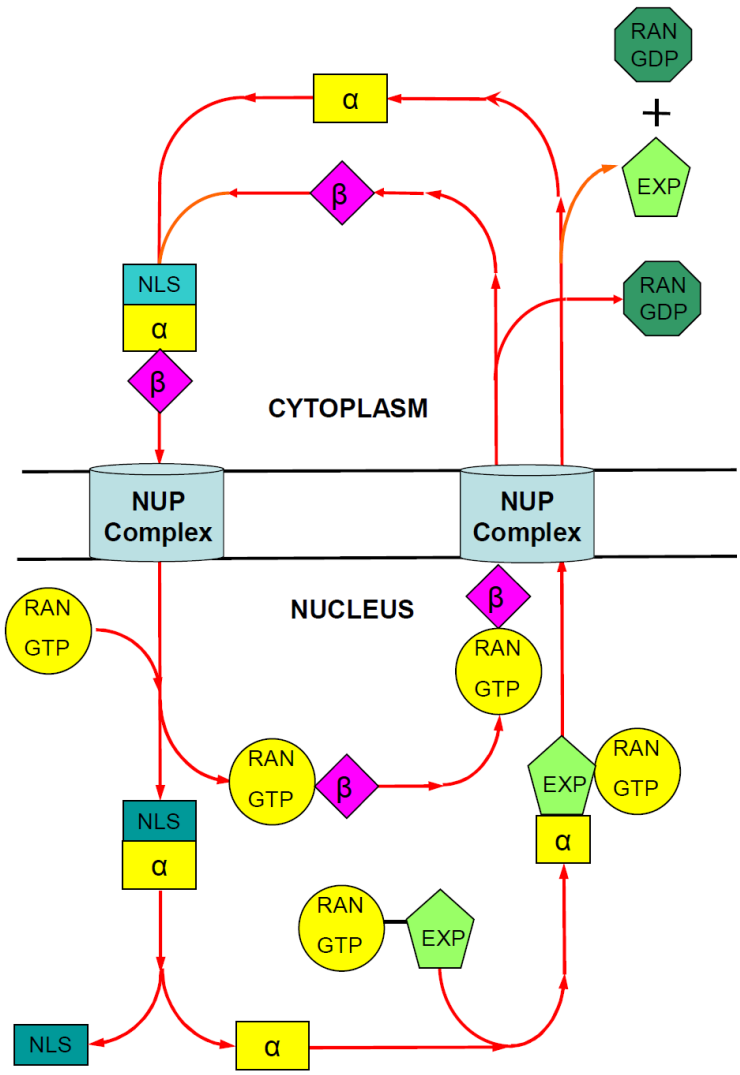


Figure 5.6. Brief overview of the nuclear transport pathway. Importin α subunits associate with proteins with nuclear localisation signals (NLSs) in the cytoplasm and this stimulates the association with the importin β subunit (Stewart et al., 2001). The trimeric complex then translocates into the nucleus, where disassociation of the carrier from the protein is achieved by binding of RanGTP to importins. Subsequent export may require the binding of exportins (EXP) such as exportin 2 which shuttle from the nucleus to the cytosol. Upon reaching the cytoplasm, importins are released at the expense of RanGTP hydrolysis, and RanGDP is imported back into the nucleus, where conversion to RanGTP occurs though the activity of Ran GEF (guanine nucleotide exchange factor). Diagram adapted from a review (Stewart et al., 2001).

Nuclear transport proteins, known as importins or exportins are frequently referred to as Ran binding proteins (RBPs) due to their ability to bind RanGTP. The importins identified in the NTAP-ORF4 purification include importin β, as well as the β-related importins 7, 8, 9, and 13. Whereas importin β binds to cargo bound adaptor molecules such as importin α, the importin β-related receptors specifically and directly bind the designated cargo without the aid of adaptor proteins (Waldmann et al., 2007). In addition to nuclear import, importin 13 also possesses exportin activity (Mingot et al.,

2001), and importin 7, 8, and 9 have all been shown to bind RanGTP which is required for export (Gorlich, 1998, Gorlich et al., 1997, Waldmann et al., 2007). Unfortunately, little is known about the function of the isolated Ran-binding protein 6 (RanBP6). However, as database searches revealed that RanBP6 shares sequence similarities to the importin β subfamily and also contains Huntington-elongation-A subunit-TOR (HEAT) repeats, RanBP6 is equally thought to have importin/exportin activity (data not shown). HEAT repeat containing proteins are proteins which contain 37-43 amino acid residues in tandem motifs of between 3 and 22 repeats (Groves et al., 1999). HEAT repeat domains are a common component of importins and exportins (Fukuhara et al., 2004). Consequently, the identified HEAT repeat domain containing protein is also likely to be involved in nuclear transport.

Similarly, many exportins were isolated, such as the abundant exportin 2, which is used to re-export the importin-α subunit (Stewart et al., 2001). Exportin 5 is responsible for the nuclear export of RNA binding proteins and non-coding RNA (Calado et al., 2002, Chen et al., 2004, Kim, 2004). Other proteins isolated by NTAP-ORF4 include the tRNA specific exportin T (Arts et al., 1998) and an exportin 1 like protein. Interestingly, exportin 1 (also known as crm1) binds to and exports survivin, an antiapoptotic protein (Mita et al., 2008, Stauber et al., 2006). In light of the fact that survivin is down-regulated during MNV infection (Bok et al., 2009), the identification of exportin 1 could indicate that by binding exportin 1, the ORF4 protein prevents survivin nuclear export upon apoptosis. Interestingly, western blot analysis has shown that survivin is indeed down-regulated more rapidly in cells infected with the ORF4 knockout virus in comparison to WT MNV (details in chapter 7). This may serve to delay the process of apoptosis induction seen in MNV-1 infected cells (evidence for which is presented in chapter 7), although overall MNV-1 infection is associated with the down-regulation of survivin and the induction of apoptosis (Bok et al., 2009). However, as shown, a great number of exportins and importins were identified in the NTAP-ORF4 purification; hence the binding to an exportin 1-like protein may be completely unrelated to survivin activity, and survivin itself was not isolated by NTAP-ORF4.

Overall, similar to the identification of many mitochondrial import proteins, the association between NTAP-ORF4 and a number of nuclear transport proteins was of considerable interest and immediately raised the question whether or not the ORF4 protein localises to the nucleus or NPC. Although unlikely that the ORF4 protein

directly associates with such a vast diversity of transport molecules, it may well be that association of the ORF4 protein with the NPC led to the co-purification of a number of transport proteins with their associated cargo.

Other isolated nuclear proteins include several DNA binding proteins and repair enzymes, which of course are targeted to the nucleus. Of these, Fanconi anemia group D2 (FANCD2) and the related group I (FANCI) proteins are involved in the repair of double-stranded DNA breaks which occur during DNA replication, presumably by interacting directly with the DNA repair protein RAD51 (Niedernhofer et al., 2005, Smogorzewska et al., 2007, Yang et al., 2005). There are a number of Fanconi anemia group proteins which form part of a nuclear E3 ubiquitin ligase, responsible for activation of FANCD2 (Patel & Joenje, 2007, Smogorzewska et al., 2007). Of this multimeric complex, it is interesting to note that Fanconi anemia group C (FANCC) protein has antiapoptotic activity by binding to and phosphorylating STAT1 (Cumming et al., 2001, Pang et al., 2000). Interestingly, a FANCC binding partner (FANZF) was identified in the ORF4 protein yeast two-hybrid screen. Although antiapoptotic activity has not been recorded for other Fanconi anemia group members, a role in apoptosis can not be ruled out and many of these proteins are still being identified and characterised.

RuvB-like 1 and RuvB-like 2 proteins are both ATP binding proteins which function in scaffolding and chromatin remodelling. RuvB-like proteins regulate DNA access of various enzymes, including those involved in DNA repair, transcription and mitosis (Jha & Dutta, 2009). Interestingly, Ruv B-like proteins also regulate expression of the oncogenic and apoptosis inducing transcription factor c-Myc (Jha & Dutta, 2009). The ATPase Werner helicase interacting protein 1 (WRNIP1) has DNA helicase and exonuclease activities. WRNIP1 interacts directly with poly (ADP-ribose) polymerase 1 (PARP), which binds both single and double-stranded DNA breaks and catalyses their repair (Comai & Li, 2004). Although PARP has antiapoptotic DNA repair activity, extensive DNA damage actually results in PARP inducing apoptosis, through the accumulation and nuclear exit of poly ADP ribose (PAR), a by-product of PARP activity. Released PAR locates to the mitochondria, resulting in the release of AIF thus triggering apoptosis, which takes place in a caspase-independent manner (Andrabi et al., 2006, Comai & Li, 2004).

Although these DNA repair enzymes may simply have been cargo of the isolated transport molecules, it is possible that the ORF4 protein localises to the nucleus

(supporting evidence in chapter 6) and directly interacts with a number of DNA repair enzymes which are involved in the process of apoptosis. Although DNA repair enzymes have antiapoptotic activity, it could be that similar to PARP, many of these enzymes are actively involved in the induction of apoptosis upon excessive DNA damage. In the case of WRNIP1 for example, it could be speculated that recruitment of WRNIP1 by the ORF4 protein may serve to block PARP-WRNIP1 interaction, thus delaying the accumulation of apoptosis-inducing PAR.

5.2.1.2.3 Golgi and endoplasmic reticulum (ER) transport proteins

The other group of proteins identified in the NTAP-ORF4 purification were enzymes of the Golgi and ER transport pathways. These included a number of non-clathrin-coated vesicular coat proteins (COPs), such as COPA, COPB1 and a COPG similar protein, all of which form part of the COPI transport system (Breakspear et al., 2007). The COPI transport system is required for the retrograde transport of proteins within the Golgi and from the Golgi to the ER (Manolea et al., 2008, Nebenfuhr et al., 2002). The COPII transport system on the other hand is used in transport from the ER to the Golgi, and employs proteins distinct from COP proteins (Barlowe, 1995, Manolea et al., 2008). From the COPII transport system, a Sec22-like protein was isolated. Sec22, a vesicle specific receptor is a key component in ER to Golgi transport and recycling of Secc22 to the ER in turn is COPI dependent (Ballensiefen et al., 1998, Mancias & Goldberg, 2007). COP binding to the membranes and subsequent budding of vesicles requires the activity of small GTPases, known as ADP-ribosylation factors (ARFs), of which ADP-ribosylation factor-like 5A (ARL5A) was isolated. ARFs in turn are regulated by guanine nucleotide exchange factors (GEFs), such as the identified Brefeldin A-inhibited guanine nucleotide-exchange protein 1 (BIG1) (Manolea et al., 2008, Orci et al., 1993, Zhao et al., 1997). BIG1 localises to the Golgi complex and plays a role in the recruitment of COPI, clathrin and adaptor proteins, which are required for packaging (Manolea et al., 2008, Nebenfuhr et al., 2002). Brefeldin A is a fungal antibiotic which inhibits the assembly of coat proteins onto Golgi membranes (Robinson & Kreis, 1992) and previous studies have shown that MNV is not sensitive to Brefeldin A (Hyde et al., 2009). Of course, the identification of these transport proteins immediately raised the question whether or not the ORF4 protein localised to the ER/Golgi network, supporting evidence of which can be found in chapter 6.

ER/Golgi localisation may be transient or could simply be a consequence ORF4 translation occurring on ER membranes. Although posttranslational modification is possible, there is currently no bioinformatic or *in vitro* evidence to suggest that the ORF4 protein is posttranslationally modified.

5.2.1.2.4 Binding partners associated with proteosomal degradation

Lastly, a number of proteins involved in proteosomal degradation were isolated, including ubiquitin and zinc finger protein 294 (ZNF294), which also plays a role in the ubiquitination process (Ivanov et al., 2007). Rapid ubiquitination and proteosomal degradation of cytotoxic viral proteins such as influenza A virus PB1-F2 protein has been demonstrated (Chen et al., 2001). Sometimes, ubiquitinated proteins can escape proteosomal degradation by removal of ubiquitin (Komander et al., 2009). An example of a deubiquitinase enzyme is FAF-X, which was identified with a high Mascot score. FAF-X, also known as FAM or USP9x removes ubiquitin associated with proteins targeted for proteosomal degradation (Dupont et al., 2009, Nathan et al., 2008). The identification of these proteosomal proteins may be the consequence of overexpression leading to ubiquitination and proteosomal degradation of NTAP-ORF4.

5.2.1.2.5 Other identified NTAP-ORF4 binding partners

Other proteins identified from the NTAP-ORF4 complex could not be localised to the four described cellular locations (mitochondria, nucleus, ER/Golgi or proteosome). Indeed, the protein which obtained the highest Mascot score was the translational regulator general control of amino-acid synthesis 1-like protein (GCN1). In response to cellular stress such as amino acid starvation, phosphorylation of eIF2 results in the down-regulation of general translation but in the up-regulation of selective translation (Holcik & Sonenberg, 2005). Phosphorylation of eIF2 occurs through GCN2, which is activated by GCN1 (Kubota et al., 2001, Marton et al., 1997). An example of a translationally upregulated gene is the transcriptional activator GCN4. Increased levels of GCN4 in turn leads to increased binding of GCN4 to the promoter region of several genes involved in amino acid biosynthesis (Kubota et al., 2001, Marton et al., 1997). It is therefore possible that binding of the ORF4 protein to GCN1 prevents the subsequent activation of GCN2, inhibiting or delaying eIF2 phosphorylation. In viral

infected cells this would consequently mean that general translation is not down-regulated even though the cell is subject to a large amount of stress resulting from viral infection. As discussed previously, MNV translation requires numerous host translation factors, and so prolonging host translation is beneficial to the virus. To date, the role of the ORF4 protein in translation has not been characterised, although as discussed in chapter 3, the ORF4 knockout virus displays reduced viral translation in cells infected at high density from 15 hours onwards. This effect may well be due to the discussed interaction between AIF and the ORF4 protein as well as an interaction between GCN1 and the ORF4 protein. Although in tissue culture this reduction in translation was not associated with a difference in virus yield between the mutant and wild-type virus, and could only be observed when cells were seeded at a high density, this may not be the case *in vivo,* where ORF4 knockout viruses displayed an attenuated phenotype (chapter 4).

Insulin receptor substrates (IRSs), including the identified IRS4 undergo tyrosine phosphorylation upon receptor binding of various substances such as insulin, growth factors as well as cytokines (Uchida et al., 2000). Upon stimulation, phosphorylated IRSs bind to SH2 domain-containing proteins such as PI3 kinase (Uchida et al., 2000). Bound PI3 kinase in turn activates several serine/threonine kinases, which play a role in a number of metabolic processes, including glucose transport and glycogen metabolism, as well as apoptotic signalling (Uchida et al., 2000). Although IRS1 and IRS2 have been shown to posses antiapoptotic activity under certain conditions (Uchida et al., 2000, Zhou et al., 2000), the role of IRS4 in apoptosis is less clear and proapoptotic (Uchida et al., 2000) as well as antiapoptotic functions (Cuevas et al., 2009) of IRS4 have been reported. Consequently, it would be difficult to speculate on the outcome of an interaction between IRS4 and the ORF4 protein, although an involvement in apoptosis may well be the case.

The identification of the cytosolic M2 type pyruvate kinase was interesting as it is a known target for other viruses. Pyruvate kinase is a glycolytic enzyme which transfers phosphate from phosphoenolpyruvate to ADP, thus generating ATP and pyruvate (Mazurek et al., 2005). As proliferating cells and virus replication preferentially require cellular metabolites over maximum ATP, pyruvate kinase isozymes are employed. These isozymes have a reduced phosphoenolpyruvate substrate specificity, thus allowing the accumulation of glycolytic precursor molecules (Mazurek et al., 2005). In order to drive the expression of these precursor molecules in favour of

glycolytic intermediate metabolites, a number of viral proteins target pyruvate kinases. The HCV RNA-dependent RNA polymerase NS5B specifically associates with M2 type pyruvate kinase and down-regulation of M2 type pyruvate kinase inhibits HCV replication (Wu et al., 2008). In human papillomavirus 16 (HPV-16) infected cells, the transforming potential of the E7 oncoprotein has been linked to the specific interaction with M2 type pyruvate kinase (Mazurek et al., 2001, Zwerschke et al., 1999). Because E7 promotes expression of an enzymatically less active form of M2 type pyruvate kinase, cell division is stimulated, thus resulting in the observed transforming tendency (Mazurek et al., 2001). Similarly, a link between M2 type pyruvate kinase and the transforming potential of Rous sarcoma virus has also been demonstrated. In this case the viral v-src protein stimulates tyrosine phosphorylation of M2 type pyruvate kinase, leading to a reduced affinity of M2 type pyruvate kinase for phosphoenolpyruvate (Presek et al., 1988). Although there is no data or experimental evidence to suggest that MNV is an oncogenic virus, the ability to alter the cell cycle phase may very well be beneficial for the virus, for example in providing copious amounts of transcription/translation factors in the G1/G2 phase. If this is the case, the question whether or not the ORF4 protein is involved in this process remains to be investigated.

5.2.2 Yeast two-hybrid screen

In a further attempt to identify binding partners of the ORF4 protein, a commercial yeast two-hybrid screen using both the previously described LexA and TetR based systems was carried out by the company Proteinlinks. It must be noted that this work was entirely undertaken by the company, but as the results have great relevance to the potential function of the ORF4 protein, the data was included in this thesis. In order to investigate protein-protein interactions for the MNV ORF4 protein, a library of 1.4 x 10^7 cDNA clones derived from mouse spleen was screened for the ability to interact with a truncation representing amino acids 1-176 of the ORF4 protein. The truncated version of the protein was employed as a full-length version of the ORF4 protein failed to transform into yeast, potentially due to toxicity.

The ORF4 yeast two-hybrid screens identified a number of interacting proteins (table 5.1). An extensive list and the identity of the clones from transformed yeast colonies gown on selective media can be seen in appendix 4 and 5. Unfortunately, the analysis of sequences revealed that repeatedly identified proteins were identical cDNA clones.

As for the TAP analysis, there is currently no direct evidence to suggest any of the identified interactions are authentic. It is therefore unlikely that these proteins would maintain the interaction with the ORF4 protein under high stringency binding conditions. Consequently, future work will focus on further characterising these interactions. For completeness of this thesis all identified proteins are discussed and the consequences of a potential interaction with the ORF4 protein are hypothesised.

The LexA screen only identified FAZF, a DNA binding transcriptional repressor (Hoatlin et al., 1999). Investigations into the function of FAZF (Dai et al., 2002, Reuter et al., 2003) revealed that FAZF interacts directly with FANCC. Given the fact that FANCC has antiapoptotic activity and studies have shown that overexpression of FAZF leads to apoptosis (Dai et al., 2002), these findings were of considerable interest. As mentioned previously, FANCD2 and the related FANCI were both identified in the NTAP-ORF4 purification. Although FAZF was not purified by NTAP-ORF4, the protein may not have been stable in the complex and may have become disassociated during the purification procedure. Another explanation is that sufficient quantities of FAZF were not present in the complex for positive identification by Mascot sequence query. In terms of understanding the consequences of a potential interaction between the ORF4 protein and FAZF, it could be that this interaction serves to delay apoptosis by preventing an interaction between FAZF and FANCC. Once again, this speculation is purely hypothetical and would of course require further investigation.

In contrast to the LexA screen, the ORF4 protein TetR based screen identified a number of proteins (table 5.1). Overall, RNA binding motif proteins are involved in RNA stabilising and processing events such as export, splicing and translation, but an increasing number also play a role in apoptosis (Martinez-Arribas et al., 2006, Sutherland et al., 2005). Interestingly, the identified RNA binding motif protein, X-linked (Rbmx) has been associated with expression of the proapoptotic Bax protein (Martinez-Arribas et al., 2006), a process which could possibly be disrupted by an interaction between Rbmx and the ORF4 protein.

Another RNA binding protein to be identified was pre-mRNA processing factor 8 (PRP8). PRP8 is an RNA-binding co-factor involved in splicing pre-mRNAs in the spliceosome complex (Ritchie et al., 2008, Wachtel & Manley, 2009). Intriguingly, a proapoptotic protein known as apoptosis regulated protein 2 (ARP2), found in *Xenopus laevis* oocytes demonstrated 99% homology with a small fragment (18%) of the total

PRP8 cDNA sequence (Tapia-Vieyra et al., 2005). To date it has not been investigated whether PRP8, or indeed a potential cleavage product has proapoptotic activity, and hence further investigation could potentially yield some extremely interesting results.

Pre-B-cell leukaemia transcription factor interacting protein 1 (PBX1) acts as a transcriptional activator and has been shown to regulate transcription of the anti-inflammatory cytokine interleukin 10 (IL-10), which is produced in response to apoptosis (Chung et al., 2007). PBX1 was initially identified as an oncogene at a site of chromosomal translocations and was also shown to play an essential role in haematopoiesis (DiMartino et al., 2001). PBX1 also acts as a transcriptional activator of integrated retroviruses such as Moloney murine leukaemia virus (MMLV), with down-regulation of PBX1 or mutation of the MMLV PBX1 binding site associated with reduced transcription (Chao et al., 2003). Consequently, binding of the ORF4 protein to PBX1 may serve to prevent the transcription of genes involved in apoptosis.

Interaction of the ORF4 protein with the nucleoporin NUP107 was of considerable interest, as several nucleoporins and nuclear transport proteins were identified during the TAP tagging analysis. As described previously, the nuclear pore is an essential component for nuclear import as well as export. The NPC is therefore employed by the many transcriptional activators and repressors identified in the NTAP purification as well as the yeast two-hybrid screen. As discussed, NUP107 associates with NUP160 (identified as a component of the NTAP-ORF4 complex) to form the central channel of the NPC (Glavy et al., 2007, Vasu et al., 2001). The fact that both TAP tagging analysis as well as yeast two-hybrid screen identified associated components of the NPC strongly indicates that ORF4 protein association with this complex is authentic. Interestingly, an interaction between the ORF4 protein and the NPC may function to inhibit nuclear transport. In terms of relating this to the process of apoptosis, such an inhibition may be highly beneficial in terms of delaying the transport of proapoptotic molecules such as AIF into the nucleus. By blocking the NPC, inhibition of nuclear export would of course also incur, and thus export of molecules such as the antiapoptotic survivin and the proapoptotic PAR may be affected. This model is however purely speculative to date, and as is the case with all identified proteins, this suspected interaction would have to be verified, for example by co-immunoprecipitation and co-localisation studies.

Although the yeast two-hybrid screen identified the proteins described above, a number of proteins were identified of which little information is available. Similarly,

the interaction between the ORF4 protein and other identified proteins could be seen as highly questionable. Peroxisomal delta3, delta2-enoyl-Coenzyme A isomerase (Peci) is an enzyme which targets the peroxisome and is involved in fatty acid metabolism by catalysing the isomerisation of 3-*cis*-octenoyl-CoA to 2-*trans*-octenoyl-CoA (Geisbrecht et al., 1999). Another identified protein, KLA1009, is an essential microtubule associated ATPase which is involved in mitosis (Leon et al., 2006). KLA1009 is found at the spindle poles of the mitotic apparatus, but during mitosis can be found associated with the centrosome and acts as a microtubule motor to drive the mitotic process (Leon et al., 2006). The screen also identified protein phosphatase 1, regulatory (inhibitor) subunit 12C, which associates with protein phosphatase 1δ and meditates myosin binding and subsequent cytoskeletal reorganisation (Tan et al., 2001).

Although cytoskeletal reorganisation during viral infection is a common phenomenon which is also employed by MNV (Hyde et al., 2009), the role of the ORF4 protein in this process has not been studied. Analysis of cytoskeletal rearrangements during infection using the ORF4 knockout virus M1 could in itself yield some interesting observations, although any differences observed would not affect viral yield (chapter 3). Unfortunately, little is known about the function of Thrombospondin, type I, domain 1 (THSD1). However, seeing that this transmembrane protein may be involved in cell adhesion and tumour angiogenesis (Ko et al., 2008), THSD1 could potentially be linked to gene expression and even to apoptosis, although extensive further investigation would be required.

Protein name[a]	Synonyms[b]	Binding region (amino acids)[c]	Total protein length[d]	Sequ direction[e]	Function[f]
KIAA1009	RIKEN cDNA 4922501C03, C6orf84, FLJ13551, Protein QN1 homolog, QN1, Kiaa1009	1241 - 1400	1403	F	Microtubule-associated ATPase involved in cell division regulating chromosome segregation and mitotic spindle assembly
Nucleoporin 107 (Nup107)	107 kDa nucleoporin, Nuclear pore complex protein Nup107, Nucleoporin Nup107, NUP84	661 - 842	926	F	Essential component of nuclear pore complex. Required for the assembly of peripheral proteins into the nuclear pore complex
Peroxisomal delta3, delta2-enoyl-Coenzyme A isomerase (Peci)	D3,D2-enoyl-CoA isomerase, DBI-related protein 1, Delta(3),delta(2)-enoyl-CoA isomerase, dJ1013A10.3, Dodecenoyl-CoA isomerase, DRS1, DRS-1, HCA88, Hepatocellular carcinoma-associated antigen 88, KIAA0536, Peroxisomal 3,2-trans-enoyl-CoA isomerase, Renal carcinoma antigen NY-REN-1, ACBD2	10 - 147	358	F	Peroxisomal enzyme that catalyzes an isomerisation step required for the beta-oxidation of unsaturated fatty acids
Pre-B-cell leukaemia transcription factor interacting protein 1 (PBX1)	Pre-B-cell leukemia transcription factor, Homeobox protein PBX1, Homeobox protein PRL, DKFZp686B09108, MGC126627	251 - 349	632	R	DNA-binding protein that acts as a transcriptional activator
Pre-mRNA processing factor 8 (PRP8)	Splicing factor Prp8, AU019467, D11Bwg0410e, DBF3/PRP8, Sfprp8l,	861 - 1057	1201	F	Central component of the spliceosome, which may play a role in aligning the pre-mRNA 5'- and 3'-exons for ligation
Protein phosphatase 1, regulatory (inhibitor) subunit 12C (PPP1R12C)	DKFZp434D0412, DKFZP434D0412, LENG3, MBS85, p84, Protein phosphatase 1 myosin-binding subunit of 85 kDa, Protein phosphatase 1 myosin-binding subunit p85, Protein phosphatase 1 regulatory subunit 12C	490 - 622	782	F	Regulates myosin phosphatase activity
RNA binding motif protein, X chromosome (Rbmx)	Glycoprotein p43, Heterogeneous nuclear ribonucleoprotein G, HNRPG, RBMXP1, RBMXRT, RNMX	60 - 229	301	R	RNA-binding protein which may be involved in pre-mRNA splicing
Thrombospondin, type I, domain 1 (THSD1)	Transmembrane molecule with thrombospondin module, MGC74971, TMTSP, UNQ3010, UNQ3010/PRO9769	520 – 644	798	F	Contains a type 1 thrombospondin domain. May be involved in cell adhesion and tumour angiogenesis. Different isoforms produced by alternative splicing.
Fanconi anemia zinc finger protein (FAZF)	FANCC-interacting protein, Zinc finger and BTB domain containing 32 (Zbtb32), FAXF, Rog, Testis zinc finger protein, TZFP, ZNF538	290 - 462	465	F	DNA-binding protein, may function as a transcriptional transactivator and transcriptional repressor

Table 5.1. Proteins identified by the ORF4 protein TetR and LexA yeast two-hybrid screens. (a) Names of the identified ORF4 protein interacting proteins, although alternative names are common (b). The ORF4 protein interacting region (c) of the identified proteins is shown in relation to the full-length protein (d). Sequencing to identify positive clones was performed by Proteinlinks using either a forward (F) or reverse (R) sequencing primer (e). Hence in the case of forward sequencing, the binding region may extend towards the C-terminus of the full-length protein, whereas in the case of reverse sequencing the binding region may extend towards the N-terminus of the identified interacting protein. (f) Short description of protein function (more detailed description can be found in the text).

5.3 Conclusions and future directions

The identification of numerous proteins in the NTAP-ORF4 purification gave a strong indication to possible mitochondrial, nuclear and / or ER/Golgi localisation (also supported in chapter 6). The fact that both yeast two-hybrid and TAP analysis identified NUP proteins was of considerable interest and strongly suggests an authentic interaction between the NPC and the ORF4 protein. Indeed, subsequent studies indicated that the ORF4 protein could be identified within the nucleus and at least partially co-localised with AIF (chapter 6). Unfortunately, preliminary attempts to co-immunoprecipitate the ORF4 protein and AIF in virus infected cells were unsuccessful (data not shown). In spite of this, the fact that both yeast two-hybrid screen and TAP analysis identified many proteins involved in the process of apoptosis was of considerable interest and has direct relevance to the predicted function of the ORF4 protein (investigated in chapter 7 and discussed in detail in chapter 8).

In terms of further experiments, the aim was to refine the list of NTAP-ORF4 binding partners by repeating this large scale TAP purification, especially as many proteins were identified in the complex even though they likely did not directly interact with NTAP-ORF4. Therefore, the discussions regarding the possible consequences of an interaction between the ORF4 protein and the identified proteins are at this stage purely speculative. There were also concerns that the $CdCl_2$ inducible system was not the best choice for the purification, due to the toxic effect $CdCl_2$ exerts on cells. Even at the comparatively low concentration of 5 μM (10 μM was used to induce NTAP-ORF4), $CdCl_2$ has indeed been shown to alter gene expression patterns, especially in relation to mitochondrial apoptosis (Cannino et al., 2008). Therefore, repeat of the NTAP-ORF4 purification in the tetracycline inducible system would serve to verify the previously identified binding partners and would possibly aid in refining the list of authentic binders. As the presence of any tag is likely to affect protein structure to some degree and hence affect the host cell factors which are identified by TAP analysis, purifications using ORF4-CTAP expressing cell lines could be used in order to compare results. Although several attempts were made to repeat this large scale TAP purification, this was not completed successfully. The most likely reason for this was due to a low yield of protein during the purification. Therefore, future analyses would require the use of a larger number of cells to carry out the purification. Furthermore, the generation of stable MNV-permissive cell lines expressing NTAP-

ORF4 or ORF4-CTAP would also be important. This would allow the purification to be performed in the presence of MNV infection, and hence proteins isolated from infected and non-infected cells could be compared. Unfortunately, previous attempts to generate a stable NTAP-ORF4 expressing RAW26.7 cells was unsuccessful potentially due to low transfection efficiency and possible toxicity of the ORF4 protein. In the future, attempts could be repeated by infecting RAW264.7 cells with lentiviruses carrying the TAP constructs.

Although results from the yeast two-hybrid screen underline many of the TAP purification findings, it must be remembered that this technique also has disadvantages. One such disadvantage is the fact that interactions identified by yeast two-hybrid screen are based on overexpressed proteins, and that interactions in yeast cells may not accurately represent authentic interactions in cells permissive to MNV infection. As the screen was performed using a truncated version of the ORF4 protein, the identified binding partners may not represent proteins which actually bind to the full-length protein. This argument is also the case for the prey protein, which frequently did not contain the entire protein sequence; hence an interaction between the full-length ORF4 protein and the full-length prey protein may not be the case.

Consequently, for both NTAP-ORF4 identified proteins as well as those identified in the yeast two-hybrid screen, an interaction between the protein of interest and the ORF4 protein must be examined more closely, for instance by immunoprecipitation. Streptavidin pulldown of the TAP tagged protein from induced lysates and subsequent western blot using antibodies against the protein of interest is one method of demonstrating an interaction. Immunoprecipitation using antibodies is a more direct approach which can be performed on infected cells and eliminates interference from additional epitope or purification tag sequences. However, this approach requires suitable antibodies for both proteins and it is possible that the antibody binding site overlaps with the protein interaction site. If suspected that large tags interfere with the interaction, immunoprecipitation using a Flag tagged version of the ORF4 protein could also be an approach as the small Flag tag is less likely to interfere with interactions. In terms of studying co-localisation, bimolecular fluorescence complementation (BiFC) could also be employed. In this relatively novel technique the C terminal portion of GFP is fused to one protein of interest, whilst the N-terminus is fused to another (Hu et al., 2005). If the proteins interact, the fluorescence signal can be detected by confocal microscopy with the added benefit that cellular localisation

can also be studied (Hu et al., 2005). This technique is beneficial not only because it is possible to study protein interactions in living cells, but also because a number of associated binding partners can be analysed at the same time by using different fluorescent tags (Hu et al., 2005). Once again however, the question of potential interference from the tag arises and a number of combinations are possible for generating the fusion proteins.

In conclusion, results from the successful NTAP-ORF4 purification were used to approach the question of cellular localisation of the ORF4 protein (chapter 6) and involvement in the process of apoptosis (chapter 7). Although verification of the interactions between the ORF4 protein and any of the identified proteins remains to be demonstrated, a hypothetical model linking a great number of these identified proteins with a proposed function of the ORF4 protein can be found in the concluding chapter (chapter 8) of this PhD thesis.

6. Localisation studies

6.1 Introduction

The next approach during the course of these studies was to investigate the cellular localisation of the ORF4 protein. As described in chapter 5, the identification of a great number of mitochondrial, nuclear and ER/Golgi enzymes in the TAP tagging analysis strongly suggested that the ORF4 protein localises to some, if not all of these organelles. There are many approaches to studying the cellular localisation of proteins, one of which is confocal microscopy. One advantage of this technique is that the analysis of localisation of a particular protein does not depend on the availability of a suitable antibody. If an antibody to a particular protein is not available or not suited for confocal microscopy, then constructs expressing fluorescently tagged fusion proteins can be expressed. Fluorescent tags include for example the widely used enhanced and optimised versions of GFP, which was first isolated from the jellyfish *Aequorea victoria* and exhibits green fluorescence when exposed to blue light (Tsien, 1998). Because the use of tags may interfere with protein folding, it is of course desirable to confirm localisation with the use of antisera. In the case of viral infection the use of antisera to localise the protein of interest is particularly important, as localisation may depend on the co-expression of other viral proteins. However, another approach to study localisation is biochemical fractionation, a procedure by which the organelles of interest can be isolated. In this chapter, the localisation of GFP fusions of the ORF4 protein were investigated by confocal microscopy and results were confirmed biochemically in infected cells. In later work described in a separate discussion section of this chapter, Guia Carrara an MSc student under my supervision generated high resolution images of the ORF4 GFP fusions, thus confirming localisation. Guia Carrara also generated truncations of the ORF4 GFP fusion proteins and examined localisation in addition to comparing the localisation of MNV ORF4 to SV ORF4E-GFP fusion proteins.

6.2. Results and Discussion

6.2.1 Confocal microscopy demonstrating mitochondrial localisation

The localisation of the MNV ORF4 protein in cells was investigated using confocal microscopy. Unfortunately, due to a high degree of non-specific cross reactivity with

other proteins, the ORF4 protein specific antibody was not suitable to use for confocal microscopy (figure 6.1).

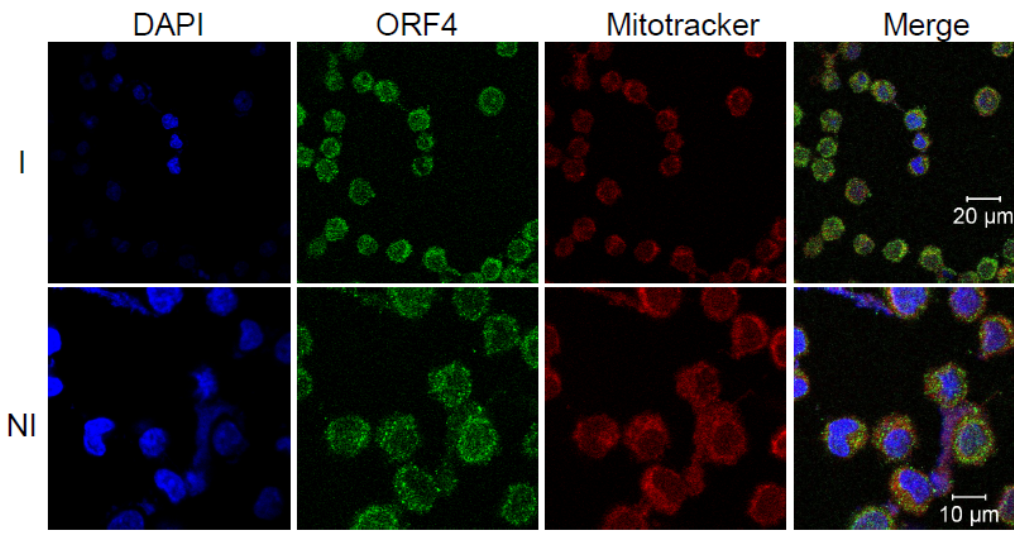


Figure 6.1. Confocal microscopy analysis of ORF4 protein localisation in infected RAW264.7 cells using the ORF4 protein specific cross reactive antibody. RAW264.7 cells were infected (I) with MNV and were fixed 16 h post transfection with 4% paraformaldehyde. Cells were incubated with Mitotracker red dye (Invitrogen) for 45 min prior to fixation in order to stain the mitochondria. Nuclear staining was carried out by mounting slides in moviol containing DAPI (4',6-diamidino-2-phenylindole). Non-infected (NI) RAW26.7 cells served as a control. Images shown here as well as subsequent images were taken using a Zeiss Meta510 confocal microscope.

Therefore, due to the non-suitability of the ORF4 protein cross reactive antibody, localisation was addressed by generating both C-terminal (ORF4-GFP) and N-terminal (GFP-ORF4) GFP fusion proteins. Unfortunately, when using MNV permissive cell lines (RAW264.7 and IC21 cells), difficulties were encountered both in expressing the ORF4 protein, as well as generating images in which cellular organelles could be easily distinguished due to the spherical nature of the mouse macrophage cell lines in our laboratory. Therefore, cell lines which allowed easy visualisation of various cytoplasmic organelles were used to visualise the GFP fusion proteins. Although permissive to MNV replication, these cell lines can not be infected with MNV, which is predicted to be because of MNV receptor specificity. Cell lines in which GFP fusions of the ORF4 protein were investigated include human embryonic kidney cells (293T), baby hamster kidney cells (BHK) and African green monkey kidney cells (COS-7).

Results from the initial confocal microscopy analysis of ORF4-GFP and GFP-ORF4 fusion proteins performed in 293T cells indicated cytoplasmic punctuated structures

reminiscent of previously published images of mitochondrial localisation. This was confirmed by co-localisation analysis, where co-staining was seen between ORF4-GFP and GFP-ORF4 fusion proteins and the MitoTracker red dye used to stain the mitochondria (figure 6.2). As expected, untagged GFP expression was uniformly distributed and was not associated with a particular cellular location (figure 6.2).

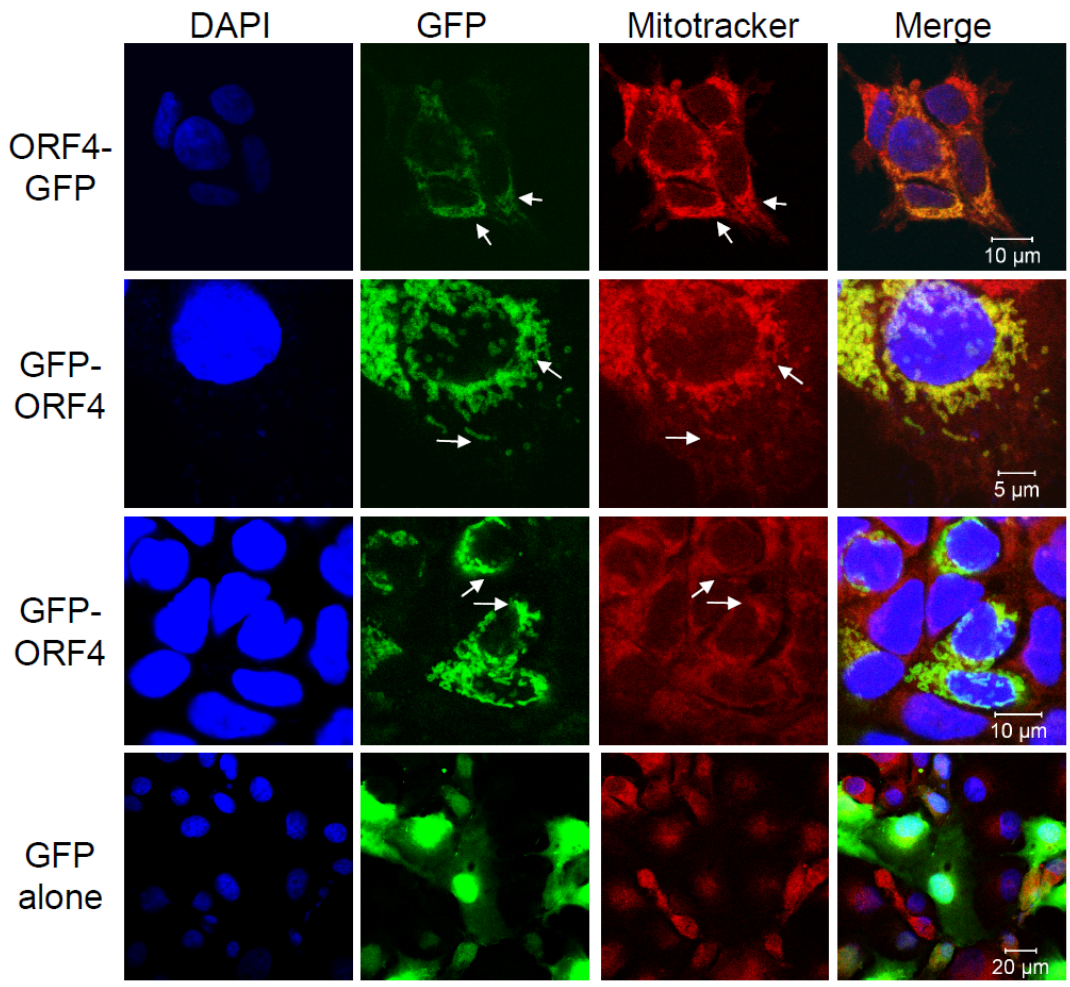


Figure 6.2. Confocal microscopy analysis of ORF4 protein localisation using GFP fusion proteins. 293T cells were transfected with GFP expression constructs and were incubated with Mitotracker red dye (Invitrogen) for 45 min prior to fixation. Cells were fixed 16 h post transfection with 4% paraformaldehyde and nuclear staining was carried out by mounting slides in moviol containing DAPI.

Although these initial results demonstrated mitochondrial localisation, the quality of the photomicrographs was not sufficient in terms of resolution, and even after several attempts it was concluded that the stacked morphology of these cell lines did not permit the generation of focused high resolution photomicrographs. Therefore, in order to generate high resolution photomicrographs, GFP fusions of the ORF4 protein were expressed in BHK cells, which improved the quality of the images in terms of

resolution (figure 6.3). Again mitochondrial localisation was observed for GFP-ORF4 as well as ORF4-GFP.

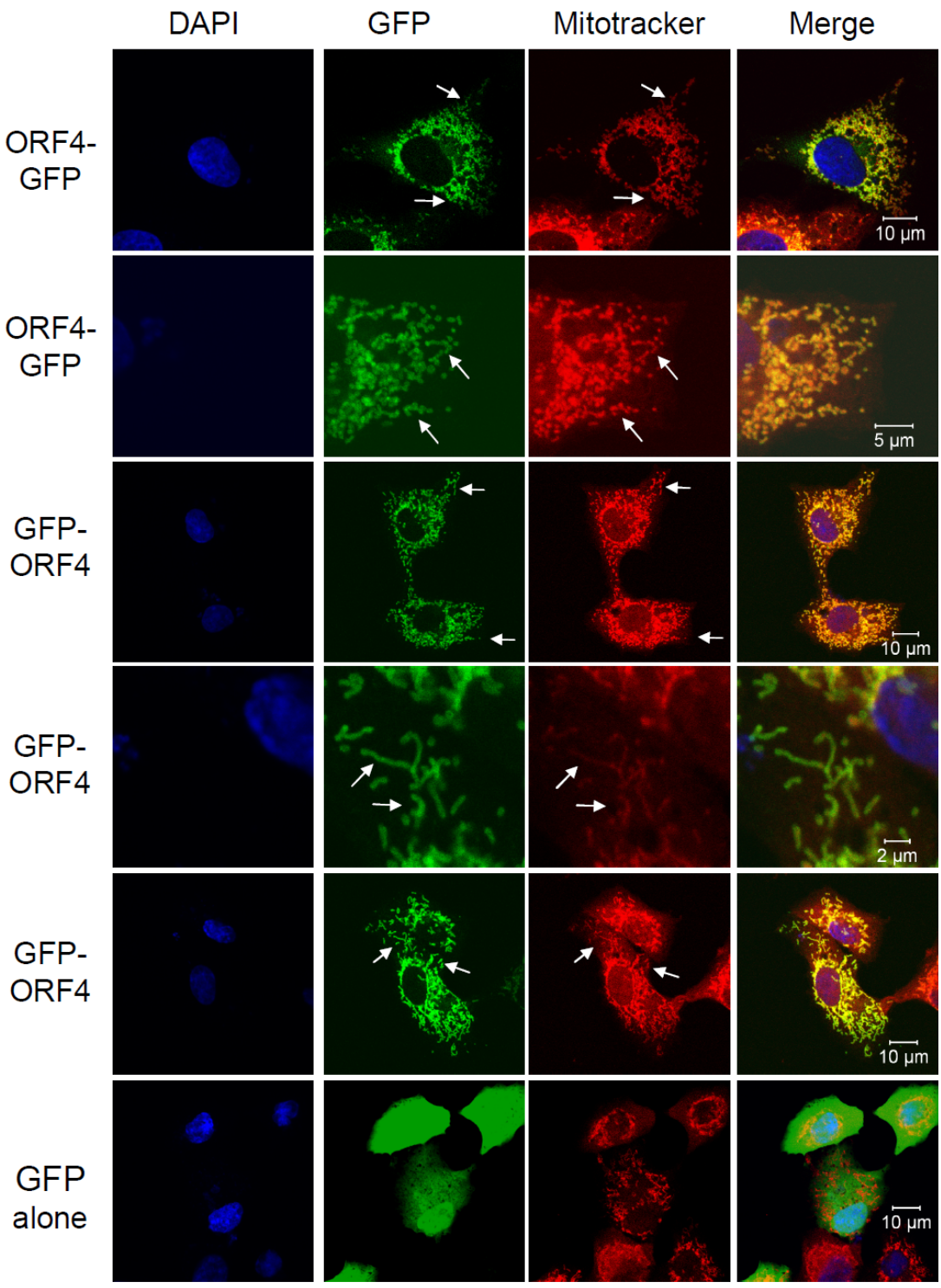


Figure 6.3. Confocal microscopy analysis of ORF4 GFP fusions in BHK cells. BHK cells were transfected with GFP expression constructs and were incubated with Mitotracker red dye (Invitrogen) for 45 min prior to fixation. Cells were fixed 16 h post transfection with 4% paraformaldehyde and nuclear staining was carried out by mounting slides in moviol containing DAPI.

These results coincide with proteomic as well as bioinformatic analysis of the ORF4 amino acid sequence, which predicted mitochondrial localisation of the ORF4 protein (data not shown). Bioinformatic predictions of this nature are carried out by comparing the sequence in query to sequences of proteins with known localisation. Components such as charge, amino acid composition, hydrophilicity, the presence of signal sequences, DNA binding domains and predicted secondary structures are also taken into account. Often a hierarchal system of exclusion is performed, whereby the protein is analysed in a series of steps. If the probability of localisation to a particular compartment is excluded at a certain step because of the properties of the protein in question, the protein is further analysed in the next step for localisation to the next compartment in question. Algorithms which predicted mitochondrial localisation of the ORF4 protein include LOCtree (Nair & Rost, 2005), MitoProt (Claros & Vincens, 1996), PSORT II (Nakai & Horton, 1999, Nakai & Kanehisa, 1992), MuliLoc (Hoglund et al., 2006) and CELLOv2.5 (Yu et al., 2006).

However, in spite of the predictions by these algorithms, no MTS could be identified within the amino acid sequence of the ORF4 protein. Similar to cellular mitochondrial proteins, viral proteins targeted to the mitochondria require a MTS. MTSs can be C-terminal, for example as is the case in influenza virus PB1-F2 (Yamada et al., 2004) and the CMV UL9 protein (Mandic et al., 2009), N-terminal as is the case for AIF or the ORF1 product of the Carnation Italian ringspot virus (Weber-Lotfi et al., 2002), or internal as is the case for cytochrome *c* (Stojanovski et al., 2007). In many cases, both N-and C-terminal MTSs can be identified by bioinformatics based on sequence comparison and predicted structure of known mitochondrial proteins. Internal signal sequences on the other hand are much more difficult to identify, as they sometimes stretch over the entire length of the protein and are dependent on protein 3D conformation (Dinur-Mills et al., 2008).

Even though these images sufficiently demonstrated mitochondrial localisation of the ORF4 protein, it was decided that higher resolution photomicrographs should be attempted in the morphogenically larger and flatter COS-7 cells, as these cell lines were the most suitable to allow easy visualisation of various cytoplasmic organelles. Furthermore the identification of the ORF4 protein MTS was attempted by generating N-terminal truncations of the ORF4-GFP proteins. As this analysis was performed by Guia Carrara as part of an MSc project the results are therefore presented in a separate discussion section as part of this chapter.

6.2.2 Biochemical localisation of the MNV ORF4 protein

After discovering that GFP fusions of the MNV ORF4 protein predominantly localised to the mitochondria, it was important to verify mitochondrial localisation of native untagged ORF4 protein during the course of infection. Due to technical difficulties in the use of our permissive cell lines as well as difficulties in the use of the ORF4 antibody for confocal microscopy, an alternative biochemical procedure was used to separate mitochondria from other cellular organelles (figure 6.4a). This technique exploits the fact that the mitochondrial membrane is not soluble in certain detergents and hence can be purified by lysis in this reagent followed by centrifugation to separate the soluble and insoluble proteins.

Using this technique, mitochondria and cytosolic fractions were isolated from infected and non-infected control cells. Subsequent SDS-PAGE and western blot analysis of these fractions demonstrated the ORF4 protein did indeed localise to the mitochondria of infected cells (figure 6.4b). To ensure purity of the fractions, the predominantly mitochondrial AIF was used as a mitochondrial control, whereas the well characterised (Berry et al., 2006) PCBP-1 was used as a control for the cytosolic fraction (figure 6.4). As can be seen, both control proteins were found in the anticipated fractions with little or no cross contamination between fractions (figure 6.4b). As a further control, the lysates of infected and non-infected cells lysed directly into reducing sample buffer were also run alongside the isolated fractions (figure 6.4b). Most importantly, the western blot using the antibody against the ORF4 protein revealed that the ORF4 protein strongly associated with the mitochondrial fraction, thus confirming the results found by confocal microscopy.

Importantly, although these results highlighted mitochondrial localisation of the ORF4 protein, alternative cellular (such as nuclear) localisation would not necessarily have been shown by this analysis, as the first step after lysis is to remove unlysed cells and other large organelles, including the nucleus by low speed centrifugation (figure 6.4a). Also, the small amount of ORF4 protein residing in the nucleus may have been undetectable by western blot analysis.

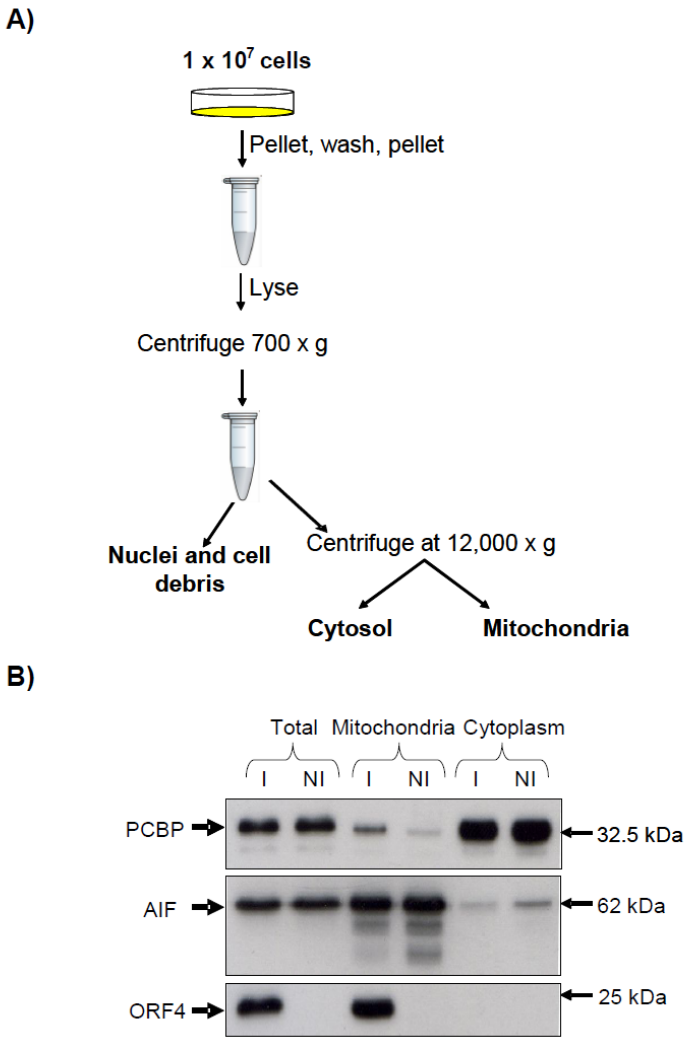


Figure 6.4. Biochemical characterisation of ORF4 protein localisation. A) Brief overview of the steps performed to separate mitochondria and cytosolic fractions of infected (I) versus non-infected (NI) cells. **B)** Proteins contained within total cell lysates and the mitochondrial and cytosolic fractions were separated by SDS-PAGE. Western blots were performed against the ORF4 protein, the cytosolic (PCBP-1) and the predominantly mitochondrial AIF.

6.3 Presentation and discussion of further work performed by Guia Carrara

6.3.1. Further characterisation of MNV ORF4 protein localisation

Using confocal microscopy and a biochemical approach, the mitochondrial localisation of the ORF4 protein was successfully demonstrated. However, after being tutored in all the relevant techniques, high resolution photomicrographs demonstrating the

mitochondrial localisation of GFP-ORF4 and ORF4-GFP in COS-7 cells were generated by Guia Carrara as part of her MSc project (figure 6.5). COS-7 cells were chosen due to the favourable morphology which makes them suitable for high resolution confocal microscopy.

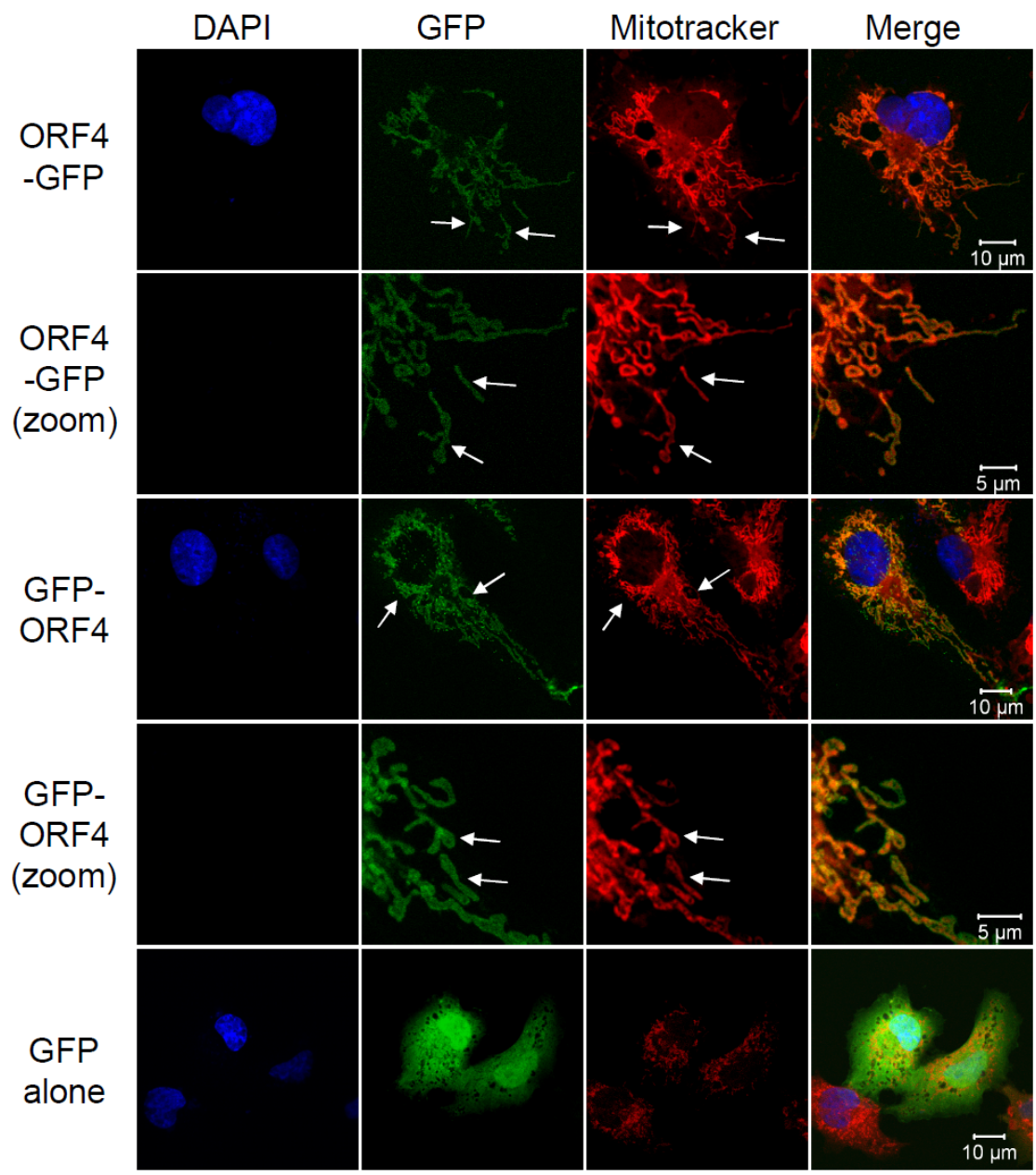


Figure 6.5. Confocal microscopy analysis of ORF4 GFP fusions in COS-7 cells. Cells were transfected with GFP expression constructs and were incubated with Mitotracker red dye (Invitrogen) for 45 min prior to fixation. Cells were fixed 16 h post transfection with 4% paraformaldehyde and nuclear staining was carried out by mounting slides in moviol containing DAPI. HM: high magnification of image displayed in higher panel.

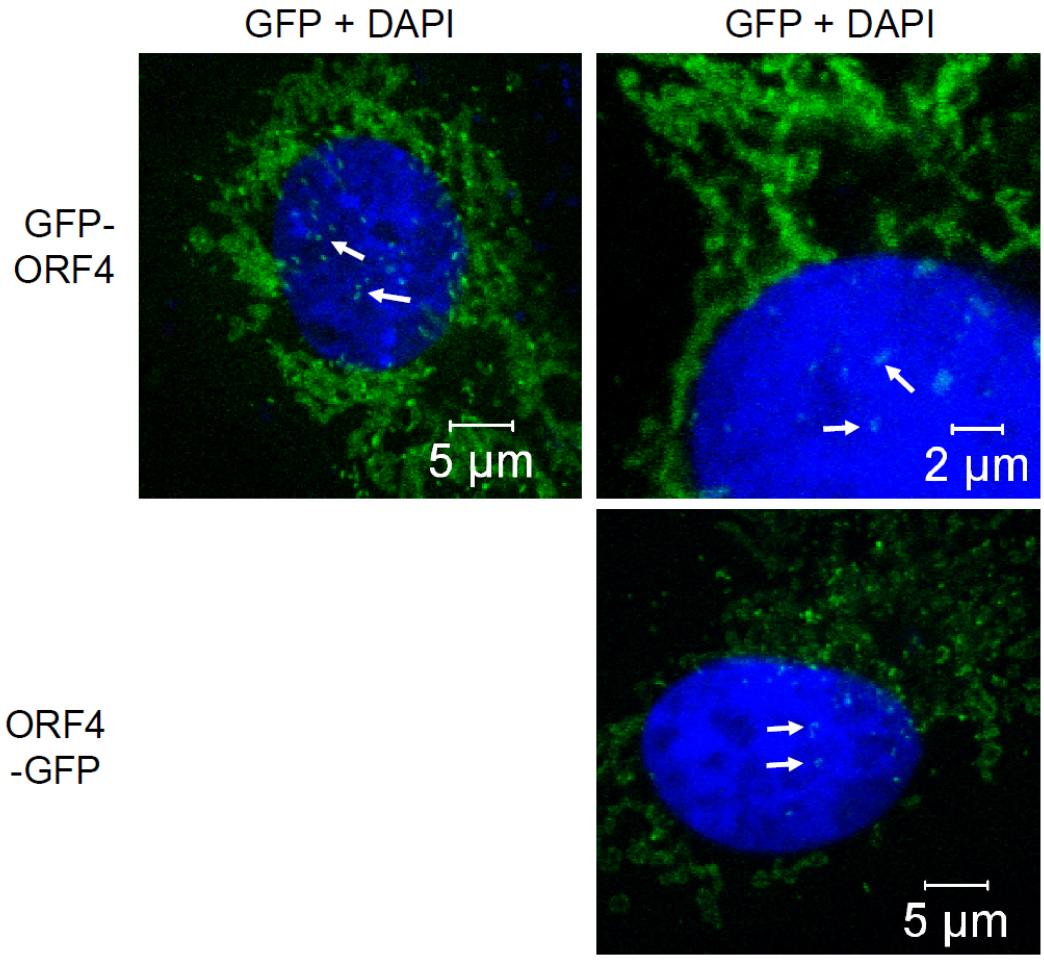


Figure 6.6. Partial nuclear localisation of the GFP-ORF4 and ORF4-GFP proteins. COS-7 cells were transfected with GFP-ORF4 or ORF4-GFP expression constructs and were fixed 16 h post transfection with 4% paraformaldehyde. Nuclear staining was carried out by mounting slides in moviol containing DAPI (4',6-diamidino-2-phenylindole). Top left image is a higher magnification image of one shown in figure 6.5.

Most interestingly, although less evident than the mitochondrial localisation, in some examples, foci of GFP-ORF4 or ORF4-GFP were also seen either in, or in very close proximity to the nucleus (figure 6.6). Although this could have been an artefact of GFP-ORF4 or ORF4-GFP overexpression, it is possible that the ORF4 protein also localised to the nuclear envelope and in some cases was translocated into the nucleus.

In order to confirm these findings, fixed and permeabilised GFP-ORF4 transfected cells were stained AIF, a predominantly mitochondrial protein. As expected, mitochondrial co-localisation between AIF and GFP-ORF4 was seen (figure 6.7).

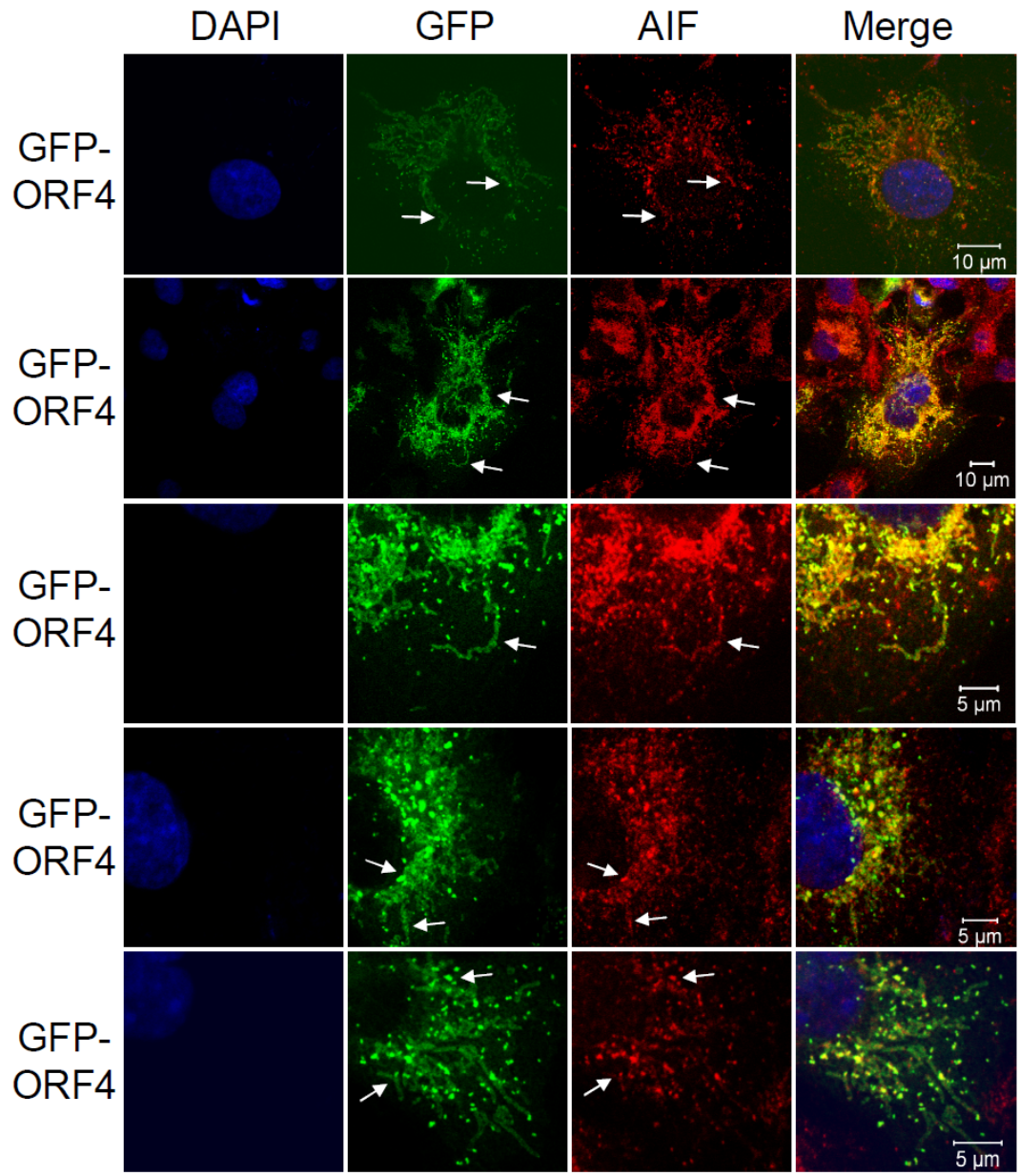


Figure 6.7. Confocal microscopy images underlining mitochondrial localisation of GFP-ORF4. COS-7 cells transfected with GFP-ORF4 were fixed, permeabilised and incubated with an AIF specific antibody, which was followed by incubating with an Alexa Fluor® 546 conjugated secondary antibody. Slides were subsequently mounted in moviol containing DAPI.

The use of the AIF antibody also served to investigate the potential co-localisation between the ORF4 protein and AIF, a protein identified as a potential binding partner of the ORF4 protein using proteomics. As mentioned previously, upon stimulation of apoptosis, AIF exits the mitochondria and translocates to the nucleus. Even though the GFP transfected cells had not been actively stimulated to undergo apoptosis, it was not surprising to see that in some cases small foci of AIF localised to the nucleus, probably

as a consequence of the transfection reagent acting as an apoptotic stimulant (figure 6.7). Interestingly, foci of GFP-ORF4 were again observed in and particularly around the nucleus, and in some cases co-localisation could be seen with AIF (figure 6.8). This co-localisation therefore greatly underlined findings from the proteomics analysis which identified mitochondrial as well as nuclear proteins from the NTAP-ORF4 purification.

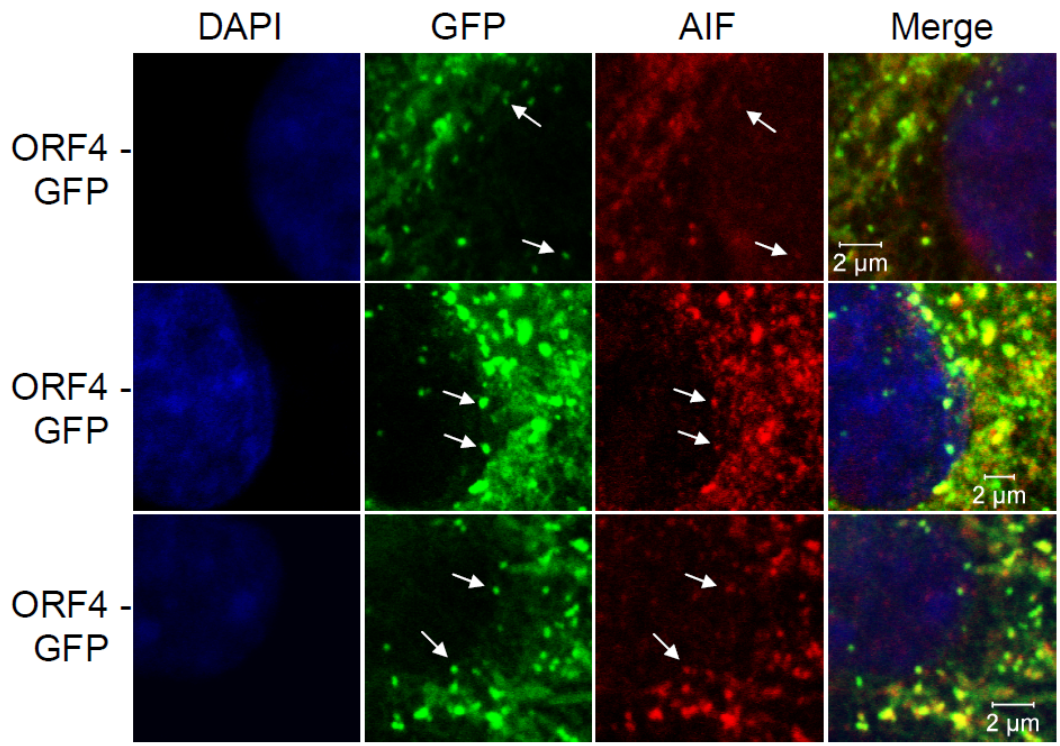


Figure 6.8. Co-localisation of GFP-ORF4 with AIF, particularly at the nuclear membrane. Samples were prepared as in figure 6.3 and represent higher magnification images of the ones shown in figure 6.3.

In order to identify the ORF4 MTS, N-terminal truncations were chosen as a starting point simply because many MTS are N-terminal (Neupert, 1997). In total, three truncations of ORF4-GFP were generated by Guia Carrara. When designing the truncations, bioinformatically predicted α-helices (using the PSIPRED predication method) were taken into account (figure 6.9). ORF4-GFP truncations were named Δ 1-19 ORF4-GFP, Δ 1-56 ORF4-GFP and Δ 1-123 ORF4-GFP, depending on the number of amino acids which has been truncated.

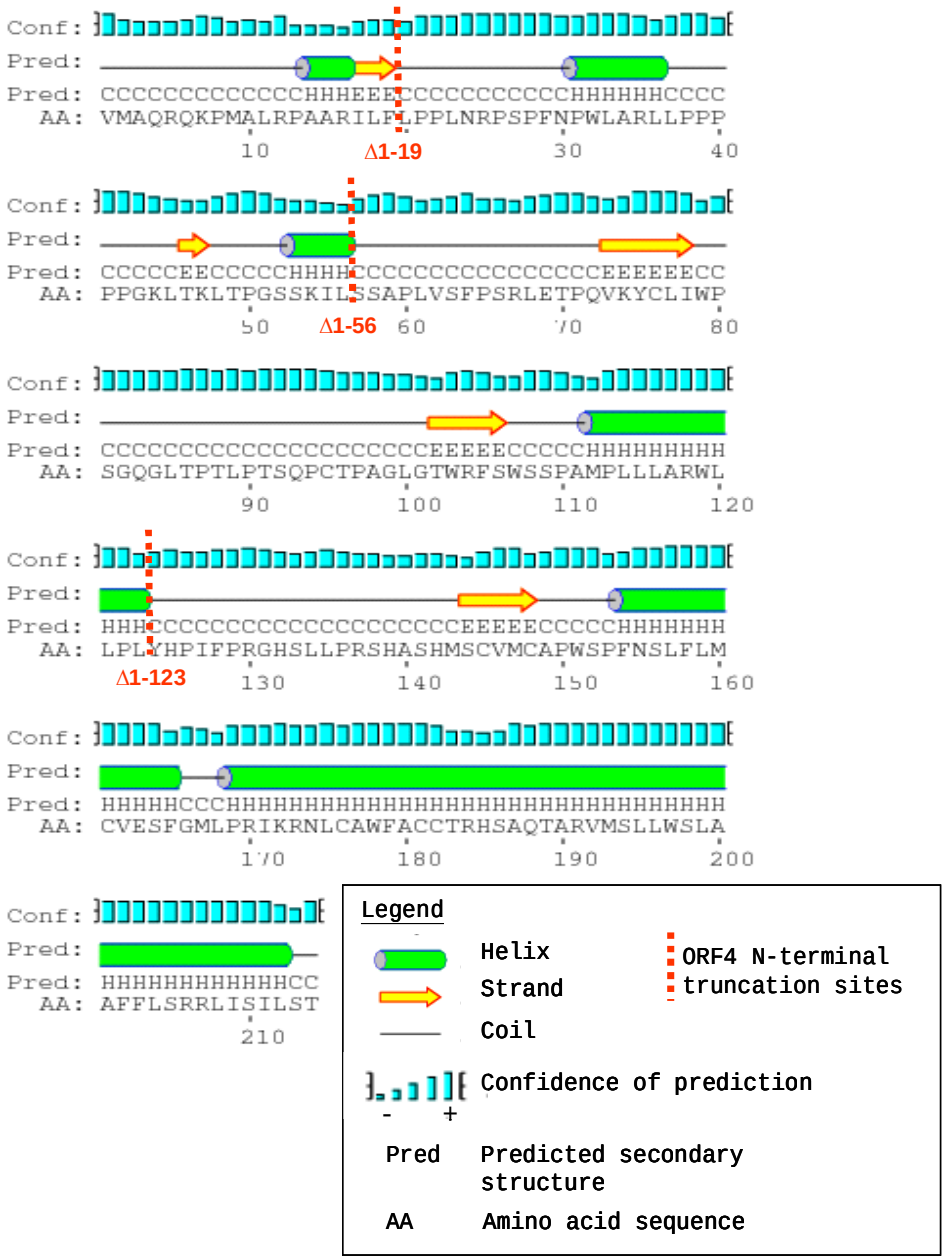


Figure 6.9. Design of N-terminal truncations of the ORF4 protein in ORF4-GFP. Figure demonstrating the predicted helices and coils in the ORF4 protein. These bioinformatic predictions were performed using the PSIPRED v2.6 software (Bryson et al., 2005). The sites of the three truncations are marked with dashed red lines. The ORF4 protein C-terminally fused to GFP was truncated after 19, 56 or 123 amino acids.

Surprisingly, confocal microscopy analysis demonstrated mitochondrial localisation of all three truncations (figure 6.10), thus narrowing down the ORF4 MTS to the last 91 C-terminal amino acids of the ORF4 protein. Therefore, it was concluded that the N-terminus is not required for mitochondrial localisation of the ORF4 protein. As a result, the ORF4 MTS was predicted in the C-terminus, which in fact is the case for an

increasing number of proteins including the UL9 protein of CMV (Mandic et al., 2009) and PB1-F2 of influenza A (Yamada et al., 2004).

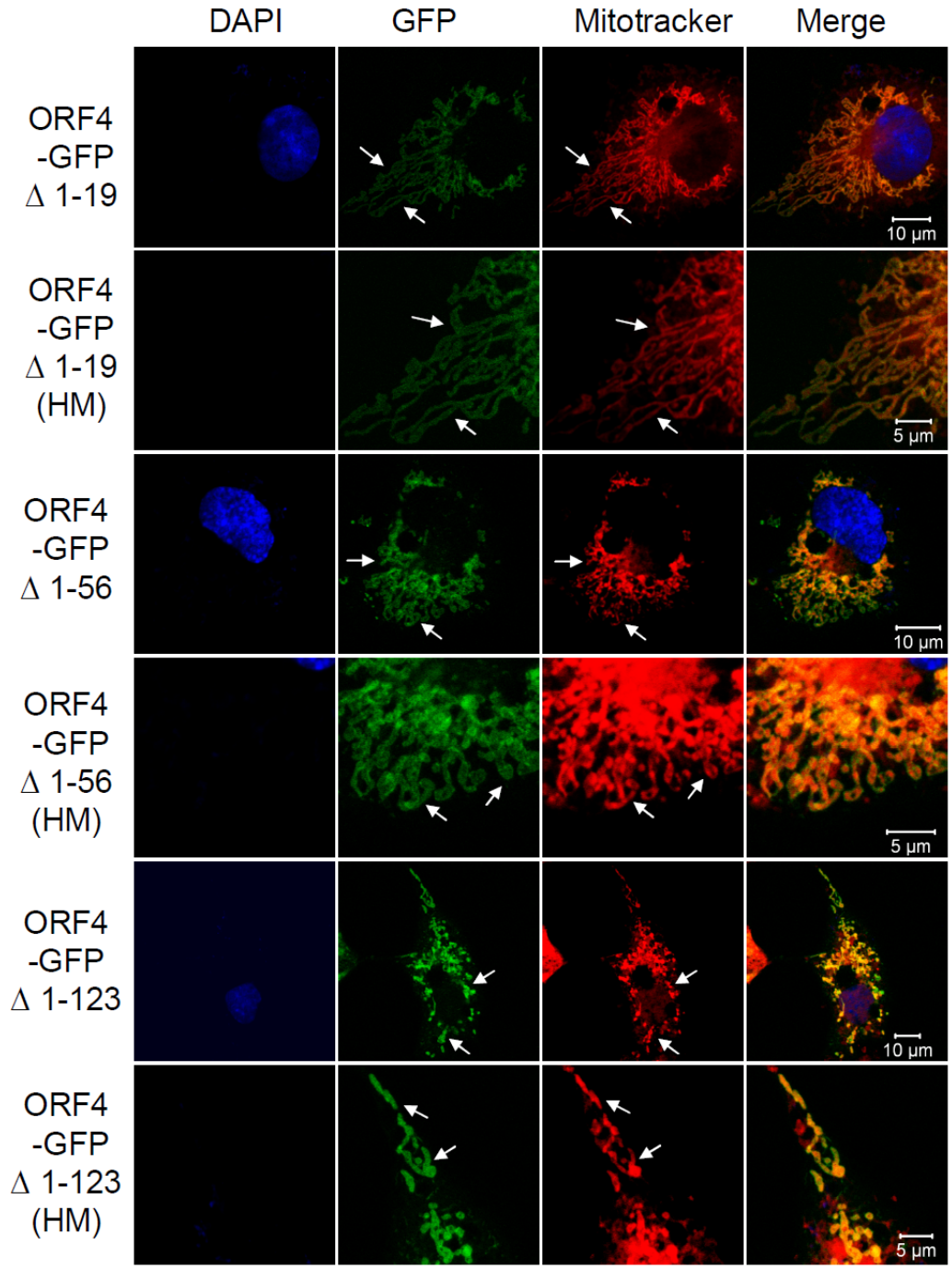


Figure 6.10 Confocal microscopy images demonstrating mitochondrial localisation of all three N-terminal truncations of ORF4-GFP. COS-7 cells were either transfected with Δ 1-19 ORF4-GFP, Δ 1-56 ORF4-GFP or Δ 1-123 ORF4-GFP. Cells were incubated with Mitotracker red dye (Invitrogen) for 45 min prior to fixation and nuclear staining, as previously described. HM: High magnification of image displayed in the higher panel.

Closer bioinformatic analysis of the C-terminal 91 amino acids did not identify a known MTS, indicating that the signal is previously unidentified MTS. As many MTS are located within α-helical regions (Endo & Kohda, 2002), it is likely that the ORF4 protein MTS is located with the C-terminal 60 amino acids, which contains two predicted α-helices (figure 6.10). Consequently, future work will focus on identifying the minimal sequence required for mitochondrial localisation. This will be done by generating further truncations in ORF4-GFP, and results could be compared to truncations generated in the N-terminal ORF4 fusion protein (GFP-ORF4). Alternatively, it is also possible that the ORF4 protein localises to the mitochondria by interacting with another mitochondrial targeted protein. Should this be the case then further analysis of binding partners by proteomic analysis as discussed in chapter 5 could yield some interesting results.

6.3.2 Analysis of the ORF4 protein equivalent of Sapovirus

The identification and characterisation of MNV ORF4 as an authentic reading frame, which expresses a protein involved in virulence, naturally raised the question whether or not the overlapping ORF4E sometimes found in human SV performs a similar function. However, the lack of a tissue culture system for human caliciviruses and the lack of a suitable antibody against the SV ORF4E protein have severely limited any kind of investigation to date. Therefore, comparative confocal microscopy analysis between GFP fusions of the MNV ORF4 protein and the SV ORF4E protein was investigated by Guia Carrara.

Like the MNV ORF4 protein, bioinformatic analysis predicted the SV ORF4E protein to be mitochondrial, in spite of the relatively little homology (nucleotide or amino acid) between the smaller, 161 amino acid SV protein and the 214 amino acid protein encoded by MNV ORF4 (data not shown). As for the MNV ORF4 protein, mitochondrial localisation predictions were performed using the algorithms LOCtree (Nair & Rost, 2005), MitoProt (Claros & Vincens, 1996) and PSORT II (Nakai & Horton, 1999, Nakai & Kanehisa, 1992) (data not shown). Interestingly, contrary to bioinformatic predictions, both C- and N-terminal SV ORF4E-GFP fusions did not localise to the mitochondria, as no co-localisation could be seen with the MitoTracker red stain used to stain the mitochondria (figure 6.11).

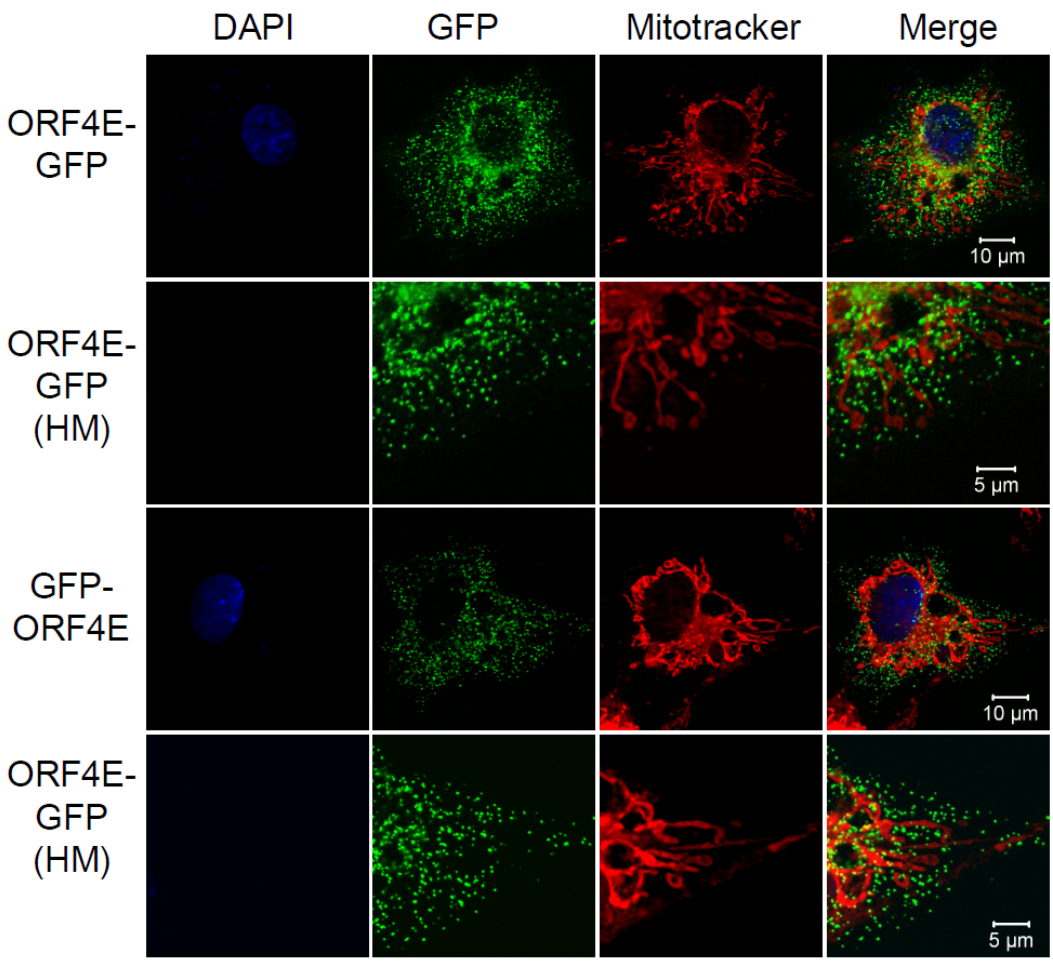


Figure 6.11. The SV ORF4E protein does not localise to mitochondria. COS7 cells transfected with GFP-ORF4E or ORF4E-GFP expressing constructs underwent mitochondrial staining with Mitotracker red dye prior to fixation, mounting and nuclear staining as previously described.

However, co-staining of the ER of GFP-ORF4E and ORF4E-GFP expressing cells using an antibody to calnexin revealed that both GFP-ORF4E and ORF4E-GFP localised to the ER (figure 6.12). This ER localisation was confirmed in GFP-ORF4E and ORF4E-GFP transfected cells by co-expressing Kdel:HRP, which localises to and is retained within the ER due to the Kdel ER retention motif (data not shown). Bioinformatic analysis could not identify an ER retention motif within the SV ORF4E protein (data not shown). Furthermore, ER localisation of the ORF4E protein did not demonstrate uniform distribution (figure 6.12), which could either indicate localisation to certain ER compartments or localisation at ER exit sites. Many cases of ER localisation of viral proteins have been reported, especially as replication complex formation is frequently associated with ER/Golgi associated membranes. For example, in related caliciviruses this has been shown for FCV (Bailey et al., 2010a) as well as

MNV non-structural proteins (Hyde et al., 2009). In order to verify these results and exclude possible interference in localisation from the relatively large GFP protein, preliminary confocal microscopy analysis using a smaller C-terminal FLAG tagged fusion of ORF4E was performed. This approach was however unsuccessful, possibly due to low expression levels or conformation constraints preventing access of the primary antibody (data not shown). Future analysis of SV ORF4E protein localisation could therefore be addressed by generating a suitable antibody against the SV ORF4E protein.

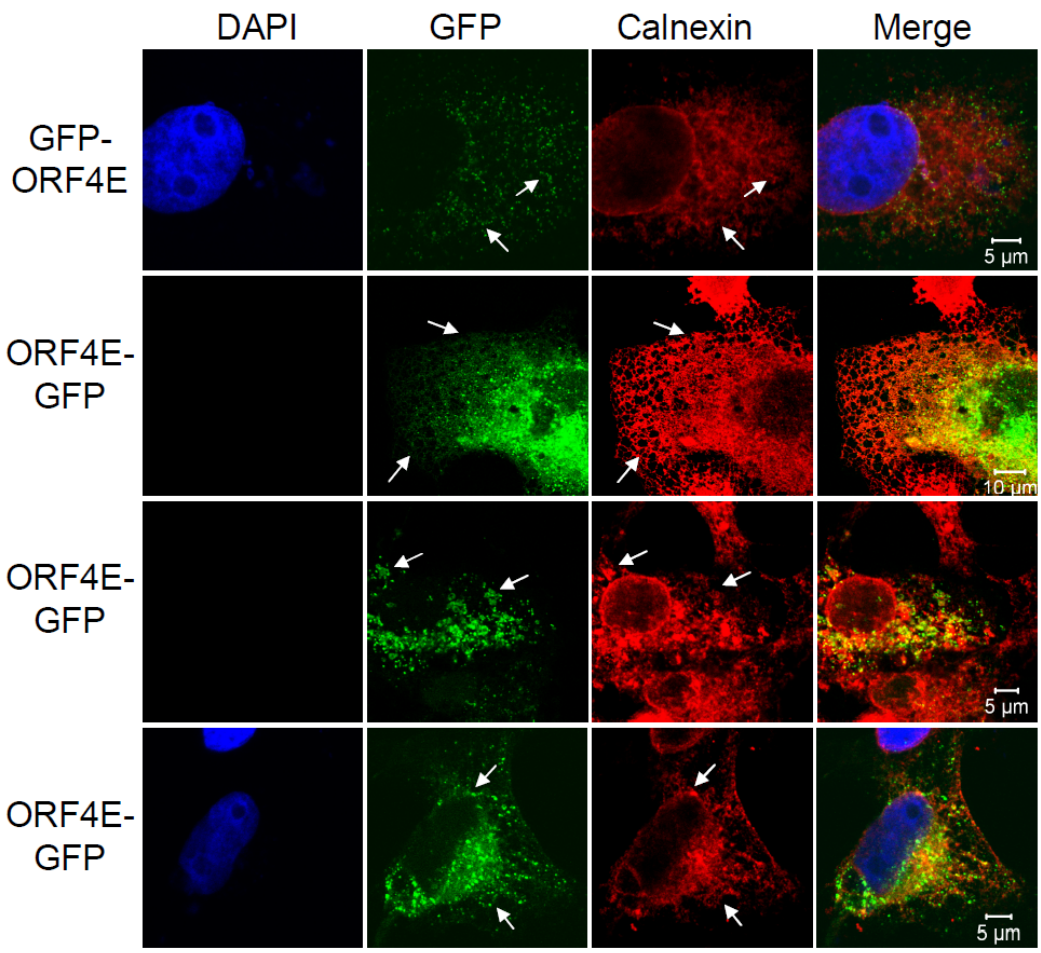


Figure 6.12. ER localisation of the SV ORF4E protein. COS7 cells transfected with GFP-ORF4E or ORF4E-GFP expression constructs were fixed, permeabilised and incubated with a calnexin specific antibody, which was followed by incubating with an Alexa Fluor® 546 conjugated secondary antibody. Slides were mounted in moviol containing DAPI.

6.4 Final conclusion

Using GFP fusions, the mitochondrial localisation of the ORF4 protein was demonstrated in 293T, BHK and COS-7 cells. Mitochondrial localisation was supported by a biochemical fractionation procedure in infected cells. In addition to mitochondrial localisation, the high resolution photomicrographs generated in COS-7 cells by Guia Carrara demonstrated distinct foci of nuclear localisation. Guia's results also demonstrated that the ORF4 protein appeared to co-localise with AIF, a predominantly mitochondrial protein which was also identified by proteomic analysis (chapter 5). Whilst the mitochondrial co-localisation between AIF and the ORF4 protein was expected, it was interesting to observe this co-localisation in foci surrounding the nucleus which may have been components of the nuclear envelope. In some cases co-localisation between AIF and the ORF4 protein within the nucleus was also observed. Especially as mitochondria play a key role in the execution of apoptosis one future approach could be to examine this co-localisation under stimulation of apoptosis. This would be especially interesting, as the ORF4 protein was later shown to be involved in the process of apoptosis (chapter 7). As described, after stimulation of apoptosis AIF is released from the mitochondria, enters the nucleus and is involved in high molecular weight DNA fragmentation. Therefore, it would be interesting to study nuclear co-localisation between AIF and the ORF4 protein under apoptotic conditions. Localisation of the ORF4 protein to the mitochondria, and possibly the nucleus would in all cases underline findings of the TAP purification. In conclusion, the results from this chapter, especially the mitochondrial localisation of the ORF4 protein and co-localisation with AIF led to the investigation and demonstration of an involvement of the ORF4 protein in the process of MNV induced apoptosis, which will be discussed in chapter 7.

Importantly, although biochemical fractionation demonstrated mitochondrial localisation of the ORF4 protein, it is important to stress that results of this fractionation procedure do not necessarily mean that the ORF4 protein is exclusively mitochondrial and nuclear localisation could not be investigated with this protocol. As described in chapter 5, the microscopy technique of BiFC could prove valuable in investigating co-localisation with the potential involvement of multiple associated binding partners.

Somewhat surprising in the work performed by Guia was the fact that despite biochemical predictions, the SV ORF4E protein did not localise to the mitochondria

but to the ER, with localisation reminiscent of clustering within specific compartments or at potential ER exit sites. As the use of the smaller FLAG tagged fusion was not successful at verifying these results, the generation of a SV ORF4E cross-reactive antibody may be an approach for further confocal microscopy investigation as well as biochemical investigation. Even if this approach is successful it must be remembered that expression of this yet uncharacterised protein during infection needs to be demonstrated, which to date is difficult due to the inability to successfully propagate human caliciviruses in tissue culture.

7. Investigation into the role of ORF4 in apoptosis

7.1 Introduction

7.1.1 The extrinsic and intrinsic pathways of apoptosis

As described in previous chapters, the ORF4 protein was found to localise predominately to the mitochondria and proteomic analysis identified a number of mitochondrial proteins, some of which are involved in the process of programmed cell death (apoptosis). Because mitochondria play a key part in this process, the role of the ORF4 protein in apoptosis was further investigated.

Apoptosis can be categorised into the extrinsic and intrinsic (also knows as mitochondrial) pathways, although both can be interlinked (figure 7.1). The extrinsic pathway is receptor mediated, whereas the intrinsic pathway relies on internal signals, with the mitochondria playing a key role. Apoptosis is characterised by mitochondrial membrane permeabilisation, DNA fragmentation, chromatin condensation and membrane blebbing leading to the death of the cell (reviewed by Vermeulen et al., 2005). The extrinsic pathway involves binding of stimuli to members of the TNF surface receptor family (such as Fas), which leads to the formation of the death induced signalling complex (DISC) (Vermeulen et al., 2005). Upon recruitment of pro-caspase 8 (a member of the initiator caspases) to DISC, caspase 8 is activated though proteolytic cleavage, which in turn cleaves procaspase 3 (Arnoult et al., 2008, Salvesen & Duckett, 2002). As an executioner caspase, caspase 3 translocates into the nucleus and activates a number of enzymes, including caspase-activated DNase (CAD) through cleavage of the associated inhibitor of caspase activated DNase (ICAD) (Fahrenkrog, 2006, Salvesen & Duckett, 2002). Caspase 3 also cleaves the DNA repair enzyme poly(ADP-ribose) polymerase (PARP), resulting in reduced DNA repair and therefore increased DNA cleavage, eventually leading to fragmentation and death of the cell (Andrabi et al., 2006, Kuribayashi et al., 2006).

Upon stimulation of apoptosis via the intrinsic pathway, proapoptotic Bcl-2 family members such as Bak and Bax oligomerise to form pores in the mitochondrial membrane. The proapoptotic Bcl-2 family members are activated by the BH3-only domain family members such as Bid, Noxa, Puma, Bad, Bik and Bim (Kuribayashi et al., 2006, Oberst et al., 2008). Caspase 3, 8, 10, granzyme B, calpains and cathepsins can all cleave and thus activate Bid (Aslan & Thomas, 2009, Kuribayashi et al., 2006). Cleavage of Bid by caspases 3 and 8 is a stage at which the intrinsic and extrinsic pathways of apoptosis can be interlinked (Arnoult et al., 2008). In the absence of

apoptotic stimuli, the antiapoptotic Bcl-2 family members such as Bcl-xL and Bcl-2 prevent activation of proapoptotic Bcl-2 family members (Kuribayashi et al., 2006, Oberst et al., 2008).

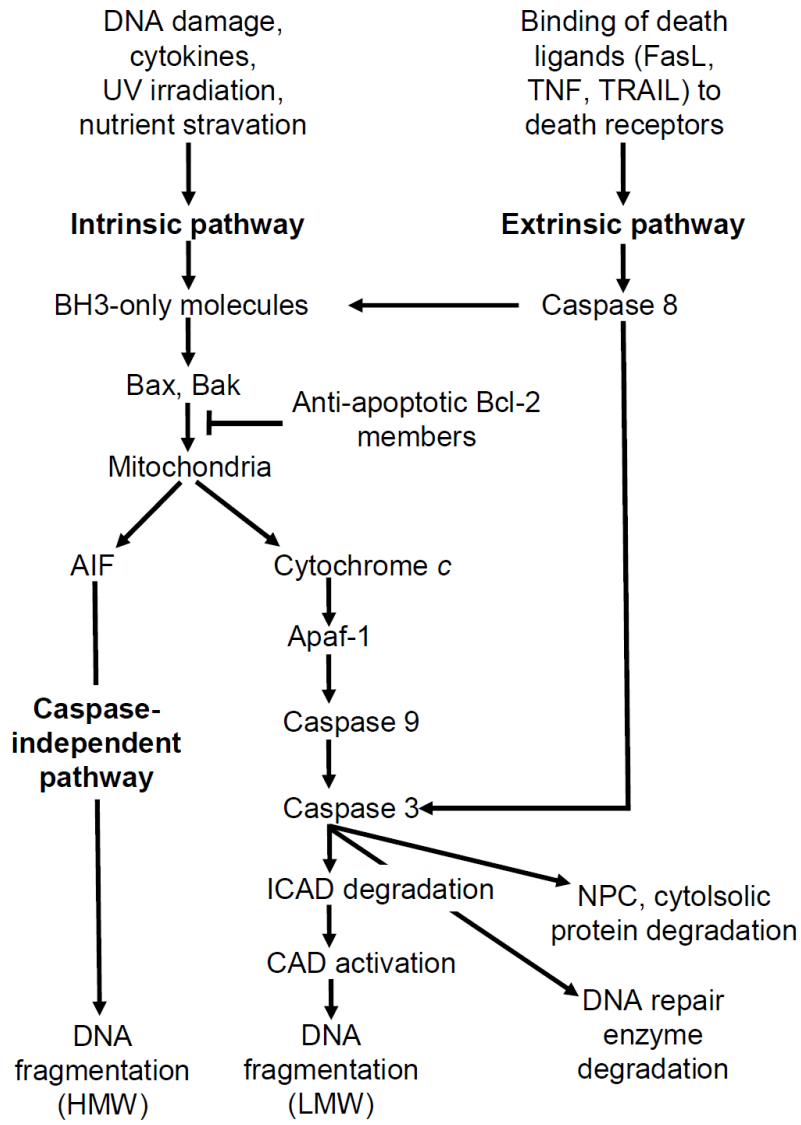


Figure 7.1. Overview of the different pathways of apoptosis. Apoptotic stimuli such as DNA damage activate the intrinsic pathway of apoptosis through a signalling cascade directly activating mitochondrial apoptosis induction. BH3-only molecules activate the proapoptotic Bcl-2 family members such as Bax and Bak. Proapoptotic Bcl-2 family members oligomerise to from pores in the mitochondrial membrane, leading to the release of cytochrome *c* and molecules such as AIF. Under non-apoptotic conditions oligomerisation of proapoptotic Bcl-2 family members is inhibited by antiapoptotic Bcl-2 family members. Released AIF translocates to the nucleus and causes high molecular weight (HMW) DNA fragmentation, a process which can occur completely independent of caspases. Released cytochrome *c* and apoptosis protease activating factor 1 (Apaf-1) lead to caspase 9 activation through formation of the apoptosome. Caspase 9 activates caspase 3, which proteolytically cleaves the inhibitor of caspase activated DNAse (ICAD), thus enabling low molecular weight (LMW) DNA fragmentation through caspase activated DNAse (CAD). Caspase 3 also degrades components of the nuclear pore complex (NPC) and cytosolic proteins, eventually leading to the destruction of the cytosol. The extrinsic pathway is induced by binding of the corresponding ligands to death receptors on the cell surface, which activates caspase 8. Caspase 8 can directly activate caspase 3 and can also activate the mitochondrial pathway via activation of BH3-only family members.

Pores in the OMM resulting from Bak and Bax oligomerisation release cytochrome *c* and other apoptotic signalling molecules, such as AIF as well as reactive oxygen species (ROS) (Salvesen & Duckett, 2002, Wei et al., 2001b). Disruption/destabilisation of the mitochondrial membrane potential resulting in the loss in ATP generation also ensues (Salvesen & Duckett, 2002). Cytosolic cytochrome *c* binds to apoptotic protease activating factor 1 (Apaf-1) which, in the presence of ATP, results in the formation of the apoptosome (Boatright & Salvesen, 2003, Salvesen & Duckett, 2002). This complex recruits the initiator procaspase 9, which is cleaved into active caspase 9, which in turn cleaves procaspase 3 (Boatright & Salvesen, 2003, Salvesen & Duckett, 2002). Again, activated caspase 3 translocates into the nucleus and activates a number of DNA degradation enzymes and inactivates a number of DNA repair enzymes (Fahrenkrog, 2006, Kuribayashi et al., 2006). Cytochrome *c* also translocates to the nucleus independently of caspase 3 and is thought to be involved in caspase independent chromatin remodelling (Fahrenkrog, 2006).

Both caspase and AIF activation are required in many cases for the successful completion of apoptosis, for example after treatment with the DNA-damaging drug camptothecin or transfection with p53. p53 is a key regulator of cellular processes (including apoptosis), which is activated in response to DNA damage or cellular stress (Joza et al., 2009). However, apoptosis via the mitochondrial pathway can also take place in a caspase independent manner, a process termed parthanatos. In this particular pathway, mitochondrial AIF release requires the activity of the DNA repair enzyme PARP-1, which produces the small molecule PAR (poly ADP ribose) (Andrabi et al., 2006, Grote et al., 2007, Susin SA, 1999). Examples of proapoptotic PARP-1 activators are the DNA-alkylating agent N-methyl-N-nitro-N-nitroso-guanidine (MNNG) and hydrogen peroxide (H_2O_2) (Joza et al., 2009). In the absence of DNA damaging agents, PARP-1 activity and the associated accumulation of PAR is limited. However, excessive DNA damage caused by apoptotic stimuli gives rise to high levels of PAR. Proapoptotic PAR exits the nucleus (the precise transport pathway of which are unknown), migrates to the mitochondria and triggers the mitochondrial release of AIF (Wang et al., 2009a). Interestingly, only PAR molecules of approximately 33.6 kDa are effective and it is unknown whether transport proteins are utilised. As the size exclusion limit of the nucleus is approximately 40 kDa, it is thought that any interference or reduction in the size of the NPC could dramatically affect the

proapoptotic action of PAR (Grote et al., 2007). To date, there is evidence to suggest that calpain cleavage releases mitochondrial AIF in the process of parthanatos, although it is currently unknown whether this action is independent of or a component of PAR-mediated events (Wang et al., 2009b).

7.1.2 The nuclear transport system in apoptosis

During apoptosis the nuclear envelope (NE) becomes disassociated from chromatin and eventually collapses, with several NE proteins, particularly lamina proteins being cleaved by caspases (Fahrenkrog, 2006). Caspases, including caspase 3 have been shown to cleave several nucleoporins (Nups), including Nup153, Nup358, Nup214, POM121 and Tpr (Fahrenkrog, 2006, Ferrando-May et al., 2001). In this highly sequential process of degradation, the targeted Nups are both peripheral as well as internal. Although the NPC itself remains intact, the process of active transport ceases (Fahrenkrog, 2006, Faleiro & Lazebnik, 2000, Grote et al., 2007). The proteosomal degradation of nuclear importins can, but does not necessarily occur, depending on apoptotic stimuli (Fahrenkrog, 2006, Ferrando-May et al., 2001). Disruption of the NPC is likely to facilitate the nuclear import of cleaved caspase 3 by diffusion (Faleiro & Lazebnik, 2000).

Although partial inhibition of nuclear transport can prevent or delay apoptosis (Yasuhara et al., 1997), significantly inhibiting nuclear transport can actually trigger the induction of apoptosis (Fahrenkrog, 2006, Grote et al., 2007). Under non-apoptotic conditions, the majority of Ran is found in the nucleus as RanGTP, but under cellular stress cytoplasmic Ran levels increase (Grote et al., 2007). Reduced levels of RanGTP lead to reduced nuclear import and this effect is accompanied by an increase in nuclear importin α levels, as importin α requires RanGTP to exit the nucleus (also shown in figure 5.6, chapter 5) (Grote et al., 2007). This in turn results in the reduced nuclear uptake of proapoptotic proteins which require importin α for nuclear import (Grote et al., 2007). One hypothesis suggested by Grote et al, is that exclusion of nuclear Ran may serve to be antiapoptotic, in order to prevent the translocation of proapoptotic molecules to the nucleus (Grote et al., 2007). Interestingly, the apoptotic response to a number of viruses is accompanied by nuclear changes, including the response to poliovirus (Belov et al., 2003, Tolskaya et al., 1995).

7.1.3 Viruses and apoptosis

From an evolutionary perspective, viruses can draw advantages from both inducing and inhibiting apoptosis. Apoptosis induction upon infection has been demonstrated for MNV (Bok et al., 2009, Furman et al., 2009) and can be seen as a mechanism for viral release. Although apoptosis may be required for viral release, viral delay of apoptosis induction may be employed to enable optimal viral yield from the infected cell. Unlike lytic viruses such as MNV, viruses which establish latent infections (e.g. herpesviruses) often benefit from the total inhibition of apoptosis, where latency rather than the release of copious amounts of viral progeny is the required outcome of infection.

A number of viruses and viral proteins are associated with the induction of apoptosis. The overlapping reading frame protein PB1-F2 of influenza A virus for example localises to the mitochondria and plays a role in inducing apoptosis, although PB1-F2 is not essential for virus viability (Chen et al., 2001, Gibbs et al., 2003). TMEV infection is also associated with apoptosis induction in tissue culture, as well as *in vivo* (Jelachich & Lipton, 2001, Schlitt et al., 2003). Poliovirus induces apoptosis via the mitochondrial pathway (Belov et al., 2003, Tolskaya et al., 1995), and expression of the 3C protease alone is sufficient to trigger apoptosis (Barco et al., 2000). The capsid protein of Rubella has been shown to block mitochondrial import and the processing of mitochondrial precursor proteins by possibly binding to a conserved component of the translocation machinery, although a direct link with apoptosis has yet to be established (Ilkow et al., 2009).

Other viruses encode antiapoptotic proteins in order to prevent or delay the onset of apoptosis. Murine CMV antiapoptotic m38.5 protein binds to and associates with proapoptotic Bax, thus preventing Bax mediated OMM permeabilisation (Arnoult et al., 2008). Human and primate CMVs on the other hand encode the Bcl-2 like mitochondrial inhibitor of apoptosis vMIA, which shares no homology to the murine m38.5 antiapoptotic protein but also acts by targeting procaspase 8 and Bax in order to block the extrinsic pathway of apoptosis (Arnoult et al., 2008, Goldmacher, 2002). Another human CMV protein vICA also targets these pathways and the combination of vMIA and vICA is essential for CMV replication, viability and prevention of otherwise dramatic apoptosis in CMV permissive cells (Arnoult et al., 2008, Goldmacher, 2002). The X-protein in Borna disease virus, which is also an overlapping reading frame protein has been shown to inhibit apoptosis and promote

persistent infection (Poenisch et al., 2009a, Poenisch et al., 2009b). Although the majority of the X-protein localises to the nucleus and regulates viral polymerase activity, a comparatively small amount localises to the mitochondria, and has antiapoptotic activity (Poenisch et al., 2009a, Poenisch et al., 2009b).

Of the caliciviruses, FCV infection has been associated with the induction of apoptosis via the intrinsic pathway, as seen by Bax translocation to the mitochondria and cytochrome *c* release (Natoni et al., 2006). FCV infection is associated with activation of the initiator caspases 2, 8 and 9 and the executioner caspases 3 and 7 (Al-Molawi et al., 2003, Sosnovtsev et al., 2003). PARP cleavage occurs during infection and treatment of cells with broad spectrum caspase inhibitors blocks apoptosis, thus excluding a primary role of the caspase-independent pathway (Al-Molawi et al., 2003, Furman et al., 2009). Furthermore, cells infected with UV-inactivated FCV, or cells treated with the protein synthesis inhibitor cyclohexamide following FCV infection do not undergo apoptosis, indicating that viral genome replication and protein synthesis is required (Sosnovtsev et al., 2003). The significant similarity between poliovirus 3C protease, which is sufficient to induce apoptosis (Barco et al., 2000), and the calicivirus protease, suggests that expression of the calicivirus protease may also be sufficient to induce apoptosis, which for FCV is currently being investigated (Natoni et al., 2006). Apoptotic cells have also been observed during RHDV infection (Alonso et al., 1998).

One of the first indicators that MNV infection was associated with the process of apoptosis came from the histopathological analysis of infected $STAT1^{-/-}$ mice, which demonstrated a significant number of apoptotic cells in the spleen and intestines of $STAT1^{-/-}$ mice compared to WT mice (Mumphrey et al., 2007). It was thus concluded that STAT1 was essential for the prevention of splenic apoptosis (Mumphrey et al., 2007). In infected mouse macrophages, MNV has been associated with the induction of apoptosis via the intrinsic pathway, as caspases 9 and 3 but not 8 become activated (Bok et al., 2009, Furman et al., 2009). In the presence of caspase inhibitors, MNV does not induce apoptosis and cells are visibly necrotic, leading to the conclusion that the caspase-independent pathway is not sufficient for the execution of apoptosis during MNV infection (Furman et al., 2009). Under non-apoptotic circumstances, inhibitors of apoptosis proteins (IAPs) bind to and inhibit proapoptotic signalling molecules. During MNV infection, the IAP survivin which prevents caspase 9 activation, is down-regulated, a process not associated with any other infectious agent to date (Bok et al.,

2009). In contrast, up-regulation of the antiapoptotic survivin in order to delay apoptosis is employed by many viruses. These include for example the Vpr protein of HIV (Zhu et al., 2003) and the X protein of hepatitis B (Zhang et al., 2005).

7.2 Results and Discussion

7.2.1 Investigation of the role of ORF4 in viral induced apoptosis

Taking previously described results into account, and in light of data collected by other groups on the process of apoptosis in MNV-1 infected cells (Bok et al., 2009, Furman et al., 2009), the role of the ORF4 protein during MNV-1 induced apoptosis in mouse macrophage cells was investigated. To do this, the ability of the ORF4 knockout virus M1 to induce apoptosis was examined and compared to WT virus. RAW264.7 cells were either infected with M1 or WT virus, alongside non-treated cells or those stimulated with staurosporine, a positive inducer of apoptosis. After 16 h, lysed cells were incubated with Glo3/7 assay reagent, which contains a caspase 3 specific substrate. As the cleavage of this substrate by caspase 3 releases aminoluciferin, a substrate for luciferase, caspase activity could be directly monitored.

As expected, no statistically significant difference could be seen between cells treated with either WT or M1 UV inactivated virus (figure 7.2a). The low luminescent signal of these inactivated viruses was comparable to NI control, thus indicating that procaspase 3 was not being cleaved, and therefore apoptosis was not being induced. In contrast, infection with M1 and WT virus was associated with the induction of apoptosis, as seen by the high luminescent signal and comparison to the staurosporine treated control (figure 7.2a). Most importantly, results from an unpaired T-test test at 95% confidence level indicated that there was a high statistically significant difference ($P<0.001$) in caspase 3 activity in cells infected with M1 in comparison to WT virus. This indicated that the ORF4 protein is either directly or indirectly involved in the process of apoptosis. In order to confirm these findings, western blot and subsequent densitometry analysis was performed (figure 7.2b). Interestingly, M1 virus infected cells contained a 43% increase in the levels of cleaved caspase 3 (CC3) in comparison to WT infected cells (figure 7.2b). As M1 infected cells demonstrated a higher production of cleaved caspase 3 than WT virus infected cells, these western blots confirmed the results of the Glo3/7 assays, indicating that cells infected with virus containing an intact ORF4 were less apoptotic at 16 h post-infection. These findings

were also verified by carrying out a Glo3/7 assay on M1 and WT infected primary bone derived mouse macrophage cells (BMMΦ) isolated from the thigh bone of BALB/c mice (figure 7.2c). Once again, a statistically significant ($P<0.05$) difference could be seen between M1 and WT infected cells, although this difference may not have been as prominent as for the RAW264.7 cells. In spite of efforts, sufficient protein could not be harvested from the amount of BMMΦs available in order to perform quantitative western blot analysis as carried out for the RAW264.7 cells (data not shown).

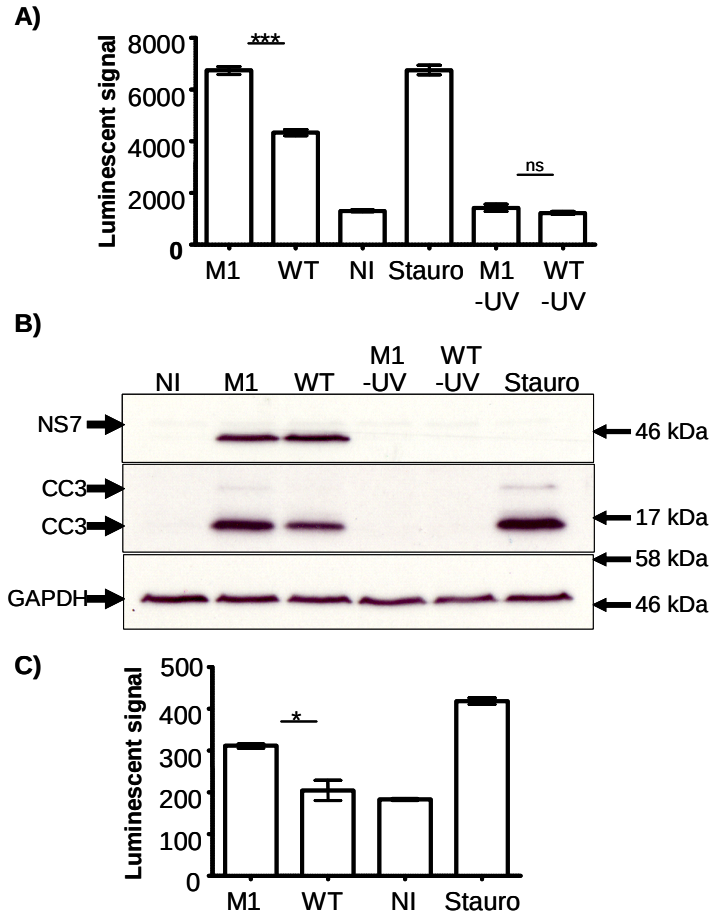


Figure 7.2. *In vitro* measurement of caspase 3 activity and caspase levels in M1 vs. WT infected cells. A) Luminescent signal by Glo 3/7 assay in RAW264.7 cells infected for 16 h (representative of three independent repeats). Cells were either treated with live or UV inactivated ORF4 M1 or WT virus. Non-infected (NI) cells were used as a negative control and cells treated with 5 µM staurosporine (Stauro) were used as a positive control. Assays were performed in triplicate and error bars depict the standard error between repeats. A high statistically significant difference ($P<0.001$, depicted with ***) was observed between M1 and WT, whereas no significant difference (ns) was observed between WT and M1 which had been UV inactivated. Differences were analysed by unpaired T-test at 95% confidence interval. **B)** Western blot analysis of SDS-PAGE separated RAW264.7 lysates treated as described above. Blots were performed using antibodies to cleaved caspase 3 (CC3), the viral polymerase NS7 as well as cellular GAPDH as a control. **C)** Luminescent signal by Glo 3/7 assay (performed in duplicate, error bars representing standard error between repeats) in primary mouse bone derived macrophages (BMMΦ) infected for 16 h again demonstrated a statistically significant difference ($P<0.05$ depicted by *) between M1 and WT.

In order to further investigate this observed difference in apoptosis induction, a timecourse of infection was performed for M1 and WT infected RAW264.7 cells. Caspase activity was monitored by Glo3/7 assays, and a series of western blots were performed. Consistent with previous findings (Bok et al., 2009, Furman et al., 2009), caspase 3 activity was not detected before 12 h post-infection (figure 7.3a). Although at 12 h post-infection there was no difference in caspase 3 activity between M1 and WT infected cells, both at 15 h ($P<0.01$) and 18 h ($P<0.001$) there were statistically significant differences which were measured using two-way ANOVA with Bonferroni post-tests (figure 7.3a). However, by 21 h post-infection, a timepoint coinciding with visible cytopathology and high viral titres (data not shown), this difference was no longer present (figure 7.3a). Noteworthy is that no consistently obvious difference in cytopathic effect between M1 and WT virus infected cells was detected by light microscopy at any of these timepoints (data not shown). Consequently, this data indicated that in M1 infected cells apoptosis was being induced earlier and to a higher degree than in WT infected cells, although the outcome of infection, i.e. apoptosis remained the same.

In order to further investigate these findings, lysates of M1 and WT infected cells taken at the given timepoints were separated by SDS-PAGE and western blots were performed (figure 7.3b). Densitometry analysis of the western blots underlined previous findings of survivin down-regulation during the timecourse of infection (Bok et al., 2009). Consistent with the results from the Glo3/7 assays was that survivin down-regulation preceded more rapidly in M1 infected cells in comparison to WT infected cells, with survivin levels in WT infected cells being 22% higher at 15 h post-infection than in M1 infected cells (figure 7.3b). Non-infected and staurosporine treated cells harvested at 9 h and 21 h post-infection were taken as controls for this experiment. Analysis of caspase levels revealed that at 15 h post-infection total levels of the initiator caspase 9 were elevated for M1 in comparison to WT infected cells, with a 27% increase observed for M1 infected cells (figure 7.3b). High levels of procaspase at these early timepoints is likely to be a consequence of up-regulated caspase gene expression following stimulation of apoptosis. As apoptosis induction appears to proceed more rapidly in M1 infected cells, this would explain the higher levels of procaspase 9 in comparison to WT infected cells. The reason why at later timepoints levels of caspase 9 were significantly lower for M1 infected cells (59% of WT levels at 18 h and 26% at 21 h) could be because the majority of procaspase 9 had

by that point been proteolytically cleaved in M1 infected cells due to the more advanced apoptotic process. A 12% increase in the 30 kDa cleaved caspase 9 was seen at 15 h post-infection for cells infected with M1, whereas higher levels of the 17 kDa cleavage product for M1 was also seen at 18 and 21 h post-infection (figure 7.3b).

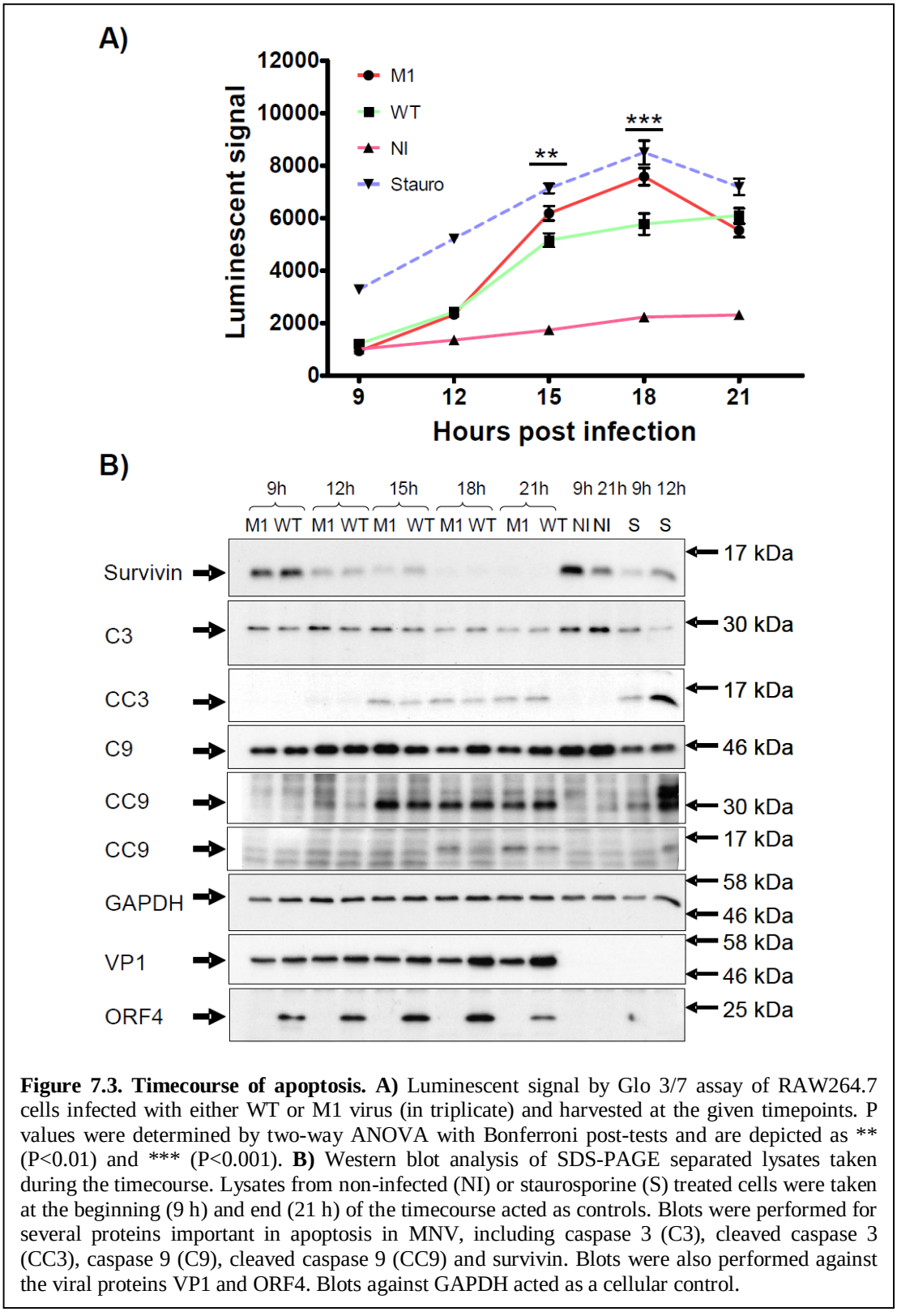


Figure 7.3. Timecourse of apoptosis. A) Luminescent signal by Glo 3/7 assay of RAW264.7 cells infected with either WT or M1 virus (in triplicate) and harvested at the given timepoints. P values were determined by two-way ANOVA with Bonferroni post-tests and are depicted as ** ($P<0.01$) and *** ($P<0.001$). **B)** Western blot analysis of SDS-PAGE separated lysates taken during the timecourse. Lysates from non-infected (NI) or staurosporine (S) treated cells were taken at the beginning (9 h) and end (21 h) of the timecourse acted as controls. Blots were performed for several proteins important in apoptosis in MNV, including caspase 3 (C3), cleaved caspase 3 (CC3), caspase 9 (C9), cleaved caspase 9 (CC9) and survivin. Blots were also performed against the viral proteins VP1 and ORF4. Blots against GAPDH acted as a cellular control.

M1 infected cells were also associated with overall higher levels of the executioner caspase 3, with the difference at 15 h post-infection being approximately 40% higher for M1 infected cells. However, by 18 h post-infection there was a 50% decrease for M1 in comparison to WT infected cells in the levels of caspase 3. In M1 infected cells, 66% (at 15 h post-infection) and 53% (at 18 h post-infection) higher levels of cleaved caspase 3 were seen compared to WT infected cells (figure7.3b).

Once again, these results emphasised and agreed with the finding from the Glo3/7 assays, which indicated that apoptosis induction occurred earlier during M1 infection. To ensure equal protein loading, GAPDH was used as a control and western blot against the ORF4 protein ensured that ORF4 was not being expressed (figure 7.3b). Western blot against the viral polymerase NS7 (data not shown) and the major capsid protein VP1 was performed in order to measure viral protein synthesis (figure 7.3b – data also shown in figure 3.11 in chapter 3). As previously described in chapter 3, higher levels of VP1 (figure 7.3b) and NS7 (data not shown) were observed between 15 h and 21 h post-infection for WT infected cells. Whilst at 15 h VP1 levels were 22% higher in WT infected cells, the difference at 18 h (79%) and 21 h (60%) was significantly higher. Importantly, as described in chapter 3, whilst previous western blot analysis of M1 and WT infected cells seeded at low density ($6x10^5$/well in $9cm^2$) revealed comparable viral protein levels at all timepoints post-infection, western blots against survivin, caspase 3, caspase 9, cleaved caspase 3 and cleaved caspase 9 did not demonstrate an observable difference between WT and M1 infected cells (data not shown).

7.3 Conclusion

The mitochondrial localisation of the ORF4 protein and data obtained from the ORF4 NTAP purification led to the investigation of the role of the ORF4 protein during the process of apoptosis. Both luminescent analysis of caspase 3 activity, as well as western blot analysis of several proteins shown to play a role in MNV induced apoptosis was performed. From this data it was concluded that cells infected with M1 virus (which lacks an intact ORF4) showed an earlier and higher degree of apoptosis induction in comparison to WT MNV infected cells. This observation was made in primary bone-derived macrophages as well as RAW264.7 cells.

To date it remains unclear whether or not the ORF4 protein actually possesses antiapoptotic activity or whether delayed apoptosis induction could be an indirect

consequence of the ORF4 protein localising to the mitochondria and interfering with mitochondrial processes. Experiments to analyse whether the ORF4 protein has antiapoptotic activity could for example include expression of the protein in the absence of infection under conditions of apoptosis stimulation. Assays to investigate apoptosis include FACS and confocal microscopy analysis to monitor annexin V staining, as well as assays to monitor cytochrome *c* release and mitochondrial membrane potential.

Interestingly, very recent studies performed by Dr Andrew MacDonald have demonstrated that the ORF4 protein interacts with a number of SH3 domain containing proteins, some of which are involved in the generation of ROS, which also play a role in apoptosis induction (unpublished observations). The involvement of the ORF4 protein in ROS generation could therefore be analysed by various *in vitro* assays to monitor ROS generation. Although at this stage purely speculative it could be hypothesised that interference in ROS production could serve to delay the generation of damaging ROS which also damage viral RNA and proteins in addition to functioning as proapoptotic molecules. Another currently purely hypothetical proposal is that mere physical association of the ORF4 protein with the mitochondria may prevent or delay the physical changes occurring in mitochondria following apoptosis stimulation. To date however, no homology has been observed between the ORF4 protein and any known antiapoptotic Bcl-2 family members.

Although there are many methods by which the ORF4 protein may either directly or indirectly be involved in apoptosis induction, two hypothetical models of ORF4 protein function linking a number of findings from the TAP purification, yeast-two hybrid screen, localisation and apoptosis studies can be found in the concluding chapter (chapter 8) of this PhD thesis.

8. Conclusion and future work

8.1 Overall conclusions

From the described studies it was concluded that in addition to the three previously characterised ORFs, MNV also contains a highly conserved fourth open reading frame which overlaps ORF2 in a +1 frame. The first indication that ORF4 encoded a protein came from *in vitro* transcription and translation reactions, which demonstrated that the protein produced from an expression plasmid containing ORF4 was the same size as a protein produced from the subgenomic RNA of MNV. Once a suitable antibody was generated, it was also shown that the ORF4 protein is expressed in mouse macrophages during the course of MNV infection, comparable to other viral proteins. However, the sera of MNV immune mice did not react with recombinant ORF4 protein by western blot, a feature which is common to all viral non-structural proteins.

Although the successful propagation of ORF4 mutants to wild-type levels in tissue culture showed that ORF4 knockout had no effect on MNV viability, serial passage of the ORF4 knockout virus under conditions of high cell seeding density led to the restoration of ORF4 expression. These results therefore indicated that even *in vitro* this ORF was important, and explains why ORF4 remains so conserved amongst MNV strains, even upon serial passage in tissue culture.

One speculation is that the reduced rate of viral translation seen in cells infected with the ORF4 knockout virus at later timepoints of infection may be a consequence of an interaction between the ORF4 protein and AIF, which was identified in the ORF4 TAP screen. As AIF is involved in the shutoff of host cell translation during apoptosis by binding to eIF3, the ORF4 protein may serve to block this interaction, thus prolonging translation. Whereas prolonged host cell translation would retain levels of cellular proteins which are required by the virus, it is also important to remember that calicivirus VPg binds to and employs eIF3 for viral translation (Daughenbaugh et al., 2003). Consequently, blocking the interaction between AIF and eIF3 also prolongs viral translation, thus resulting in higher viral protein levels in cells infected with WT virus compared to M1 infected cells. A similar speculation is that an interaction between the ORF4 protein and the translational regulator GCN1 may also serve to prolong translation during virus infection.

In vivo analysis using STAT1$^{-/-}$ mice demonstrated that ORF4 plays a role in viral pathogenesis, even though abolishing ORF4 expression did not alter the lethal nature of MNV-1 in these severely immunocompromised mice. However, analysis of bodyweight and qPCR demonstrated that the ORF4 knockout virus was attenuated in

STAT1$^{-/-}$ mice. Consequently, it appeared that similar to other overlapping reading frame proteins, such as influenza A virus PB1-F2, the ORF4 protein acts as an accessory virulence factor. Although no histopathology data was available at the time of writing it has since been established that the M1-v infected arbitrarily selected tissue samples for histopathology closer resembled the tissues of mock infected animals than those infected with WT-v. This is somewhat surprising as it was hoped that comparative analysis of apoptotic cells in the intestines, spleens and livers of M1-v and WT-v infected STAT1$^{-/-}$ mice would demonstrate differences. In retrospect, cytokine production in WT-v and M1-v infected animals could also have been monitored during these experiments and this aspect should definitely be examined in the future.

Comparable to other lytic viruses, it is clear that MNV must replicate in the most efficient manner in order to allow transmission. In the case of MNV infection controlling apoptosis appears to be essential and early induction of apoptosis would result in the infected cells being picked up by immune cells earlier. This could result in the clearance of apoptotic infected cells, reducing the levels of virus. If future more in-depth and extensive analysis shows that the tissues of M1-v infected mice also demonstrate an earlier and higher degree of apoptosis induction, then it is plausible to suggest clearance of a number of apoptotic infected cells and with it the delayed onset of infection was the reason M1-v attenuation in infected animals. This clearance resulting in reduced viral titre would of course be amplified during multiple rounds of infection, therefore leading to the delayed onset of M1-v induced disease. One explanation regarding the variations between inoculation and onset of symptoms which varied largely amongst individual animals is that in some mice inoculation with this attenuated virus resulted in an abortive infection. However, the successful establishment of infection in some animals and high excretion levels in addition to constant exposure to the virus may have enabled the spread of M1-v. In order to therefore limit the possibility of inner cage transmission, mice should be housed in the minimum number of two per cage should an experiment of this kind be repeated.

Because STAT1$^{-/-}$ mice are so susceptible to the lethal nature of MNV-1, the system may not be best suited for studying the potentially subtle effects of the ORF4 protein. As MNV-1 is the only MNV stain associated with lethal infection (and only in severely immunocompromised mice), it was decided that future *in vivo* work will focus on the role of ORF4 in persistent MNV strains such as MNV-3. For this work, immunocompetent mice will be inoculated with WT MNV-3 and MNV-3 containing

the ORF4 knockout mutation M1. Analysis of bodyweight, faecal shedding, seroconversion, intestinal viral load and cytokine production can subsequently be compared.

A large scale tandem affinity purification procedure identified a number of mitochondrial, nuclear, ER/Golgi and proteosome associated proteins, although the purification procedure must be repeated in the future with the less toxic tetracycline inducible system, using both C- and N- terminal TAP tags in order to confirm these results. The generation of stable permissive cell lines expression ORF4 TAP fusions would also enable the pulldown in the presence or absence of infection and may affect the number and identification of purified proteins. It is important to remember that the number of proteins able to bind under high stringency conditions is likely to be far lower than the number of binding partners identified by TAP. Therefore, closer analysis of interactions between individual proteins and the ORF4 protein remains to be confirmed, for example by co-immunoprecipitation or co-localisation studies. Especially techniques such as BiFC could be used to analyse interactions as well as co-binding partners. If interactions between the proteins of interest are confirmed, then mutational analysis may be used to establish the precise interaction site(s).

The great number of identified mitochondrial proteins strongly suggests that the ORF4 protein utilises mitochondrial import pathways to localise to the mitochondria, a finding supported by confocal microscopy and biochemical fractionation. Unfortunately, preliminary attempts by Guia Carrara to localise the minimum MTS of the ORF4 protein using N-terminal truncations of ORF4-GFP were unsuccessful, and it was concluded that the ORF4 MTS resides within the C-terminal 91 amino acids of the ORF4 protein. Hence, further analysis will focus on generating further truncations in order to precisely identify the MTS of the ORF4 protein. Interestingly, the comparative analysis of SV ORF4E localisation also performed by Guia Carrara did not reveal mitochondrial, but ER localisation. However, there were concerns that the large GFP protein was interfering with localisation by potentially blocking ER exit of SV ORF4E protein. To date, it remains to be determined whether or not SV ORF4E is in fact expressed during infection and an antibody to the ORF4E protein would have to be generated. However, analysis as was the case for MNV ORF4 would prove difficult due to the lack of a tissue culture or reverse genetics system for human sapoviruses.

The first indication that the ORF4 protein is involved in the process of apoptosis came from the identification of a number of apoptosis-associated proteins by proteomic

analysis as well studies showing partial co-localisation of the ORF4 protein with AIF. Importantly, it was subsequently shown that cells infected with the ORF4 knockout virus led to an earlier and higher degree of apoptosis induction in comparison to WT infected cells. Whether or not this effect on apoptosis was a direct consequence of antiapoptotic activity of the ORF4 protein or the result of other processes remains to be investigated.

The role of AIF in down-regulating host translation and the involvement in apoptosis make further investigations into the interaction of AIF and the ORF4 protein particularly interesting. Co-localisation studies under stimulation of apoptosis could be performed in the future. Similarly, associated ORF4-AIF binding partners may also function to stabilise the interactions. *In vivo* investigations using persistent MNV strains and Harlequin mice which have 80% reduced AIF could further be used to characterise the nature of the ORF4 protein (Klein et al., 2002).

The fact that TAP purification as well as the yeast two-hybrid screen identified components of the NPC strongly suggests that the ORF4 protein interacts with the complex, a finding also supported by confocal microscopy. One speculation regarding such an interaction could be that by binding to the NPC the ORF4 protein serves to block nuclear transport, which would explain why such a vast number of nuclear transport proteins were identified by TAP purification. Interestingly, inhibiting nuclear transport can delay the process of apoptosis and would explain why apoptosis is seen earlier and to a higher degree in infections with M1. Because the activated caspase 3 eventually degrades components of the NPC, nuclear transport is no longer controlled and hence the apoptosis programme is executed. Even though no difference in virus yield between M1 and WT was seen in tissue culture, this was possibly not the case *in vivo*, where early clearance of infected apoptotic cells is ensured by immune cells in the absence of ORF4 expression. Therefore, the purpose of the ORF4 protein may be to delay apoptosis in order to avoid early immune cell detection and optimise virus yield. Consequently, reduced viral genome copy numbers of M1-v infected tissues following *in vivo* infection of $STAT1^{-/-}$ mice were observed. In future experiments, viral titres in infected tissues could be directly measured by performing $TCID_{50}$ assays, something which was not possible from the tissue samples taken in the US, due to the Southwestern Medical Centre local regulations as well as UK customs regulations for the import of biological samples.

Both yeast two-hybrid as well as TAP purification identified a number of DNA binding proteins and repair enzymes. It could be speculated that an interaction of the ORF4 protein with these nuclear proteins would also explain the nuclear foci of ORF4 localisation seen by confocal microscopy. As a number of these identified transcription regulatory genes are involved in the process of apoptosis, such an interaction could potentially serve to delay the process of apoptosis, although further concrete evidence for this would have to be generated.

Because the spherical nature of the mouse macrophage cell lines in our laboratory make the distinction of cellular organelles difficult by confocal microscopy, future microscopy work could involve purchasing alternative MNV permissive cell lines. With these cell lines, ORF4 protein localisation in the presence of infection could be investigated. As the current ORF4 antibody is not suited for confocal microscopy analysis, cells infected with the ORF4 knockout virus could also be transfected with constructs expressing GFP fusions of the ORF4 protein. Alternatively, COS-7 cells, which allow easy visualisation of various cytoplasmic organelles, could be transfected with viral RNA in addition to ORF4 GFP expressing plasmids.

8.2 Hypothetical model of function

Although at this stage extremely preliminary and highly speculative, a proposed model of the involvement of the ORF4 protein in apoptosis can be seen in figure 8.1. The model is based on the findings presented in this thesis, and the discussed proposals are not necessarily mutually exclusive. Importantly, all suggestions require further investigation and there is no concrete evidence to date to suggest they are authentic.

MNV replication causes cellular stress leading to the activation of proapoptotic Bcl-2 family members. The newly synthesised ORF4 protein associates with and is imported into the mitochondria. One possibility is that excessive amounts of ORF4 protein could physically block and hence delay oligomerisation and pore formation by proapoptotic Bcl2 family members. Significant homology between the ORF4 protein and known Bcl-2 family members does however not exist at the amino acid level (data not shown). Association of the ORF4 protein with AIF at the mitochondria ensures that when AIF is released, associated ORF4 protein migrates with AIF to the nucleus. At the same time released cytochrome *c* activates the caspase cascade.

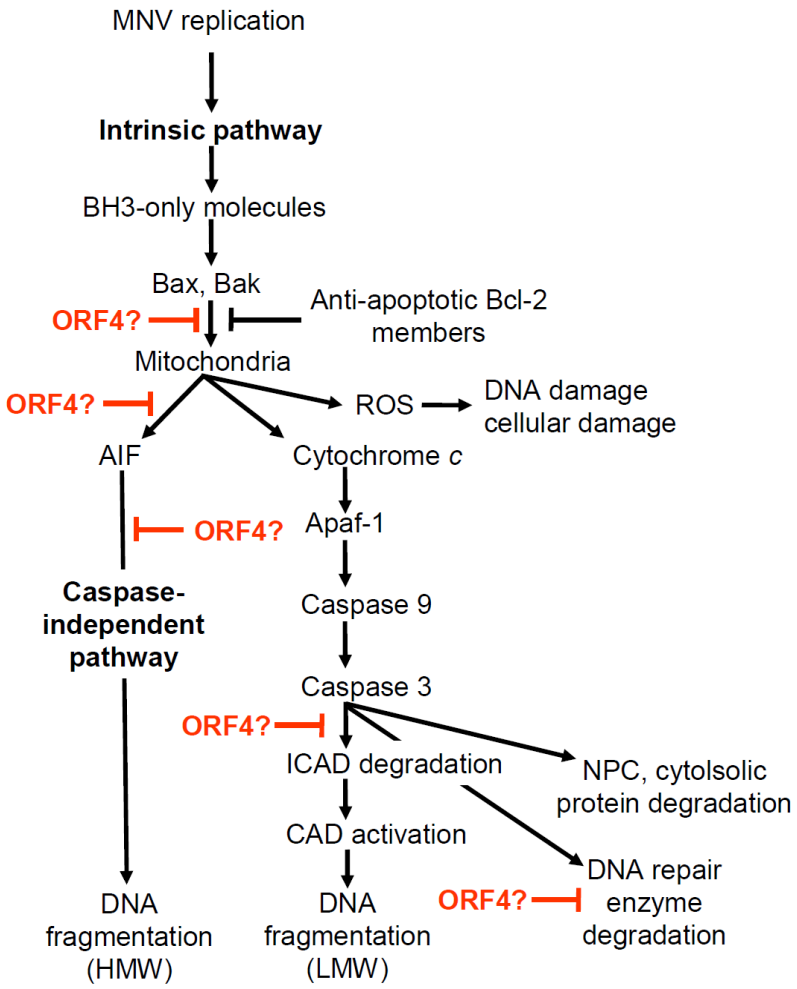


Figure 8.1. Proposals of ORF4 protein function. In this model the execution of MNV-induced apoptosis is delayed by the ORF4 protein which localises to the mitochondria. The ORF4 protein may physically prevent oligomerisation of proapoptotic Bcl-2 family members, or may physically block the exit of proapoptotic signalling molecules including reactive oxygen species (ROS) from the mitochondria. Alternatively, the ORF4 protein associates with AIF and translocates with AIF to the nucleus, where association with the nuclear pore complex (NPC) prevents further AIF translocation as well as translocation of the executioner caspase 3. Some of the ORF4 protein may also enter the nucleus and associate with DNA repair enzymes. This may serve to prevent the accumulation of proapoptotic signalling molecules such as PAR, which would further drive the process of apoptosis. Alternatively, association with DNA repair enzymes could sterically hinder effective degradation of these enzymes by caspase 3. Eventually however, caspase 3 mediated degradation of the NPC and cytosol lead to the execution of the apoptotic programme. As the precise mechanisms of ORF4 protein function are unknown, possible points of intervention are highlighted in red with ORF4?

Upon migration to the nucleus, the ORF4 protein associates with the NPC in order to restrict nuclear transport and delay apoptotic events. The delay would be achieved because the nuclear import of proteins or activators of proteins involved in DNA fragmentation (such as AIF and caspase 3) could not occur, and the export of proteins further driving the process of apoptosis such as PAR and survivin can not be released from the nucleus. Interestingly, the nuclear exit of PAR polymers is severely affected by the size of the NPC, as only PAR molecules of approximate 33.6 kDa are

effectively transported from the nucleus (Grote et al., 2007), hence any restriction in size is likely to be of consequence. As binding to the NPC may not be effective in all cases, small amounts of the ORF4 protein also localise to the nucleus, where an interaction with a number of DNA binding and repair enzymes may prevent the accumulation of proapoptotic by-products of these repair enzymes, such as PAR or the mRNAs of further proapoptotic proteins. Association of the ORF4 protein with DNA binding and repair enzymes could also sterically hinder and prevent degradation of these enzymes by caspase 3.

In spite of this predicted activity of the ORF4 protein, the programme of apoptosis is eventually carried out because activated caspase 3 degrades components of the NPC, which leads to the uncontrolled influx and efflux of molecules into the nucleus and the role of the ORF4 protein in restricting the NPC becomes redundant. Therefore, AIF and caspase 3 activated CAD can fragment DNA, whilst proapoptotic PAR and p53 can further stimulate the intrinsic pathway of apoptosis. Consequently, the final outcome of infection (i.e. apoptosis) is the same for both WT and the ORF4 knockout virus. However, in the absence of ORF4 expression, apoptosis is induced earlier and to a greater extent than for WT infected cells.

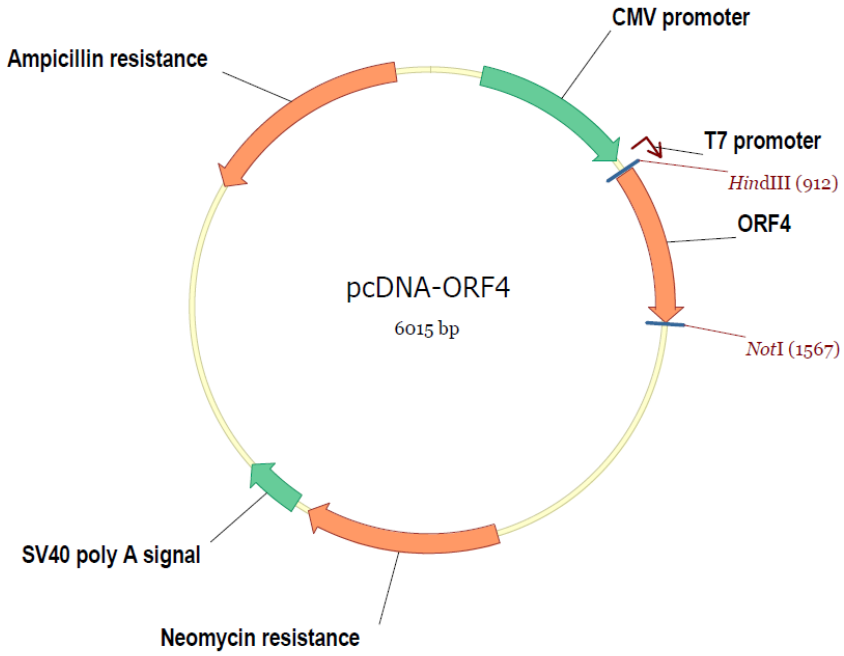
Another hypothesis relating to the interaction between the ORF4 protein and the mitochondria is that the ORF4 protein could block the formation of the permeability transition pore (PTP) and prevent the subsequent mitochondrial release of apoptotic signalling molecules and ROS. Alternatively, by binding to SH3 domain containing proteins involved in ROS generation via conserved polyproline motifs, the ORF4 protein may delay the production of proapoptotic ROS. In support of this theory are recent unpublished studies performed by Dr Andrew MacDonald, demonstrating that the ORF4 protein interacts with a number of proteins involved in ROS generation *in vitro*. Hence, a delay in apoptosis could serve to prevent cytosolic ROS damaging susceptible viral genomes and proteins during the replication cycle and the events of apoptosis may simply be an artefact of such a block. As ROS cause RNA as well as DNA damage, it would be interesting to monitor the viral mutation frequency in cells infected with M1 compared to those infected with WT virus after multiple passages. Overall, it is possible that a combination of both models is the case and further work must be performed in order to identify the precise function of the ORF4 protein.

8.3 Final summary

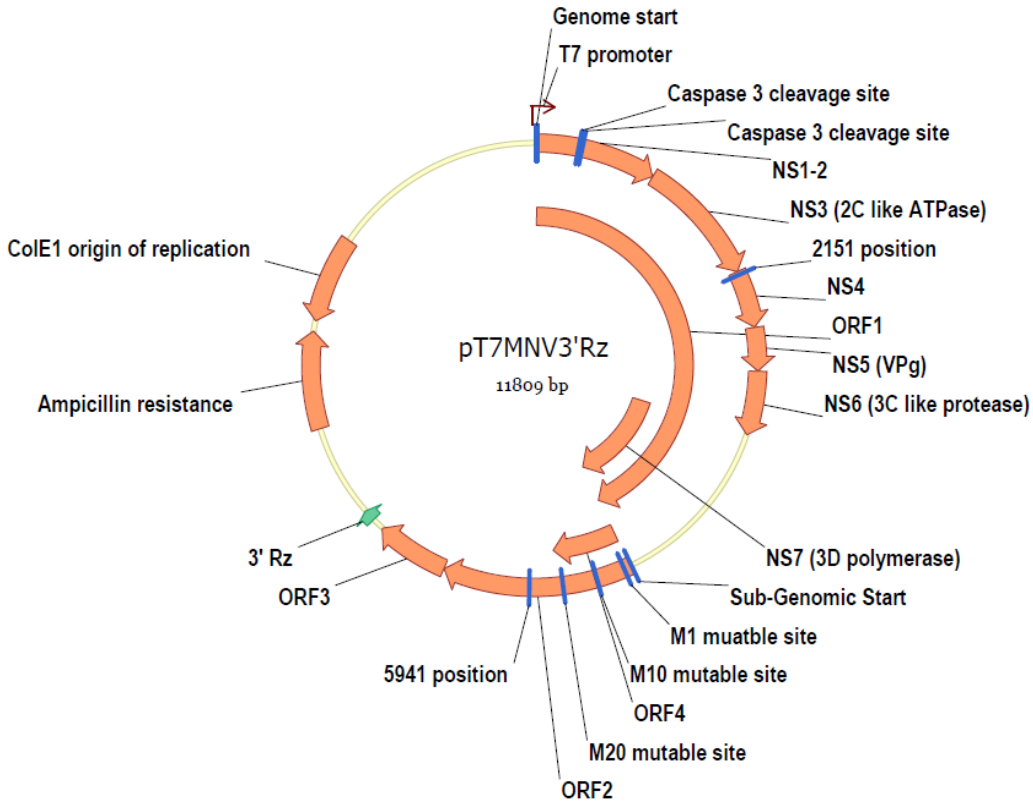
During the course of this work evidence has been gathered demonstrating that MNV contains a fourth overlapping reading frame in the capsid encoding region. Although not essential for viability of MNV in tissue culture, there was pressure to restore expression from this reading frame upon serial passage in tissue culture. *In vivo*, ORF4 knockout viruses gave rise to an attenuated phenotype. Mitochondrial localisation of the ORF4 protein and the identification of a number proteins involved in the process of apoptosis led to the investigation of the role of the ORF4 protein in MNV induced apoptosis. Results demonstrated that cells infected with the ORF4 knockout virus showed an earlier and higher degree of apoptosis induction than WT MNV infected cells, thus indicating that the ORF4 protein is involved in the process of apoptosis. To date however, the precise mechanism of ORF4 protein involvement in the process of apoptosis is unknown and requires further investigation, although several potential mechanisms of function have been presented. Overall, this work has identified a new viral component which regulates the host response to infection and yields further insights into the pathogen-host interface.

Appendix

A)

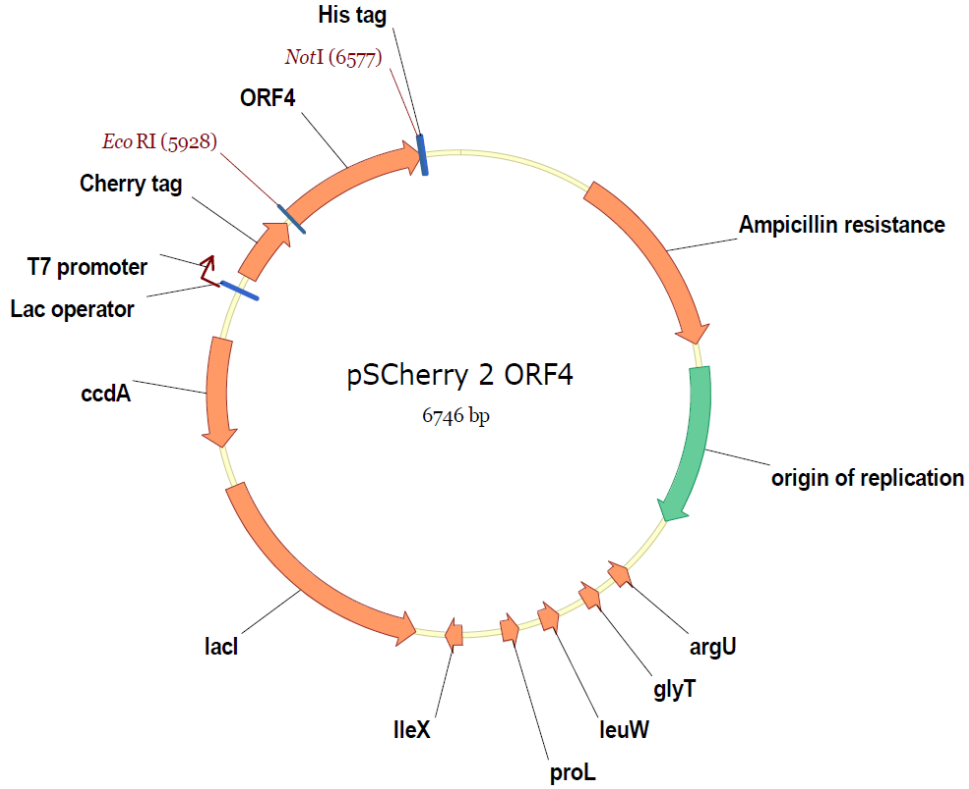


B)

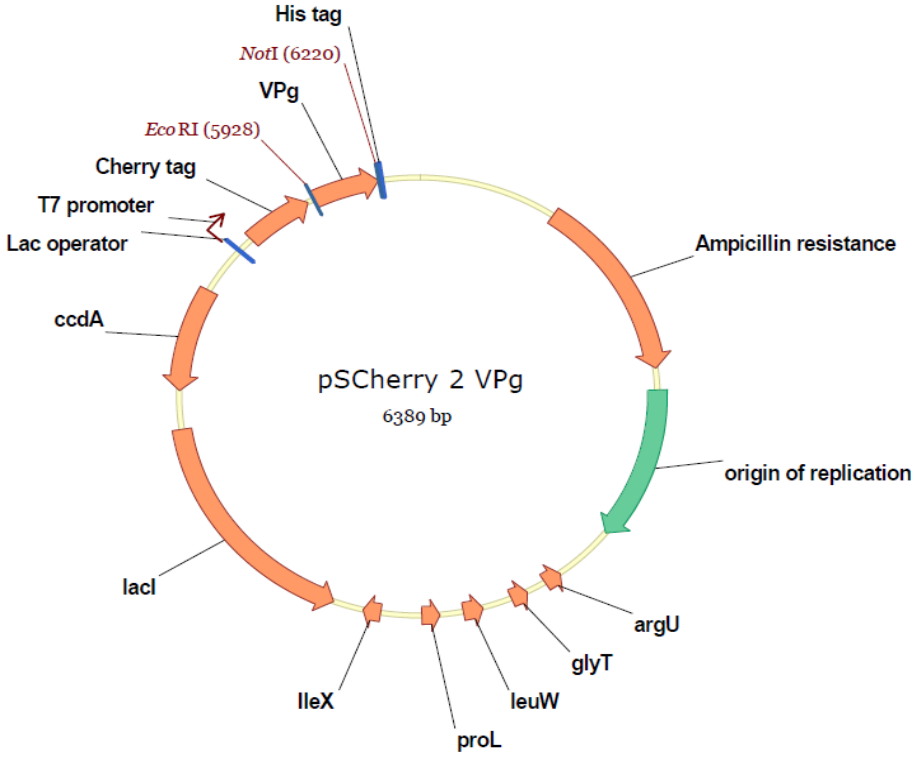


Appendix 1. Maps of plasmids used during the course of this work. Restriction sites used for cloning and selection markers are depicted on the maps **A)** Map pf pcDNA-ORF4 used during *in vitro* translations. **B)** Map of full-length MNV infectious clone used for virus recovery. The sites mutated on order to generate the individual ORF4 mutants M1, M10 and M20 are highlighted as well the *in vivo* virulence defining mutations at genome positions 2151 and 5941.

C)

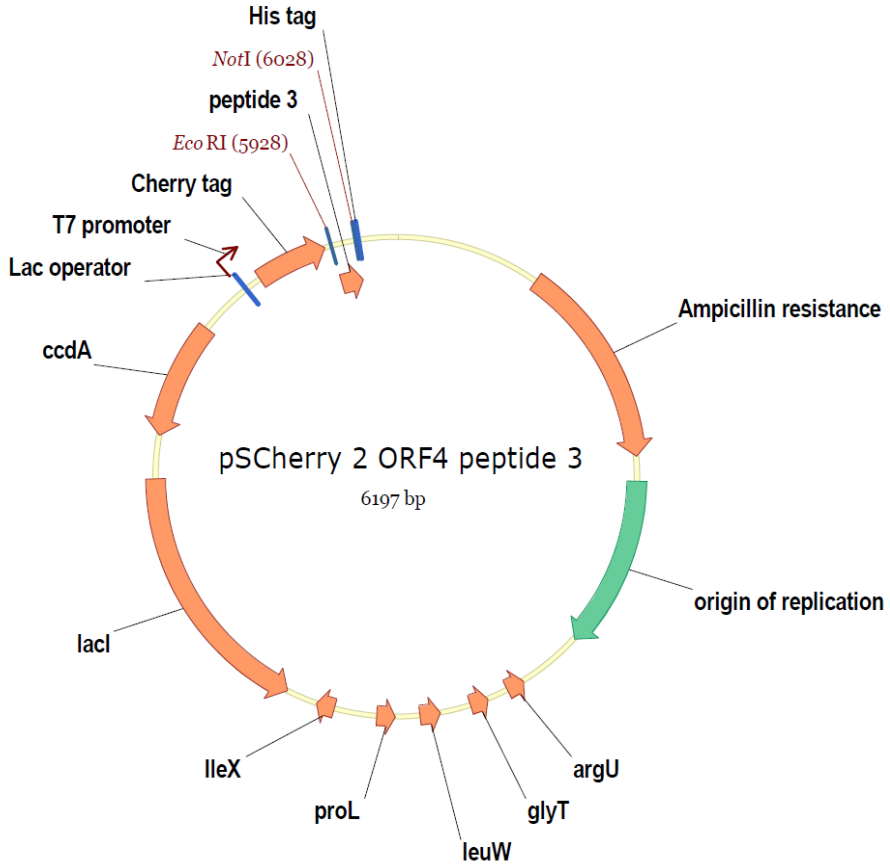


D)

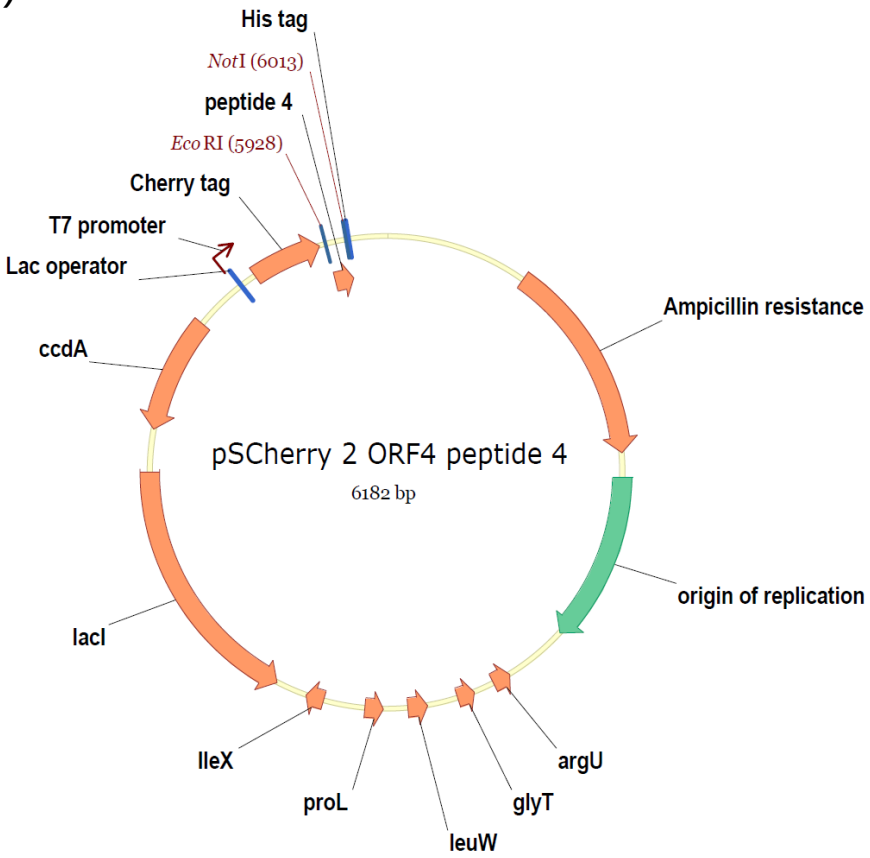


Appendix 1 (cont.). Maps of Cherry ORF4 his **(C)** and Cherry VPg his **(D)** expression constructs. The pSCherry 2 vector additional encodes the tRNA genes of the six rare codons. In the presence of glucose LacI represses both the expression of the T7 RNA polymerase in the SE21 bacteria as well as expression of the gene of interest which is under thee control of the lac operator. The *ccdA* gene is involved in plasmid stabilisation.

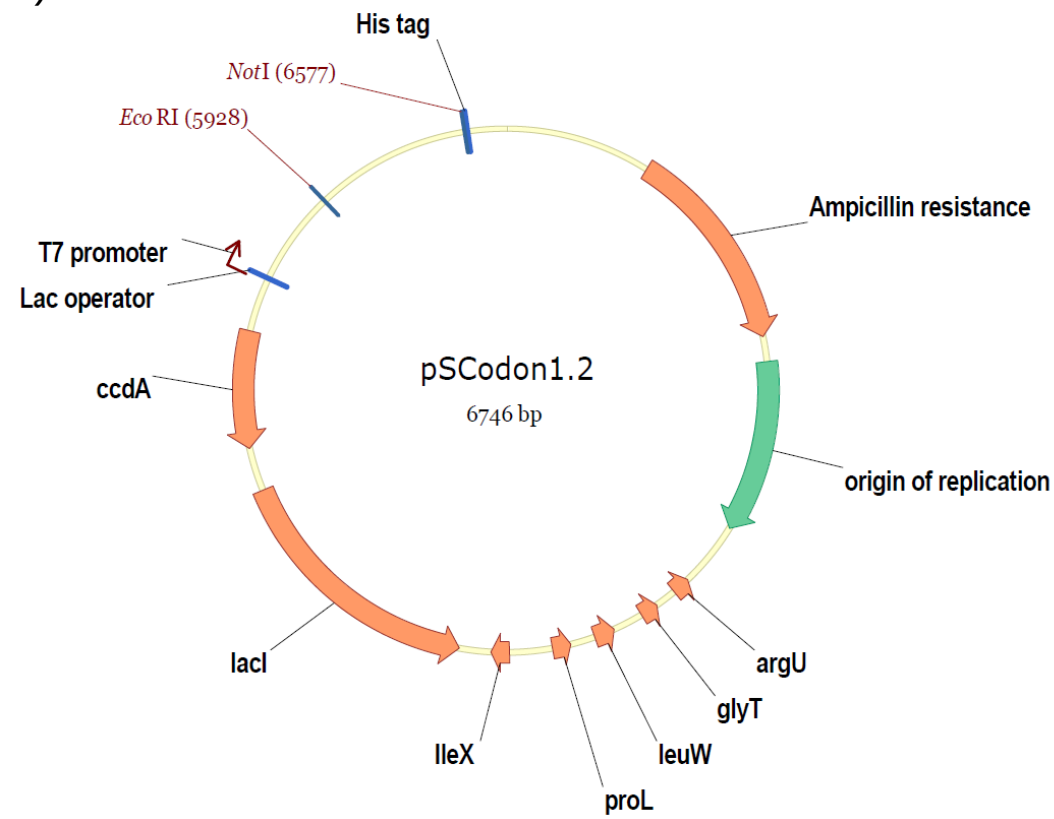
E)



F)

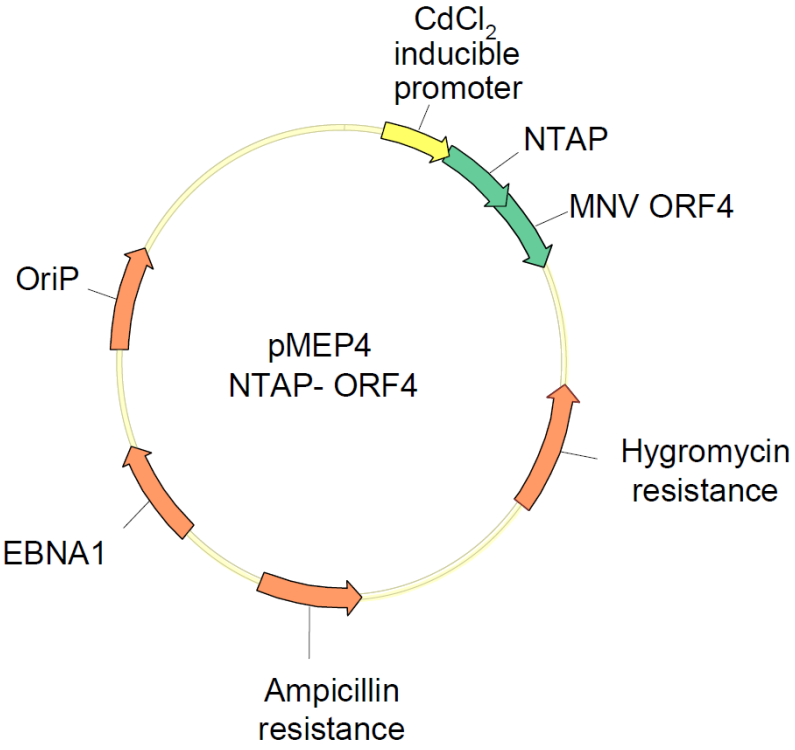


Appendix 1 (cont.). Maps of Cherry ORF4 peptide 3 his fusion **(E)** and Cherry ORF4 peptide 4 his **(F)** expression constructs.

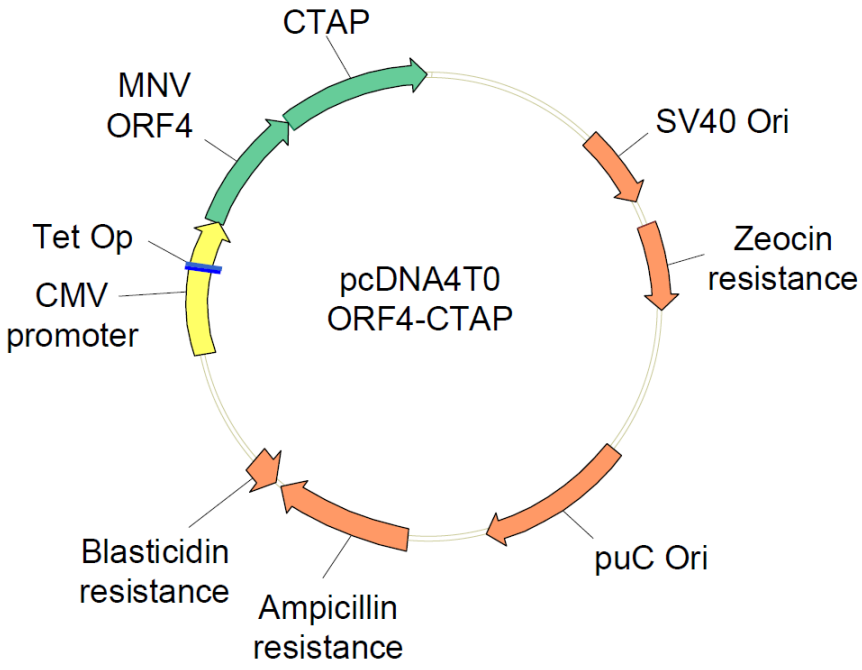


Appendix 1 (cont.). G) Map of pSCodon1.2 which does not contain the cherry tag and was used as a negative control in the cherry expression experiments.

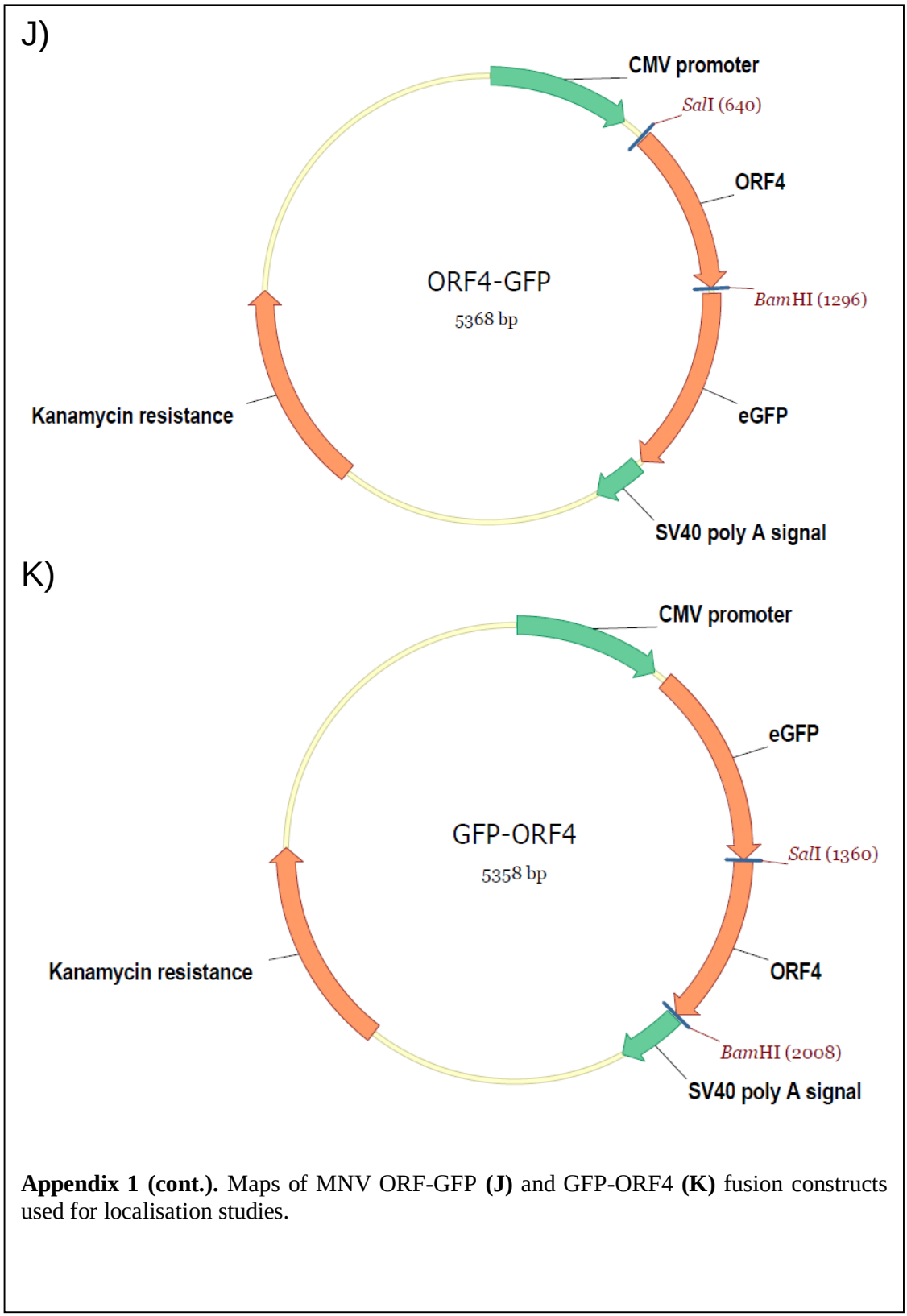
H)



I)

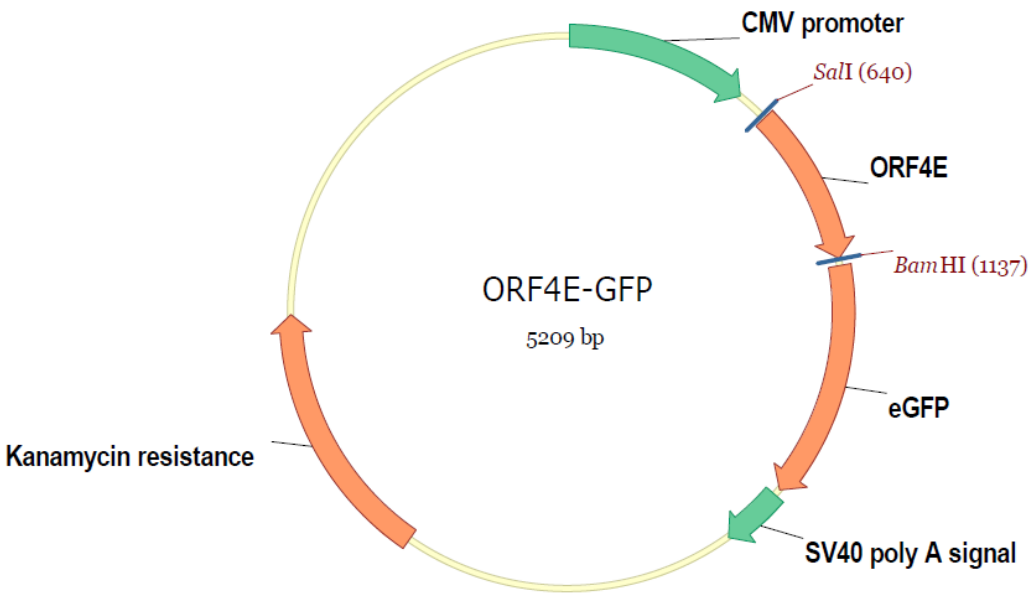


Appendix 1 (cont.). H) NTAP-ORF4 in the $CdCl_2$ inducible plasmid. I) ORF4-CTAP in the tetracycline inducible plasmid

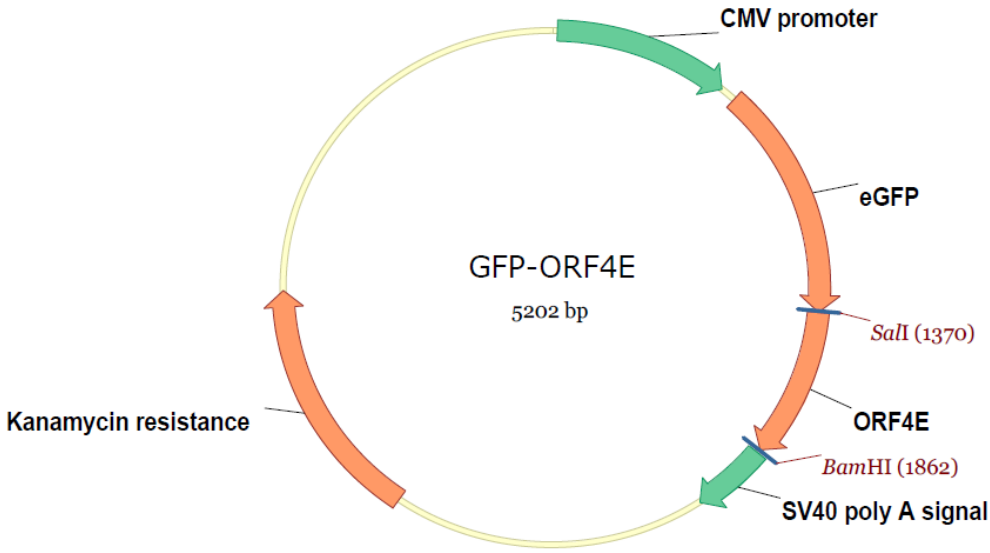


Appendix 1 (cont.). Maps of MNV ORF-GFP **(J)** and GFP-ORF4 **(K)** fusion constructs used for localisation studies.

L)



M)



Appendix 1 (cont.). Maps of SV ORFE-GFP **(L)** and GFP-ORF4E **(M)** fusion constructs GFP used for localisation studies.

		Mascot query	
Protein name[1]	**Band[2]**	**Score[3]**	**No of peptides[4]**
GCN1 general control of amino-acid synthesis 1-like 1	1	1198	15
Probable ubiquitin carboxyl-terminal hydrolase FAF-X	1	682	7
Brefeldin A-inhibited guanine nucleotide-exchange protein 1 (BIG1)	2	633	8
Exportin 2	3,6	447	7
HEAT repeat containing 1	2	360	5
Exportin T	6	318	3
Coatomer subunit beta 1 (COPB1)	4	311	5
Tubulin, gamma complex associated protein 2 variant	6	256	5
Insulin receptor substrate 4	3,6	234	4
Importin 13	6	227	4
Pyruvate kinase isozymes M1/M2	9	220	4
Importin 8	5	218	3
Apoptosis-inducing factor 1 (AIF), mitochondrial precursor	9	212	3
Coatomer subunit alpha (COPA)	3	210	3
DnaJ	13	204	1
cDNA FLJ78054, highly similar to *Homo sapiens* proteasome	16	192	3
Importin 7	5	190	2
Importin 9	5	189	3
Translocase of outer mitochondrial membrane 70 homolog A (TOM70)	8,9	185	4
Fanconi anemia group D2 protein	3	166	2
Proteasome-associated protein ECM29 homolog	4	158	2
Zinc finger protein 294 (ZFP294)	4	148	2
Mitochondrial import inner membrane translocase subunit Tim13	25	145	2
Fanconi anemia group I protein	3	144	2
Uncharacterized protein KIAA0406	5	143	1
DnaJ homolog subfamily A member 2	11,12	126	2
LRPPRC protein (leucine rich PPR motif cont. protein) - mitochondrial precursor	3	115	1
Methionyl-tRNA synthetase, cytoplasmic	6	99	2
Importin subunit beta-1	6	97	1

Peroxisomal biogenesis factor 19	14	89	1
cDNA FLJ78427, highly similar to *Homo sapiens* exportin 1	5	83	1
ATPase WRNIP1	7	74	1
cDNA FLJ11224 fis, clone PLACE1008273, moderately similar to coatomer gamma subunit	6,7	74	2
cDNA FLJ31237 fis, clone KIDNE2004846, highly similar to 26S proteasome regulatory subunit S3	9	70	1
Exportin 5	5	65	1
SHINC3	18	61	1
TATA-binding protein-associated factor 172	2	57	1
LP6054	13	54	1
HCLS1 associated protein X-1 (HAX-1)	15	53	1
Uncharacterized protein ENSP00000376341 (ribosomal)	24	53	1
Telomere length regulation protein TEL2 homolog	7	49	1
EH domain-containing protein 1	3	49	1
cDNA FLJ75591, highly similar to Homo sapiens SEC22 vesicle trafficking protein-like 1	19	47	1
Ig kappa chain V-I region CAR	17	46	1
Aladin	10	44	1
Ran-binding protein 6 (RanBP6)	5	42	1
Putative uncharacterized protein DKFZp761D0223	8	41	1
Proteasome subunit alpha type-3	17	40	1
ADP-ribosylation factor-like protein 5A (ARL5A)	21	40	1
Paraoxonase nirs variant 1 (PON1)	12	40	1

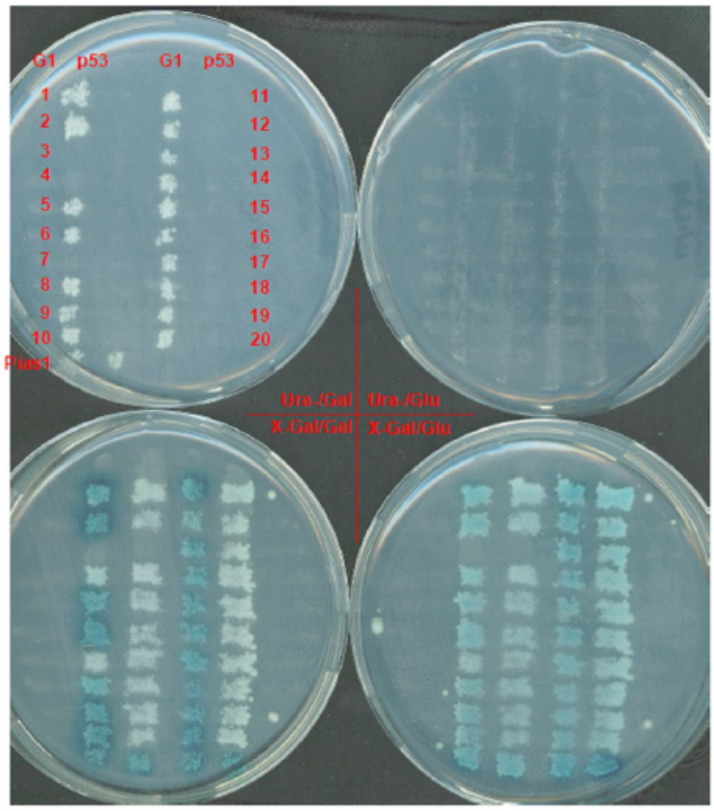
Appendix 2. **Proteins identified in the NTAP-ORF4 purification which were not identified in the purification of other NTAP-MNV proteins**. [1] Name of the protein is the name referred to if the protein is discussed in this thesis. Alternative nomenclatures of these proteins do frequently exist and can be obtained from http://www.ihop-net.org. [2] Band refers to the segment of the SDS-PAGE gel the protein was identified in. A picture of the SDS-PAGE gel and the corresponding segments was shown in figure 5.4. Note: Numbering was not shown in this figure but began with band 1 being the first segment (boxed black immediately adjacent to the gel picture) from the top of the gel. In total the SDS-PAGE gel was sliced into 25 adjoining segments. [3] Score indicates the total Mascot sequence query score of the identified protein calculated from the scores of the individually identified peptide sequences. [4] No of peptides refers to the number of peptides which were positively identified by Mascot sequence query as being a peptide component of the listed protein.

Protein name[1]	Band[2]	Mascot query		No of other interactors[5]	Other interactors (no of peptides)[6]
		Score[3]	No of peptides[4]		
60 kDa heat shock protein, mitochondrial precursor (HSP60)	9	611	9	1	VP2 (11)
Coatomer subunit beta	6	525	8	1	VP1 (3)
Nucleoporin 160kDa	3	522	7	1	VP2 (2)
Nuclear pore complex protein Nup205	2	341	4	1	VP1 (1)
RuvB-like 1	10,11	300	4	1	VP1 (6)
Uncharacterized protein ATP2A2	6	295	4	1	VP1 (1)
ATP synthase subunit alpha	10	283	4	1	VP1 (2)
Sodium/potassium-transporting ATPase subunit alpha-1 precursor	6	218	2	1	VP1 (2)
T-complex protein 1 subunit alpha	9	215	3	1	VP1 (3)
26S proteasome non-ATPase regulatory subunit 2	6	213	2	1	VP1 (1)
DnaJ homolog subfamily A member 1	12	204	3	1	VP1 (3)
IARS protein (=isoleucyl t-RNA synthetase)	3	175	3	1	VP1 (1)
DNA damage-binding protein	5	171	1	1	VP1 (3)
Import inner membrane translocase subunit TIM50, mitochondrial precursor	14	133	2	1	VP1 (2)
Dolichyl-diphosphooligosaccharide--protein glycosyltransferase 48 kDa subunit precursor	12	102	2	1	VP1 (1)
Ras-related protein Rab-35	19	102	1	1	VP1 (1)
60S ribosomal protein L38	25	94	2	1	VP1 (2)
ADP/ATP translocase 2	16	75	1	1	VP1 (4)
Protein NipSnap homolog 1	17	70	1	1	VP1 (1)
cDNA FLJ78394, highly similar to Homo sapiens RAN, member RAS oncogene family	17	68	1	1	VP1 (2)
Solute carrier family 25	16	50	1	1	VP1 (1)
D-3-phosphoglycerate dehydrogenase	10	49	1	1	VP1 (3)
NADH dehydrogenase [ubiquinone] 1 alpha subcomplex subunit 4	25	44	1	1	VP1 (1)

Anti-mucin1 light chain variable region	18	42	1	1	VP1 (1)
26S protease regulatory subunit 4	12	41	1	1	VP1 (1)
cDNA FLJ75514, highly similar to *S.scrofa* putative 26S protease subunit	12	41	1	1	VP1 (3)
Putative uncharacterized protein RAB10	19		1	1	VP1 (1)
Putative uncharacterized protein CAD (carbamoyl-phosphate synthetase 2, aspartate transcarbamylase, and dihydrotase)	1,2	1132	14	2	VP1 (12), VP2 (1)
RuvB-like 2	10,11	726	13	2	VP1 (11), VP2 (1)
Putative uncharacterized protein (beta actin variant)	13	292	5	2	VP1 (7), VP2 (9)
Heat shock protein HSP 90-beta	6, 7	224	3	2	VP1 (11), VP2 (1)
6-phosphofructokinase, liver type	7	191	1	2	VP1 (1), VP2 (1)
Actin, alpha 1, skeletal muscle	13	164	2	2	VP1 (5), VP2 (2)
PFKM protein	7	135	1	2	VP1 (3), VP2 (1)
BAG family molecular chaperone regulator 2	18	130	2	2	VP1, VP2
Protein beta-actin-like	13	127	1	2	VP1 (2), VP2 (2)
cDNA FLJ36025 fis, clone TESTI2016701, highly similar to tumour necrosis factor type I associated protein	7	94	1	2	VP1 (1), VP2 (1)
Actin-like protein	13	72	1	2	VP1 (2), VP2 (1)
60S ribosomal protein L12	20	47	1	2	VP1(3), VPg (1)
Ubiquitin			2	2	NS3 (4), VP1 (2)
HSP90AA1 protein	7		2	2	VP1 (10), VP2 (1)
Elongation factor 1-alpha	11	255	4	3	VPg (2), VP1 (6), VP2 (1)
40S ribosomal protein S3	16	80	4	3	NS33 (1),NS4 (1),VP1 (7)
40S ribosomal protein S25	20	143	2	4	NS3 (1), VPg (3), VP1 (1), VP2 (1)
Tubulin alpha-8 chain	2 to 19		6	4	NS3 (2),VPg (3), VP1 (6), VP2 (2)
Putative tubulin-like protein alpha-4B	10,11,12		2	4	NS3 (1),VPg (1), VP1 (2), VP2 (1)
COL14A1 protein	20		1	5	NS4 (1), VP1 (1), VP2 (1)

Appendix 3. **Proteins identified in the NTAP-ORF4 purification which were not identified in the purification of other NTAP-MNV proteins.** [1-4] as described in appendix 1. [5] number of other MNV NTAP proteins in which the protein was also identified by TAP purification. [6] Identification of the other MNV NTAP proteins in which the protein was also isolated by TAP purification

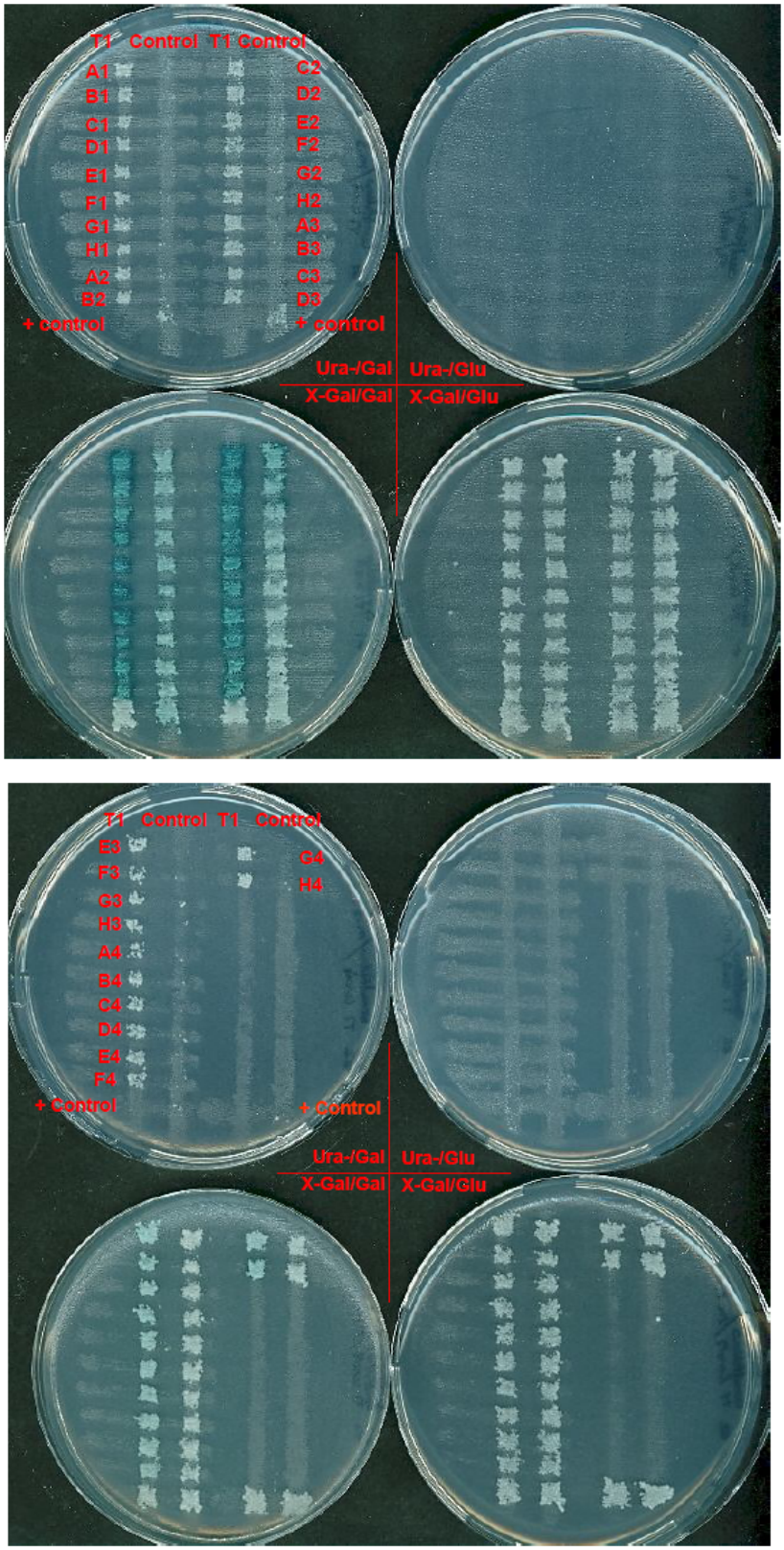
A)



B)

Clone number	Genbank accession	Identity
5	BC119603.2	*Mus musculus* thrombospondin, type I, domain 1
6	NM_001006966.1	*Rattus norvegicus* peroxisomal delta3, delta2-enoyl-Coenzyme A isomerase (Peci)
8	NM_011252.2	*Mus musculus* RNA binding motif protein, X chromosome (Rbmx)
9	BC093481.1	*Mus musculus* pre-mRNA processing factor 8
11	NM_134010.2	*Mus musculus* nucleoporin 107 (Nup107)
12	BC034200.1	pre-B-cell leukemia transcription factor interacting protein 1
13	NM_001006966.1	*Rattus norvegicus* peroxisomal delta3, delta2-enoyl-Coenzyme A isomerase (Peci),
14	BC093481.1	*Mus musculus* pre-mRNA processing factor 8
15	NM_199316.2	*Mus musculus* RIKEN cDNA 4922501C03 gene
16	NM_134010.2	*Mus musculus* nucleoporin 107 (Nup107)
17	NM_029834.3	*Mus musculus* protein phosphatase 1, regulatory (inhibitor) subunit 12C (Ppp1r12c)
18	BC003710.1	*Mus musculus* nucleoporin 107 (Nup107)
19	NM_134010.2	RNA binding motif protein, X chromosome
20	NM_134010.2	*Mus musculus* nucleoporin 107 (Nup107)

Appendix 4. Proteins which interacted with the ORF4 protein by TetR yeast two hybrid screen. A) Interacting clones were characterised by their ability to grow on media deficient of uracil in the presence of galactose but not glucose. In the presence of X-gal blue colonies can be seen for interacting clones. The p53-PIAS1 interaction served as a positive control. **B)** Only the identity of clones in which the interaction was confirmed after retransformation into yeast are listed in the table.



Appendix 5. Proteins which interacted with the ORF4 protein by LexA yeast two hybrid screen. Interacting clones were characterised by their ability to grow on media deficient of uracil in the presence of galactose but not glucose. In the presence of X-gal blue colonies were be seen for interacting clones. The p53-PIAS1 interaction served as a positive control. All interacting clones were sequenced and identified as *Mus musculus* Fanconi anemia zinc finger. The p53-PIAS1 interaction served as a positive control.

Bibliography

Agirre, A., Barco, A., Carrasco, L. & Nieva, J. L. (2002). Viroporin-mediated membrane permeabilization. Pore formation by nonstructural poliovirus 2B protein. *J Biol Chem* **277**, 40434-41.

Al-Molawi, N., Beardmore, V. A., Carter, M. J., Kass, G. E. & Roberts, L. O. (2003). Caspase-mediated cleavage of the feline calicivirus capsid protein. *J Gen Virol* **84**, 1237-44.

Alonso, C., Oviedo, J. M., Martin-Alonso, J. M., Diaz, E., Boga, J. A. & Parra, F. (1998). Programmed cell death in the pathogenesis of rabbit hemorrhagic disease. *Arch Virol* **143**, 321-32.

Ammann, C. G., Messer, R. J., Varvel, K., Debuysscher, B. L., Lacasse, R. A., Pinto, A. K. & Hasenkrug, K. J. (2009). Effects of acute and chronic murine norovirus infections on immune responses and recovery from Friend retrovirus infection. *J Virol* **83**, 13037-41.

Andrabi, S. A., Kim, N. S., Yu, S. W., Wang, H., Koh, D. W., Sasaki, M., Klaus, J. A., Otsuka, T., Zhang, Z., Koehler, R. C., Hurn, P. D., Poirier, G. G., Dawson, V. L. & Dawson, T. M. (2006). Poly(ADP-ribose) (PAR) polymer is a death signal. *Proc Natl Acad Sci U S A* **103**, 18308-13.

Arnoult, D., Skaletskaya, A., Estaquier, J., Dufour, C. & Goldmacher, V. S. (2008). The murine cytomegalovirus cell death suppressor m38.5 binds Bax and blocks Bax-mediated mitochondrial outer membrane permeabilization. *Apoptosis* **13**, 1100-10.

Arts, G. J., Kuersten, S., Romby, P., Ehresmann, B. & Mattaj, I. W. (1998). The role of exportin-t in selective nuclear export of mature tRNAs. *EMBO J* **17**, 7430-41.

Aslan, J. E. & Thomas, G. (2009). Death by committee: organellar trafficking and communication in apoptosis. *Traffic* **10**, 1390-404.

Aubert, C., Chamorro, M. & Brahic, M. (1987). Identification of Theiler's virus infected cells in the central nervous system of the mouse during demyelinating disease. *Microbial Pathogenesis* **3**, 319-326.

Baert, L., Wobus, C. E., Van Coillie, E., Thackray, L. B., Debevere, J. & Uyttendaele, M. (2008). Detection of murine norovirus 1 by using plaque assay, transfection assay, and real-time reverse transcription-PCR before and after heat exposure. *Appl Environ Microbiol* **74**, 543-6.

Bailey, D. & Goodfellow, I. G. (2009). Noroviruses. In *Encyclopedia of Life Sciences*. Chichester: John Wiley & Sons.

Bailey, D., Kaiser, W. J., Hollinshead, M., Moffat, K., Chaudhry, Y., Wileman, T., Sosnovtsev, S. V. & Goodfellow, I. G. (2010a). Feline calicivirus p32, p39 and p30 proteins localize to the endoplasmic reticulum to initiate replication complex formation. *J Gen Virol* **91**, 739-49.

Bailey, D., Karakasiliotis, I., Vashist, S., Chung, L. M., Reese, J., McFadden, N., Benson, A., Yarovinsky, F., Simmonds, P. & Goodfellow, I. (2010b). Functional analysis of RNA structures present at the 3' extremity of the murine norovirus genome: the variable polypyrimidine tract plays a role in viral virulence. *J Virol* **84**, 2859-70.

Bailey, D., Thackray, L. B. & Goodfellow, I. G. (2008). A single amino acid substitution in the murine norovirus capsid protein is sufficient for attenuation in vivo. *J Virol* **82**, 7725-8.

Bain, C., Parroche, P., Lavergne, J. P., Duverger, B., Vieux, C., Dubois, V., Komurian-Pradel, F., Trepo, C., Gebuhrer, L., Paranhos-Baccala, G., Penin, F. & Inchauspe, G. (2004). Memory T-cell-mediated immune responses specific to an alternative core protein in hepatitis C virus infection. *J Virol* **78**, 10460-9.

Ballensiefen, W., Ossipov, D. & Schmitt, H. D. (1998). Recycling of the yeast v-SNARE Sec22p involves COPI-proteins and the ER transmembrane proteins Ufe1p and Sec20p. *J Cell Sci* **111**, 1507-20.

Barco, A., Feduchi, E. & Carrasco, L. (2000). Poliovirus protease 3C(pro) kills cells by apoptosis. *Virology* **266**, 352-60.

Baril, M. & Brakier-Gingras, L. (2005). Translation of the F protein of hepatitis C virus is initiated at a non-AUG codon in a +1 reading frame relative to the polyprotein. *Nucleic Acids Res* **33**, 1474-86.

Barlowe, C. (1995). COPII: a membrane coat that forms endoplasmic reticulum-derived vesicles. *FEBS Lett* **369**, 93-6.

Basu, A., Steele, R., Ray, R. & Ray, R. B. (2004). Functional properties of a 16 kDa protein translated from an alternative open reading frame of the core-encoding genomic region of hepatitis C virus. *J Gen Virol* **85**, 2299-306.

Belov, G. A., Romanova, L. I., Tolskaya, E. A., Kolesnikova, M. S., Lazebnik, Y. A. & Agol, V. I. (2003). The major apoptotic pathway activated and suppressed by poliovirus. *J. Virol.* **77**, 45-56.

Belshaw, R., Pybus, O. G. & Rambaut, A. (2007). The evolution of genome compression and genomic novelty in RNA viruses. *Genome Res* **17**, 1496-504.

Bergin, I. L., Wise, A. G., Bolin, S. R., Mullaney, T. P., Kiupel, M. & Maes, R. K. (2009). Novel calicivirus identified in rabbits, michigan, USA. *Emerg Infect Dis* **15**, 1955-62.

Berry, A. M., Flock, K. E., Loh, H. H. & Ko, J. L. (2006). Molecular basis of cellular localization of poly C binding protein 1 in neuronal cells. *Biochem Biophys Res Commun* **349**, 1378-86.

Bhella, D., Gatherer, D., Chaudhry, Y., Pink, R. & Goodfellow, I. G. (2008). Structural insights into calicivirus attachment and uncoating. *J Virol* **82**, 8051-8.

Blaustein, M., Quadrana, L., Risso, G., Mata Mde, L., Pelisch, F. & Srebrow, A. (2009). SF2/ASF regulates proteomic diversity by affecting the balance between translation initiation mechanisms. *J Cell Biochem* **107**, 826-33.

Boatright, K. M. & Salvesen, G. S. (2003). Mechanisms of caspase activation. *Curr Opin Cell Biol* **15**, 725-31.

Bok, K., Prikhodko, V. G., Green, K. Y. & Sosnovtsev, S. V. (2009). Apoptosis in murine norovirus-infected RAW264.7 cells is associated with downregulation of survivin. *J Virol* **83**, 3647-56.

Breakspear, A., Langford, K. J., Momany, M. & Assinder, S. J. (2007). CopA:GFP localizes to putative Golgi equivalents in Aspergillus nidulans. *FEMS Microbiol Lett* **277**, 90-7.

Bruns, K., Studtrucker, N., Sharma, A., Fossen, T., Mitzner, D., Eissmann, A., Tessmer, U., Roder, R., Henklein, P., Wray, V. & Schubert, U. (2007). Structural characterization and oligomerization of PB1-F2, a proapoptotic influenza A virus protein. *J Biol Chem* **282**, 353-63.

Bryson, K., McGuffin, L. J., Marsden, R. L., Ward, J. J., Sodhi, J. S. & Jones, D. T. (2005). Protein structure prediction servers at University College London. *Nucleic Acids Res* **33**, W36-8.

Burckstummer, T., Bennett, K. L., Preradovic, A., Schutze, G., Hantschel, O., Superti-Furga, G. & Bauch, A. (2006). An efficient tandem affinity purification procedure for interaction proteomics in mammalian cells. *Nat Methods* **3**, 1013-9.

Burroughs, J. N. & Brown, F. (1978). Presence of a covalently linked protein on calicivirus RNA. *J Gen Virol* **41**, 443-6.

Calado, A., Treichel, N., Muller, E. C., Otto, A. & Kutay, U. (2002). Exportin-5-mediated nuclear export of eukaryotic elongation factor 1A and tRNA. *EMBO J* **21**, 6216-24.

Cannino, G., Ferruggia, E., Luparello, C. & Rinaldi, A. M. (2008). Effects of cadmium chloride on some mitochondria-related activity and gene expression of human MDA-MB231 breast tumor cells. *J Inorg Biochem* **102**, 1668-76.

Cappello, F., de Macario, E. C., Marasa, L., Zummo, G. & Macario, A. J. (2008). Hsp60 expression, new locations, functions and perspectives for cancer diagnosis and therapy. *Cancer Biol Ther* **7**, 801-9.

Carre, M., Andre, N., Carles, G., Borghi, H., Brichese, L., Briand, C. & Braguer, D. (2002). Tubulin is an inherent component of mitochondrial membranes that interacts with the voltage-dependent anion channel. *J Biol Chem* **277**, 33664-9.

Carter, M. J., Milton, I. D., Meanger, J., Bennett, M., Gaskell, R. M. & Turner, P. C. (1992). The complete nucleotide sequence of a feline calicivirus. *Virology* **190**, 443-8.

Cash, E., Chamorro, M. & Brahic, M. (1986). Quantitation, with a new assay, of Theiler's virus capsid protein in the central nervous system of mice. *J Virol* **60**, 558-563.

Castro, C., Arnold, J. J. & Cameron, C. E. (2005). Incorporation fidelity of the viral RNA-dependent RNA polymerase: a kinetic, thermodynamic and structural perspective. *Virus Res* **107**, 141-9.

Chachu, K. A., LoBue, A. D., Strong, D. W., Baric, R. S. & Virgin, H. W. (2008a). Immune mechanisms responsible for vaccination against and clearance of mucosal and lymphatic norovirus infection. *PLoS Pathog* **4**, e1000236.

Chachu, K. A., Strong, D. W., LoBue, A. D., Wobus, C. E., Baric, R. S. & Virgin, H. W. t. (2008b). Antibody is critical for the clearance of murine norovirus infection. *J Virol* **82**, 6610-7.

Chandra, D., Choy, G. & Tang, D. G. (2007). Cytosolic accumulation of HSP60 during apoptosis with or without apparent mitochondrial release: evidence that its pro-apoptotic or pro-survival functions involve differential interactions with caspase-3. *J Biol Chem* **282**, 31289-301.

Chandra, V., Kar-Roy, A., Kumari, S., Mayor, S. & Jameel, S. (2008). The hepatitis E virus ORF3 protein modulates epidermal growth factor receptor trafficking, STAT3 translocation, and the acute-phase response. *J Virol* **82**, 7100-10.

Chang, K. O., Sosnovtsev, S. S., Belliot, G., Wang, Q., Saif, L. J. & Green, K. Y. (2005). Reverse genetics system for porcine enteric calicivirus, a prototype sapovirus in the *Caliciviridae*. *J Virol* **79**, 1409-16.

Chang, K. O., Sosnovtsev, S. V., Belliot, G., King, A. D. & Green, K. Y. (2006). Stable expression of a Norwalk virus RNA replicon in a human hepatoma cell line. *Virology* **353**, 463-73.

Chang, L. Y., Shih, S. R., Shao, P. L., Huang, D. T. & Huang, L. M. (2009). Novel swine-origin influenza virus A (H1N1): the first pandemic of the 21st century. *J Formos Med Assoc* **108**, 526-32.

Chao, S. H., Walker, J. R., Chanda, S. K., Gray, N. S. & Caldwell, J. S. (2003). Identification of homeodomain proteins, PBX1 and PREP1, involved in the transcription of murine leukemia virus. *Mol Cell Biol* **23**, 831-41.

Chaudhry, Y., Nayak, A., Bordeleau, M.-E., Tanaka, J., Pelletier, J., Belsham, G. J., Roberts, L. O. & Goodfellow, I. G. (2006). Caliciviruses differ in their functional requirements for eIF4F components. *J Biol Chem* **281**, 25315-25325.

Chaudhry, Y., Skinner, M. A. & Goodfellow, I. G. (2007). Recovery of genetically defined murine norovirus in tissue culture by using a fowlpox virus expressing T7 RNA polymerase. *J Gen Virol* **88**, 2091-100.

Cheetham, S., Souza, M., Meulia, T., Grimes, S., Han, M. G. & Saif, L. J. (2006). Pathogenesis of a genogroup II human norovirus in gnotobiotic pigs. *J Virol* **80**, 10372-81.

Chen, S. Y., Tsai, C. N., Lai, M. W., Chen, C. Y., Lin, K. L., Lin, T. Y. & Chiu, C. H. (2009). Norovirus infection as a cause of diarrhea-associated benign infantile seizures. *Clin Infect Dis* **48**, 849-55.

Chen, T., Brownawell, A. M. & Macara, I. G. (2004). Nucleocytoplasmic shuttling of JAZ, a new cargo protein for exportin-5. *Mol Cell Biol* **24**, 6608-19.

Chen, W., Calvo, P. A., Malide, D., Gibbs, J., Schubert, U., Bacik, I., Basta, S., O'Neill, R., Schickli, J., Palese, P., Henklein, P., Bennink, J. R. & Yewdell, J. W. (2001). A novel influenza A virus mitochondrial protein that induces cell death. *Nat Med* **7**, 1306-12.

Chien, C. T., Bartel, P. L., Sternglanz, R. & Fields, S. (1991). The two-hybrid system: a method to identify and clone genes for proteins that interact with a protein of interest. *Proc Natl Acad Sci U S A* **88**, 9578-82.

Chowdhury, I., Tharakan, B. & Bhat, G. K. (2008). Caspases - an update. *Comp Biochem Physiol B Biochem Mol Biol* **151**, 10-27.

Chung, B. Y., Miller, W. A., Atkins, J. F. & Firth, A. E. (2008). An overlapping essential gene in the *Potyviridae*. *Proc Natl Acad Sci U S A* **105**, 5897-902.

Chung, E. Y., Liu, J., Homma, Y., Zhang, Y., Brendolan, A., Saggese, M., Han, J., Silverstein, R., Selleri, L. & Ma, X. (2007). Interleukin-10 expression in macrophages during phagocytosis of apoptotic cells is mediated by homeodomain proteins Pbx1 and Prep-1. *Immunity* **27**, 952-64.

Chung, K. M., Lee, J., Kim, J. E., Song, O. K., Cho, S., Lim, J., Seedorf, M., Hahm, B. & Jang, S. K. (2000). Nonstructural protein 5A of hepatitis C virus inhibits the function of karyopherin beta3. *J Virol* **74**, 5233-41.

Cilenti, L., Soundarapandian, M. M., Kyriazis, G. A., Stratico, V., Singh, S., Gupta, S., Bonventre, J. V., Alnemri, E. S. & Zervos, A. S. (2004). Regulation of HAX-1 anti-apoptotic protein by Omi/HtrA2 protease during cell death. *J Biol Chem* **279**, 50295-301.

Clarke, I. N. & Lambden, P. R. (1997). Viral zoonoses and food of animal origin: caliciviruses and human disease. *Arch Virol Suppl* **13**, 141-52.

Clarke, I. N. & Lambden, P. R. (2000). Organization and expression of calicivirus genes. *J Infect Dis* **181 Suppl 2**, S309-16.

Claros, M. G. & Vincens, P. (1996). Computational method to predict mitochondrially imported proteins and their targeting sequences. *Eur J Biochem* **241**, 779-86.

Cohen, M., Bachmatov, L., Ben-Ari, Z., Rotman, Y., Tur-Kaspa, R. & Zemel, R. (2007). Development of specific antibodies to an ARF protein in treated patients with chronic HCV infection. *Dig Dis Sci* **52**, 2427-32.

Coleman, J. R. (2007). The PB1-F2 protein of Influenza A virus: increasing pathogenicity by disrupting alveolar macrophages. *Virol J* **4**, 9.

Comai, L. & Li, B. (2004). The Werner syndrome protein at the crossroads of DNA repair and apoptosis. *Mech Ageing Dev* **125**, 521-8.

Conenello, G. M. & Palese, P. (2007). Influenza A virus PB1-F2: a small protein with a big punch. *Cell Host Microbe* **2**, 207-9.

Corcelette, S., Masse, T. & Madjar, J. J. (2000). Initiation of translation by non-AUG codons in human T-cell lymphotropic virus type I mRNA encoding both Rex and Tax regulatory proteins. *Nucleic Acids Res* **28**, 1625-34.

Cuevas, E. P., Escribano, O., Monserrat, J., Martinez-Botas, J., Sanchez, M. G., Chiloeches, A., Hernandez-Breijo, B., Sanchez-Alonso, V., Roman, I. D., Fernandez-Moreno, M. D. & Guijarro, L. G. (2009). RNAi-mediated silencing of insulin receptor substrate-4 enhances actinomycin D- and tumor necrosis factor-alpha-induced cell death in hepatocarcinoma cancer cell lines. *J Cell Biochem* **108**, 1292-301.

Cumming, R. C., Lightfoot, J., Beard, K., Youssoufian, H., O'Brien, P. J. & Buchwald, M. (2001). Fanconi anemia group C protein prevents apoptosis in hematopoietic cells through redox regulation of GSTP1. *Nat Med* **7**, 814-20.

Dai, M. S., Chevallier, N., Stone, S., Heinrich, M. C., McConnell, M., Reuter, T., Broxmeyer, H. E., Licht, J. D., Lu, L. & Hoatlin, M. E. (2002). The effects of the Fanconi anemia zinc finger (FAZF) on cell cycle, apoptosis, and proliferation are differentiation stage-specific. *J Biol Chem* **277**, 26327-34.

Danishuddin, M., Khan, S. N. & Khan, A. U. (2010). Molecular interactions between mitochondrial membrane proteins and the C-terminal domain of PB1-F2: an in silico approach. *J Mol Model* **16**, 535-41.

Daughenbaugh, K. F., Fraser, C. S., Hershey, J. W. & Hardy, M. E. (2003). The genome-linked protein VPg of the Norwalk virus binds eIF3, suggesting its role in translation initiation complex recruitment. *EMBO J* **22**, 2852-9.

Daughenbaugh, K. F., Wobus, C. E. & Hardy, M. E. (2006). VPg of murine norovirus binds translation initiation factors in infected cells. *Virol J* **3**, 33.

Delhaye, S., van Pesch, V. & Michiels, T. (2004). The leader protein of Theiler's virus interferes with nucleocytoplasmic trafficking of cellular proteins. *J Virol* **78**, 4357-62.

DiMartino, J. F., Selleri, L., Traver, D., Firpo, M. T., Rhee, J., Warnke, R., O'Gorman, S., Weissman, I. L. & Cleary, M. L. (2001). The Hox cofactor and proto-oncogene Pbx1 is required for maintenance of definitive hematopoiesis in the fetal liver. *Blood* **98**, 618-26.

Dinur-Mills, M., Tal, M. & Pines, O. (2008). Dual targeted mitochondrial proteins are characterized by lower MTS parameters and total net charge. *PLoS One* **3**, e2161.

Dolin, R. (2007). Noroviruses--challenges to control. *N Engl J Med* **357**, 1072-3.

Donaldson, E. F., Lindesmith, L. C., Lobue, A. D. & Baric, R. S. (2008). Norovirus pathogenesis: mechanisms of persistence and immune evasion in human populations. *Immunol Rev* **225**, 190-211.

Doom, C. M., Turula, H. M. & Hill, A. B. (2009). Investigation of the impact of the common animal facility contaminant murine norovirus on experimental murine cytomegalovirus infection. *Virology* **392**, 153-61.

Drescher, K. M. & Sosnowska, D. (2008). Being a mouse in a man's world: what TMEV has taught us about human disease. *Front Biosci* **13**, 3775-85.

Dubuisson, J. (2007). Hepatitis C virus proteins. *World J Gastroenterol* **13**, 2406-15.

Duizer, E., Schwab, K. J., Neill, F. H., Atmar, R. L., Koopmans, M. P. G. & Estes, M. K. (2004). Laboratory efforts to cultivate noroviruses. *J Gen Virol* **85**, 79-87.

Dupont, S., Mamidi, A., Cordenonsi, M., Montagner, M., Zacchigna, L., Adorno, M., Martello, G., Stinchfield, M. J., Soligo, S., Morsut, L., Inui, M., Moro, S., Modena, N., Argenton, F., Newfeld, S. J. & Piccolo, S. (2009). FAM/USP9x, a deubiquitinating enzyme essential for TGFbeta signaling, controls Smad4 monoubiquitination. *Cell* **136**, 123-35.

Dziembowski, A. & Seraphin, B. (2004). Recent developments in the analysis of protein complexes. *FEBS Lett* **556**, 1-6.

Dziembowski, A., Ventura, A. P., Rutz, B., Caspary, F., Faux, C., Halgand, F., Laprevote, O. & Seraphin, B. (2004). Proteomic analysis identifies a new complex required for nuclear pre-mRNA retention and splicing. *EMBO J* **23**, 4847-56.

Emerson, S. U., Nguyen, H., Torian, U. & Purcell, R. H. (2006). ORF3 protein of hepatitis E virus is not required for replication, virion assembly, or infection of hepatoma cells *in vitro*. *J Virol* **80**, 10457-64.

Endo, T. & Kohda, D. (2002). Functions of outer membrane receptors in mitochondrial protein import. *Biochim Biophys Acta* **1592**, 3-14.

Ernst, H. & Shatkin, A. J. (1985). Reovirus hemagglutinin mRNA codes for two polypeptides in overlapping reading frames. *Proc Natl Acad Sci U S A* **82**, 48-52.

Estes, M. K., Prasad, B. V. & Atmar, R. L. (2006). Noroviruses everywhere: has something changed? *Curr Opin Infect Dis* **19**, 467-74.

Ettayebi, K. & Hardy, M. E. (2003). Norwalk virus nonstructural protein p48 forms a complex with the SNARE regulator VAP-A and prevents cell surface expression of vesicular stomatitis virus G protein. *J Virol* **77**, 11790-7.

Fahrenkrog, B. (2006). The nuclear pore complex, nuclear transport, and apoptosis. *Can J Physiol Pharmacol* **84**, 279-86.

Faleiro, L. & Lazebnik, Y. (2000). Caspases disrupt the nuclear-cytoplasmic barrier. *J Cell Biol* **151**, 951-9.

Fankhauser, R. L., Noel, J. S., Monroe, S. S., Ando, T. & Glass, R. I. (1998). Molecular epidemiology of "Norwalk-like viruses" in outbreaks of gastroenteritis in the United States. *J Infect Dis* **178**, 1571-8.

Farkas, T., Nakajima, S., Sugieda, M., Deng, X., Zhong, W. & Jiang, X. (2005). Seroprevalence of noroviruses in swine. *J Clin Microbiol* **43**, 657-61.

Farkas, T., Sestak, K., Wei, C. & Jiang, X. (2008). Characterization of a rhesus monkey calicivirus representing a new genus of *Caliciviridae*. *J Virol* **82**, 5408-16.

Faure, E. (2006). Alternative peptide-fusion proteins generated by out-of-frame mutations, just upstream ORFs or elongations in mutants of human hepatitis B viruses. *Virus Res* **117**, 185-201.

Ferrando-May, E., Cordes, V., Biller-Ckovric, I., Mirkovic, J., Gorlich, D. & Nicotera, P. (2001). Caspases mediate nucleoporin cleavage, but not early redistribution of nuclear transport factors and modulation of nuclear permeability in apoptosis. *Cell Death Differ* **8**, 495-505.

Fiorucci, M., Boulant, S., Fournillier, A., Abraham, J. D., Lavergne, J. P., Paranhos-Baccala, G., Inchauspe, G. & Bain, C. (2007). Expression of the alternative reading frame protein of Hepatitis C virus induces cytokines involved in hepatic injuries. *J Gen Virol* **88**, 1149-62.

Firth, A. E. (2008). Bioinformatic analysis suggests that the Orbivirus VP6 cistron encodes an overlapping gene. *Virol J* **5**, 48.

Firth, A. E. & Atkins, J. F. (2008a). Bioinformatic analysis suggests that a conserved ORF in the waikaviruses encodes an overlapping gene. *Arch Virol* **153**, 1379-83.

Firth, A. E. & Atkins, J. F. (2008b). Bioinformatic analysis suggests that the Cypovirus 1 major core protein cistron harbours an overlapping gene. *Virol J* **5**, 62.

Firth, A. E. & Atkins, J. F. (2009). A case for a CUG-initiated coding sequence overlapping torovirus ORF1a and encoding a novel 30 kDa product. *Virol J* **6**, 136.

Fleischer, T. C., Weaver, C. M., McAfee, K. J., Jennings, J. L. & Link, A. J. (2006). Systematic identification and functional screens of uncharacterized proteins associated with eukaryotic ribosomal complexes. *Genes Dev* **20**, 1294-307.

Fontoura, B. M., Faria, P. A. & Nussenzveig, D. R. (2005). Viral interactions with the nuclear transport machinery: discovering and disrupting pathways. *IUBMB Life* **57**, 65-72.

Fukuhara, N., Fernandez, E., Ebert, J., Conti, E. & Svergun, D. (2004). Conformational variability of nucleo-cytoplasmic transport factors. *J Biol Chem* **279**, 2176-81.

Fukushi, S., Kojima, S., Takai, R., Hoshino, F. B., Oka, T., Takeda, N., Katayama, K. & Kageyama, T. (2004). Poly(A)- and primer-independent RNA polymerase of Norovirus. *J Virol* **78**, 3889-96.

Fullerton, S. W., Blaschke, M., Coutard, B., Gebhardt, J., Gorbalenya, A., Canard, B., Tucker, P. A. & Rohayem, J. (2007). Structural and functional characterization of sapovirus RNA-dependent RNA polymerase. *J Virol* **81**, 1858-71.

Furman, L. M., Maaty, W. S., Petersen, L. K., Ettayebi, K., Hardy, M. E. & Bothner, B. (2009). Cysteine protease activation and apoptosis in Murine norovirus infection. *Virol J* **6**, 139.

Gallimore, C. I., Lewis, D., Taylor, C., Cant, A., Gennery, A. & Gray, J. J. (2004). Chronic excretion of a norovirus in a child with cartilage hair hypoplasia (CHH). *J Clin Virol* **30**, 196-204.

Gallimore, C. I., Taylor, C., Gennery, A. R., Cant, A. J., Galloway, A., Iturriza-Gomara, M. & Gray, J. J. (2006). Environmental monitoring for gastroenteric viruses in a pediatric primary immunodeficiency unit. *J Clin Microbiol* **44**, 395-9.

Gaur, A. & Green, W. R. (2005). Role of a cytotoxic-T-lymphocyte epitope-defined, alternative gag open reading frame in the pathogenesis of a murine retrovirus-induced immunodeficiency syndrome. *J Virol* **79**, 4308-15.

Geisbrecht, B. V., Zhang, D., Schulz, H. & Gould, S. J. (1999). Characterization of PECI, a novel monofunctional Delta(3), Delta(2)-enoyl-CoA isomerase of mammalian peroxisomes. *J Biol Chem* **274**, 21797-803.

Ghadge, G. D., Ma, L., Sato, S., Kim, J. & Roos, R. P. (1998). A protein critical for a Theiler's virus-induced immune system-mediated demyelinating disease has a cell type-specific antiapoptotic effect and a key role in virus persistence. *J Virol* **72**, 8605-12.

Ghosh, J. C., Dohi, T., Kang, B. H. & Altieri, D. C. (2008). Hsp60 regulation of tumor cell apoptosis. *J Biol Chem* **283**, 5188-94.

Gibbs, J. S., Malide, D., Hornung, F., Bennink, J. R. & Yewdell, J. W. (2003). The influenza A virus PB1-F2 protein targets the inner mitochondrial membrane via a predicted basic amphipathic helix that disrupts mitochondrial function. *J Virol* **77**, 7214-24.

Glavy, J. S., Krutchinsky, A. N., Cristea, I. M., Berke, I. C., Boehmer, T., Blobel, G. & Chait, B. T. (2007). Cell-cycle-dependent phosphorylation of the nuclear pore Nup107-160 subcomplex. *Proc Natl Acad Sci U S A* **104**, 3811-6.

Gohara, D. W., Ha, C. S., Kumar, S., Ghosh, B., Arnold, J. J., Wisniewski, T. J. & Cameron, C. E. (1999). Production of "authentic" poliovirus RNA-dependent RNA polymerase (3D(pol)) by ubiquitin-protease-mediated cleavage in *Escherichia coli*. *Protein Expr Purif* **17**, 128-38.

Goldmacher, V. S. (2002). vMIA, a viral inhibitor of apoptosis targeting mitochondria. *Biochimie* **84**, 177-85.

Goodfellow, I., Chaudhry, Y., Gioldasi, I., Gerondopoulos, A., Natoni, A., Labrie, L., Laliberte, J. F. & Roberts, L. (2005). Calicivirus translation initiation requires an interaction between VPg and eIF 4 E. *EMBO Rep* **6**, 968-72.

Goodfellow, I. G., Chaudhry, Y., Richardson, A., Meredith, J. M., Almond, J. W., Barclay, W. S. & Evans, D. J. (2000). Identification of a *cis*-acting replication element (CRE) within the poliovirus coding region. *J Virol* **74**, 4590-4600.

Gorlich, D. (1998). Transport into and out of the cell nucleus. *EMBO J* **17**, 2721-7.

Gorlich, D., Dabrowski, M., Bischoff, F. R., Kutay, U., Bork, P., Hartmann, E., Prehn, S. & Izaurralde, E. (1997). A novel class of RanGTP binding proteins. *J Cell Biol* **138**, 65-80.

Gorska, M. M., Cen, O., Liang, Q., Stafford, S. J. & Alam, R. (2006). Differential regulation of interleukin 5-stimulated signaling pathways by dynamin. *J Biol Chem* **281**, 14429-39.

Gotoh, B., Komatsu, T., Takeuchi, K. & Yokoo, J. (2001). Paramyxovirus accessory proteins as interferon antagonists. *Microbiol Immunol* **45**, 787-800.

Graff, J., Torian, U., Nguyen, H. & Emerson, S. U. (2006). A bicistronic subgenomic mRNA encodes both the ORF2 and ORF3 proteins of hepatitis E virus. *J Virol* **80**, 5919-26.

Green, K. Y., Ando, T., Balayan, M. S., Berke, T., Clarke, I. N., Estes, M. K., Matson, D. O., Nakata, S., Neill, J. D., Studdert, M. J. & Thiel, H. J. (2000). Taxonomy of the caliciviruses. *J Infect Dis* **181 Suppl 2**, S322-30.

Green, K. Y., Kapikian, A. Z., Valdesuso, J., Sosnovtsev, S., Treanor, J. J. & Lew, J. F. (1997). Expression and self-assembly of recombinant capsid protein from the antigenically distinct Hawaii human calicivirus. *J Clin Microbiol* **35**, 1909-14.

Green, K. Y., Mory, A., Fogg, M. H., Weisberg, A., Belliot, G., Wagner, M., Mitra, T., Ehrenfeld, E., Cameron, C. E. & Sosnovtsev, S. V. (2002). Isolation of enzymatically active replication complexes from feline calicivirus-infected cells. *J Virol* **76**, 8582-95.

Grote, P., Schaeuble, K. & Ferrando-May, E. (2007). Commuting (to) suicide: an update on nucleocytoplasmic transport in apoptosis. *Arch Biochem Biophys* **462**, 156-61.

Groves, M. R., Hanlon, N., Turowski, P., Hemmings, B. A. & Barford, D. (1999). The structure of the protein phosphatase 2A PR65/A subunit reveals the conformation of its 15 tandemly repeated HEAT motifs. *Cell* **96**, 99-110.

Guix, S., Asanaka, M., Katayama, K., Crawford, S. E., Neill, F. H., Atmar, R. L. & Estes, M. K. (2007). Norwalk virus RNA is infectious in mammalian cells. *J Virol* **81**, 12238-48.

Gupta, S. & Knowlton, A. A. (2002). Cytosolic heat shock protein 60, hypoxia, and apoptosis. *Circulation* **106**, 2727-33.

Han, Y., Chen, Y. S., Liu, Z., Bodyak, N., Rigor, D., Bisping, E., Pu, W. T. & Kang, P. M. (2006). Overexpression of HAX-1 protects cardiac myocytes from apoptosis through caspase-9 inhibition. *Circ Res* **99**, 415-23.

Hensley, S. E., Pinto, A. K., Hickman, H. D., Kastenmayer, R. J., Bennink, J. R., Virgin, H. W. & Yewdell, J. W. (2009). Murine norovirus infection has no significant effect on adaptive immunity to vaccinia virus or influenza A virus. *J Virol* **83**, 7357-60.

Herbert, T. P., Brierley, I. & Brown, T. D. (1997). Identification of a protein linked to the genomic and subgenomic mRNAs of feline calicivirus and its role in translation. *J Gen Virol* **78**, 1033-40.

Higashi, K., Kashiwagi, K., Taniguchi, S., Terui, Y., Yamamoto, K., Ishihama, A. & Igarashi, K. (2006). Enhancement of +1 frameshift by polyamines during translation of polypeptide release factor 2 in Escherichia coli. *J Biol Chem* **281**, 9527-37.

Himeda, T., Ohara, Y., Asakura, K., Kontani, Y. & Sawada, M. (2005). A lentiviral expression system demonstrates that L* protein of Theiler's murine encephalomyelitis virus (TMEV) has an anti-apoptotic effect in a macrophage cell line. *Microb Pathog* **38**, 201-7.

Ho, O. & Green, W. R. (2006). Alternative translational products and cryptic T cell epitopes: expecting the unexpected. *J Immunol* **177**, 8283-9.

Hoatlin, M. E., Zhi, Y., Ball, H., Silvey, K., Melnick, A., Stone, S., Arai, S., Hawe, N., Owen, G., Zelent, A. & Licht, J. D. (1999). A novel BTB/POZ transcriptional repressor protein interacts with the Fanconi anemia group C protein and PLZF. *Blood* **94**, 3737-47.

Hoglund, A., Donnes, P., Blum, T., Adolph, H. W. & Kohlbacher, O. (2006). MultiLoc: prediction of protein subcellular localization using N-terminal targeting sequences, sequence motifs and amino acid composition. *Bioinformatics* **22**, 1158-65.

Holcik, M. & Sonenberg, N. (2005). Translational control in stress and apoptosis. *Nat Rev Mol Cell Biol* **6**, 318-27.

Hoyt, C. C., Bouchard, R. J. & Tyler, K. L. (2004). Novel nuclear herniations induced by nuclear localization of a viral protein. *J Virol* **78**, 6360-9.

Hoyt, C. C., Richardson-Burns, S. M., Goody, R. J., Robinson, B. A., Debiasi, R. L. & Tyler, K. L. (2005). Nonstructural protein sigma1s is a determinant of reovirus virulence and influences the kinetics and severity of apoptosis induction in the heart and central nervous system. *J Virol* **79**, 2743-53.

Hsu, C. C., Riley, L. K. & Livingston, R. S. (2007). Molecular characterization of three novel murine noroviruses. *Virus Genes* **34**, 147-55.

Hu, C. D., Grinberg, A. V. & Kerppola, T. K. (2005). Visualization of protein interactions in living cells using bimolecular fluorescence complementation (BiFC) analysis. *Curr Protoc Protein Sci* **Chapter 19**, Unit 19 10.

Huang, X. & Miller, W. (1991). A tool for analyzing and annotating genomic sequences. *Adv. Appl. Math.* **12**, 373-381.

Huang, Y. W., Opriessnig, T., Halbur, P. G. & Meng, X. J. (2007). Initiation at the third in-frame AUG codon of open reading frame 3 of the hepatitis E virus is essential for viral infectivity in vivo. *J Virol* **81**, 3018-26.

Huang, Z., Elkin, G., Maloney, B. J., Beuhner, N., Arntzen, C. J., Thanavala, Y. & Mason, H. S. (2005). Virus-like particle expression and assembly in plants: hepatitis B and Norwalk viruses. *Vaccine* **23**, 1851-8.

Hutson, A. M., Atmar, R. L., Graham, D. Y. & Estes, M. K. (2002). Norwalk virus infection and disease is associated with ABO histo-blood group type. *J Infect Dis* **185**, 1335-7.

Hyde, J. L., Sosnovtsev, S. V., Green, K. Y., Wobus, C., Virgin, H. W. & Mackenzie, J. M. (2009). Mouse norovirus replication is associated with virus-induced vesicle clusters originating from membranes derived from the secretory pathway. *J Virol* **83**, 9709-19.

Ilkow, C. S., Weckbecker, D., Cho, W. J., Meier, S., Beatch, M. D., Goping, I. S., Herrmann, J. M. & Hobman, T. C. (2009). The rubella virus capsid protein inhibits mitochondrial import. *J Virol*.

Ina, Y., Mizokami, M., Ohba, K. & Gojobori, T. (1994). Reduction of synonymous substitutions in the core protein gene of hepatitis C virus. *J Mol Evol* **38**, 50-6.

Ito, T., Tahara, S. M. & Lai, M. M. (1998). The 3'-untranslated region of hepatitis C virus RNA enhances translation from an internal ribosomal entry site. *J Virol* **72**, 8789-96.

Ivanov, I., Lo, K. C., Hawthorn, L., Cowell, J. K. & Ionov, Y. (2007). Identifying candidate colon cancer tumor suppressor genes using inhibition of nonsense-mediated mRNA decay in colon cancer cells. *Oncogene* **26**, 2873-84.

Janin, J. & Seraphin, B. (2003). Genome-wide studies of protein-protein interaction. *Curr Opin Struct Biol* **13**, 383-8.

Jao, D. L. & Chen, K. Y. (2006). Tandem affinity purification revealed the hypusine-dependent binding of eukaryotic initiation factor 5A to the translating 80S ribosomal complex. *J Cell Biochem* **97**, 583-98.

Jelachich, M. L. & Lipton, H. L. (2001). Theiler's murine encephalomyelitis virus induces apoptosis in gamma interferon-activated M1 differentiated myelomonocytic cells through a mechanism involving tumor necrosis factor alpha (TNF-alpha) and TNF-alpha-related apoptosis-inducing ligand. *J Virol* **75**, 5930-8.

Jha, S. & Dutta, A. (2009). RVB1/RVB2: running rings around molecular biology. *Mol Cell* **34**, 521-33.

Jiang, X., Wang, M., Graham, D. Y. & Estes, M. K. (1992). Expression, self-assembly, and antigenicity of the Norwalk virus capsid protein. *J. Virol.* **66**, 6527-6532.

Johnson, P. C., Mathewson, J. J., DuPont, H. L. & Greenberg, H. B. (1990). Multiple-challenge study of host susceptibility to Norwalk gastroenteritis in US adults. *J Infect Dis* **161**, 18-21.

Jones, D. T., Taylor, W. R. & Thornton, J. M. (1994). A model recognition approach to the prediction of all-helical membrane protein structure and topology. *Biochemistry* **33**, 3038-49.

Jordan, I. & Lipkin, W. I. (2001). Borna disease virus. *Rev Med Virol* **11**, 37-57.

Joza, N., Pospisilik, J. A., Hangen, E., Hanada, T., Modjtahedi, N., Penninger, J. M. & Kroemer, G. (2009). AIF: not just an apoptosis-inducing factor. *Ann N Y Acad Sci* **1171**, 2-11.

Joza, N., Susin, S. A., Daugas, E., Stanford, W. L., Cho, S. K., Li, C. Y., Sasaki, T., Elia, A. J., Cheng, H. Y., Ravagnan, L., Ferri, K. F., Zamzami, N., Wakeham, A., Hakem, R., Yoshida, H., Kong, Y. Y., Mak, T. W., Zuniga-Pflucker, J. C., Kroemer, G. & Penninger, J. M. (2001). Essential role of the mitochondrial apoptosis-inducing factor in programmed cell death. *Nature* **410**, 549-54.

Kaiser, W. J., Chaudhry, Y., Sosnovtsev, S. V. & Goodfellow, I. G. (2006). Analysis of protein-protein interactions in the feline calicivirus replication complex. *J Gen Virol* **87**, 363-8.

Kang, S. M., Kim, S. J., Kim, J. H., Lee, W., Kim, G. W., Lee, K. H., Choi, K. Y. & Oh, J. W. (2009). Interaction of hepatitis C virus core protein with Hsp60 triggers the production of reactive oxygen species and enhances TNF-alpha-mediated apoptosis. *Cancer Lett* **279**, 230-7.

Kannan, H., Fan, S., Patel, D., Bossis, I. & Zhang, Y. J. (2009). The hepatitis E virus open reading frame 3 product interacts with microtubules and interferes with their dynamics. *J Virol* **83**, 6375-82.

Kapikian, A. Z. (2000). The discovery of the 27-nm Norwalk virus: an historic perspective. *J Infect Dis* **181 Suppl 2**, S295-302.

Karakasiliotis, I., Chaudhry, Y., Roberts, L. O. & Goodfellow, I. G. (2006). Feline calicivirus replication: requirement for polypyrimidine tract-binding protein is temperature dependent. *J Gen Virol* **87**, 3339-3347.

Karst, S. M., Wobus, C. E., Lay, M., Davidson, J. & Virgin, H. W. t. (2003). STAT1-dependent innate immunity to a Norwalk-like virus. *Science* **299**, 1575-8.

Katpally, U., Wobus, C. E., Dryden, K., Virgin, H. W. t. & Smith, T. J. (2008). Structure of antibody-neutralized murine norovirus and unexpected differences from viruslike particles. *J Virol* **82**, 2079-88.

Kim, J. T., Kim, K. D., Song, E. Y., Lee, H. G., Kim, J. W., Kim, J. W., Chae, S. K., Kim, E., Lee, M. S., Yang, Y. & Lim, J. S. (2006). Apoptosis-inducing factor (AIF) inhibits protein synthesis by interacting with the eukaryotic translation initiation factor 3 subunit p44 (eIF3g). *FEBS Lett* **580**, 6375-83.

Kim, V. N. (2004). MicroRNA precursors in motion: exportin-5 mediates their nuclear export. *Trends Cell Biol* **14**, 156-9.

Kind, B., Koehler, K., Lorenz, M. & Huebner, A. (2009). The nuclear pore complex protein ALADIN is anchored via NDC1 but not via POM121 and GP210 in the nuclear envelope. *Biochem Biophys Res Commun* **390**, 205-10.

Kirchhoff, S. R., Gupta, S. & Knowlton, A. A. (2002). Cytosolic heat shock protein 60, apoptosis, and myocardial injury. *Circulation* **105**, 2899-904.

Klein, J. A., Longo-Guess, C. M., Rossmann, M. P., Seburn, K. L., Hurd, R. E., Frankel, W. N., Bronson, R. T. & Ackerman, S. L. (2002). The harlequin mouse mutation downregulates apoptosis-inducing factor. *Nature* **419**, 367-74.

Knox, C., Sass, E., Neupert, W. & Pines, O. (1998). Import into mitochondria, folding and retrograde movement of fumarase in yeast. *J Biol Chem* **273**, 25587-93.

Ko, J. M., Chan, P. L., Yau, W. L., Chan, H. K., Chan, K. C., Yu, Z. Y., Kwong, F. M., Miller, L. D., Liu, E. T., Yang, L. C., Lo, P. H., Stanbridge, E. J., Tang, J. C., Srivastava, G., Tsao, S. W., Law, S. & Lung, M. L. (2008). Monochromosome transfer and microarray analysis identify a critical tumor-suppressive region mapping to chromosome 13q14 and THSD1 in esophageal carcinoma. *Mol Cancer Res* **6**, 592-603.

Kobayashi, T., Zhang, G., Lee, B. J., Baba, S., Yamashita, M., Kamitani, W., Yanai, H., Tomonaga, K. & Ikuta, K. (2003). Modulation of Borna disease virus phosphoprotein nuclear localization by the viral protein X encoded in the overlapping open reading frame. *J Virol* **77**, 8099-107.

Komander, D., Clague, M. J. & Urbe, S. (2009). Breaking the chains: structure and function of the deubiquitinases. *Nat Rev Mol Cell Biol* **10**, 550-63.

Komurian-Pradel, F., Rajoharison, A., Berland, J. L., Khouri, V., Perret, M., Van Roosmalen, M., Pol, S., Negro, F. & Paranhos-Baccala, G. (2004). Antigenic relevance of F protein in chronic hepatitis C virus infection. *Hepatology* **40**, 900-9.

Kong, W. P. & Roos, R. P. (1991). Alternative translation initiation site in the DA strain of Theiler's murine encephalomyelitis virus. *J Virol* **65**, 3395-9.

Korkaya, H., Jameel, S., Gupta, D., Tyagi, S., Kumar, R., Zafrullah, M., Mazumdar, M., Lal, S. K., Xiaofang, L., Sehgal, D., Das, S. R. & Sahal, D. (2001). The ORF3 protein of hepatitis E virus binds to Src homology 3 domains and activates MAPK. *J Biol Chem* **276**, 42389-400.

Kozak, M. (1984). Complimentation & analysis of sequences upstream from the translational start site in eukaryotic mRNA's. *Nucleic Acids Research* **12**, 857-872.

Krull, S., Thyberg, J., Bjorkroth, B., Rackwitz, H. R. & Cordes, V. C. (2004). Nucleoporins as components of the nuclear pore complex core structure and Tpr as the architectural element of the nuclear basket. *Mol Biol Cell* **15**, 4261-77.

Kubota, H., Ota, K., Sakaki, Y. & Ito, T. (2001). Budding yeast GCN1 binds the GI domain to activate the eIF2alpha kinase GCN2. *J Biol Chem* **276**, 17591-6.

Kuribayashi, K., Mayes, P. A. & El-Deiry, W. S. (2006). What are caspases 3 and 7 doing upstream of the mitochondria? *Cancer Biol Ther* **5**, 763-5.

Kuyumcu-Martinez, M., Belliot, G., Sosnovtsev, S. V., Chang, K. O., Green, K. Y. & Lloyd, R. E. (2004). Calicivirus 3C-like proteinase inhibits cellular translation by cleavage of poly(A)-binding protein. *J Virol* **78**, 8172-82.

Lamb, R. A. & Takeda, M. (2001). Death by influenza virus protein. *Nat Med* **7**, 1286-8.

Lee, C. H., Leung, B., Lemmon, M. A., Zheng, J., Cowburn, D., Kuriyan, J. & Saksela, K. (1995). A single amino acid in the SH3 domain of Hck determines its high affinity and specificity in binding to HIV-1 Nef protein. *Embo J* **14**, 5006-15.

Lee, S. H., Kim, Y. K., Kim, C. S., Seol, S. K., Kim, J., Cho, S., Song, Y. L., Bartenschlager, R. & Jang, S. K. (2005). E2 of hepatitis C virus inhibits apoptosis. *J Immunol* **175**, 8226-35.

Lee, S. K., Park, S. O., Joe, C. O. & Kim, Y. S. (2007). Interaction of HCV core protein with 14-3-3epsilon protein releases Bax to activate apoptosis. *Biochem Biophys Res Commun* **352**, 756-62.

Lencioni, K. C., Seamons, A., Treuting, P. M., Maggio-Price, L. & Brabb, T. (2008). Murine norovirus: an intercurrent variable in a mouse model of bacteria-induced inflammatory bowel disease. *Comp Med* **58**, 522-33.

Leon, A., Omri, B., Gely, A., Klein, C. & Crisanti, P. (2006). QN1/KIAA1009: a new essential protein for chromosome segregation and mitotic spindle assembly. *Oncogene* **25**, 1887-95.

Liston, P. & Briedis, D. J. (1995). Ribosomal frameshifting during translation of measles virus P protein mRNA is capable of directing synthesis of a unique protein. *J Virol* **69**, 6742-50.

Liu, B. L., Clarke, I. N., Caul, E. O. & Lambden, P. R. (1995). Human enteric caliciviruses have a unique genome structure and are distinct from the Norwalk-like viruses. *Arch Virol* **140**, 1345-56.

Liu, G., Ni, Z., Yun, T., Yu, B., Chen, L., Zhao, W., Hua, J. & Chen, J. (2008a). A DNA-launched reverse genetics system for rabbit hemorrhagic disease virus reveals that the VP2 protein is not essential for virus infectivity. *J Gen Virol* **89**, 3080-5.

Liu, G. Q., Ni, Z., Yun, T., Yu, B., Zhu, J. M., Hua, J. G. & Chen, J. P. (2008b). Rabbit hemorrhagic disease virus poly(A) tail is not essential for the infectivity of the virus and can be restored in vivo. *Arch Virol* **153**, 939-44.

Lopman, B. A., Reacher, M. H., Van Duijnhoven, Y., Hanon, F. X., Brown, D. & Koopmans, M. (2003). Viral gastroenteritis outbreaks in Europe, 1995-2000. *Emerg Infect Dis* **9**, 90-6.

Lopman, B. A., Reacher, M. H., Vipond, I. B., Hill, D., Perry, C., Halladay, T., Brown, D. W., Edmunds, W. J. & Sarangi, J. (2004). Epidemiology and cost of nosocomial gastroenteritis, Avon, England, 2002-2003. *Emerg Infect Dis* **10**, 1827-34.

Ma, H. C., Lin, T. W., Li, H., Iguchi-Ariga, S. M., Ariga, H., Chuang, Y. L., Ou, J. H. & Lo, S. Y. (2008). Hepatitis C virus ARFP/F protein interacts with cellular MM-1 protein and enhances the gene trans-activation activity of c-Myc. *J Biomed Sci* **15**, 417-25.

Macdonald, A., Mazaleyrat, S., McCormick, C., Street, A., Burgoyne, N. J., Jackson, R. M., Cazeaux, V., Shelton, H., Saksela, K. & Harris, M. (2005). Further

studies on hepatitis C virus NS5A-SH3 domain interactions: identification of residues critical for binding and implications for viral RNA replication and modulation of cell signalling. *J Gen Virol* **86**, 1035-44.

Machin, A., Martin Alonso, J. M. & Parra, F. (2001). Identification of the amino acid residue involved in rabbit hemorrhagic disease virus VPg uridylylation. *J Biol Chem* **276**, 27787-92.

Madan, V., Sanchez-Martinez, S., Vedovato, N., Rispoli, G., Carrasco, L. & Nieva, J. L. (2007). Plasma membrane-porating domain in poliovirus 2B protein. A short peptide mimics viroporin activity. *J Mol Biol* **374**, 951-64.

Makino, A., Shimojima, M., Miyazawa, T., Kato, K., Tohya, Y. & Akashi, H. (2006). Junctional adhesion molecule 1 is a functional receptor for feline calicivirus. *J Virol* **80**, 4482-90.

Mancias, J. D. & Goldberg, J. (2007). The transport signal on Sec22 for packaging into COPII-coated vesicles is a conformational epitope. *Mol Cell* **26**, 403-14.

Mandic, L., Miller, M. S., Coulter, C., Munshaw, B. & Hertel, L. (2009). Human cytomegalovirus US9 protein contains an N-terminal signal sequence and a C-terminal mitochondrial localization domain, and does not alter cellular sensitivity to apoptosis. *J Gen Virol* **90**, 1172-82.

Manktelow, E., Shigemoto, K. & Brierley, I. (2005). Characterization of the frameshift signal of Edr, a mammalian example of programmed -1 ribosomal frameshifting. *Nucleic Acids Res* **33**, 1553-63.

Mann, M. & Wilm, M. (1994). Error-tolerant identification of peptides in sequence databases by peptide sequence tags. *Anal Chem* **66**, 4390-9.

Manolea, F., Claude, A., Chun, J., Rosas, J. & Melancon, P. (2008). Distinct functions for Arf guanine nucleotide exchange factors at the Golgi complex: GBF1 and BIGs are required for assembly and maintenance of the Golgi stack and trans-Golgi network, respectively. *Mol Biol Cell* **19**, 523-35.

Marin, M. S., Casais, R., Alonso, J. M. & Parra, F. (2000). ATP binding and ATPase activities associated with recombinant rabbit hemorrhagic disease virus 2C-like polypeptide. *J Virol* **74**, 10846-51.

Marks, P. J., Vipond, I. B., Carlisle, D., Deakin, D., Fey, R. E. & Caul, E. O. (2000). Evidence for airborne transmission of Norwalk-like virus (NLV) in a hotel restaurant. *Epidemiol Infect* **124**, 481-7.

Martella, V., Campolo, M., Lorusso, E., Cavicchio, P., Camero, M., Bellacicco, A. L., Decaro, N., Elia, G., Greco, G., Corrente, M., Desario, C., Arista, S., Banyai, K., Koopmans, M. & Buonavoglia, C. (2007). Norovirus in captive lion cub (*Panthera leo*). *Emerg Infect Dis* **13**, 1071-3.

Martella, V., Lorusso, E., Decaro, N., Elia, G., Radogna, A., D'Abramo, M., Desario, C., Cavalli, A., Corrente, M., Camero, M., Germinario, C. A., Banyai, K., Di Martino, B., Marsilio, F., Carmichael, L. E. & Buonavoglia, C. (2008). Detection and molecular characterization of a canine norovirus. *Emerg Infect Dis* **14**, 1306-8.

Martinez-Arribas, F., Agudo, D., Pollan, M., Gomez-Esquer, F., Diaz-Gil, G., Lucas, R. & Schneider, J. (2006). Positive correlation between the expression of X-chromosome RBM genes (RBMX, RBM3, RBM10) and the proapoptotic Bax gene in human breast cancer. *J Cell Biochem* **97**, 1275-82.

Marton, M. J., Vazquez de Aldana, C. R., Qiu, H., Chakraburtty, K. & Hinnebusch, A. G. (1997). Evidence that GCN1 and GCN20, translational regulators of GCN4, function on elongating ribosomes in activation of eIF2alpha kinase GCN2. *Mol Cell Biol* **17**, 4474-89.

Matsuda, D. & Dreher, T. W. (2006). Close spacing of AUG initiation codons confers dicistronic character on a eukaryotic mRNA. *RNA* **12**, 1338-49.

Matsufuji, S., Matsufuji, T., Miyazaki, Y., Murakami, Y., Atkins, J. F., Gesteland, R. F. & Hayashi, S. (1995). Autoregulatory frameshifting in decoding mammalian ornithine decarboxylase antizyme. *Cell* **80**, 51-60.

Mazurek, S., Boschek, C. B., Hugo, F. & Eigenbrodt, E. (2005). Pyruvate kinase type M2 and its role in tumor growth and spreading. *Semin Cancer Biol* **15**, 300-8.

Mazurek, S., Zwerschke, W., Jansen-Durr, P. & Eigenbrodt, E. (2001). Effects of the human papilloma virus HPV-16 E7 oncoprotein on glycolysis and glutaminolysis: role of pyruvate kinase type M2 and the glycolytic-enzyme complex. *Biochem J* **356**, 247-56.

McAuley, J. L., Hornung, F., Boyd, K. L., Smith, A. M., McKeon, R., Bennink, J., Yewdell, J. W. & McCullers, J. A. (2007). Expression of the 1918 influenza A virus PB1-F2 enhances the pathogenesis of viral and secondary bacterial pneumonia. *Cell Host Microbe* **2**, 240-9.

McCartney, S. A., Thackray, L. B., Gitlin, L., Gilfillan, S., Virgin, H. W. & Colonna, M. (2008). MDA-5 recognition of a murine norovirus. *PLoS Pathog* **4**, e1000108.

McIntosh, M. T., Behan, S. C., Mohamed, F. M., Lu, Z., Moran, K. E., Burrage, T. G., Neilan, J. G., Ward, G. B., Botti, G., Capucci, L. & Metwally, S. A. (2007). A pandemic strain of calicivirus threatens rabbit industries in the Americas. *Virol J* **4**, 96.

McMullan, L. K., Grakoui, A., Evans, M. J., Mihalik, K., Puig, M., Branch, A. D., Feinstone, S. M. & Rice, C. M. (2007). Evidence for a functional RNA element in the hepatitis C virus core gene. *Proc Natl Acad Sci U S A* **104**, 2879-84.

Meeroff, J. C., Schreiber, D. S., Trier, J. S. & Blacklow, N. R. (1980). Abnormal gastric motor function in viral gastroenteritis. *Ann Intern Med* **92**, 370-3.

Meyers, G. (2003). Translation of the minor capsid protein of a calicivirus is initiated by a novel termination-dependent reinitiation mechanism. *J Biol Chem* **278**, 34051-60.

Meyers, G. (2007). Characterization of the sequence element directing translation reinitiation in RNA of the calicivirus rabbit hemorrhagic disease virus. *J. Virol.* **81**, 9623-9632.

Meyers, G., Tautz, N., Dubovi, E. J. & Thiel, H. J. (1991). Viral cytopathogenicity correlated with integration of ubiquitin-coding sequences. *Virology* **180**, 602-616.

Mills, R. D., Trewhella, J., Qiu, T. W., Welte, T., Ryan, T. M., Hanley, T., Knott, R. B., Lithgow, T. & Mulhern, T. D. (2009). Domain organization of the monomeric form of the Tom70 mitochondrial import receptor. *J Mol Biol* **388**, 1043-58.

Mingot, J. M., Kostka, S., Kraft, R., Hartmann, E. & Gorlich, D. (2001). Importin 13: a novel mediator of nuclear import and export. *EMBO J* **20**, 3685-94.

Mita, A. C., Mita, M. M., Nawrocki, S. T. & Giles, F. J. (2008). Survivin: key regulator of mitosis and apoptosis and novel target for cancer therapeutics. *Clin Cancer Res* **14**, 5000-5.

Mitzner, D., Dudek, S. E., Studtrucker, N., Anhlan, D., Mazur, I., Wissing, J., Jansch, L., Wixler, L., Bruns, K., Sharma, A., Wray, V., Henklein, P., Ludwig, S. & Schubert, U. (2009). Phosphorylation of the influenza A virus protein PB1-F2 by PKC is crucial for apoptosis promoting functions in monocytes. *Cell Microbiol* **11**, 1502-16.

Modjtahedi, N., Giordanetto, F., Madeo, F. & Kroemer, G. (2006). Apoptosis-inducing factor: vital and lethal. *Trends Cell Biol* **16**, 264-72.

Mokranjac, D. & Neupert, W. (2009). Thirty years of protein translocation into mitochondria: unexpectedly complex and still puzzling. *Biochim Biophys Acta* **1793**, 33-41.

Moradpour, D., Cerny, A., Heim, M. H. & Blum, H. E. (2001). Hepatitis C: an update. *Swiss Med Wkly* **131**, 291-8.

Muller, B., Klemm, U., Mas Marques, A. & Schreier, E. (2007). Genetic diversity and recombination of murine noroviruses in immunocompromised mice. *Arch Virol* **152**, 1709-19.

Mumphrey, S. M., Changotra, H., Moore, T. N., Heimann-Nichols, E. R., Wobus, C. E., Reilly, M. J., Moghadamfalahi, M., Shukla, D. & Karst, S. M. (2007). Murine norovirus 1 infection is associated with histopathological changes in immunocompetent hosts but clinical disease is prevented by STAT1-dependent interferon responses. *J Virol* **81**, 3251-63.

Munder, P. G., Modolell, M., and Wallach, D. F. H. (1971). Cell propagation of films of polymeric fluorocarbon as a means to regulate pericellular pH and pO2 in cultured monolayers. *FEBS Lett.* **15**, 191-196.

Murata, T., Katsushima, N., Mizuta, K., Muraki, Y., Hongo, S. & Matsuzaki, Y. (2007). Prolonged norovirus shedding in infants <or=6 months of age with gastroenteritis. *Pediatr Infect Dis J* **26**, 46-9.

Nair, R. & Rost, B. (2005). Mimicking cellular sorting improves prediction of subcellular localization. *J Mol Biol* **348**, 85-100.

Nakai, K. & Horton, P. (1999). PSORT: a program for detecting sorting signals in proteins and predicting their subcellular localization. *Trends Biochem Sci* **24**, 34-6.

Nakai, K. & Kanehisa, M. (1992). A knowledge base for predicting protein localization sites in eukaryotic cells. *Genomics* **14**, 897-911.

Napthine, S., Lever, R. A., Powell, M. L., Jackson, R. J., Brown, T. D. & Brierley, I. (2009). Expression of the VP2 protein of murine norovirus by a translation termination-reinitiation strategy. *PLoS One* **4**, e8390.

Narechania, A., Terai, M. & Burk, R. D. (2005). Overlapping reading frames in closely related human papillomaviruses result in modular rates of selection within E2. *J Gen Virol* **86**, 1307-13.

Nathan, J. A., Sengupta, S., Wood, S. A., Admon, A., Markson, G., Sanderson, C. & Lehner, P. J. (2008). The ubiquitin E3 ligase MARCH7 is differentially regulated by the deubiquitylating enzymes USP7 and USP9X. *Traffic* **9**, 1130-45.

Natoni, A., Kass, G. E., Carter, M. J. & Roberts, L. O. (2006). The mitochondrial pathway of apoptosis is triggered during feline calicivirus infection. *J Gen Virol* **87**, 357-61.

Nebenfuhr, A., Ritzenthaler, C. & Robinson, D. G. (2002). Brefeldin A: deciphering an enigmatic inhibitor of secretion. *Plant Physiol* **130**, 1102-8.

Neill, J. D. (2002). The subgenomic RNA of feline calicivirus is packaged into viral particles during infection. *Virus Res* **87**, 89-93.

Neupert, W. (1997). Protein import into mitochondria. *Annu Rev Biochem* **66**, 863-917.

Niedernhofer, L. J., Lalai, A. S. & Hoeijmakers, J. H. (2005). Fanconi anemia (cross)linked to DNA repair. *Cell* **123**, 1191-8.

Nilsson, J., Rydell, G. E., Le Pendu, J. & Larson, G. (2009). Norwalk virus-like particles bind specifically to A, H and difucosylated Lewis but not to B histo-blood group active glycosphingolipids. *Glycoconj J* **26**, 1171-80.

Obenauer, J. C., Denson, J., Mehta, P. K., Su, X., Mukatira, S., Finkelstein, D. B., Xu, X., Wang, J., Ma, J., Fan, Y., Rakestraw, K. M., Webster, R. G., Hoffmann, E., Krauss, S., Zheng, J., Zhang, Z. & Naeve, C. W. (2006). Large-scale sequence analysis of avian influenza isolates. *Science* **311**, 1576-80.

Oberst, A., Bender, C. & Green, D. R. (2008). Living with death: the evolution of the mitochondrial pathway of apoptosis in animals. *Cell Death Differ* **15**, 1139-46.

Obuchi, M., Odagiri, T., Asakura, K. & Ohara, Y. (2001). Association of L* protein of Theiler's murine encephalomyelitis virus with microtubules in infected cells. *Virology* **289**, 95-102.

Obuchi, M. & Ohara, Y. (1999). Theiler's murine encephalomyelitis virus (TMEV): the role of a small out-of-frame protein in viral persistence and demyelination. *Jpn J Infect Dis* **52**, 228-33.

Oliver, S. L., Asobayire, E., Dastjerdi, A. M. & Bridger, J. C. (2006). Genomic characterization of the unclassified bovine enteric virus Newbury agent-1 (Newbury1) endorses a new genus in the family *Caliciviridae*. *Virology* **350**, 240-50.

Olsen, C. W., Kehren, J. C., Dybdahl-Sissoko, N. R. & Hinshaw, V. S. (1996). bcl-2 alters influenza virus yield, spread, and hemagglutinin glycosylation. *J Virol* **70**, 663-6.

Orci, L., Palmer, D. J., Ravazzola, M., Perrelet, A., Amherdt, M. & Rothman, J. E. (1993). Budding from Golgi membranes requires the coatomer complex of non-clathrin coat proteins. *Nature* **362**, 648-52.

Ostermann, J., Horwich, A. L., Neupert, W. & Hartl, F. U. (1989). Protein folding in mitochondria requires complex formation with hsp60 and ATP hydrolysis. *Nature* **341**, 125-130.

Panda, S. K., Thakral, D. & Rehman, S. (2007). Hepatitis E virus. *Rev Med Virol* **17**, 151-80.

Pang, Q., Fagerlie, S., Christianson, T. A., Keeble, W., Faulkner, G., Diaz, J., Rathbun, R. K. & Bagby, G. C. (2000). The Fanconi anemia protein FANCC binds to and facilitates the activation of STAT1 by gamma interferon and hematopoietic growth factors. *Mol Cell Biol* **20**, 4724-35.

Parrino, T. A., Schreiber, D. S., Trier, J. S., Kapikian, A. Z. & Blacklow, N. R. (1977). Clinical immunity in acute gastroenteritis caused by Norwalk agent. *N Engl J Med* **297**, 86-9.

Patel, K. J. & Joenje, H. (2007). Fanconi anemia and DNA replication repair. *DNA Repair (Amst)* **6**, 885-90.

Patel, M. M., Hall, A. J., Vinje, J. & Parashar, U. D. (2009). Noroviruses: a comprehensive review. *J Clin Virol* **44**, 1-8.

Perry, J. W., Taube, S. & Wobus, C. E. (2009). Murine norovirus-1 entry into permissive macrophages and dendritic cells is pH-independent. *Virus Res* **143**, 125-9.

Pfister, T. & Wimmer, E. (2001). Polypeptide p41 of a Norwalk-like virus is a nucleic acid-independent nucleoside triphosphatase. *J Virol* **75**, 1611-9.

Poenisch, M., Burger, N., Staeheli, P., Bauer, G. & Schneider, U. (2009a). Protein X of Borna disease virus inhibits apoptosis and promotes viral persistence in the central nervous systems of newborn-infected rats. *J Virol* **83**, 4297-307.

Poenisch, M., Staeheli, P. & Schneider, U. (2008). Viral accessory protein X stimulates the assembly of functional Borna disease virus polymerase complexes. *J Gen Virol* **89**, 1442-5.

Poenisch, M., Wille, S., Ackermann, A., Staeheli, P. & Schneider, U. (2007). The X protein of borna disease virus serves essential functions in the viral multiplication cycle. *J Virol* **81**, 7297-9.

Poenisch, M., Wille, S., Schneider, U. & Staeheli, P. (2009b). Second-site mutations in Borna disease virus overexpressing viral accessory protein X. *J Gen Virol* **90**, 1932-6.

Poyry, T. A., Kaminski, A., Connell, E. J., Fraser, C. S. & Jackson, R. J. (2007). The mechanism of an exceptional case of reinitiation after translation of a long ORF reveals why such events do not generally occur in mammalian mRNA translation. *Genes Dev* **21**, 3149-62.

Presek, P., Reinacher, M. & Eigenbrodt, E. (1988). Pyruvate kinase type M2 is phosphorylated at tyrosine residues in cells transformed by Rous sarcoma virus. *FEBS Lett* **242**, 194-8.

Pringle, C. R. (1998). Virus taxonomy--San Diego 1998. *Arch Virol* **143**, 1449-59.

Putics, A., Vashist, S., Bailey, D. & Goodfellow, I. (in press). Murine Norovirus Translation, Transation and Reverse Genetics.

Qureshi, S. A. (2007). Hepatitis C virus--biology, host evasion strategies, and promising new therapies on the horizon. *Med Res Rev* **27**, 353-73.

Radford, A. D., Coyne, K. P., Dawson, S., Porter, C. J. & Gaskell, R. M. (2007). Feline calicivirus. *Vet Res* **38**, 319-35.

Ramakrishnan, M. A., Gramer, M. R., Goyal, S. M. & Sreevatsan, S. (2009). A Serine12Stop mutation in PB1-F2 of the 2009 pandemic (H1N1) influenza A: a possible reason for its enhanced transmission and pathogenicity to humans. *J Vet Sci* **10**, 349-51.

Raschke, W. C., Baird, S., Ralph, P. & Nakoinz, I. (1978). Functional macrophage cell lines transformed by Abelson leukemia virus. *Cell* **15**, 261-7.

Reed, L. J. & Muench, H. (1938). A simple method of estimating fifty per cent end points. *American Journal of Hygiene* **27**, 493-497.

Rehling, P., Brandner, K. & Pfanner, N. (2004). Mitochondrial import and the twin-pore translocase. *Nat Rev Mol Cell Biol* **5**, 519-30.

Reuter, T. Y., Medhurst, A. L., Waisfisz, Q., Zhi, Y., Herterich, S., Hoehn, H., Gross, H. J., Joenje, H., Hoatlin, M. E., Mathew, C. G. & Huber, P. A. (2003). Yeast two-hybrid screens imply involvement of Fanconi anemia proteins in transcription regulation, cell signaling, oxidative metabolism, and cellular transport. *Exp Cell Res* **289**, 211-21.

Rice, P., Longden, I. & Bleasby, A. (2000). EMBOSS: the European Molecular Biology Open Software Suite. *Trends Genet* **16**, 276-7.

Ritchie, D. B., Schellenberg, M. J., Gesner, E. M., Raithatha, S. A., Stuart, D. T. & Macmillan, A. M. (2008). Structural elucidation of a PRP8 core domain from the heart of the spliceosome. *Nat Struct Mol Biol* **15**, 1199-205.

Robinson, M. S. & Kreis, T. E. (1992). Recruitment of coat proteins onto Golgi membranes in intact and permeabilized cells: effects of brefeldin A and G protein activators. *Cell* **69**, 129-38.

Rodriguez, I., Garcia, P. & Suarez, J. E. (2005). A second case of -1 ribosomal frameshifting affecting a major virion protein of the Lactobacillus bacteriophage A2. *J Bacteriol* **187**, 8201-4.

Roussel, J., Pillez, A., Montpellier, C., Duverlie, G., Cahour, A., Dubuisson, J. & Wychowski, C. (2003). Characterization of the expression of the hepatitis C virus F protein. *J Gen Virol* **84**, 1751-9.

Rydell, G. E., Nilsson, J., Rodriguez-Diaz, J., Ruvoen-Clouet, N., Svensson, L., Le Pendu, J. & Larson, G. (2009). Human noroviruses recognize sialyl Lewis x neoglycoprotein. *Glycobiology* **19**, 309-20.

Saksela, K., Cheng, G. & Baltimore, D. (1995). Proline-rich (PxxP) motifs in HIV-1 Nef bind to SH3 domains of a subset of Src kinases and are required for the enhanced growth of Nef+ viruses but not for down-regulation of CD4. *Embo J* **14**, 484-91.

Salvesen, G. S. & Duckett, C. S. (2002). IAP proteins: blocking the road to death's door. *Nat Rev Mol Cell Biol* **3**, 401-10.

Saulquin, X., Scotet, E., Trautmann, L., Peyrat, M. A., Halary, F., Bonneville, M. & Houssaint, E. (2002). +1 Frameshifting as a novel mechanism to generate a cryptic cytotoxic T lymphocyte epitope derived from human interleukin 10. *J Exp Med* **195**, 353-8.

Schaffer, F. L., Ehresmann, D. W., Fretz, M. K. & Soergel, M. I. (1980). A protein, VPg, covalently linked to 36S calicivirus RNA. *J Gen Virol* **47**, 215-20.

Schlitt, B. P., Felrice, M., Jelachich, M. L. & Lipton, H. L. (2003). Apoptotic cells, including macrophages, are prominent in Theiler's virus-induced inflammatory, demyelinating lesions. *J Virol* **77**, 4383-8.

Schneider, U. (2005). Novel insights into the regulation of the viral polymerase complex of neurotropic Borna disease virus. *Virus Res* **111**, 148-60.

Schneider, U., Naegele, M., Staeheli, P. & Schwemmle, M. (2003). Active borna disease virus polymerase complex requires a distinct nucleoprotein-to-phosphoprotein ratio but no viral X protein. *J Virol* **77**, 11781-9.

Schwardt, M., Mayer, D., Frank, R., Schneider, U., Eickmann, M., Planz, O., Wolff, T. & Schwemmle, M. (2005). The negative regulator of Borna disease virus polymerase is a non-structural protein. *J Gen Virol* **86**, 3163-9.

Schwemmle, M., Salvatore, M., Shi, L., Richt, J., Lee, C. H. & Lipkin, W. I. (1998). Interactions of the borna disease virus P, N, and X proteins and their functional implications. *J Biol Chem* **273**, 9007-12.

Scipioni, A., Mauroy, A., Vinje, J. & Thiry, E. (2008). Animal noroviruses. *Vet J* **178**, 32-45.

Shao, S. W., Wu, W. B., Bian, Z. Q., Yu, J. G., Zhao, P., Zhao, L. J., Zhu, S. Y. & Qi, Z. T. (2009). Hepatitis C virus F protein inhibits cell apoptosis by activation of intracellular NF-kappaB pathway. *Hepatol Res* **39**, 282-9.

Sharp, T. V., Wang, H. W., Koumi, A., Hollyman, D., Endo, Y., Ye, H., Du, M. Q. & Boshoff, C. (2002). K15 protein of Kaposi's sarcoma-associated herpesvirus is latently expressed and binds to HAX-1, a protein with antiapoptotic function. *J Virol* **76**, 802-16.

Shigemoto, K., Brennan, J., Walls, E., Watson, C. J., Stott, D., Rigby, P. W. & Reith, A. D. (2001). Identification and characterisation of a developmentally regulated mammalian gene that utilises -1 programmed ribosomal frameshifting. *Nucleic Acids Res* **29**, 4079-88.

Simmonds, P., Karakasiliotis, I., Bailey, D., Chaudhry, Y., Evans, D. J. & Goodfellow, I. G. (2008). Bioinformatic and functional analysis of RNA secondary structure elements among different genera of human and animal caliciviruses. *Nucleic Acids Res* **36**, 2530-46.

Singh, S. & Khar, A. (2005). Differential gene expression during apoptosis induced by a serum factor: role of mitochondrial F0-F1 ATP synthase complex. *Apoptosis* **10**, 1469-82.

Smith, D. B. & Simmonds, P. (1997). Characteristics of nucleotide substitution in the hepatitis C virus genome: constraints on sequence change in coding regions at both ends of the genome. *J Mol Evol* **45**, 238-46.

Smith, E., Meyerrose, T. E., Kohler, T., Namdar-Attar, M., Bab, N., Lahat, O., Noh, T., Li, J., Karaman, M. W., Hacia, J. G., Chen, T. T., Nolta, J. A., Muller, R., Bab, I. & Frenkel, B. (2005). Leaky ribosomal scanning in mammalian genomes: significance of histone H4 alternative translation in vivo. *Nucleic Acids Res* **33**, 1298-308.

Smogorzewska, A., Matsuoka, S., Vinciguerra, P., McDonald, E. R., 3rd, Hurov, K. E., Luo, J., Ballif, B. A., Gygi, S. P., Hofmann, K., D'Andrea, A. D. & Elledge, S. J. (2007). Identification of the FANCI protein, a monoubiquitinated FANCD2 paralog required for DNA repair. *Cell* **129**, 289-301.

Sosnovtsev, S. & Green, K. Y. (1995). RNA transcripts derived from a cloned full-length copy of the feline calicivirus genome do not require VPg for infectivity. *Virology* **210**, 383-90.

Sosnovtsev, S. V., Belliot, G., Chang, K.-O. K., Prikhodko, V. G., Thackray, L. B., Wobus, C. E., Karst, S. M., Virgin, H. W. & Green, K. Y. (2006). Cleavage Map and Proteolytic Processing of the Murine Norovirus Nonstructural Polyprotein in Infected Cells. *J Virol* **80**, 7816-7831.

Sosnovtsev, S. V., Garfield, M. & Green, K. Y. (2002). Processing map and essential cleavage sites of the nonstructural polyprotein encoded by ORF1 of the feline calicivirus genome. *J Virol* **76**, 7060-72.

Sosnovtsev, S. V., Prikhod'ko, E. A., Belliot, G., Cohen, J. I. & Green, K. Y. (2003). Feline calicivirus replication induces apoptosis in cultured cells. *Virus Res* **94**, 1-10.

Spiropoulou, C. F. & Nichol, S. T. (1993). A small highly basic protein is encoded in overlapping frame within the P gene of vesicular stomatitis virus. *J Virol* **67**, 3103-10.

Springfeld, C., Darai, G. & Cattaneo, R. (2005). Characterization of the Tupaia rhabdovirus genome reveals a long open reading frame overlapping with P and a novel gene encoding a small hydrophobic protein. *J Virol* **79**, 6781-90.

Stanasila, L., Abuin, L., Diviani, D. & Cotecchia, S. (2006). Ezrin directly interacts with the alpha1b-adrenergic receptor and plays a role in receptor recycling. *J Biol Chem* **281**, 4354-63.

Stauber, R. H., Rabenhorst, U., Rekik, A., Engels, K., Bier, C. & Knauer, S. K. (2006). Nucleocytoplasmic shuttling and the biological activity of mouse survivin are regulated by an active nuclear export signal. *Traffic* **7**, 1461-72.

Stavrou, S., Baida, G., Viktorova, E., Ghadge, G., Agol, V. I. & Roos, R. P. (2010). Theiler's murine encephalomyelitis virus (TMEV) L* amino acid position 93 is important for virus persistence and virus-induced demyelination. *J Virol* **84**, 1348-54.

Stewart, M., Baker, R. P., Bayliss, R., Clayton, L., Grant, R. P., Littlewood, T. & Matsuura, Y. (2001). Molecular mechanism of translocation through nuclear pore complexes during nuclear protein import. *FEBS Lett* **498**, 145-9.

Stojanovski, D., Pfanner, N. & Wiedemann, N. (2007). Import of proteins into mitochondria. *Methods Cell Biol* **80**, 783-806.

Straub, T. M., Bentrup, K. H. z., Orosz-Coghlan, P., Dohnalkova, A., Mayer, B. K., Bartholomew, R. A., O.Valdez, C., Bruckner-Lea, C. J., Gerba, C. P.,

Abbaszadegan, M. & Nickerson, C. A. (2007). *In vitro* cell culture infectivity assay for human noroviruses. *Emerging Infectious Diseases* **13**, 396-403.

Stuart, A. D. & Brown, T. D. (2007). Alpha2,6-linked sialic acid acts as a receptor for Feline calicivirus. *J Gen Virol* **88**, 177-86.

Stuart, A. D. & Brown, T. D. K. (2006). Entry of feline calicivirus is dependent on clathrin-mediated endocytosis and acidification in endosomes. *J. Virol.* **80**, 7500-7509.

Surjit, M., Jameel, S. & Lal, S. K. (2004). The ORF2 protein of hepatitis E virus binds the 5' region of viral RNA. *J Virol* **78**, 320-8.

Susin SA, L. H., Zamzami N, Marzo I, Snow BE, Brothers GM, Mangion J, Jacotot E, Costantini P, Loeffler M, Larochette N, Goodlett DR, Aebersold R, Siderovski DP, Penninger JM, Kroemer G. (1999). Molecular characterization of mitochondrial apoptosis-inducing facto. *Nature* **4;397(6718)**, 441-6.

Sutherland, L. C., Rintala-Maki, N. D., White, R. D. & Morin, C. D. (2005). RNA binding motif (RBM) proteins: a novel family of apoptosis modulators? *J Cell Biochem* **94**, 5-24.

Suzuki, N., Sugawara, M., Nuss, D. L. & Matsuura, Y. (1996). Polycistronic (tri- or bicistronic) phytoreoviral segments translatable in both plant and insect cells. *J Virol* **70**, 8155-9.

Suzuki, T., Aizaki, H., Murakami, K., Shoji, I. & Wakita, T. (2007a). Molecular biology of hepatitis C virus. *J Gastroenterol* **42**, 411-23.

Suzuki, T., Ishii, K., Aizaki, H. & Wakita, T. (2007b). Hepatitis C viral life cycle. *Adv Drug Deliv Rev* **59**, 1200-12.

Tam, A. W., Smith, M. M., Guerra, M. E., Huang, C. C., Bradley, D. W., Fry, K. E. & Reyes, G. R. (1991). Hepatitis-E Virus (HEV) - Molecular Cloning and Sequencing of the Full-Length Viral Genome. *Virology* **185**, 120-131.

Tamura, M., Natori, K., Kobayashi, M., Miyamura, T. & Takeda, N. (2004). Genogroup II noroviruses efficiently bind to heparan sulfate proteoglycan associated with the cellular membrane. *J Virol* **78**, 3817-26.

Tan, I., Ng, C. H., Lim, L. & Leung, T. (2001). Phosphorylation of a novel myosin binding subunit of protein phosphatase 1 reveals a conserved mechanism in the regulation of actin cytoskeleton. *J Biol Chem* **276**, 21209-16.

Tapia-Vieyra, J. V., Arellano, R. O. & Mas-Oliva, J. (2005). ARP2 a novel protein involved in apoptosis of LNCaP cells shares a high degree homology with splicing factor Prp8. *Mol Cell Biochem* **269**, 189-201.

Taube, S., Kurth, A. & Schreier, E. (2005). Generation of recombinant norovirus-like particles (VLP) in the human endothelial kidney cell line 293T. *Arch Virol* **150**, 1425-31.

Taube, S., Perry, J. W., Yetming, K., Patel, S. P., Auble, H., Shu, L., Nawar, H. F., Lee, C. H., Connell, T. D., Shayman, J. A. & Wobus, C. E. (2009). Ganglioside-linked terminal sialic acid moieties on murine macrophages function as attachment receptors for Murine Noroviruses (MNV). *J Virol* **83**, 4092-101.

Teunis, P. F., Moe, C. L., Liu, P., Miller, S. E., Lindesmith, L., Baric, R. S., Le Pendu, J. & Calderon, R. L. (2008). Norwalk virus: how infectious is it? *J Med Virol* **80**, 1468-76.

Thackray, L. B., Wobus, C. E., Chachu, K. A., Liu, B., Alegre, E. R., Henderson, K. S., Kelley, S. T. & Virgin, H. W. t. (2007). Murine noroviruses comprising a single genogroup exhibit biological diversity despite limited sequence divergence. *J Virol* **81**, 10460-73.

Tolskaya, E. A., Romanova, L. I., Kolesnikova, M. S., Ivannikova, T. A., Smirnova, E. A., Raikhlin, N. T. & Agol, V. I. (1995). Apoptosis-inducing and apoptosis-preventing functions of poliovirus. *J Virol* **69**, 1181-1189.

Trifonov, V. & Rabadan, R. (2009). The Contribution of the PB1-F2 Protein to the Fitness of Influenza A Viruses and its Recent Evolution in the 2009 Influenza A (H1N1) Pandemic Virus. *PLoS Curr Influenza*, RRN1006.

Tsao, M. L., Chao, C. H. & Yeh, C. T. (2006). Interaction of hepatitis C virus F protein with prefoldin 2 perturbs tubulin cytoskeleton organization. *Biochem Biophys Res Commun* **348**, 271-7.

Tsien, R. Y. (1998). The green fluorescent protein. *Annu Rev Biochem* **67**, 509-44.

Turcios-Ruiz, R. M., Axelrod, P., St John, K., Bullitt, E., Donahue, J., Robinson, N. & Friss, H. E. (2008). Outbreak of necrotizing enterocolitis caused by norovirus in a neonatal intensive care unit. *J Pediatr* **153**, 339-44.

Tyagi, S., Jameel, S. & Lal, S. K. (2001). Self-association and mapping of the interaction domain of hepatitis E virus ORF3 protein. *J Virol* **75**, 2493-8.

Tyagi, S., Korkaya, H., Zafrullah, M., Jameel, S. & Lal, S. K. (2002). The phosphorylated form of the ORF3 protein of hepatitis E virus interacts with its non-glycosylated form of the major capsid protein, ORF2. *J Biol Chem* **277**, 22759-67.

Uchida, T., Myers, M. G., Jr. & White, M. F. (2000). IRS-4 mediates protein kinase B signaling during insulin stimulation without promoting antiapoptosis. *Mol Cell Biol* **20**, 126-38.

van Eyll, O. & Michiels, T. (2002). Non-AUG-initiated internal translation of the L* protein of Theiler's virus and importance of this protein for viral persistence. *J Virol* **76**, 10665-73.

van Pesch, V., van Eyll, O. & Michiels, T. (2001). The leader protein of Theiler's virus inhibits immediate-early alpha/beta interferon production. *J Virol* **75**, 7811-7.

Varaklioti, A., Vassilaki, N., Georgopoulou, U. & Mavromara, P. (2002). Alternate translation occurs within the core coding region of the hepatitis C viral genome. *J Biol Chem* **277**, 17713-21.

Vashist, S., Bailey, D., Putics, A. & Goodfellow, I. (2009). Model systems for the study of human norovirus biology. *Future Virology* **4**, 353.

Vassilaki, N., Boleti, H. & Mavromara, P. (2007). Expression studies of the core+1 protein of the hepatitis C virus 1a in mammalian cells. The influence of the core protein and proteasomes on the intracellular levels of core+1. *Febs J* **274**, 4057-74.

Vassilaki, N., Boleti, H. & Mavromara, P. (2008a). Expression studies of the HCV-1a core+1 open reading frame in mammalian cells. *Virus Res* **133**, 123-35.

Vassilaki, N., Friebe, P., Meuleman, P., Kallis, S., Kaul, A., Paranhos-Baccala, G., Leroux-Roels, G., Mavromara, P. & Bartenschlager, R. (2008b). Role of the hepatitis C virus core+1 open reading frame and core cis-acting RNA elements in viral RNA translation and replication. *J Virol* **82**, 11503-15.

Vassilaki, N., Kalliampakou, K. I. & Mavromara, P. (2008c). Differences in the expression of the hepatitis C virus core+1 open reading frame between a nuclear and a cytoplasmic expression system. *J Gen Virol* **89**, 222-31.

Vassilaki, N. & Mavromara, P. (2003). Two alternative translation mechanisms are responsible for the expression of the HCV ARFP/F/core+1 coding open reading frame. *J Biol Chem* **278**, 40503-13.

Vassilaki, N. & Mavromara, P. (2009). The HCV ARFP/F/core+1 protein: production and functional analysis of an unconventional viral product. *IUBMB Life* **61**, 739-52.

Vasu, S., Shah, S., Orjalo, A., Park, M., Fischer, W. H. & Forbes, D. J. (2001). Novel vertebrate nucleoporins Nup133 and Nup160 play a role in mRNA export. *J Cell Biol* **155**, 339-54.

Vermeulen, K., Van Bockstaele, D. R. & Berneman, Z. N. (2005). Apoptosis: mechanisms and relevance in cancer. *Ann Hematol* **84**, 627-39.

Wachtel, C. & Manley, J. L. (2009). Splicing of mRNA precursors: the role of RNAs and proteins in catalysis. *Mol Biosyst* **5**, 311-6.

Waldmann, I., Walde, S. & Kehlenbach, R. H. (2007). Nuclear import of c-Jun is mediated by multiple transport receptors. *J Biol Chem* **282**, 27685-92.

Walewski, J. L., Keller, T. R., Stump, D. D. & Branch, A. D. (2001). Evidence for a new hepatitis C virus antigen encoded in an overlapping reading frame. *RNA* **7**, 710-21.

Wang, Y., Dawson, V. L. & Dawson, T. M. (2009a). Poly(ADP-ribose) signals to mitochondrial AIF: a key event in parthanatos. *Exp Neurol* **218**, 193-202.

Wang, Y., Kim, N. S., Li, X., Greer, P. A., Koehler, R. C., Dawson, V. L. & Dawson, T. M. (2009b). Calpain activation is not required for AIF translocation in PARP-1-dependent cell death (parthanatos). *J Neurochem* **110**, 687-96.

Ward, J. M., Wobus, C. E., Thackray, L. B., Erexson, C. R., Faucette, L. J., Belliot, G., Barron, E. L., Sosnovtsev, S. V. & Green, K. Y. (2006). Pathology of immunodeficient mice with naturally occurring murine norovirus infection. *Toxicol Pathol* **34**, 708-15.

Ward, V. K., McCormick, C. J., Clarke, I. N., Salim, O., Wobus, C. E., Thackray, L. B., Virgin, H. W. t. & Lambden, P. R. (2007). Recovery of infectious murine norovirus using pol II-driven expression of full-length cDNA. *Proc Natl Acad Sci U S A* **104**, 11050-5.

Watanabe, Y., Ohtaki, N., Hayashi, Y., Ikuta, K. & Tomonaga, K. (2009). Autogenous translational regulation of the Borna disease virus negative control factor X from polycistronic mRNA using host RNA helicases. *PLoS Pathog* **5**, e1000654.

Weber-Lotfi, F., Dietrich, A., Russo, M. & Rubino, L. (2002). Mitochondrial targeting and membrane anchoring of a viral replicase in plant and yeast cells. *J Virol* **76**, 10485-96.

Wei, L., Huhn, J. S., Mory, A., Pathak, H. B., Sosnovtsev, S. V., Green, K. Y. & Cameron, C. E. (2001a). Proteinase-polymerase precursor as the active form of feline calicivirus RNA-dependent RNA polymerase. *J Virol* **75**, 1211-9.

Wei, M. C., Zong, W. X., Cheng, E. H., Lindsten, T., Panoutsakopoulou, V., Ross, A. J., Roth, K. A., MacGregor, G. R., Thompson, C. B. & Korsmeyer, S. J. (2001b). Proapoptotic BAX and BAK: a requisite gateway to mitochondrial dysfunction and death. *Science* **292**, 727-30.

Whitton, J. L., Cornell, C. T. & Feuer, R. (2005). Host and virus determinants of picornavirus pathogenesis and tropism. *Nat Rev Microbiol* **3**, 765-76.

Willcocks, M. M., Carter, M. J. & Roberts, L. O. (2004). Cleavage of eukaryotic initiation factor eIF4G and inhibition of host-cell protein synthesis during feline calicivirus infection. *J Gen Virol* **85**, 1125-30.

Wise, H. M., Foeglein, A., Sun, J., Dalton, R. M., Patel, S., Howard, W., Anderson, E. C., Barclay, W. S. & Digard, P. (2009). A complicated message: Identification of a novel PB1-related protein translated from influenza A virus segment 2 mRNA. *J Virol* **83**, 8021-31.

Wobus, C. E., Karst, S. M., Thackray, L. B., Chang, K. O., Sosnovtsev, S. V., Belliot, G., Krug, A., Mackenzie, J. M., Green, K. Y. & Virgin, H. W. (2004).

Replication of Norovirus in cell culture reveals a tropism for dendritic cells and macrophages. *PLoS Biol* **2**, e432.

Wobus, C. E., Thackray, L. B. & Virgin, H. W. t. (2006). Murine norovirus: a model system to study norovirus biology and pathogenesis. *J Virol* **80**, 5104-12.

Wolf, M., Dimitrova, M., Baumert, T. F. & Schuster, C. (2008). The major form of hepatitis C virus alternate reading frame protein is suppressed by core protein expression. *Nucleic Acids Res* **36**, 3054-64.

Wu, W. B., Shao, S. W., Zhao, L. J., Luan, J., Cao, J., Gao, J., Zhu, S. Y. & Qi, Z. T. (2007). Hepatitis C virus F protein up-regulates c-myc and down-regulates p53 in human hepatoma HepG2 cells. *Intervirology* **50**, 341-6.

Wu, X., Zhou, Y., Zhang, K., Liu, Q. & Guo, D. (2008). Isoform-specific interaction of pyruvate kinase with hepatitis C virus NS5B. *FEBS Lett* **582**, 2155-60.

Xanthoudakis, S., Roy, S., Rasper, D., Hennessey, T., Aubin, Y., Cassady, R., Tawa, P., Ruel, R., Rosen, A. & Nicholson, D. W. (1999). Hsp60 accelerates the maturation of pro-caspase-3 by upstream activator proteases during apoptosis. *EMBO J* **18**, 2049-56.

Xu, C. W., Mendelsohn, A. R. & Brent, R. (1997). Cells that register logical relationships among proteins. *Proc Natl Acad Sci U S A* **94**, 12473-8.

Xu, Z., Choi, J., Lu, W. & Ou, J. H. (2003). Hepatitis C virus f protein is a short-lived protein associated with the endoplasmic reticulum. *J Virol* **77**, 1578-83.

Xu, Z., Choi, J., Yen, T. S., Lu, W., Strohecker, A., Govindarajan, S., Chien, D., Selby, M. J. & Ou, J. (2001). Synthesis of a novel hepatitis C virus protein by ribosomal frameshift. *EMBO J* **20**, 3840-8.

Yamada, H., Chounan, R., Higashi, Y., Kurihara, N. & Kido, H. (2004). Mitochondrial targeting sequence of the influenza A virus PB1-F2 protein and its function in mitochondria. *FEBS Lett* **578**, 331-6.

Yamamoto, H., Fukui, K., Takahashi, H., Kitamura, S., Shiota, T., Terao, K., Uchida, M., Esaki, M., Nishikawa, S., Yoshihisa, T., Yamano, K. & Endo, T. (2009). Roles of Tom70 in import of presequence-containing mitochondrial proteins. *J Biol Chem* **284**, 31635-46.

Yang, Y. G., Herceg, Z., Nakanishi, K., Demuth, I., Piccoli, C., Michelon, J., Hildebrand, G., Jasin, M., Digweed, M. & Wang, Z. Q. (2005). The Fanconi anemia group A protein modulates homologous repair of DNA double-strand breaks in mammalian cells. *Carcinogenesis* **26**, 1731-40.

Yasuhara, N., Eguchi, Y., Tachibana, T., Imamoto, N., Yoneda, Y. & Tsujimoto, Y. (1997). Essential role of active nuclear transport in apoptosis. *Genes Cells* **2**, 55-64.

Yedavalli, V. S., Shih, H. M., Chiang, Y. P., Lu, C. Y., Chang, L. Y., Chen, M. Y., Chuang, C. Y., Dayton, A. I., Jeang, K. T. & Huang, L. M. (2005). Human immunodeficiency virus type 1 Vpr interacts with antiapoptotic mitochondrial protein HAX-1. *J Virol* **79**, 13735-46.

Yewdell, J. W. & Hickman, H. D. (2007). New lane in the information highway: alternative reading frame peptides elicit T cells with potent antiretrovirus activity. *J Exp Med* **204**, 2501-4.

Yu, C. S., Chen, Y. C., Lu, C. H. & Hwang, J. K. (2006). Prediction of protein subcellular localization. *Proteins* **64**, 643-51.

Yu, S. W., Wang, Y., Frydenlund, D. S., Ottersen, O. P., Dawson, V. L. & Dawson, T. M. (2009). Outer mitochondrial membrane localization of apoptosis-inducing factor: mechanistic implications for release. *ASN Neuro* **1**, 275-281.

Yuksek, K., Chen, W. L., Chien, D. & Ou, J. H. (2009). Ubiquitin-independent degradation of hepatitis C virus F protein. *J Virol* **83**, 612-21.

Zafrullah, M., Ozdener, M. H., Panda, S. K. & Jameel, S. (1997). The ORF3 protein of hepatitis E virus is a phosphoprotein that associates with the cytoskeleton. *J Virol* **71**, 9045-53.

Zamarin, D., Garcia-Sastre, A., Xiao, X., Wang, R. & Palese, P. (2005). Influenza virus PB1-F2 protein induces cell death through mitochondrial ANT3 and VDAC1. *PLoS Pathog* **1**, e4.

Zamarin, D., Ortigoza, M. B. & Palese, P. (2006). Influenza A virus PB1-F2 protein contributes to viral pathogenesis in mice. *J Virol* **80**, 7976-83.

Zell, R., Krumbholz, A., Eitner, A., Krieg, R., Halbhuber, K. J. & Wutzler, P. (2007). Prevalence of PB1-F2 of influenza A viruses. *J Gen Virol* **88**, 536-46.

Zhang, M., Purcell, R. H. & Emerson, S. U. (2001). Identification of the 5' terminal sequence of the SAR-55 and MEX-14 strains of hepatitis E virus and confirmation that the genome is capped. *J Med Virol* **65**, 293-5.

Zhang, X., Dong, N., Yin, L., Cai, N., Ma, H., You, J., Zhang, H., Wang, H., He, R. & Ye, L. (2005). Hepatitis B virus X protein upregulates survivin expression in hepatoma tissues. *J Med Virol* **77**, 374-81.

Zhao, L., Helms, J. B., Brugger, B., Harter, C., Martoglio, B., Graf, R., Brunner, J. & Wieland, F. T. (1997). Direct and GTP-dependent interaction of ADP ribosylation factor 1 with coatomer subunit beta. *Proc Natl Acad Sci U S A* **94**, 4418-23.

Zhou, H., Li, X. M., Meinkoth, J. & Pittman, R. N. (2000). Akt regulates cell survival and apoptosis at a postmitochondrial level. *J Cell Biol* **151**, 483-94.

Zhu, Y., Roshal, M., Li, F., Blackett, J. & Planelles, V. (2003). Upregulation of survivin by HIV-1 Vpr. *Apoptosis* **8**, 71-9.

Zuker, M. (2003). Mfold web server for nucleic acid folding and hybridization prediction. *Nucleic Acids Res* **31**, 3406-15.

Zwerschke, W., Mazurek, S., Massimi, P., Banks, L., Eigenbrodt, E. & Jansen-Durr, P. (1999). Modulation of type M2 pyruvate kinase activity by the human papillomavirus type 16 E7 oncoprotein. *Proc Natl Acad Sci U S A* **96**, 1291-6.